RADAR CROSS SECTION OF WIRES ATTACHED TO BODIES OF REVOLUTION

(THEORETICAL STUDY)

A Thesis

Submitted to the College of Science
University of Basrah
as a Partial Fulfillment of the Requirements for
the Degree of Doctor of Philosophy in Physics
(*Electromagnetic Computations*)

By

Akeel S. Tahir

B. Sc. 1997 Basrah University

M. Sc. 2000 Basrah University

UNDER THE SUPERVISION OF

PROF. Dr. AHMAD H. ABOOD AND ASST. PROF. Dr. WA'IL A. GODAYMI

1436 **2014**

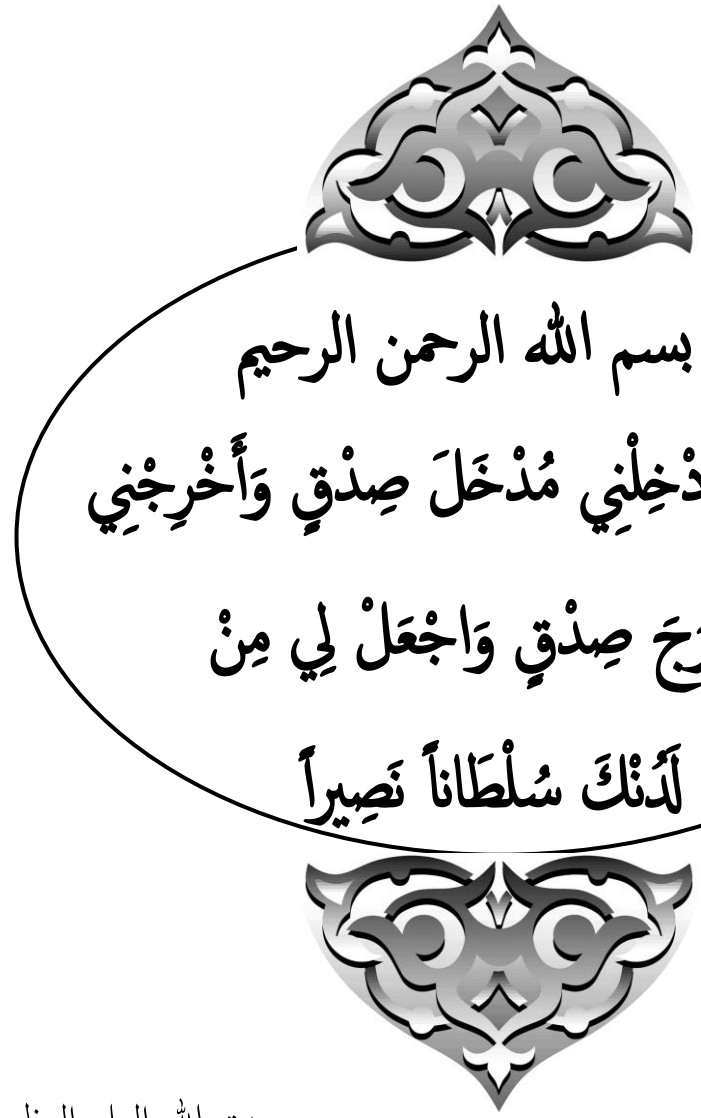

صدق الله العلي العظيم
(الاسراء، آية 80)

CERTIFICATION

We certify that this thesis, which is entitled **(RADAR CROSS SECTION OF WIRES ATTACHED TO BODIES OF REVOLUTION)** Presented by **Akeel S. Tahir,** was prepared under our supervision at the Physics Department, College of Science, Basrah University as a partial requirement for the degree of Doctor of philosophy in physics **(Electromagnetic Computations).**

Signature:

Supervisor: Dr. Ahmad H. Abood

Academic Title : Professor

Date : 30/10/2014

Signature:

Supervisor: Dr. Wa'il A. Godaymi

Academic Title : Assist. Professor

Date : 30/10/2014

In view of the available recommendations, I forward this thesis for debate by the examining committee.

Signature:

Adviser : Dr. H. A. AL Khursan

Title : Assist. Professor

Head of Physics Department

Date : 30/10/2014

COMMIUTTEE CERTIFICATION

We the examining committee have read this thesis **(RADAR CROSS SECTION OF WIRES ATTACHED TO BODIES OF REVOLUTION)** Presented by the student **(Akeel S. Tahir)**. We have examined the student in its content and in what is related to it, and that in our opinion it is qualified for pursuing the degree of **Doctor of philosophy in physics** with the specially of ***Electromagnetic Computations***.

Signature:
Name: **Dr. Zeki A. Ahmed**
Academic Title : Professor
(Chairman)
Date : **16/ 9/ 2015**

Signature:
Name: **Dr. Jamal W. Salman**
Academic Title : Professor
(Member)
Date : **16 /4 / 2015**

Signature:
Name: **Dr. Ahmad K. Ahmad**
Academic Title : Professor
(Member)
Date : **16/4 / 2015**

Signature:
Name: **Dr. Sabah M. Mohammed-Ameen**
Academic Title: Asst. Professor
(Member)
Date : **16 /4 / 2015**

Signature:
Name: **Dr. Qusay M. Ali**
Academic Title: Asst. Professor
(Member)
Date : **16 /4 / 2015**

Signature:
Name: **Dr. Ahmad H. Abood**
Academic Title : Professor
(Member & Supervisor)
Date : **16 /4 / 2015**

Signature:
Name: **Dr. Wa'il A. Godaymi**
Academic Title : Asst. Professor
(Member & Supervisor)
Date : **16/ 4/ 2015**

Approve by the Deanery of the College of Science/University of Basrah.

Signature :
Name: **Dr. Falhi. A. Ali**
Academic Title : Professor
(Dean of the College of Science)
Date : **/ / 2015**

DEDICATION

With all love I dedicate my work

To

My father, for his spirit and his memory fragrant

To

My address in life

The wonderful family, My wife and my children

Akeel

ACKNOWLEDGEMENT

First, I would like to thank the almighty Allah for my healthy life, and granting me a blessed family, and everyone who has shared something with me or supported me during the hard time.

I am extremely grateful to my supervisors' professor Dr. **Ahmad H. Abood** and Asst. professor Dr. **Wa'il A. Godaymi** for their time and patience that guides me to develop analytic thinking and scientific knowledge to build up the core of my thesis; without their valuable advises and assistance, the completion of this thesis would not be possible.

I would like to express my appreciation to Basrah University and College of Science for their support to postgraduates to raise the scientific path of great Iraq; especially to the Dean of the College.

Deep thanks are due to the Head of the Physics Department for his support and facilitating my work during the research period and for staff of Physics Department.

I owe many debts of gratitude to my professorial Dr. **Zeki A. Ahmed** of Basrah University, College of Science for providing a supportive intellectual environment and so much kindness, guidance, and encouragement during this Doctoral research. Deep gratitude is also extended to Mr. **Ra'ad Abdul-Jabar Al-Assdi** and Mr. **Awn E. Salman** of Basrah University, College of Science, and Dr. **Shamaail A. Saewan** of Basrah University, College of Agriculture to help me during this work. I'm also grateful to my friend's colleagues and all those who contributed to the shaping of this thesis.

Finally, I would like to express my thanks to my family for their care, patient, and help.

TABLE OF CONTENTS

LIST OF TABLES

LIST OF FIGURES

LIST OF ABBREVIATION

Terms	Abbreviation
Body of Revolution	BOR
Body of Translation	BOT
Combined Field Integral Equation	CFIE
Computational Electromagnetic	CEM
Conducting Body of Revolution	CBOR
Dielectric Body of Revolution	DBOR
Dielectrically Coated Body of Revolution	DCBOR
Electric Field Integral Equation	EFIE
Electromagnetic	EM
Fast Fourier Transform	FFT
Finite Difference Time Domain	FDTD
Finite Element Method	FEM
Geometric Theory of Diffraction	GTD
High-Frequency Methods	HFMs
Horizontal Polarization	HP

Integral Boundary Condition	IBC
Integral Equation	IE
Low-Frequency Methods	LFMs
Magnetic Field Integral Equation	MFIE
Method of Moment	MoM
Partial Differential Equation	PDE
Perfect Electric Conductor	PEC
Physical Optics	PO
Physical Theory of Diffraction	PTD
Poggio-Miller- Chang-Harrington-Wu-Tsai	PMCHWT
Radar Absorbing Material	RAM
Radar Cross Section	RCS
Radar Cross Section Reduction	RCSR
Radar Range Equation	RRE
Surface Integral Equation	SIE
Vertical Polarization	VP
Volume Integral Equation	VIE

LIST OF SYMBOLS

$\bar{E}$	Electric field
$\bar{H}$	Magnetic field
ε_e	Free space permittivity
μ_e	Free space permeability
ε_r	Relative permittivity
ε_d	Dielectric permittivity
μ_d	Dielectric permeability
$\bar{A}$	Magnetic vector potential
$\bar{F}$	Electric vector potential
w	Angular frequency
k	Wave number
$G(\bar{r},\bar{r}')$	Scalar Green's function
$\sigma^{\theta\theta}$	Cross section area in θθ-polarized
$\sigma^{\theta\phi}$	Cross section area in θϕ-polarized
$\sigma^{\phi\theta}$	Cross section area in ϕθ-polarized
$\sigma^{\phi\phi}$	Cross section area in ϕϕ-polarized
η_e	Free space intrinsic impedance (377 Ω)
η_d	Impedance of dielectric region $(\mu_d/\varepsilon_d)^{1/2}$
$\bar{D}$	Electric flux density

$\bar{B}$	Magnetic flux density
$\bar{M}$	Equivalent magnetic surface current
$\bar{J}$	Equivalent electric surface current
ρ_e	Electric charge
σ	The conductivity
d	Dielectric medium
e	Empty medium
S_{ce}	Surface between conducting and empty media
S_{cd}	Surface between conducting and dielectric media
S_{de}	Surface between dielectric and empty media
S_{we}	Surface between conducting wire and empty media
S_{wd}	Surface between conducting wire and dielectric media
S_{je}	Surface between conducting junction and empty media
S_{jd}	Surface between conducting junction and dielectric media
$\bar{J}_{ce}$	The equivalent electric surface current on S_{ce} surface
$\bar{J}_{cd}$	The equivalent electric surface current on S_{cd} surface
$\bar{J}_{de}$	The equivalent electric surface current on S_{de} surface
$\bar{J}_{we}$	The equivalent electric surface current on S_{we} surface
$\bar{J}_{je}$	The equivalent electric surface current on S_{je} surface
$\bar{E}^d, \bar{H}^d$	The electromagnetic fields in dielectric region
$\bar{E}^e, \bar{H}^e$	The electromagnetic fields in empty region
$\bar{E}^a(\bar{J}, \bar{M})$,	Electric and magnetic fields due to $\bar{J}$ and $\bar{M}$ in "e" or

$\bar{H}^a(\bar{J},\bar{M})$	"d" homogeneous medium, respectively
Φ^a , Ψ^a	Electric and magnetic scalar potential in "e" or "d" medium, respectively
N	Total number of basis function
N_s	Number of data points on the conducting surface
N_d	Number of data points on the dielectric surface
N_w	Number of data points on the wire segment
N_a	Number of data points on the attachment part of junction
$f_i(t)$	Subsectional function
$I_{ni}^{t,\varphi}, I^w, I^j$	Unknown electric current coefficients
$K_{ni}^{t,\varphi}$	Unknown magnetic current coefficients
$\bar{J}_{ni}^{t,\varphi}$	Components of the electric current density along $\hat{u}_{t'}, \hat{u}_{\varphi'}$
$\bar{M}_{ni}^{t,\varphi}$	Components of the magnetic current density along $\hat{u}_{t'}, \hat{u}_{\varphi'}$
$\bar{J}_l^w$	Components of the electric current density along $\hat{u}_l^w$
$\bar{J}_a^d, \bar{J}_j^d$	Components of the electric current density along $\hat{u}_a, \hat{u}_r$
T(t)	Triangle function
JE	Denote impedance matrix due to the electric field with electric current density
MH	Denote impedance matrix due to the magnetic field with magnetic current density
JH	Denote admittance matrix due to the magnetic field with electric current density
ME	Denote admittance matrix due to the electric field with magnetic current density

k_e	Propagation constant for free space ($2\pi/\lambda$)
k_d	Propagation constant for dielectric region
$\overline{E}_{\theta}^{s}$	The θ-component of far-field scattered
$\overline{E}_{\phi}^{s}$	The ϕ-component of far-field scattered
$\overline{W}(\bar{r})$	Testing function
[Z]	Impedance matrix
[Y]	Admittance matrix
[V]	Excitation matrix
[R]	Measurement matrix

ABSTRACT

This thesis presents a treatment of the problems of electromagnetic (EM) wave scattering from conducting, dielectric and dielectrically coated Bodies of Revolution (BOR) with attached wires and wings with different angles, which are the most important factors that affect the Radar Cross Section (RCS). The solution to these problems depends on the contribution of the BOR, wires, wings and junctions (junction is the connected region between the wire and BOR surface) and the interactions among which are taken into consideration. The formulation of the EM scattering is based on the equivalence principle which treats the equivalent unknown surface current density on the conducting BOR, and the surface electric and magnetic current densities on the dielectric surface.

The Electric Field Integral Equation (EFIE) is used to formulate the EM scattering from the conducting bodies, while the formulation of the EM scattering from dielectric and dielectrically coated objects depend on the boundary conditions for the problems produces four integral equations (IEs), which reduces to two set of IEs using PMCHWT method to formulate the Combined Field Integral Equation CFIE, that convert to liner equations using the Method of Moments (MoM) using the Galerkin's approach. This method provides accurate results for regular and irregular bodies.

A source code was written using a Fortran Power Station 90 programming language to simulate the theoretical part of this thesis to calculate the Bistatic and Monostatic RCS to the EM scattering problems from conducting, dielectric and dielectrically coated BOR with different constitutive parameters such as conductivity σ, permittivity ε, and permeability μ in case of with and without wire and/or wings and junctions.

The computed results refer to the validity of our formulation when our results are compared with the published results.

One of the basic and important aims in our research is to study the effect of the shape by wires in addition to the coated by Radar Absorbing Material (RAM) on the RCS pattern. This RCS be known for regular and simple objects, as in sphere and cylinder, before adding the effect of the wires and find a new form of RCS pattern. The main application is to find a developer model for this study carries known RCS, if it is an approximation with other objects close to his form.

The proposed model in this study, which is used to realize our results by compared the RCS with known RCS figure, is the rocket of US Navy with four wings. The effect of the wings dimensions on the RCS was studied, also the effect of Radar Absorbing Material (RAM) in case of its thickness and constitutive parameters, as a RCS reduction, on the RCS was studied. The computed results revealed the significant effect of the coated layer on the RCS reduction with respect the conducting body, rather than the effect of wire/wings on the RCS. The imaginary part of the permittivity and permeability showed a clear effect on the RCS reduction and distortion, and the important aim of this current study when the rocket body is coating and the other parts remain as conductors.

Chapter One
General introduction

1.1 Introduction

Radar did not come to the forefront as a useful sensor until world war II, when tremendous strides were made in both the theory and practice of radar technology. Before the 1950s, the scientific community in general felt the theoretical calculation of a complex targets Radar Cross Section (RCS) was beyond the capabilities of the known technology. By the early 1950s approximation technique began evolving that allowed the estimation of the RCS for such complex shapes as airplane, missiles, and satellite. Consequently the development of radar over the past fifty years has focused on two primary radar technologies: monostatic and bistatic.

Radar detects or tracks a target, and sometimes can identify it, only because there is an echo signal. The intensity of echo is described explicitly by the RCS of the objects, which frequently ought to be reduced. Control of the echo characteristics of some targets is of vital tactical importance. There are two important practical ways of doing so: shaping and radar absorbers. Shaping is the selection or design of surface profiles so that little or no energy is reflected back toward the radar, while, Radar Absorbing Material (RAM) actually soak up radar energy, also reducing the energy reflected back to the radar [1].

Several Electromagnetic (EM) problems like scattering, radiation, wave guiding etc., are not analytically calculable, for the multitude of irregular geometries found in actual devices. Computational numerical techniques can overcome the ability to derive closed form solutions of Maxwell's equations under various constitutive relations of media, and boundary conditions. This makes Computational Electromagnetic (CEM), important to design, and modeling of antenna, radar, satellite and other communication systems [2].

Maxwell's equations tell us that EM waves are a combination of electric ($\bar{E}$) and magnetic ($\bar{H}$) fields which are perpendicular to each other and perpendicular to the direction of propagation. When an EM wave is incident on a body, such as BOR, the boundary conditions on the body require that surface currents flow. These currents, in turn, re-radiate a scattered EM wave. The strength of the reflected and transmitted for planar surface are given by Fresnel coefficients, which are functions of the incident polarization and material properties [3].

CEM typically solves the problem of computing the *E* and *H* fields across the problem domain. Also calculating scattering from this fields. CEM models may or may not assume symmetry, extensively make use of symmetry, and solve for reduced dimensionality from 3 spatial dimensions to 2D even 1D by choosing the right technique for solving problem. Moreover, CEM problems require super computer; high performance clusters, vector processor and/or parallel computer. Typical formulations involve either time-stepping through the equations over the whole domain for each time instant; or through banded matrix inversion to calculate the weights of basis functions, when modeled by Finite Element Method (FEM); or matrix products when using transfer matrix method; or calculating integrals when using MoM; or using Fast Fourier Transforms (FFT), and time iterations when calculating by split-step method [2].

The ability to produce the systems that exhibit stringent operating requirements with feasible cost efficiency is only made possible through the application of numerical methods to develop the fundamental models used to predict such systems. Applied numerical methods, with respect to the EM applications[4], can be employed in such a way as to develop unique tools that characterize segments of the complete analysis of a system.

1.2 The scattering problem and radar cross section

EM waves, with any specified polarization, are normally diffracted or scattered in all directions when incident on a target. These scattered waves are broken down into two parts. The first part is made of waves that have the same polarization as the receiving antenna. The other portion of the scattered waves will have a different polarization to which the receiving antenna does not respond. The two polarization are orthogonal and are referred to as the principle polarization (pp) and orthogonal polarization (op), respectively. The intensity of the backscattered energy that has the same polarization as the radar's receiving antenna is used to define the target RCS.

An object exposed to an EM waves, with a given polarization, disperses incident energy in all directions. This spatial distribution of energy is called scattering and the object itself is often called scatterer [5].

Scattering problems can be considered as radiation problems where the locally radiating current are generated by other currents or field. Therefore RCS problems involved incident EM radiation generated by external source, creating on the scatterer that re-radiated a scattered field.

Basic scattering configuration is depicted in Fig.(1-1). Assuming $e^{j\omega t}$ time dependence and suppressing it, the incident electric and magnetic fields are given by [6], as follow:

$$\bar{E}^i = \bar{E}^i_\circ e^{-jk_i \hat{k}_i \cdot \bar{r}} \quad (1\text{-}1)$$

$$\bar{H}^i = \bar{H}^i_\circ e^{-jk_i \hat{k}_i \cdot \bar{r}} \quad (1\text{-}2)$$

$$\bar{H}^i_\circ = \frac{1}{\eta} \hat{k}_i \times \bar{E}^i_\circ \quad (1\text{-}3)$$

Where $\bar{E}^i_\circ$ and $\bar{H}^i_\circ$ are real and constant amplitude vector, η is the intrinsic impedance of free space. The propagation vector $\hat{k}_i$ is given by:

$$\hat{k}_i = -(\hat{x}\, sin\theta^i cos\varphi^i + \hat{y}\, sin\theta^i sin\varphi^i + \hat{z}\, cos\theta^i) \quad (1\text{-}4)$$

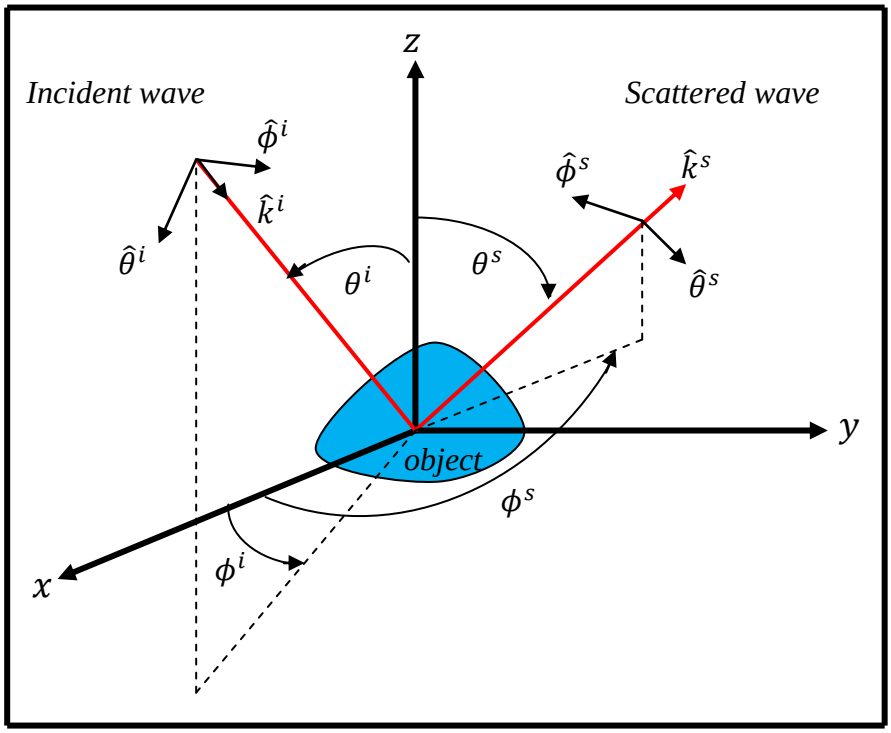

Fig.(1-1): Basic scattering configuration

The incident electric field can also be expressed in terms of its orthogonal components as:

$$\bar{E}^i = E_\theta^i \hat{\theta}^{\,i} + E_\phi^i \hat{\phi}^{\,i} \tag{1-5}$$

Since, for RCS calculations, the observation point is in the far field of the scattering structure, the direction of the observation point can safely be assumed to be equal to k_s in Fig.(1-1) everywhere on the scatterer surface. The scattered electric far field can be expressed as:

$$\bar{E}^s = \bar{E}_\circ^s \frac{e^{-jk_s r}}{r} \tag{1-6}$$

Where $\bar{E}_\circ^s$ is complex amplitude vector. Similar to the incident field, scattered electric field can be expressed along $\hat{\theta}^{\,s}$ and $\hat{\phi}^{\,s}$ as:

$$\bar{E}^s = E_\theta^s \hat{\theta}^{\,s} + E_\phi^s \hat{\phi}^{\,s} \tag{1-7}$$

Formally, RCS is a measured of the power that is returned or scattered in a given directions normalized with respect to the power density of the

incident field. RCS is a characteristic property of the scatterer (property of the target reflectivity). It is defined in [7] as the area required to be cut of the incident wave front, at the position of the scatterer, so the power thereby intercepted would, if radiated isotropically, create the same power density at the observation point as does the scatterer itself. The expression for RCS is [8]:

$$\sigma = \lim_{r\to\infty} 4\pi r^2 \frac{|\bar{E}^s|^2}{|\bar{E}^i|^2} \tag{1-8}$$

$$\sigma = \lim_{r\to\infty} 4\pi r^2 \frac{|\bar{H}^s|^2}{|\bar{H}^i|^2} \tag{1-9}$$

To make the RCS quantity be independent of the distance between the scatterer and the observation point, the scattered power should be normalized so that decay due to spherical spreading of the scattered wave is eliminated. This is achieved by the multiplication factor 4πr. Equations (1-8) or (1-9) is general definition and does not contain any information about the polarization of the incident and scattered fields. The following definitions, which make use of the components defined in Eqs.(1-5) and (1-7), are introduced to emphasize the polarizations.

$$\sigma^{\theta\theta} = \lim_{r\to\infty} 4\pi r^2 \frac{|\bar{E}_\theta^s|^2}{|\bar{E}_\theta^i|^2} \tag{1-10}$$

$$\sigma^{\theta\phi} = \lim_{r\to\infty} 4\pi r^2 \frac{|\bar{E}_\theta^s|^2}{|\bar{E}_\phi^i|^2} \tag{1-11}$$

$$\sigma^{\phi\phi} = \lim_{r\to\infty} 4\pi r^2 \frac{|\bar{E}_\phi^s|^2}{|\bar{E}_\phi^i|^2} \tag{1-12}$$

$$\sigma^{\phi\theta} = \lim_{r\to\infty} 4\pi r^2 \frac{|\bar{E}_\phi^s|^2}{|\bar{E}_\theta^i|^2} \tag{1-13}$$

In the same way RCS can also be expressed in terms of the incident and scattering magnetic fields, Eq.(1-9), by replacing the E-field terms with

corresponding magnetic field quantities in Eqs.(1-10) to (1-13). From these definitions of RCS, it can be concluded that RCS is a function of:-

1-Target geometry, its material properties, and its orientation relative to radar.

2-The frequency and wavelength of the incident wave.

3-Polarization of incident and scattered wave.

4-Polarization of transmitter and receiver radar.

1.3 Radar range equation

The Radar Range Equation (RRE) provides the most useful mathematical relationship available to engineer in assessing both the need for and the resulting effectiveness of efforts RCS. In its complete form [7], the radar equation accounts for:

1. Radar system parameters.
2. Target parameters.
3. Background effects (clutter, noise, interference, and jamming).
4. Propagation effects (reflection, refraction, and diffraction).
5. Propagation medium (absorption and scatter).

The RCS of radar target is the hypothetical area required to intercept the transmitted power density at the target such that if the total intercepted power were re-radiated isotropically, the power density actually observed at the receiver is produced [9]. This is a complex statement that can be understood by examining radar transmitter and receiver co-located, radar equation one term at a time.

$$P_r = \left(\frac{P_t G_t}{4\pi r^2}\right) \sigma \left(\frac{1}{4\pi r^2}\right) A_{eff} \qquad (1\text{-}14)$$

Where P_r is the power received back from the target by the radar (watt), P_t is the power transmitted by the radar (watts), G_t is the gain of the radar transmitted antenna (dimensionless), σ is the RCS of the target (m^2), r is the

distance from the radar to the target (m), A_{eff} is the effective area of the radar receiving antenna (m^2).

The term $\left(\frac{P_t G_t}{4\pi r^2}\right)$ is present the power density (watt/m^2) that the radar transmitter produces at the target. This power density is intercepted by the target with radar cross section σ, which has units of area (m^2). Thus, the product $\left(\frac{P_t G_t}{4\pi r^2}\right)\sigma$ has the dimensions of power (watts), and represents a hypothetical total power intercepted by the radar target. The second term $\left(\frac{1}{4\pi r^2}\right)$ represents isotropic spreading of this intercepted power from the target back to the radar receiver. The third term represents the amount of the returned power, which is captured by the receiving antenna as a result of its effective area.

The radar equation can be used to estimate radar system performance. Therefore, a thorough knowledge of radar equation and its simplification are vitally necessary in the area of RCS range, and since the far field conditions are implicate in the RCS definition, so that the isolation between receiver and transmitter can be determined by RRE.

The examination radar detection range is, (for co-located transmitter and receiver).

$$R_{max} = \left[\frac{P_t G_t \lambda^2 \sigma}{(4\pi)^3 L_s}\right]^{1/4} \quad (1\text{-}15)$$

and for non co-located

$$(R_t R_r)_{max} = \left[\frac{P_t G_t G_r \lambda^2 \sigma}{(4\pi)^3 L_s}\right]^{1/2} \quad (1\text{-}16)$$

Where R_t is the transmitter-to-target range, R_r is the receiver-to-target range, λ is the wavelength, G_r is the gain of the radar receive antenna, Fig.(1-2), and L_s is the total system loss and given by [10].

$$L_s = L_t L_{atm} L_r L_{sp} \quad (1\text{-}17)$$

Where: L_t is the transmitte loss, L_{atm} is the atmospheric loss, L_r is the receiver loss, and L_{sp} is the processing loss.

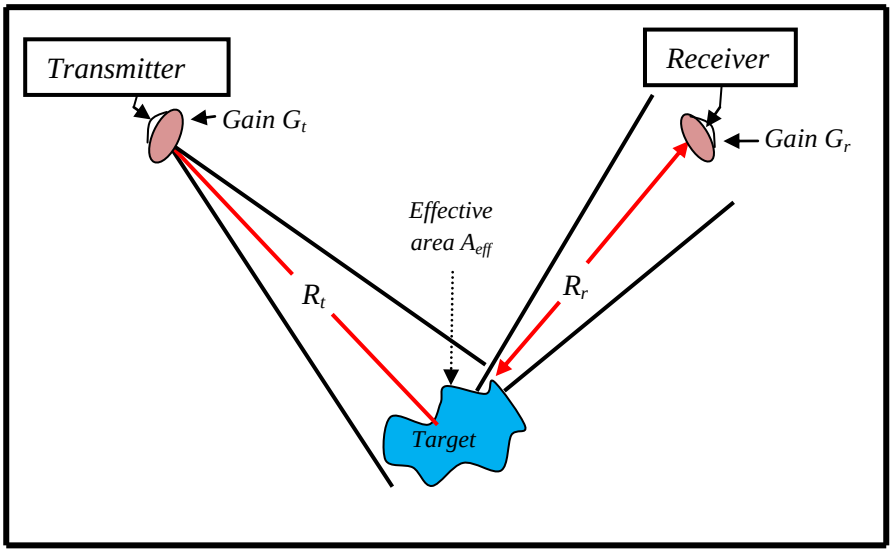

Fig.(1-2): Link geometry for radar measurement.

1.4 Radar cross section technologies

The definitions of RCS give the general notation for indicating polarization and angle as:

$$\sigma^{tr}(\theta^t, \phi^t, \theta^r, \phi^r) \quad (1\text{-}18)$$

The superscripts *t* and *r* refer to transmitter and receiver polarization, typically horizontal or vertical, and angular coordinate. From this notation of RCS three cases of technologies can be distinguished as follow:

1- **Bistatic** cross section is for the case when the transmitter and receiver are at different locations.

2- **Forward** cross section is the measure of scattered power in the forward direction; that is, in the same direction as the incident field. This forward scattered power is usually 180° out of phase with the incident field so that when added to the incident field a shadow region is found behind the scattering object.

3- **Monostatic** or backscatter cross section is the used case of interest for most radar system where the receiver and transmitter are collocated.

The most common of these technologies are monostatic and bistatic cross section. In monostatic case only one of angular coordinates is needed. Most experimental measurements are of monostatic cross section. Whereas analytical RCS predictions are much easier to do for bistatic cross section, with illumination source fixed and receiver position moved. Far-field monostatic or bistatic scattering measurements can provide information on radiated fields from a target, but supply little information on evanescent fields such as surface waves or local cavity modes. In general the bistatic signature will be lower than the monostatic [11].

Bistatic RCS measurements are inherently more difficult and complex than monostatic measurements simply because the receiving antenna must be moved for each measurement, for this reason many studies developed a relationship between monostatic RCS and bistatic, whereby bistatic RCS can be predicted from monostatic RCS measurements under certain condition [12].

Polarization is one source of the additional complexity. Radar systems, that operate on a single polarization may only need a single transmit (T_x) channel and a single receiver (R_x) channel. However, fully polarized systems duplicate both the T_x and R_x channels. Figure (1-3) depicts both monostatic and bistatic radar configurations. A monostatic system use a single location for both transmit and receive, whereas a bistatic system locates the transmitter and receiver at separate locations. Monostatic radars operating a single polarization only and no cross-polarized components, just vertical and horizontal polarized [13].

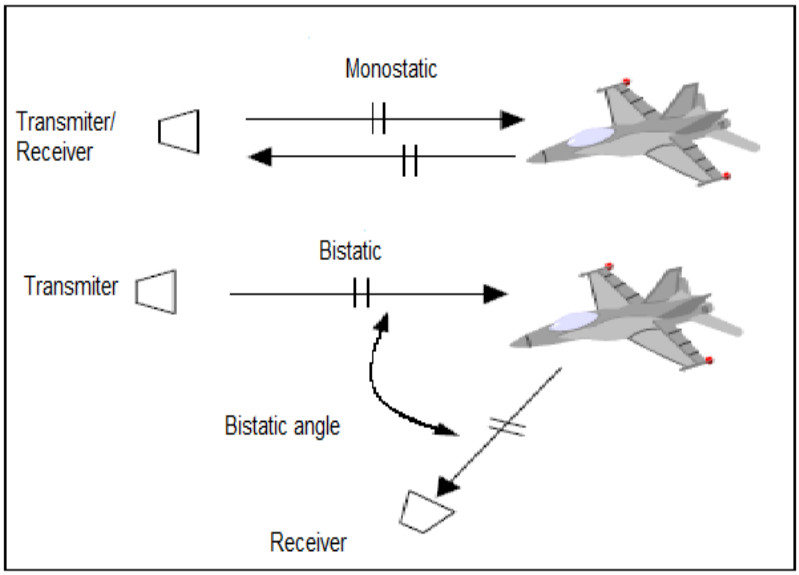

Fig. (1-3): Monostatic and Bistatic geometry

1.5 The scattering regions

The scattering process which takes place when an EM wave encounters a material object can be characterized in two ways [14]. The simple specular reflection model assumes that the angle of incidence is the same as the angle of reflection. A more general (and physical) approach is to consider the interaction in detail, involving induced charges and currents on the object. The incident waves induce charges and currents on the surface that re-radiate EM fields which can emanate also into non-specular directions.

Generally, when an EM wave propagating in free space encounters, different media characterized by μ and ε, energy is reflected, transmitted or absorbed. Calculation of the scattered fields requires solving of the Maxwell equations, and analytical solutions exist only for some simple surfaces like cylinders and spheres. An introduction to the theory of EM scattering can be found in [15].

Three characteristic scattering regions can be distinguished depending on the ratio of wavelength to object size: Rayleigh, resonant, and optics scattering regions. These regions and the associated scattering mechanisms are

illustrated in Fig.(1-4). In the figure below, the normalized RCS of a metallic sphere (radius = *a*) as a function of its circumference in wavelengths is shown.

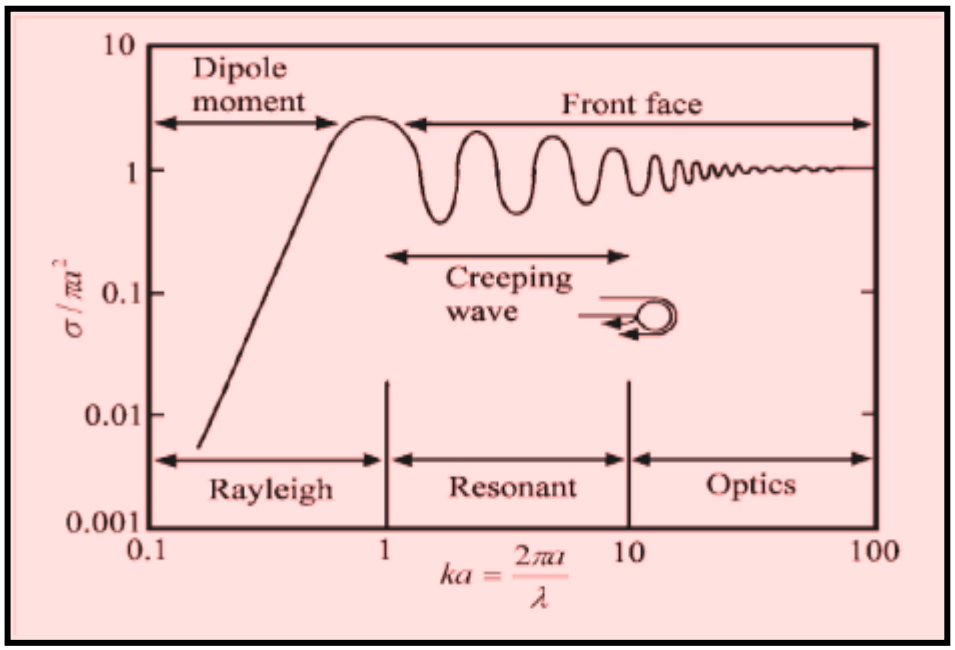

Fig.(1-4): Normalized RCS of a metallic sphere (radius = a) as a function of its circumference in wavelengths [14].

The region where the wavelength λ of the incident EM wave is considerably larger than the object size *L*, i.e., λ>> *L*, is called the low-frequency or Rayleigh scattering region [14-15]. In this case, the phase of the incident field over the object surface can be considered to be the same at each time instant. The dominant scattering mechanism in the Rayleigh region is induced dipole moment scattering. The strengths of the induced dipole moments and thus the scattered fields depend on the size and orientation of the object with respect to the incident vector EM field. Characteristics of the Rayleigh scattering are that the scattering cross-section is proportional to the fourth power of the frequency, and that it does not depend on the object's detailed shape [14]. Rayleigh scattering problems can be solved with the scalar analysis methods developed for electrostatics. Rayleigh scattering is of

little practical interest to most applied EM problems, because usually the objects are large measured in wavelengths.

In the resonant scattering region, where the wavelength is comparable to the object's dimension, i.e., $L \leq \lambda \leq 10\ L$, surface wave and front-face optics-like scattering mechanisms dominate [14]. The surface wave types present are traveling, creeping, and edge traveling waves. Surface wave scattering is relatively independent of the objects size, and the scattering cross-section produced is proportional to the square of frequency. Also, the overall geometry of the object has a great effect on the observed scattered fields in this region, since the field at any part of the object surface is a sum of the incident field and the scattered fields from any other part of the object. The optics-like scattering occurs in the specular direction from the objects front-face. Calculation of the scattered fields in the resonant region requires an exact solution of the Maxwell's equations [14].

The optics scattering region begins when the wavelength becomes much smaller than the objects dimensions, i.e., $\lambda < 10\ L$. In this region, scattering from individual local scattering centers due to detailed object surface geometry dominates. The observed scattered field is a complex sum of the contributions from the individual scattering centers. The dominant scattering mechanisms in the optics region are specular (mirror-like) scattering, end-region scattering, edge diffraction, and multiple-bouncing. Specular scattering is the major scattering mechanism for many radar targets [14].

1.6 Computational Electromagnetic Methods

The scattering is one of the most important branches in CEM. Since the RCS is a term that is companied by scattering problems, so the calculation methods of RCS fall within the CEM. The calculation of RCS is classified into three basic lines, they are prediction, reduction, and measurement.

1.6.1 Prediction Methods

The RCS predicted can be classified into two types: analytical and numerical. Analytical methods are available in the frequency or time domain when the target coincides with the coordinate systems (rectangular, spherical or cylindrical). This method is separation of variable [3][16]. The other methods, numerical methods, are developed to solve RCS for the complex target. These methods are typically classified as so-called "low-frequency" and "high-frequency" methods and further sub-classified into time- or frequency- domain methods, in accordance with the scattering regimes and target geometry.

1.6.1.1 Low-Frequency Methods

Low Frequency Methods (LFMs) are so-named because they solve Maxwell's equations with no implicit approximations and are typically limited to problems of small electrical size due to limitations of computation time and systems memory. These methods are:

1- Method of Moments

The Method of Moments is a technique to solve EM boundary or volume integral equations in the frequency domain. It takes in to the account the entire EM phenomenon and the polarization effects for excite field. Because the EM sources are the quantities of interest, the MoM is very useful in solving radiation and scattering problems. In this thesis, we focus on the practical solution of boundary integral equations of scattering using this method, see Appendix (A) for information about an explanation of this method .

2- Finite Element Method

The Finite Element Method (FEM) is a method used to solve frequency-domain boundary valued EM problems by using a variational form. The features of this method can be summarized in the following:

1- It is used to find solution of Partial Differential Equation (PDE) and integral equations.

2- It can be used with two-and three dimensional canonical elements of differing shape, allowing for highly accurate discretization of the solution.

3- It is often used in the frequency domain for computing the frequency field distribution in complex, closed region such as cavities and wave guide.

4- It is unsuitable solution for radiation or scattering problems unless combined with a boundary integral equation approach [17-18].

3- Finite Difference Time Domain Method

The Finite Difference Time-Domain (FDTD) method uses the method of finite differences to solve Maxwell's equations in the time-domain. The solution is typically discretized into small rectangular or curvilinear elements, with a leap frog in time used to compute the electric and magnetic fields from one others. FDTD excels at analysis of inhomogeneous and nonlinear media, though its demands for system memory are high due to the discretization of the entire solution domain, and it suffers from dispersion issues as well and the need to artificially truncate the solution boundary. FDTD finds applications in packaging and waveguide problems, as well as in the study of wave propagation in complex dielectric [19-20].

1.6.1.2 High-Frequency Methods

The High-Frequency Methods (HFMs) can be classified into:

1- Geometrical Theory of Diffraction

The Geometrical Theory of Diffraction (GTD) [21] uses ray-optics to determine EM wave propagation. This method comes as an extension of Geometrical Optics (GO) method to account the non-zero field in the shadow regions, and state that "the incident ray excites a fictitious cone of diffracted rays; all subtend the same angle with respect to the edge as that subtended by the incident ray", as shown in Fig.(1-5) .

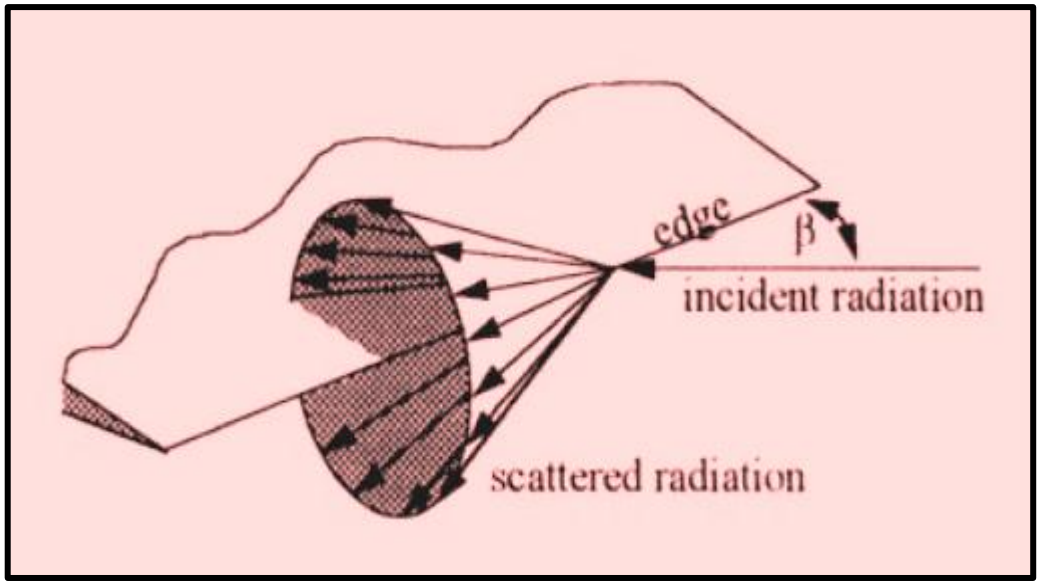

Fig.(1-5): Diffracted ray cone from a line of discontinuity

Some features for this method are :

1- The spreading, amplitude intensity and decay in ray bundle are computed using from Fermats principle and the radius of curvature at reflection point.

2- The observation point must be laid within the fictitious Keller cone, otherwise yields precisely zero.

3- It attempts to account for the fields diffracted by edges, allowing for a calculation of the fields in shadow regions.

4- The GTD is fast but often yields poor accuracy for more complex geometries.

2- Physical Optics Method

Physical Optics (PO) is a method for approximating high-frequency surface currents, allowing a boundary integration to be performed to obtain the fields. It is based on tangent plane approximation, where the integration element is assumed to be a tangent plane to the incident field, and far field approximation and through which the gradient of Greens function is replaced by Greens function itself multiplied by constant factor, more of the characteristic of this method [22]:

1- It does not account for the fields diffracted by edges or those from multiple reflections, so supplemental corrections are usually added to it.

2- It is used extensively in high-frequency reflector antenna analysis, as well as many radar cross section prediction codes.

3- The simplified integral equation can be evaluated exactly for a few special structures.

4- It has no polarization dependency, since the polarization of the scattered wave is precisely that of the incident wave.

5- The PO and the MoM are used to solve the same integral equation, through the MoM calculates the surface currents directly instead of approximating.

3- Physical Theory of Diffraction

The Physical Theory of Diffraction (PTD) [23] is a means for supplementing the PO solution by adding the effect of non uniform currents at the diffracting edges of an object. PTD is commonly used in high-frequency radar cross section and scattering analysis.

1.6.2 Reduction Methods

The detectability of a target is measured in terms of the RCS. The RCS is a property of the target size, shape and the material from which it is fabricated and is a ratio of the incident and reflected power.

Stealth technique is the main base for reduction methods of RCS. The concept of stealth means, the alter of surface characteristics of target. This in turn helps to reduce the effective area of the target reflecting the EM waves as seen by the radar [9]. The stealth techniques initially employed were frequency dependent and thus limited in their overall effectiveness. Moreover, over the years, radar technology improved drastically with the use of high-powered large bandwidth transmitters, thereby reducing the effectiveness of such primitive stealth technology [9,24,25].

There are four methods for reducing the RCS [1,26]; shaping; RAM, passive cancelation and active cancelation. The two most practical and most often applied RCS reduction techniques are shaping and RAM [1,25]. In current RCS designs, shaping techniques are first employed to create a planform design with inherently low RCS in the primary threat sectors. RAM is then used to treat areas whose shape could not be optimized or to reduced the effects of creeping waves or traveling waves on the signature. The other two methods, active and passive cancelation, employing elements at selected points on the target (where reflections are maximum), reduce the overall RCS by phase cancellation. In both techniques, the major scattering centers are first identified and each of these are treated separately, note that they operate in the range of narrow bandwidth methods [7]. The four methods show in briefly as follow:

1- Shaping

Shaping is the primary method of RCS Reduction (RCSR). It is involves modifying the external features of the target to reduce the radar returns in a

specified (usually the backscatter) direction [27]. Normally reduction is achieved only in a limited angular region and at the expense of increased RCS in other regions. So, although shaping is very important, it redirects the radiation through specular reflection hence increasing the probability of detection from bistatic radars [28]. Indeed shaping requirements are often in conflict with structural and aerodynamics requirements in designing the complex targets.

2- Radar Absorbing Materials RAM

RAM or distributed loading technique essentially consists of covering the scatterer with suitable materials. The RCSR in this case is achieved by both absorption and redirection of EM energy [29]. RAM are essentially materials characterized by large values for the imaginary part of the permittivity or permeability. The ratio of the imaginary to real parts of these EM parameters is known as tangent loss. The corresponding materials are identified as the dielectric RAM and the magnetic RAM, respectively. The mechanism reduction in the backscatter is thus partly due to scattering in the forward direction through the material and significant absorption of EM waves as it propagates through the coating [27].

3- Passive Cancellation

It is also called passive loading technique. In this method, special configurations, such as resistive sheets are placed over the scattering centers to modify the surface impedance in order to cancel the reflections [1].

4- Active Cancellation

In this method, active devices are employed to sense the incident radar waves and to send out signals to cancel the echoes from these points [1].

1.7 Bodies of Revolution

The search for the body suit with problems of EM scattering was in line with the BOR to the attribute of the recipes qualify to facilitate the process of analyzing the scattering problems. Therefore, the problem of EM scattering by a BOR has been given a great attention due to its significance in radar application.

A large number of structures in the field of EMs have symmetry around an axis of rotation. Among these structures there are certain types of simple shapes such as, sphere, finite cylinder, and cone-sphere. There are also structures that have this rotational symmetry, on to which it is desirable to mount certain electromagnetic device, for example, the fuselage of an aircraft or missile. Since the periodic behavior of EM fields around this type of structure is known, it is possible to extract this behavior analytically, and then solve Maxwell's equations on single two dimensional (2D) plane [30] .

BOR is a three-dimensional object which is formed by rotating a planar curve called the generating arc about the axis of symmetry. By taking the advantage of the rotational symmetry of BOR, the Fourier series used to convert the original three-dimensional problem illuminated by incident plane wave into a series of two-dimensional problems, which called Fourier components or modes. This results in a considerable saving in both the time of computation and memory storage [31-32].

The BOR is formed by rotating a planar curve *C* about an axis which chosen as *Z*-axis of a Cartesian coordinate system as shown in Fig.(1-6). Region 1, exterior to the body, and region 2, interior the body, are characterized by medium parameters (μ_1, ε_1) and (μ_2, ε_2), respectively, where μ and ε are the permeability and permittivity of the region, respectively. The coordinates system on the surface *S* introduced by $(t\ ,\phi)$, where t is the arc length along the generating curve and ϕ is the azimuthal angle measured from

the *XY*-plane. The unit vectors of the orthogonal right-handed triad (u_n, u_ϕ, u_t) are normal to *S* and tangent to the ϕ and *t*-coordinate lines, respectively. For numerical purpose, the generating arc is approximated as a sequence of linear segments as shown in Fig. (1-6) [33].

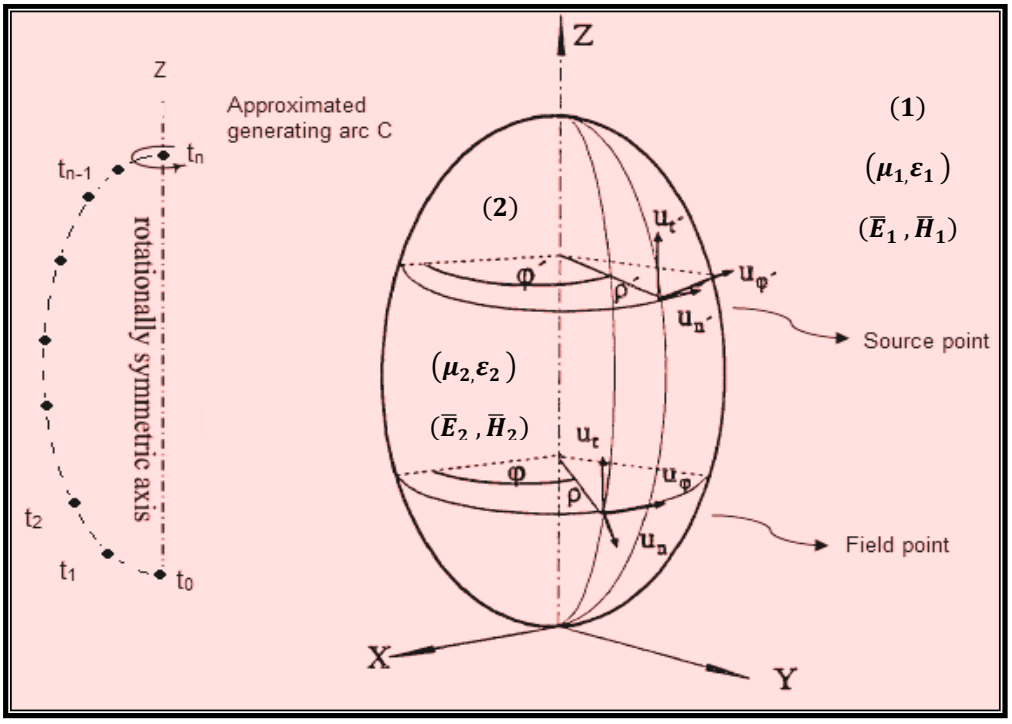

Fig.(1-6): Geometry and approximation of generating arc (C) by linear segments for BOR and the coordinate systems.

1-8 Electromagnetic integral equations and the method of moments

The radar cross sections of simple bodies can be computed exactly by a solution of the wave equation in a coordinate system for which a constant coordinate coincides with the surface of the body. The exact solution requires that the electric and magnetic fields just inside and just outside the surface satisfy certain conditions that depend on the electromagnetic properties of the material of the body (conductor or dielectric) is made. The exact solutions of the wave equation are, at best, guide lines for gauging other (approximate) methods of computing scattered fields [9].

The solution of the Integral Equations (IEs) governing the distribution of the induced fields on target surface. The most useful approach at solution is known as the MoM, in which the IEs are reduced to a system of linear homogeneous equations which are solved to determine parameters of interest [34]. The attractive of the method is that the surface profile of the body is unrestricted, allowing the computation of the scattering from truly tactical object.

The MoM, widely used in EMs due to the work of Roger Harrington and Miller [35,36], was originally popular for structural analysis and has since become common in CEM analysis. After the IE has been derived, there are four steps in implementation of the MoM, these steps are as follows [37]:

* Expansion of the unknown function using basis or expansion functions.
* Evaluation of the IE using weighting or testing functions.
* Evaluation of the moment matrices elements.
* Solving the systems of matrix equation obtaining the parameters of interest.

Maxwell's equations provide the starting point for the study of EM problems, together with certain principles and theorems such as superposition, reciprocity, equivalence, etc.[38].

The IE formulation of Maxwell's equations valid for very large or very small bodies compared to a wavelength. This formulation starts with the representation of fields as a linear superposition of the fields produced by a point source, followed by imposition of appropriate boundary conditions, depending on the geometry and parameters of the medium [39].

The boundary IEs are a powerful and elegant for the formulation analysis, and numerical solutions of a wide class of problems in EMs. By means of boundary integral equations, it is possible to deal with radiation, scattering, and resonance problems involving objects of homogeneous dielectric and/or conductor media, in both two and three dimensions. The unknowns in boundary integral equations are magnetic and electric surface current configurations under analysis [40].

The EM integral equation were obtained by using the vector Greens theorem in conjunction with Maxwell's equations. This equation gives the prescription for scattered fields in terms of surface current density. The scattered E and H fields are given by [14]:

$$\bar{E}^s = \oint_s [-j\omega\mu(\hat{n}\times\bar{H})G + (\hat{n}\times\bar{E})\times\bar{\nabla}G + (\hat{n}\cdot\bar{E})\bar{\nabla}G]\cdot d\bar{s} \qquad (1\text{-}19)$$

$$\bar{H}^s = -\oint_s [-j\omega\varepsilon(\hat{n}\times\bar{E})G - (\hat{n}\times\bar{H})\times\bar{\nabla}G - (\hat{n}\cdot\bar{H})\bar{\nabla}G]\cdot d\bar{s} \qquad (1\text{-}20)$$

where ω is the fixed angular frequency of the problem, μ and ε are the permeability and permittivity of medium, and $\hat{n}$ is the outward unit normal to the surface *S*, and *G* is the Greens function.

The physical meaning of the results in Eqs.(1-19) and (1-20) will be interpreted in terms of the Greens function *G* and its gradient ∇G (Huygens wavelets). That is, each element will be related to the field at one point on a scattering body produced by the currents flowing on another port of the same body. The three-dimensional Greens function is an outward scalar spherical wave whose intensity falls as inverse to distance, given as:

$$G(\bar{r},\acute{\bar{r}}) = \frac{e^{-jkR}}{4\pi R} = \frac{e^{-jk|\bar{r}-\acute{\bar{r}}|}}{4\pi|\bar{r}-\acute{\bar{r}}|} \qquad (1\text{-}21)$$

Where $k=\omega\sqrt{\mu\varepsilon}$ is the wave number. The term $e^{j\omega t}$, which is time–dependence, is assumed and suppressed throughout the thesis.

Primed coordinates are used for points in the source region, $\bar{r}'$, and unprimed coordinates for the point of observation, $\bar{r}$. The gradient of Greens function is an outward vector spherical wave

$$\overline{\nabla}G = -(1 - jk\bar{R})\ \frac{e^{-jkR}}{4\pi R^2}\ \hat{R} \tag{1-22}$$

where vector direction $\hat{R}$ is the radially outward from each elemental source. Eqs (1-19) and (1-20) can be re-written in a new form by meaning of the magnetic vector potential $\bar{A}$, and electric vector potential $\bar{F}$, as follow [41]:

$$\bar{E}^s = -j\omega\bar{A}\ - \frac{j\omega}{k^2}\ \overline{\nabla}(\overline{\nabla}\cdot\bar{A}\,) - \frac{1}{\epsilon}\ \overline{\nabla}\times\bar{F} \tag{1-23}$$

$$\bar{H}^s = -j\omega\bar{F} - \frac{j\omega}{k^2}\ \overline{\nabla}(\overline{\nabla}\cdot\bar{F}) + \frac{1}{\mu}\ \overline{\nabla}\times\bar{A} \tag{1-24}$$

where

$$\bar{A}\ = \mu\ \int_s\ \bar{J}\,(\bar{r}')G(\bar{r},\bar{r}')d\acute{s} \tag{1-25}$$

$$\bar{F}\ = \epsilon\ \int_s\ \bar{M}\,(\bar{r}')G(\bar{r},\bar{r}')ds \tag{1-26}$$

Equations (1-23) and (1-24) are known as the Electric Field Integral Equation (EFIE) and the Magnetic Field Integral Equation (MFIE), which are the most popular forms, respectively. The EFIE enforces the boundary condition on the tangential components of the electric field, while the MFIE enforces the boundary condition on the tangential components of the magnetic field. A linear combination of EFIE and MFIE formulations is normally used to form the Combined Field Integral Equation (CFIE) [41].

1.9 Electromagnetic Boundary Conditions

In a uniform medium an electromagnetic plane wave travels without blending; at an interface reflection and refraction of the incident wave occur. Reflection and refraction at the interface between dissimilar media are governed by boundary conditions implied by Maxwell's equations.

Boundary conditions are the cornerstones in EMs [42,43]. Although it is well known that for time-varying EM fields on a source free boundary, satisfying the continuity of electric ($\bar{E}$) and magnetic ($\bar{H}$) fields at the interface implies that the continuity conditions of the normal components of the magnetic induction vector ($\bar{B}$) and the electric displacement vector ($\bar{D}$) are satisfied, the converse is not true. In other words, for time-varying EM fields, the satisfaction of the continuity conditions for the tangential $\bar{E}$ and $\bar{H}$ fields at dielectric interface is a necessary and sufficient requirement, while the satisfaction of the continuity conditions for the normal $\bar{B}$ and $\bar{D}$ at that interface is only a necessary but not sufficient requirement.

For time-independent (static) electric or magnetic fields, satisfying the continuity conditions on tangential $\bar{E}$ does not imply the satisfaction of the continuity of the normal component of $\bar{B}$ at the dielectric interface, and satisfying the continuity on tangential $\bar{H}$ does not imply the satisfaction of the continuity of the normal component of $\bar{D}$ at the interface [42,44].

At the interface between regions of different dielectric parameters as shown in Fig.(1-7), the generalized EM boundary conditions are written as [41]:

$$\left.\begin{aligned} -\hat{n}\times(\bar{E}_2-\bar{E}_1)&=\bar{M}_s\\ \hat{n}\times(\bar{H}_2-\bar{H}_1)&=\bar{J}_s\\ \hat{n}\cdot(\bar{D}_2-\bar{D}_1)&=\rho_e\\ \hat{n}\cdot(\bar{B}_2-\bar{B}_1)&=\rho_m \end{aligned}\right\} \qquad (1\text{-}27)$$

Where $\bar{J}_s$ is the electric surface current density, $\bar{M}_s$ is the magnetic surface current density, ρ_e and ρ_m are the electric and magnetic charge density, respectively, $\hat{n}$ and $\hat{t}$ are outgoing vectors normal and tangential to the surface of the boundary from region 2 to 1.

For the interface between a dielectric (region 2) and a Perfect Electric Conductor (PEC, region 1), the boundary conditions become:

$$\left.\begin{aligned} -\hat{n}\times\bar{E}_2 &= 0\\ \hat{n}\times\bar{H}_2 &= \bar{J}_s\\ \hat{n}\cdot\bar{D}_2 &= \rho_e\\ \hat{n}\cdot\bar{B}_2 &= 0 \end{aligned}\right\} \qquad (1\text{-}28)$$

and between a dielectric and perfect magnetic conductor (PMC) they are:

$$\left.\begin{aligned} -\hat{n}\times\bar{E}_2 &= \bar{M}_s\\ \hat{n}\times\bar{H}_2 &= 0\\ \hat{n}\cdot\bar{D}_2 &= 0\\ \hat{n}\cdot\bar{B}_2 &= \rho_m \end{aligned}\right\} \qquad (1\text{-}29)$$

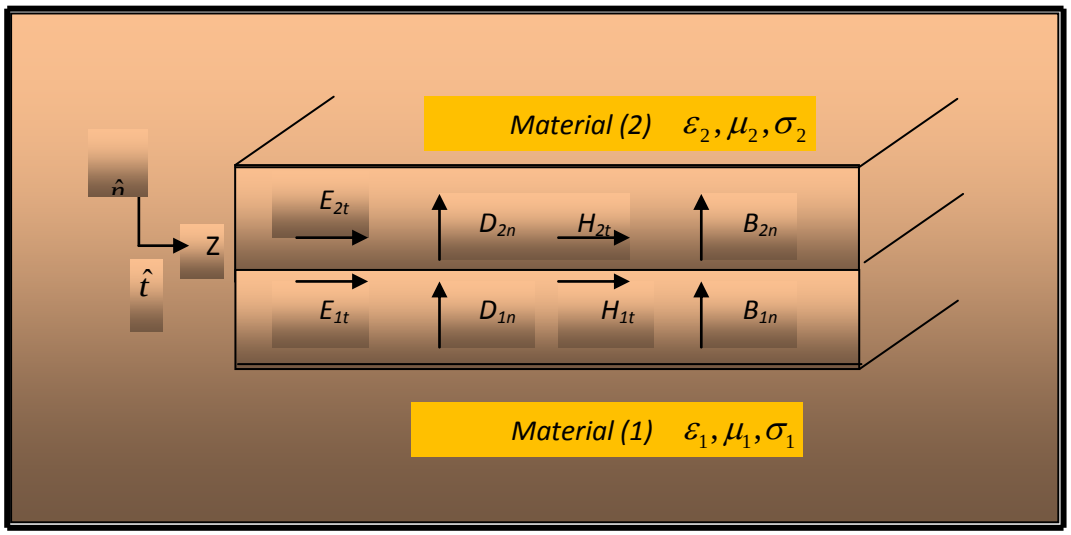

Fig.(1-7): Boundary between two media.

1.10 Surface Integral Equations

The MoM can be applied to complex conducting or penetrable bodies. Generally, a Surface Integral Equation (SIE) formulated is used to describe the physics of the scattering process for conducting, dielectric, and coated bodies. Therefore, SIE is widely used to solve problems of EM scattering by an interface *S* between two homogeneous regions of space lead to many different formulations [45,46].

If one of the regions is PEC, it is sufficient to find the electric current on S by solving a single IE such as the EFIE, MFIE, or CFIE [46,47]. In the

case of dielectric media, the usual procedure is to solve a pair of coupled IEs for the equivalent electric and magnetic current on *S* by linearly combined in several forms [48,49] as shown in Fig.(1-8). For single region or multi-regions, the three forms of SIEs can be expressed as [32, 50]:

$$EFIE: \hat{n} \times [LJ_s(\acute{r}) - KM_s(\acute{r})] = \hat{n} \times E^{inc} \quad (1\text{-}30)$$

$$MFIE: \frac{J_s(\acute{r})}{2} + \hat{n} \times KJ_s(\acute{r}) + \hat{n} \times L\frac{M_s(\acute{r})}{\eta^2} = \hat{n} \times H^{inc} \quad (1\text{-}31)$$

$$CFIE = \alpha \cdot EFIE + \frac{j}{k}(1-\alpha) \cdot MFIE \quad (1\text{-}32)$$

Where J_s and M_s are the electric and magnetic surface currents induced at point $\acute{r}$, respectively. $\hat{n}$ is the normal unit vector on surface, η is the impedance of the region, and k is the propagation constant. The constant α is chosen so that the spurious solution is eliminated, with $0.2 \leq \alpha \leq 0.5$ typically representing a good choice [51].

The integro-differential operators L and K are defined as [50]:

$$L(F_s) = jk \iint_s F_s(\acute{r})G(R)d\acute{s} - \frac{1}{jk}\iint_s \left[\acute{\nabla}_s \cdot F_s(\acute{r})\right]\nabla G(R)d\acute{s} \quad (1\text{-}33)$$

$$K(F_s) = \iint_s F_s(\acute{r}) \times \nabla G(R)d\acute{s} \quad (1\text{-}34)$$

Where F_s can represent either J_s or M_s and $R = |\bar{r} - \bar{\acute{r}}|$ is the distance between source and field points. Therefore, solving a scattering problem by SIE involves two steps:

1-Solving an IE for unknown local current J or M created by an external but known incident field E^{inc} or H^{inc}.

2- Integrating the induced currents J or M to obtain the scattered fields E^s , H^s

Although the EFIE has been used as a basis for the numerical solution of scattering or antenna problems involving (large) BOR, the MFIE is more attractive for general shaped voluminous structures [52]. For thin wires or thin cylinders or plates, however, the MFIE is known to fail, and one is forced to use the EFIE equation in such cases, because of the difficulty in adequately

representation ∇G in the MFIE for these cases [14]. Furthermore, the EFIE formulation, in contrast to the MFIE, is applied to open structures and allows voltage and local conditions to be easily specified at terminals defined on the structure [49].

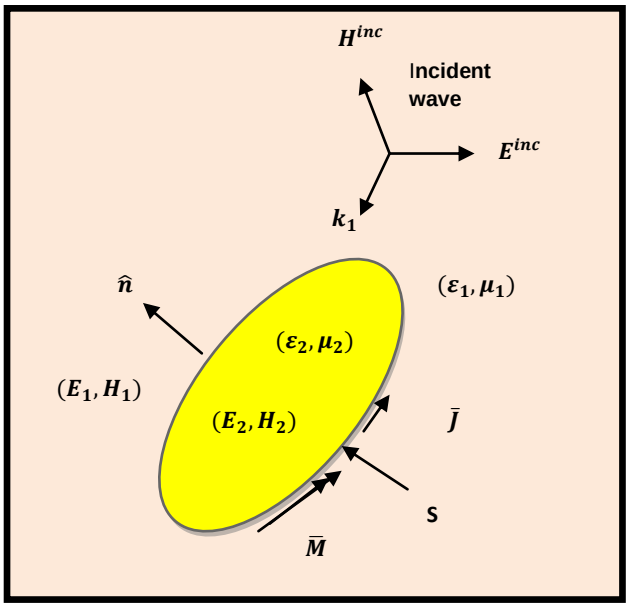

Fig.(1-8): Homogeneous dielectric object $(\varepsilon_2\ , \mu_2)$ embedded in a homogenous medium $(\varepsilon_1\ , \mu_1)$. (J,M) are the equivalent currents for the exterior region.

1.11 The concept of RAM and ideal requirements

RAM is very effective means of RCSR in the context of stealth technology. It can be applied on the complex targets and this changes the exterior profile of these target structures and interferes with their flight characteristics. The complex targets [28], like aircraft, missiles, rockets, ships and other shapes, can be represented as collections of basic geometric elements such as flat plates, spheroid, cylinder, finite cones, cone frusta, edges, vertices, or blended surfaces [53].

An enhancement in the absorption due to the RAM coating on a target results in lower scattered EM fields and hence RCSR of the target. The wave

analysis involves not only free space propagation and interaction at the interface of two media, but also through bounded material medium [54].

The wave propagation through a material medium, for example Fig.(1-9), is governed by the intrinsic physical parameters of medium, viz. its permittivity ϵ, permeability μ and conductivity σ. The well known classes of dielectric and magnetic RAM are essentially a manifestation of these intrinsic EM parameters of the medium. It is also possible to explain the various properties, such as isotropy, linearity and reciprocity of the medium in terms of the nature of these parameters [55]. RAM may be broadly separated into categories, resonant absorbers and broadband absorbers. These materials are made from resistive and/or magnetic materials [29]. There are some ideal requirements for RAM, it is possible to include briefly as follow [1,29,56]:

1- The total weight of RAM applied on the surface be as small as possible. Two desirable properties of RAM therefore would be low density, and the requirement that a very thin coating be sufficient for the purpose of RCSR.

2- The RAM must be chemically stable. It must be able to withstand electrical hazards such as static charges and lighting. In other hand, RAM should be anticorrosive in nature, i.e., it should not damage the surface of the body on which it is applied.

3- The RAM must be of high mechanical strength (flexural, Young's modulus, hardness etc.) and should be able to withstand structural stresses and other in-flight conditions.

4- From the counter-stealth perspective, in order to be effective, RAM must have ultra-wideband RCS reduction characteristics at all polarizations. Since, the bistatic radar configuration is a powerful technique of identifying radar evading targets, RAM must be effective for all angles of incidence, and should be ideally reduce the scattering in all directions.

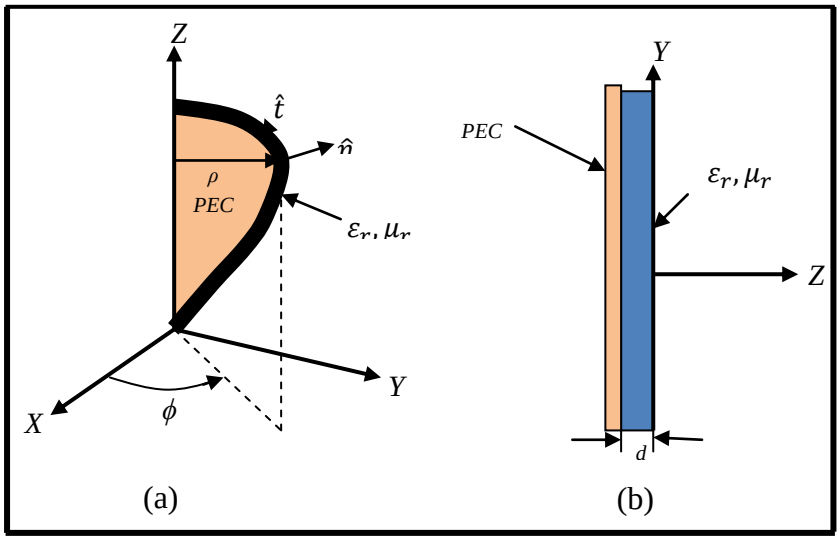

Fig.(1-9): (a) Geometry for a dielectric coated body of revolution. (b) Geometry for a dielectric coated ground plane.

1.12 Electromagnetic parameters of RAM

The EM parameters of medium are considered of the most important features, that can be dealt with very seriously, where the imposing nature of these parameters when the wave propagates through it. This rule applies to the absorbing medium, where the absorber absorbs wave energy of the incident wave. This often results in significant reduction in EM energy scattered in the direction of the radar. Theses parameters can be classified into three sections:

1.12.1 Loss mechanisms

Lossy materials attenuate EM waves that pass through them. This can be modeled with the refraction index, relative permittivity, or relative permeability which are all complex numbers. The imaginary component causes the loss in the material. Physically, the absorbed power is converted into heat. In practical engineering applications where only the cumulative loss is of interest, the different loss mechanisms are combined into one set of normalized complex permittivity and permeability values ε_r and μ_r , given as [57]:

$$\varepsilon_r = \acute{\varepsilon}_r + j\acute{\varepsilon}_r \qquad (1\text{-}35)$$

$$\mu_r = \acute{\mu_r} + j\acute{\acute{\mu}}_r \quad (1\text{-}36)$$

In the above equations, the real parts showing the energy storage are denoted by single primes, and the complex parts showing the loss with double primes. If we specify the electric and magnetic loss tangents as [54]:

$$tan\delta_e = \frac{\acute{\acute{\varepsilon}}_r}{\acute{\varepsilon}_r} \qquad (electric) \quad (1\text{-}37)$$

$$tan\delta_m = \frac{\acute{\acute{\mu}}_r}{\acute{\mu}_r} \qquad (magnetic) \quad (1\text{-}38)$$

Equations (1-35) and (1-36) can be written in polar form as:

$$\varepsilon_r = |\varepsilon_r| e^{j\delta_e} \quad (1\text{-}39)$$

$$\mu_r = |\mu_r| e^{j\delta_m} \quad (1\text{-}40)$$

The refraction index between free-space and a lossy material is

$$n = k/k_\circ = \sqrt{\varepsilon_r \mu_r} \quad (1\text{-}41)$$

where k and $k_\circ = 2\pi f\sqrt{\mu_\circ \varepsilon_\circ}$ are the wave numbers in a lossy material and in free space, respectively. If $Z_\circ = 120\pi$ (Ω) is the free-space impedance, the intrinsic impedance of a material with $\varepsilon_r \neq 1$ and/or $\mu_r \neq 1$ can be defined as

$$Z = Z_\circ \sqrt{\frac{\mu_r}{\varepsilon_r}} \quad (1\text{-}42)$$

For normal incidence, the reflection coefficient of the material interface is calculated as

$$R = \frac{Z - Z_\circ}{Z + Z_\circ} = \frac{Z/Z_\circ - 1}{Z/Z_\circ + 1} \quad (1\text{-}43)$$

In many practical applications, the dielectric absorbing material (with thickness d) has a metal backing, and its normalized input impedance (for normal incidence) can be shown to be [14]:

$$Z_{mb} = \sqrt{\frac{\mu_r}{\varepsilon_r}} \tanh\left(-jk_\circ d\sqrt{\varepsilon_r \mu_r}\right) \quad (1\text{-}44)$$

In most cases we are only interested in the amplitude of the reflection coefficient in decibels, i.e.,

$$|R|(\text{dB}) = 20\log|R| \quad (1\text{-}45)$$

However, the phase angle of R is important in some narrowband RAM applications where resonant energy cancellation is used.

1.12.2 Bianisotropic materials

Anisotropic material coating on some objects surface is a common method of RCSR which is a very important technology in military fields. It can not only absorb the incident wave, but also redistribute the scattering energy by controlling the principal axis of anisotropic material [58].

The concept of anisotropy can be further generalized to account for the magnetic polarization, leading to the class of bianisotropic material. Since isotropy and reciprocity are two commonly assumed characteristics of the material medium, the incorporation of non reciprocity in these media offers the possibility of the non reciprocal bianisotropic materials [1].

Amore convenient form incorporating non reciprocity and bianisotropic can be written as [1]:

$$\bar{D} = \bar{\bar{\varepsilon}} \cdot \bar{E} + \sqrt{\mu_\circ \varepsilon_\circ}\left(\bar{\bar{\chi}}^T - j\bar{\bar{\xi}}^T\right).\bar{H} \quad (1\text{-}46)$$

$$\bar{B} = \sqrt{\mu_\circ \varepsilon_\circ}\left(\bar{\bar{\chi}}^T - j\bar{\bar{\xi}}^T\right).\bar{E} + \bar{\bar{\mu}} \cdot \bar{H} \quad (1\text{-}47)$$

Where $\bar{E}$ is the electric field intensity, $\bar{H}$ is the magnetic field intensity, $\bar{D}$ is the electric flux density, $\bar{B}$ is the magnetic flux density, $\bar{\bar{\xi}}$ is called the chirality dyadic, whereas $\bar{\bar{\chi}}$ is known as the nonreciprocity dyadic.

For bi-isotropic material, the tensor involved in Eqs.(1-46) and (1-47) reduce to scalars. Thus the constitutive relations for non reciprocal bi-isotropic medium becomes [43]

$$\bar{D} = \varepsilon\bar{E} + \sqrt{\mu_\circ \varepsilon_\circ}(\chi - j\xi)\bar{H} \quad (1\text{-}48)$$

$$\bar{B} = \sqrt{\mu_\circ \varepsilon_\circ}(\chi - j\xi)\bar{E} + \mu\bar{H} \quad (1\text{-}49)$$

1.12.3 Chiral media

A chiral body is defined when the target have a partially covered by a thin shield, such as a thin conducting shield [59]. Chiral media exhibit electromagnetic chirality which embraces optical activity and circular dichroism. optical activity refers to the relation of plane of polarization of optical waves by a medium while circular dichroism indicates a change in the polarization elliptically of optical wave medium.

A chiral medium is a particular case of bi-isotropic medium, characterized by linear constitutive relations which couple the electric and magnetic field by three scalars (ε, μ, ξ) [59]. That is satisfied by setting the condition for reciprocity, that is $\chi = 0$, in equations (1-48) and (1-49) to give the constitutive relations of chiral media as follow:

$$\bar{D} = \varepsilon \bar{E} - j\sqrt{\mu_\circ \varepsilon_\circ}\, \xi \bar{H} \qquad (1\text{-}50)$$

$$\bar{B} = j\sqrt{\mu_\circ \varepsilon_\circ}\, \xi \bar{E} + \mu \bar{H} \qquad (1\text{-}51)$$

which involve a chirally parameter ξ (chairlity admittance) in addition to the commonly conceived EM parameters ε and μ [60].

1.13 Historical Review

In this section, the papers and thesis that interested with the field of the present work and the other related papers in the over mentioned field are historically demonstrated.

1.13.1 Conducting bodies

The problem of scattering of a plane EM wave from an arbitrarily shaped metallic BOR is solved by an IE method which is, in principle, an exact method [61]. In this method, the incident plane EM wave is expanded in a set of orthogonal modes TE and TM to the axis of the BOR. Each of these incident modes will induce a current distribution on the surface of the body. Due to the mode orthogonality, the total induced current distribution is represented by the sum of the induced mode current distributions.

The solution to the scattering problem was implemented by utilizing the MoM as a numerical solution. The mathematical formulation is an integro-differential equation, obtained from the potential integral plus boundary conditions at the conducting body. This leads to find the current distribution on scatterer by using a set of expansion functions, Galerkin expansions, chosen for the solution [8]. A variety of 2-D configurations have been analyzed by comparing the Galerkin expansions, mixed-domain, sub-domain, and entire-domain. The mixed-domain approach combines the geometric flexibility inherent in sub-domain expansions with the computational efficiencies of entire-domain formulations. So, the mixed-domain is found to be more accurate [62].

The main limitation of MoM is the number of the basis function N. Yahuda, L. et .al. in 1988 [63] studied the convergence of the numerical solution, MoM, with exact solution by changing the N for perfectly conducting bodies such as spheres and rounded cylinder**.**

Hurst, M. P. and Medgyesi-Mitschange, L. in 1990 [64] applied the MoM on coupled integral equations to investigate the EM scattering from classes of partial BOR bounded by PEC or PMC. Galerkin technique is used with a harmonic circumferential expansion, and the numerical solutions found that the two operators involved are simply related to the corresponding operators in the previously treated full-BOR case, as are excitation vector.

As an alternative to CFIE, a BOR solution was formulated using the dual-surface MFIE. Applications of dual-surface MFIE leads to eliminated the spurious resonances from the MFIE, and although identical in the form and comparable in complexity to the MFIE, dual-surface MFIE provides a unique solution for the electric surface current at all frequencies [65].

Datthanasombat, S. and Prata, A. in 1999 [66] presented a compact implementation of a MoM solution for the IE that yields scattering from a perfectly conducting BOR. The method is conceptually simple to derive and implement, and avoids most of the associated integrals. Its effectiveness stems from two basic facts: It is based on the radiation by loops of currents and charges, and point matching is used to handle the integral equation.

Hashim A., in 2002 [67] proved that, the efficient of using the EFIE, MFIE, and CFIE to solve EM scattering problems for conducting, lossy dielectric and single layer coated BOR in both simple and complex shape. This formulations solved numerically by MoM, with Galerkin's approach and triangle function to represent the sub-domain basis function or testing function, gives a good results comparison with that of exact or available data.

RCS technologies have focused on two primary radar configurations; monostatic and bistatic. So, scattering problem of EM waves by arbitrary shapes, simple or complex, using these technologies with appropriate solution, prediction, reduction or measurement, are the relationships between monostatic and bistatic radar are reviewed and discussed in [12, 13, 68-70].

AL-Assdi, R. A. in 2006 [71] presented an enhancement of computational ability to solve the scattering problems, including the shape effects, for complex CBOR. The EM scattering problem from 3-D-PEC bodies solved by using of EFIE, where Fourier technique is subjected to transform process, was published and the detailed computational analysis to find the numerical solutions had been taken by the use of MoM. The author suggested two applications, which are close to two samples exist in practical life and specially in military side, to be analyzed for the RCS after confirming the total length for each sample in the range of 1.5λ, so the change on RCS size and shape was found.

Godaymi, W. A., in 2007 [33] used the equivalence principle that introduced an unknown electric current density on the conducting surface, and both unknowns equivalent electric and magnetic surface current densities on the dielectric surface. These currents densities satisfy the IEs for the radiation problems. The formulation based on CFIE coupled with the MoM, as numerical solution, to translate them to a set of linear equations.

In 2008, Yu, W. M. and Cui, T. J., [32] suggested closed form Modal Green's Functions(MGF) for accelerating computation of bodies of revolution. The MGF is defined as the radiation field of a circular loop antenna with sinusoidal current distribution. They study proposed a closed form expressions for near-axis far-distance modal Green's functions in order to accelerate the computation of BOR problems. They also presented a criterion based on rigorous error analysis to guarantee MGF's range of applications.

Cakir, C. and Sevgi, L. in 2010 [72] used the FDTD and MoM as numerical methods to deal with realistic high frequency surface wave radar HFSWR targets. The author finds the possibility to compare RCS of these target, that computed by FDTD and the MoM-based NEC (Numerical Electromagnetic Code), in both bistatic and monostatic configuration, and the variety of illuminations over the whole HF band (3-30 MHz).

Mackenzie, A. I. et. al. in 2010 [73] developed a new MoM solution procedure for calculating EM scattering from conductor/dielectric composite structures. The solution is obtained using triangular patch modeling and a recently developed pair of mutually orthogonal pulse basis functions. These basis functions, which model equivalent J and M surface currents, allow for the correct implementation of the EFIE and MFIE for dielectric and PEC bodies.

1.13.2 Conducting BOR-Wire-Junction

Many studies have been used to numerical scattering computation by applying wire-grid model, to allow a detailed representation of a complex structure.[74] used accuracy of this model for aircraft modeled by "wire sticks", the aircraft shape is approximated by a grid of thin wires, leading to mathematical representation of the aircraft in the form of an impedance matrix equivalent to MoM and based on the EFIE.

In 1978, Newman, E. H. and Pozar, D. M. [75] used the Galerkin solution based on the sinusoidal reaction method to solve the IE for the current on composite wire and surface, open as well as close, structures. The continuity of current is enforced on the wire, on the surfaces, and at the wire/surface junctions.

A special junction basis function has been used [76-77] to determine the radiated and scattered pattern for multiple wires by using MOM.

In [78], scattering from wires and open circular cylinders of finite length is obtained using entire domain Galerkin expansions. The case of a straight wire, viewed as a thin cylinder, is examined in this context. The salient features of this study are (a) use of the EFIE as a starting point,(b) solving of this equation by Galerkin method, and (c) representation of axial variation of the current on the scatterer by an entire domain (Fourier series) expansion.

Perez-Leal, R. and Catedra, M. F. in 1988 [79] determined the input impedance of a thin wire attached on-axis to conducting BOR and fed at the attachment points. The study of the wire antenna is carried by using IEs of both reduced and exact kernel, where the analysis of BOR, MoM, takes the symmetry of revolution that allows the expansion of the current in Fourier series.

Qiu, Z. and Butler, C. M. in 1997 [80] studied an accurate and computationally efficient method to determine the currents on a wire and on an open BOR, circular hollow BOR, with the wire partially contained within the BOR shell, a technique for modeling a wire antenna in the presence and attached to the BOR. Full account is taken of the coupling between the wire and BOR, including the effects of wire-to-BOR and BOR-to-wire coupling for all Fourier modes.

Tekin, I. and Newman, E. H. in 1998 [81] presented a MoM solution to the problem of a wire attached to an arbitrary faceted surface by developing a special attachment basis function, which enforce continuity of current at the wire/plate junction. This new attachment mode contains a nonplanar disk, which conforms to the faceted surface, it is applicable near or at the edge and corners of the faceted.

The determination of the input characteristics of a wire mounted on a circumferentially invariant conducting body is great interest and the coupling between thin-wire antennas and general BOR have been studied by numerous researchers. Because the junction between the wire and conducting body presents computational difficulty, [82] improved an efficient method, that obviates these difficulties, when the wire attached to a planar surface of the BOR. The original problem is divided into two equivalent problems or models formulated by solving IEs, hard to take advantage of circumferentially invariant of BOR.

Taboda, J. M. et al. in 2000 [83] presented a comparison of different testing procedures, reduce the total number of unknowns, for sub-domain MoM formulations for arbitrarily shaped bodies, including attached wires.

Ozturk, A. K. in 2002 [6] developed the PO and PTD, high-frequency methods, to calculate the RCS of perfectly conducting targets with arbitrary shape including edges or linear parasitic.

Young, J., and Butler, C. M. 2005 [84] presented a technique to efficiently solve for the currents on appendage attached to a planar surface of conducting body. A coupling of IEs are needed to compute the current on a thin wire antenna attached to planar surface of an axisymmetric, for that appendage may be embedded in homogeneous, dielectric material.

Cao, X. and Gao, J. in 2008 [85] presented a method based on suitable changes of coordinates and domain to extract singular point of the self-impedance element calculation at junction region, and accurate impedance can be obtained in accordance with introducing an attachment mode to ensure the continuity of current density at the junction region between wire antenna and cylindrical surface.

1.13.3 Dielectric bodies

The problem of EM scattering from a homogeneous material BOR is formulated in terms of equivalent electric and magnetic currents over the surface which defines the body[48]. Application of the boundary conditions leads to four simultaneous surface integral equations to be satisfied by the two unknown equivalent currents, electric and magnetic. Linear combinations of these four equations is reduced to a coupled pair of two equations. The latter two equations were solved via the MoM. One choice of combination constants gives the formulation which has been applied to material cylinders, and to material BOR. This choice is called the PMCHWT formulation (a solution proposed by Poggio, Muller, Chang, Harrington, Wu, and Tasi) [86-88].

Fowler, B. W. and Sung, C. C. in 1979 [89] obtained the cross sections for an EM waves scattered from dielectric bodies of irregular shape. The boundary conditions are reduced to a set of linear algebraic equations whose variables are the expansion coefficients of the electric and magnetic field.

In 1986, Korada, U. et al. [49] developed an extension of the MoM technique for analyzing EM scattering by arbitrary shaped 3-dimensional homogeneous lossy dielectric objects, based on CFIE. The surfaces of the arbitrary geometrical shapes are modeled using surface triangular patches, similar to the case of arbitrary shaped conducting objects.

Gong, Z. and Glisson, A. W. in 1990 [90] presented a numerical procedure for the solution of EM scattering problems involving inhomogeneous dielectric cylinders of arbitrary cross section. The formulation has been implemented for both TM and TE cases via hybrid integral equation/partial differential equation approach. It is modeled by PDE for electric field in the interior region, and SIE for the equivalent electric and magnetic surface currents in the exterior region, which founded by MoM.

The problem of EM scattering by a homogeneous dielectric object is usually formulated as a pair of coupled IEs involving two unknown currents on the surface of the object. The problem is formulated as a single SIE in terms of an equivalent electric current defined at the body surface, solve by the MoM using Galerkin test procedure, and numerical results for dielectric sphere demonstrated the validity of the method [47,91,92].

Kucharski, A. in 2000 [93] used an efficient method of calculating the EM fields scattered from and penetrating into inhomogeneous dielectric BOR. The electric flux density is chosen as the unknown quantity, which, together with the special construction of basis and testing functions, enables considerable reduction of the number of unknowns. The testing procedure used for the MoM solution is typical mode-by-mode solution scheme of Galerkin, and the solution remains within the convenient mixed potential EFIE scheme.

Composite structures of metallic and homogeneous dielectric materials have many important applications. [94] applied the SEI method for the EM

analysis of general metallic and dielectric structures of arbitrary shape based on the EFIE-CFIE-PMCHWT integral equation formulation with Galerkin's type discretization. The task is divided into three steps: 1) present and discrete the EFIE and MFIE in each homogeneous dielectric sub-domain separately. 2) enforce the boundary conditions on the metallic surfaces, the electric interfaces and at the junctions. 3) enforce the wanted integral equation formulation.

Kucharski, A. in 2005 [95] applied methods for computation of EM scattering by partially inhomogeneous dielectric bodies. The formulations are based on hybrid volume/surface integral equations (VIE/SIE), where volume-equivalent current are used to model the inhomogeneous parts of the body while surface currents are responsible for satisfying the boundary conditions at the body surface.

Yla-Oijala, P. and Taskinen, M. in 2008 [51] studied a solution of CFIE for EM scattering by an arbitrary shaped dielectric object. A novel CFIE formulation in which the EFIE and MFIE are combined in usual outside the object is derived. Inside the object CFIE is composed by changing the roles of EFIE and MFIE. Furthermore, empirical formulas are derived for the optimum number of basis functions [96]. These empirical formulas are used in the choice of the number of basis function for dielectric or composed body.

Necmi, S. T. in 2008 [97] proposed a new and computational effective method, based on Taylor series expansion of fields with unknown coefficients, related to EM scattering from arbitrary shaped dielectric object. From boundary condition, series equations are obtained, solved by using orthogonality properties of Fourier expansion functions. Transform method and MoM are compared, the differences are just in computational time.

Rui, X. et al. in 2010 [98] developed a fast inhomogeneous plane wave algorithm to solve the EM scattering problem for homogeneous dielectric

BOR, by using the Wely identity and designing a proper integration path to express the Green's functions. Compared with the traditional MoM, both the memory and CPU time requirements are reduced for large-scale homogeneous dielectric BOR.

In 2011, Resende, U. C. et al. [50] analyzed the EM scattering from dielectric and composite BOR by the Electric-Magnetic Field Integral Equation (EMFIE) and the Magnetic-Electric Field Integral Equation (MEFIE), which are simpler than classical CFIE, with standard MoM. Dielectric and composite analysis and results are compared with these of well-established Muller and PMCHWT.

1.13.4 Dielectric BOR-Wire

Junker, G. P. et. al., in 1993 [99] presented formulation for parasitic wire radiators in the presence of dielectric bodies of revolution (DBOR/Wire). This work is in essence an extension of techniques for the MoM solution of wire radiators in the presence of conducting BOR. The formulation is general in that the wire radiators may be interior or exterior to the dielectric bodies of revolution DBOR. The utility of the MoM has been used to given accurately predicted to the input impedance of DBOR/Wire radiators, and more accurately for electrically thin wire [100].

1.13.5 Coated bodies

The different cases used with formulation of imperfectly conducting BOR are: impedance boundary condition IBC, resistive sheet boundary condition RBC, and magnetically conducting sheet boundary conducting MBC. The results of such different cases are compared with each other's, and they are compared finally with the Mie solution for impedance coated spheres

and MoM for EFIE, MFIE, and CFIE formulation of impedance coated bodies [39].

Kishk, A. A. and Shafai, L. in 1986 [101] solved the EM scattering from coated conducting BOR by different formulations, seven different formulations, to find surface currents. The performance of different formulations to solve the coated conducting problems was found to be satisfactory when the coating permittivities was small but not equal to unity.

Huddleston, P. L. et al. in 1986 [102] generalized the CFIE formulation for EM scattering from perfectly conducting BOR with single layer dielectric coating. This formulation provides unique solutions at all frequencies. They used the MoM to solve the resulting system of IE, solutions in terms of two integral operators for BOR.

Rao, S. M. and Wilkes, D. L. in 1991 [103] used IE_s formulated by equivalent electric and magnetic surface currents, solved by MoM, to determining the EM field scattered by arbitrary shaped, 3D conducting objects coated with lossy dielectric material of arbitrary thickness.

Putnam, J. M. and Medgyesi-Mitschang, L. N. in 1991 [104] derived a combined integral equation CFIE formulation for two-and-three dimensional bodies with discrete inhomogeneous regions, this formulation solved using a MoM with Galerkin's procedure. The penetrable regions are nonuniform in thickness, multilayered, and can be lossy dielectric and ferromagnetic materials, characterized by complex permittivity and permeability. Whereas [105] make a special choice for the number of basis functions between the regions of dielectrically coated bodies.

Researchers studied the polarization scattering (vertical and horizontal polarization) properties of various radar targets with size in the resonance region and of complex composition, partially coated with a lossy dielectric materials as well as partially coated with a lossy magnetic materials. To take

advantage of rotationally symmetric geometries of BOR, they formulate problem in terms of the equivalent currents, on the surface of scatterer, leading to surface IEs which are solved using the MoM and getting the backscattering polarization matrix [106-109].

Kishk, A. A. and Gorden, R. K. in1994 [110] used the coating of the conducting objects with thin layers of magnetic materials to reduce the backscattering from axisymmetric objects. They used the concept of the Impedance Boundary Condition (IBC) to predict the coating material permeability and thickness.

In 2002, Yang, H. et al. [111] predicted the RCS of large complex targets coated with uniaxial anisotropic RAM, simple and effective method used for that. According to the equivalence principle, high frequency approximation and boundary conditions, for the case of thin coating, the IEs for scattered fields can be simplified and this for is similar to the PO integral formula. But for the conducting body coating by thin-layer material, plenty of discretize the geometry in the traditional FEM. The hybrid shell vector element with the boundary integral method is used to expedite the solution of thin coating problems [112].

More accurate solutions for 3D conducting objects with arbitrary shaped coated with dielectric materials, compared with other available solutions obtained using commercial software are presented by [113].

He, S., Nie, Z., and Hu, J. in 2009 [114] presented an alternative method to the IBC to simulate the scattering from the dielectric-coated metallic structures by combining the thin dielectric sheet approximation altogether with the explicit PEC boundary condition. This method removes the need to solve the field in dielectric layer in a manner like IBC. Both the EFIE, MFIE, and CFIE are convert to a matrix equation by Galerkin's method

and solved with Multilevel Fast Multipole Algorithm (MLFMA) to obtain the far- fields scattered from coated objects.

Yuyuan, A., Zhu, J., and Chen, R. in 2010 [115] are developed the MoMs for BOR to analyze EM scattering from conducting BOR coated with chiral material. The PMCHWT integral equation is formulated using the surface equivalence principle, the boundary condition, to split a chiral media into two equivalent homogeneous media. Thy axisymmetric property of the BOR expanded all currents, fields, and scalar Greens function in Fourier series, and selected suitable basis functions reduced a 3D problem to 2D one.

Raju, A.U. and Balakrishnan, J. in 2012 [26] they introduced a novel method of partial coating to reduce the RCS of a complex shaped PEC aircraft, of electrically large size. The modified physical optics method is used to compute RCS. It is shown that, with an appropriate choice of the partial coating level, the RCS can be reduced to the same level as that of a fully coated air craft, over a wide frequency range.

1.14 Aim of thesis

The main concern of the work described in this thesis is to present a theoretical analysis to the problems of EM scattering in both bistatic and monostatic configuration. The problem further complicated were not confined to the body (BOR) alone, which gives the form a regular. The problem her, added attached wire with junction region between wire and the BOR surface.

One of the basic and important aims is to study the effect of the shape by wires in addition to the coated by Radar Absorbing Material (RAM) on the RCS pattern. This RCS be known for regular and simple objects, as in sphere and cylinder, before adding the effect of the wires and find a new form of RCS. The new application is to find a developer model for this study carries known RCS, if it is an approximation with other objects close to his form.

The computation time consumed in solving the IE of the (BOR-wire-junction) depends primarily on the evaluation of what are called the modal Greens functions and evaluated using an adaptive numerical integration method. Finally, in this study the system consist of a BOR with attached wires, in the presence of junction region, analyzed by using of MoM as numerical solution for different shapes and materials to calculate the RCS.

1.15 Organization of the thesis

Work described in this thesis was based on providing a theoretical analysis to the problems of EM scattering from BOR with attached wires in both radar configurations, bistatic and monostatic. These problems include the perfect conductor, dielectric, and coated BOR with attached wire and junction region, combined together to form a composite body (BOR-wire-junction). The formulations of the problem are different from one to another according to the material object.

This thesis is composed of five chapters and five appendices:

In **chapter One,** the same concept with a historical background that is related to the subject of the thesis such as methods of solution, problem formulation, radar cross section and radar cross section reduction, and other related concept in radar problems is introduced.

Chapter Two contains the formula analysis to the scattering problem of EM waves from conducting BOR, CBOR-wire-junction, by using EFIE and rigorous solution by MoM with Galerkin's approach. Numerical results for RCS to the CBOR and composite body are presented. The validity of formulation is proved and compared with the available data. The effect of wires and junctions on the RCS pattern of CBOR, and the shape effect of the proposed model are studied.

In **chapter Three**, the composite body consists of dielectric BOR (DBOR)-wire-junction. The EFIE-PMCHWT formulations via the MoM steps and Galerkin's approach are used to get the RCS. The EFIE was applied in wire-junction regions with surface electric current, while PMCHWT applied in the DBOR region with coupled pair of electric and magnetic surface currents. Numerical results are presented to validate these formulations. Furthermore, in this chapter an investigation involves the effect of changing body material such as lossy dielectric, dielectric constant, also the effect of wire-junction and they differ from the second chapter.

Dielectrically Coated BORs (DCBOR) are considered with wire and junction to formulate. We used the EFIE-PMCHWT formulations via MoM to confirm the suitability and effectiveness of these formulas**.** The reduced of the computational offers is the first task of **chapter Four**, and the study of the effect of layer thickness and RAM on the RCSR was the second. Also, numerical results are presented to validate these formulations in comparison with data of chapter two.

Chapter Five consists of general conclusions and presents some suggestions for future work.

The general procedure for MoM and the numerical solution of EFIE and calculating the impedance, admittance and measurement submatrices elements equations are presented in **Appendices A, B, C, D and E**, respectively.

Chapter Two

Scattering from conducting BOR with attached wires

2.1 Introduction

There are some solutions available for the problem of EM wave scattered by perfectly conducting objects. These solutions are complicated in calculations and for limited general shapes like elliptical, cylindrical and spherical objects. A new system occurs for conducting objects arises from the coupling between a wire and general CBOR. This coupling is a new path in the process of being mathematical analysis adds further complexity in the calculations because of the overlap between the regions of the body and wires. The flexibility inherent in thin wire. In the case of the wire, thin shall mean that the wire radius, is small enough in terms of wavelengths in the medium in which it resides so that the only component of current induced on the wire is that which is axially directed and circumferentially invariant. This definition is the same as that given by the well developed thin wire theory[35]. In early time accomplished for conducting BOR-wire system by introducing the junction region in the point that the wire is attached to the CBOR [76 ,85].

The most useful numerical evaluation is the use of the IEs formulation in the above cases. The IE is the representation of the field vector for both interior and exterior of the body, also the wire and junction.

In this chapter, the formulation builds on the BOR-wire-junction analysis where the voltage vector for the matrix analysis is due to an incident plane wave. The method described here is based on the EFIE, which is exact in its formulation. The IE is solved using the MoM scattering analysis for bodies possessing rotational symmetry i.e., BOR, with attached wires, by expanding the unknowns surface current distribution in series of suitable basis

function. Then the IE can be reduced to a set of simultaneous linear equations, whose solution gives the required surface current distribution.

2.2 Formulation of the problem of CBOR-wire-junction

The general model of CBOR-wire-junction as shown in Fig.(2-1). The formulation begins with EFIE, by imposing the usual boundary conditions on the perfectly conducting surface require that the total electric field vanish on the surface and just the tangential component is required, that is lead to:

$$\bar{\mathrm{E}}^{\mathrm{i}}(\bar{\mathrm{r}})\big|_{\tan} + \bar{\mathrm{E}}^{\mathrm{s}}(\bar{\mathrm{r}})|_{\tan} = 0 \qquad (2\text{-}1)$$

where $\bar{\mathrm{E}}^{\mathrm{i}}{}_{\tan}$ and $\bar{\mathrm{E}}^{\mathrm{s}}{}_{\tan}$ are the tangential components of the incident and scattered electric fields on the body surface, respectively, so

$$\bar{\mathrm{E}}^{\mathrm{i}}(\bar{\mathrm{r}})\big|_{\tan} = -\bar{\mathrm{E}}^{\mathrm{s}}(\bar{r}')\big|_{\tan} = \mathrm{j}\omega\mu \iint_{\mathrm{s}} \bar{J}(\bar{r}')G(\bar{R})d\acute{s} - \frac{1}{\mathrm{j}\omega\epsilon}\bar{\nabla}_s \iint_s \left[\bar{\nabla}\cdot\bar{J}(\bar{r}')\right]G(\bar{R})d\acute{s} \qquad (2\text{-}2)$$

in which $\bar{\mathrm{R}} = \bar{r} - \bar{r}'$ is the vector distance between the source point r' to the observation point r , and given by [85]

$$R = |\bar{R}| = \sqrt{\acute{r}^2 + r^2 - 2r\acute{r}cos\,(\phi - \acute{\phi})} \qquad (2\text{-}3)$$

and,

$$G(\bar{R}) = \frac{e^{-jkR}}{4\pi R} \qquad (2\text{-}4)$$

is the free-space Greens function. $\bar{J}(\bar{r}')$ is the surface electric current density on the conducting surface, presented by the form of;

$$\bar{J}(\bar{r}') = \bar{J}^{s}(\bar{r}') + \bar{J}^{w}(\bar{r}') + \bar{J}^{j}(\bar{r}') \qquad (2\text{-}5)$$

Where $\bar{J}^{s}$, $\bar{J}^{w}$, and $\bar{J}^{j}$ represent the electric current density on the BOR surface, wire, and junction region .

The generalized EFIE expressed in terms of integro-differential operators $L(\cdot)$ on the BOR, wire, and junction is given by:

$$\bar{\mathrm{E}}^{\mathrm{i}}(\bar{r})\big|_{\tan} = \mathrm{L_s}\left(\bar{J}^{s}(\bar{r}')\right) + \mathrm{L_w}\left(\bar{J}^{w}(\bar{r}')\right) + \mathrm{L_j}\left(\bar{J}^{j}(\bar{r}')\right) \qquad (2\text{-}6a)$$

The operator L_s refers to BOR surface S_s and written as

$$L_s(\bar{J}^s) = \left\{ j\omega\mu \iint_{S_s} \bar{J}^s G \, d\acute{s} - \frac{1}{j\omega\epsilon} \nabla_s \iint_{S_s} (\nabla_s \cdot \bar{J}^s) G \, d\acute{s} \right\}\Big|_{tan} \quad (2\text{-}6b)$$

Where ∇_s is the surface gradient on the BOR, ω is the radian frequency, μ and ϵ are the permeability and permittivity of the medium, respectively.

Analogously for the wire part we have

$$L_w(\bar{J}^w) = j\omega\mu \int_h \bar{J}^w G \, dh' - \frac{1}{j\omega\epsilon} \hat{u}_w \frac{d}{dh} \int_h \frac{d\bar{J}^w}{d\acute{h}} G d\acute{h} \quad (2\text{-}6c)$$

Where $L_w(\bar{J}^w)$ is the one-dimensional operator on the total wire current in the thin wire approximation and $\hat{u}_w$ is a unit vector along the wire.

The operator in the junction region $L_j(\cdot)$ is $L_w(\bar{J}^w)$ when the domain of integration is restricted to the attachment segment S_a; $L_j(\cdot)$ is $L_s(\bar{J}^s)$ when the surface integration is confined to the disk part of the junction region S_d as shown in Fig.(2-2).

To solve Eqs.(2-6) for the unknown J on the entire surface, explicit expressions must be obtained for all operators via the MoM with Galerkin's technique to expand the currents specific to each region. In this method the regions are sub-divided; specifically, the BOR is divided into annular segments, the wire into connected straight-wire segments, and the junction region into an attachment and disk part [76].

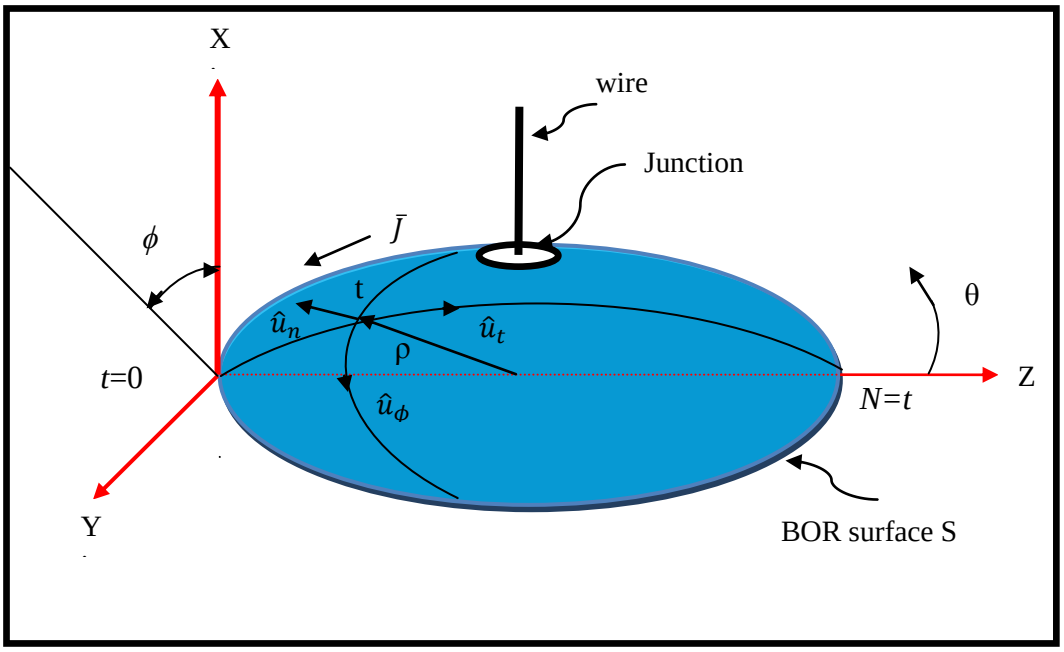

Fig.(2-1): CBOR coordinate system with attached wire and junction.

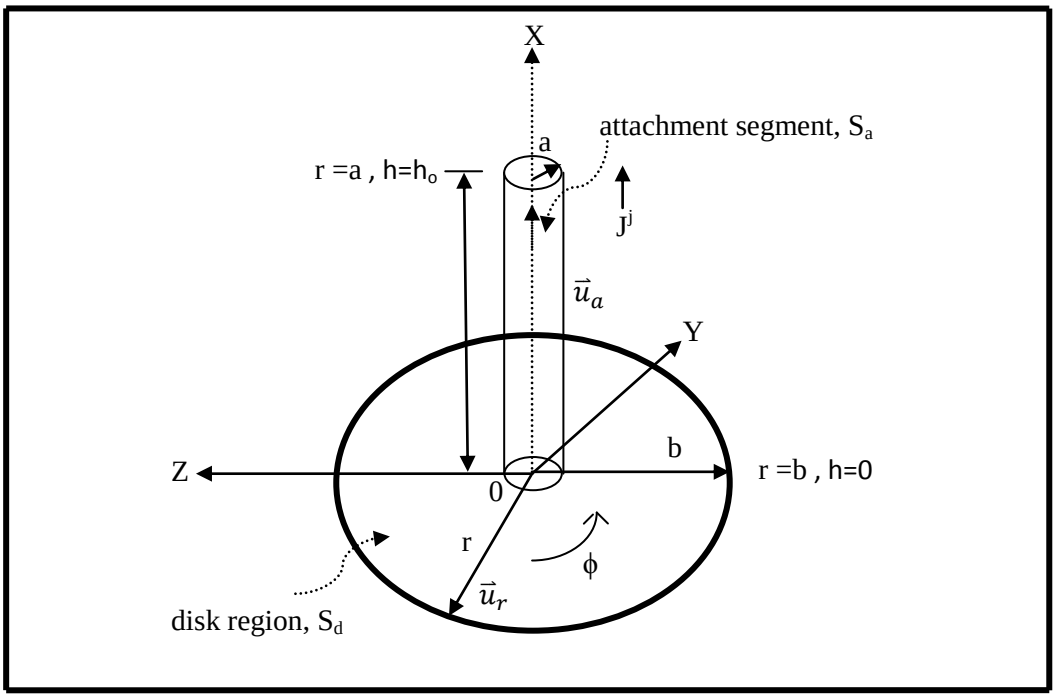

Fig.(2-2): Attachment region at the wire/BOR surface.

2.2.1 Expansion of the unknown currents

In the present formulation, appropriate sets of basis functions for the unknown surface electric current densities on the three regions the BOR, wire, and junction can be represented by:

- Modal expansion functions on the BOR.
- Piecewise continuous functions on the wire.
- Continuity-preserving expansion function for the vicinity of the junction.

Therefore each geometric part of the composite body has its own class of current expansion functions.

1- BOR basis functions

Considering the rotational symmetry geometry characteristic of the BOR, the equivalent current is a vector quantity and can be expressed as superposition of two orthogonal vectors at any points on the surface. The obvious choice for the current vectors is surface tangential vector $\hat{u}_t$, which rotationally about the angle ϕ, and the azimuthal vector $\hat{u}_\phi$. Therefore the surface current density of the BOR on the i_{th} annular segment is expanded in terms of a modal expansion in ϕ and overlapping triangle functions in t-direction as shown in Fig.(2.3a), and can be expressed by using the notation of [8] as follow:-

$$\bar{J}^s = \hat{u}_t \bar{J}^t + \hat{u}_\phi \bar{J}^\phi = \sum_{i=1}^{N_s-1} (I_{ni}^{st} \bar{J}_{ni}^{st} + I_{ni}^{s\phi} \bar{J}_{ni}^{s\phi}) \qquad (\frac{A}{m^2}) \qquad (2\text{-}7a)$$

Where

$$\bar{J}_{ni}^{st} = \hat{u}_t \frac{T(t-t_i)}{\rho} e^{jn\phi} \qquad (2\text{-}7b)$$

$$\bar{J}_{ni}^{s\phi} = \hat{u}_\phi \frac{T(t-t_i)}{\rho} e^{jn\phi} \qquad (2\text{-}7c)$$

Where $\hat{u}_t$ and $\hat{u}_\phi$ are the unit vectors along *t*- and ϕ -direction, and ρ is the radius of BOR, $T(t\text{-}t_i)$ is the triangle base function about the i_{th} segment, the

subscript *n* denote the Fourier mode number along ϕ direction, I_{ni}^{st} and $I_{ni}^{s\phi}$ are the unknown current coefficients of corresponding annulus.

2- Wire basis functions

The wire–basis functions are overlapping triangle functions on the ℓ_{th} segment with a vector direction coinciding with the wire as shown in Fig.(2.3b). The filamentary wire current distribution J^w is expanded with piecewise triangular basis function as in [116], and can be expressed as

$$\bar{J}^w = \hat{u}_\ell^w \, I_\ell^w \, T_\ell(h) = \sum_{\ell=1}^{N_w-1} \hat{u}_\ell^w \; I_\ell^w T_\ell(h) \qquad (\frac{A}{m}) \qquad (2\text{-}8)$$

Where, $\hat{u}_\ell^w$ is the unit vector of the ℓ_{th} segment a long wire, $T_\ell(h)$ represents a triangular function, and I_ℓ^w is the unknown wire current coefficient of corresponding segment. For a wire segment nearest the attachment point, one – half of a wire triangle function overlaps the half–triangle basis term on the attachment segment. This representation yields a piecewise continuous current from the junction to the wire.

3- Junction basis functions

The basis functions for surface or wire currents, must be chosen to simulate the physical realizable currents. A junction basis functions was introduced to represent the currents in the vicinity of the body – wire – junction which enable a radiation analysis for BOR with attached radiating and parasitic elements. A special attachment made is introduced wherever wire is connected with BOR surface, as shown in Fig.(2-2), at this attachment point (junction) the current has the following features.

- The surface current is radially inward toward the wire base, varying as *1/r* (singular point).
- The wire current at the base is non–zero and equal to the junction current.
- The surface current flowing into the junction must equal the wire current out of the junction.

According to these points, no discontinuity occurs at any conductive joint part.

For a point *p* in the junction region, the basis function of which is defined as follow:

$$\bar{J}^j(p) = I^j \begin{cases} J_a^j \ , & p \in S_a \\ J_d^j \ , & p \in S_d \end{cases} \tag{2-9}$$

Where

$$\bar{J}_a^j = \hat{u}_a \frac{T_a(h)}{2\pi a} \tag{2-9a}$$

$$\bar{J}_d^j = -\hat{u}_r \frac{1}{2\pi r} \left(\frac{b-r}{b-a}\right) \tag{2-9b}$$

Where $\bar{J}^j$ is the total current density on junction, as shown in Fig.(2-3c). While $\bar{J}_a^j$ is the current density on the wire segment nearest the junction region, i.e., wire attachment segment S_a, $\bar{J}_d^j$ is the current density over the BOR surface near the junction regions (disk region) S_d, $\hat{u}_a$ and $T_a(h)$ are an outward–directed unit vector and half–triangle function on the attachment segment, respectively; $\hat{u}_r$ is a unit vector on the (annular) disk surface away from the wire, *r* is the radial distance on the disk, *b* is the outer disk radius, *a* is the wire radius, and I^j is the unknown junction current coefficient. A similar formulation for the junction currents is given in [75] and [76].

The $\left(\frac{b-r}{b-a}\right)$ factor truncates the *1/r* behavior of $\bar{J}_d^j$ at *r=b* beyond the BOR basis functions provide an adequate representation. Thus *1/r* behavior is prevented from extending over the entire BOR surface. The basis functions meet the Kirchhoff current continuity requirement: namely, the surface disk current equals the wire current at the wire base, i.e., *r=a* , *h=0*.

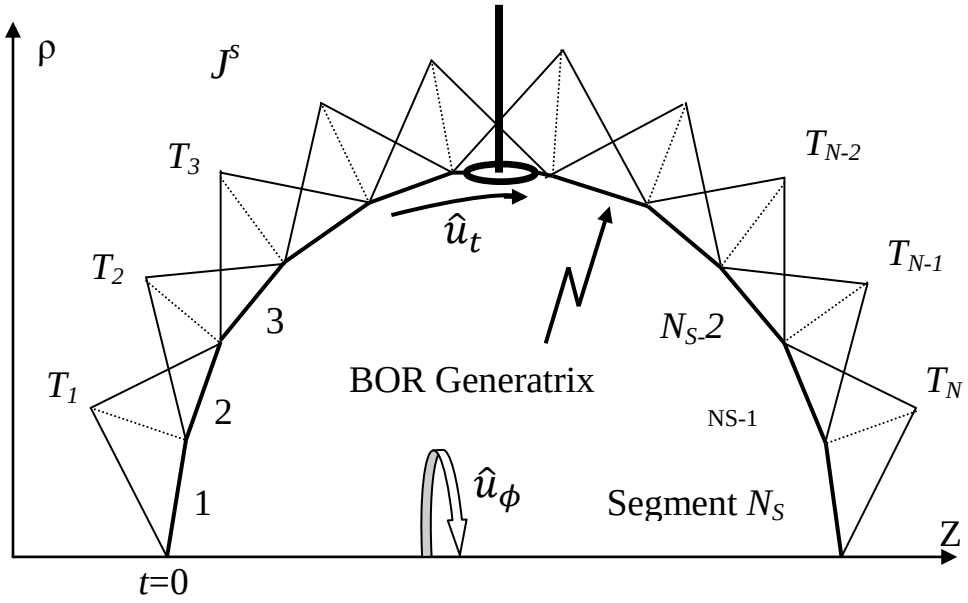

(a)

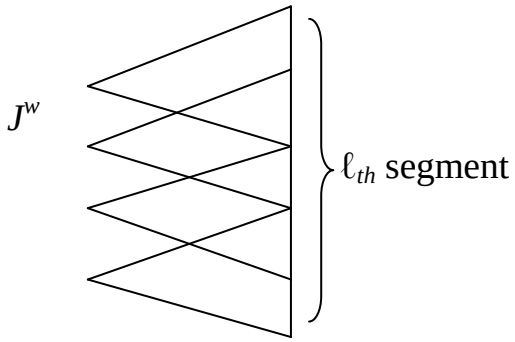

(b)

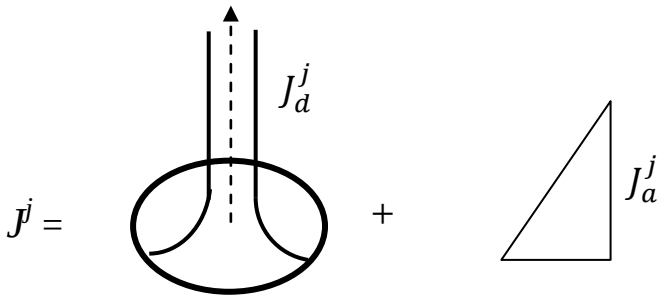

(c)

Fig.(2-3): Triangular basis functions (a) over the BOR generatrix.(b) on l_{th} segment of attachment wire. (c) junction region representation.

2.2.2 Method of solution

The MoM is used here as a numerical technique whose solutions satisfying the boundary conditions only at discrete points [35]. The procedure of numerical solutions, in coupling with Galerkin's approach, begin with reducing the Eqs.(2-6) to the set of linear equation in matrix form.

The Galerkin's expansions fall into category of sub domain. Sub domain basis functions are defined over a domain of an integral operator L(•) such that they are vanishing over part of this domain. Examples of such bases include plus, triangle, and piecewise sinusoidal functions.

Traditionally, sub-domain expansions have been favored because of their flexibility, easier evaluation of the multiple integrals arising in the MoM technique, and the ability of handle localized surface features in scattering problems [62].

According to the MoM procedure, the unknown surface currents on the different surface of the body one expressed in a finite modal expansion [33]. On the BOR as in Fig.(2-4), the variation $\acute{\phi}$ is known as a continues sinusoidal distribution with $e^{jn\acute{\phi}}$, and the t' variation is an unknown function which can be expanded as a linear combination of N_s. The electric current $\bar{J}^s$, exists on the conduction surface S, can be re-written as follow:

$$\bar{J}_{ni}^{st}(t') = \hat{u}_{t'} \sum_{i=1}^{N_s-1} I_{ni}^{st} \; f_i(t') \qquad (2\text{-}10\ a)$$

$$\bar{J}_{ni}^{st}(t') = \hat{u}_{\phi'} \sum_{i=1}^{N_s-1} I_{ni}^{s\phi} \; f_i(t') \qquad (2\text{-}10b)$$

Where $f_i(t') = \frac{T\,(t'-t'_i)}{\rho'}$ (2-11)

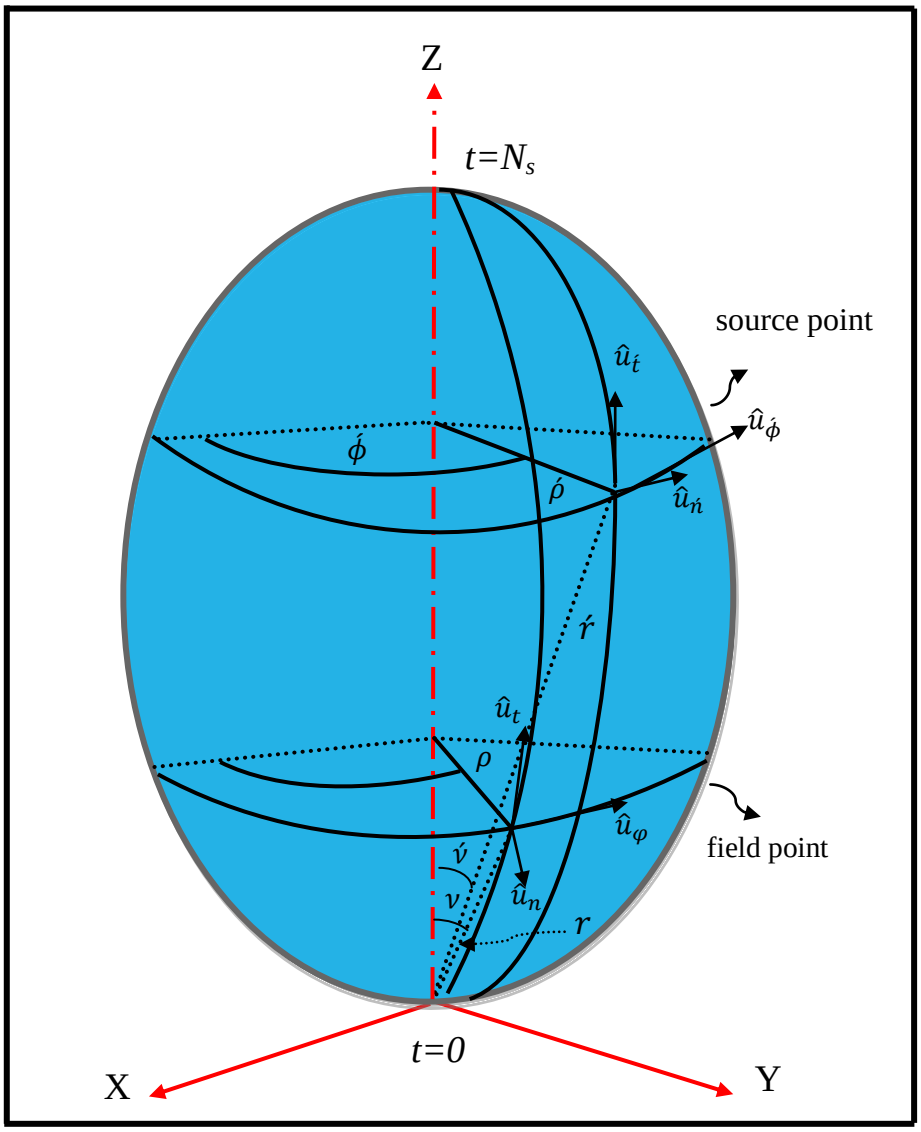

Fig.(2-4) Coordinates system of BOR.

As discussed in the body, the triangle and rooftop basis functions are used on the wire and junction, respectively. The BOR and wire both use four weighted impulses as a representation for the triangle function, whereas the junction uses only two weighted impulse in the attachment segment part. For explicit evaluation of the currents, one must choose $f_i(t')$ as triangle function. A

minor deviation from the literature is to be expanded $\rho' f_i(t')$. Thus the BOR triangle function is given in [100] as:

$$\acute{\rho}\, f_i(t') = \sum_{p=1}^{4} T_{p+4i-4}(t')\delta\left(t' - t'_{p+2i-2}\right) \quad (2\text{-}12a)$$

where *T* is the triangle function

$$T(t') = \begin{cases} 1 - |t'|, & |t'| < 1 \\ 0, & |t'| > 1 \end{cases} \quad (2\text{-}12b)$$

and $\delta(t)$ is the unit impulse function (Dirac delta function) and its coefficients *T* is defined as shown in Fig.(2-5a).

Similarly, the derivative of $f_i(t')$ is approximated by four impulse as:-

$$\frac{d}{dt}\left[\acute{\rho}\, f_i(t')\right] = \sum_{p=1}^{4} T'_{p+4i-4}(t')\ \delta\left(t' - t'_{p+2i-2}\right) \quad (2\text{-}13a)$$

where *T'* is the derivative of triangle function

$$T'(t') = \begin{cases} 1, & -1 < t' < 0 \\ -1, & 0 < t' < 1 \\ 0, & |t'| > 1 \end{cases} \quad (2\text{-}13b)$$

and are shown in figure (2-5b). So, the triangle function for the wire and its derivative as shown in the Fig.(2-5), can be written as:

$$f_\ell(h') = \sum_{p=1}^{4} T_{\ell(p+4i-4)}(h')\ \delta(h' - h'_{p+2i-2}) \quad (2\text{-}14a)$$

$$\frac{d}{dh'} f_\ell(h') = \sum_{p=1}^{4} \acute{T}_{\ell(p+4i-4)}(h')\ \delta(h' - h'_{p+2i-2}) \quad (2\text{-}14b)$$

In contrast, for the junction region in attachment part

$$f_\ell(h') = \sum_{p=1}^{2} T_{a(p+2i-2)}(h')\ \delta(h' - h'_{p+2i-2}) \quad (2\text{-}15a)$$

$$\frac{d}{dh'} f_\ell(h') = \sum_{p=1}^{2} \acute{T}_{a(p+2i-2)}(h')\ \delta(h' - h'_{p+2i-2}) \quad (2\text{-}15b)$$

Where $f_\ell(h') = T_\ell(h')\ or\ T_a(h')$ (2-16)

For computations, the generating curve of conducting BOR surfaces is approximated by choosing a succession of points t_i ($i=1,2,.....,N_s$) on the generating curve and then connecting these points by straight–line segments, where N_s is the total number of points, t_i is called a data point as shown in Fig. (2-4). The number of data point on the wire segment is N_w. The last data

points is the attachment segment of the junction region N_a. The scattered is thus modeled by adding the three region data points [75]. Then, $N=N_s+N_w+N_a$.

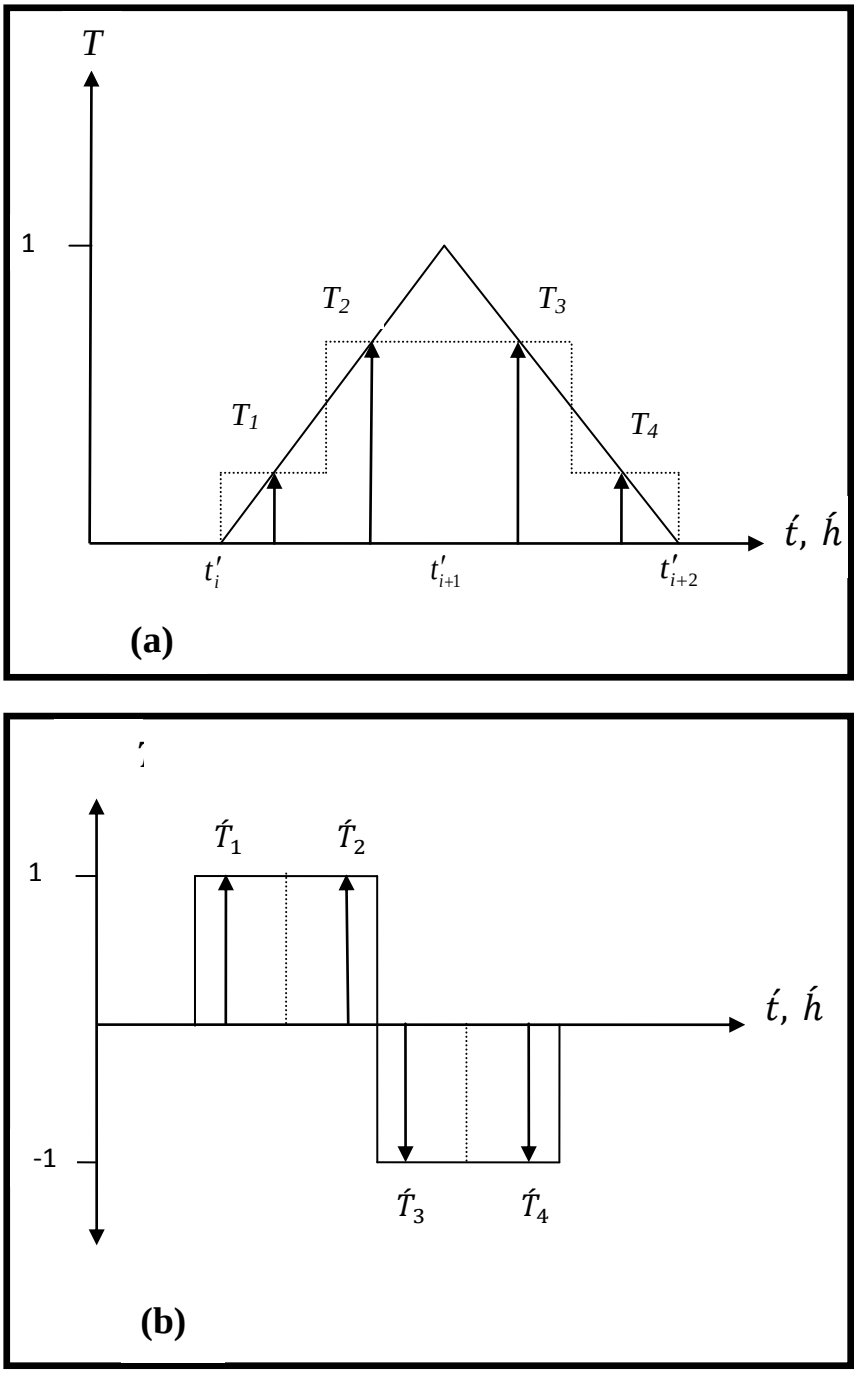

Fig.(2-5): (a) Triangle function (solid), four pulse approximation (dashed), impulse approximation (arrows) (b) Derivative of the triangle function (solid), four pulse representation (dashed), impulse approximation (arrows).

It is useful to focus on the other side of the solution which is complemented to the process of inner product, which is to choose the weighting (testing) function. The choice of weighting functions *W* is important in that the elements of this functions must be linearly independent, so that the resulting equations will be linearly independent. Furthermore, it will generally be advantageous to choose weighting functions that minimize the computations required to evaluate the inner products, because of this, similar types of functions are often used for both weighting and expansion functions (i.e. $W=J^*$, where * denotes a complex conjugate), which is known as Galerkin's approach [41].The testing functions for conducting BOR are defined by:-

$$\bar{W}^s(t,\phi) = \bar{W}^t(t,\phi) + \bar{W}^\phi(t,\phi)$$

$$= \sum_{m=-\infty}^{m=\infty} \sum_{i=1}^{Ns-1} (\bar{W}_{mi}^{st}(t,\phi) + \bar{W}_{mi}^{s\phi}(t,\phi)) \quad (2\text{-}17a)$$

$$\bar{W}_{mi}^{st} = \hat{u}_t \, f_i(t) e^{-jm\phi} \quad (2\text{-}17b)$$

$$\bar{W}_{mi}^{s\phi} = \hat{u}_\phi \, f_i(t) e^{-jm\phi} \quad (2\text{-}17c)$$

The expansion $\bar{J}_{ni}$ and testing $\bar{W}_{mi}$ functions, as defined in the last equations are orthogonal over the period 0 to 2π in ϕ, for ($n \neq m$). This means that the inner products of these functions vanish for $m \neq n$. This fact allowed each mode to be treated separately [8].

For the wire and junction elements, whose basis functions are real, that is mean ($W=J$), we find

$$\bar{J}^w = \bar{W}^w \quad (2\text{-}18)$$

$$\bar{J}^j = \bar{W}^j \quad (2\text{-}19)$$

2.2.2.1 Coordinate system of BOR – Wire – Junction

The property of an axisymmetric for BOR can be shown in Fig.(2-4). Because of the rotationally symmetric, the coordinates can be represented contently in terms of ρ , ϕ and z in a cylindrical systems with the origin on the

axis of the body. t and ϕ are forms an orthogonal curvilinear coordinate system on the surface of the BOR where $\hat{u}_t$ and $\hat{u}_\phi$ are orthogonal unit vectors in the t and ϕ directions, respectively. The outward normal to the surface is defined as:

$$\hat{u}_n = \hat{u}_\phi \times \hat{u}_t \tag{2-20}$$

Source and field quantities are denoted as primed and unprimed, respectively. On the body surface, we define a field point by its coordinates (t, ϕ, z) or (ρ, ϕ, z) and for source point by (t',ϕ',z') or (ρ',ϕ',z'). Their respective unit tangent vector are ($\hat{u}_t, \hat{u}_\phi$) and ($\hat{u}_{t'}, \hat{u}_{\phi'}$). The angle between the Z-axis and $\hat{u}_t$ is denoted as v at (t, ϕ) point and between the Z-axis and $\hat{u}_{t'}$ as v ' at (t', ϕ') point. These unit vectors can be determined in cylindrical coordinates as follow [8]:

$$\hat{u}_t = \hat{u}_\rho \sin v + \hat{u}_z \cos v \tag{2-21a}$$

$$\hat{u}_\phi = \hat{u}_\phi \tag{2-21b}$$

$$\hat{u}_{t'} = \hat{u}_\rho \sin v' \cos(\phi - \phi') + \hat{u}_\phi \sin v' \sin(\phi - \phi') + \hat{u}_z \sin v' \tag{2-21c}$$

$$\hat{u}_{\phi'} = -\hat{u}_\rho \sin(\phi - \phi') + \hat{u}_\phi \cos(\phi - \phi') \tag{2-21d}$$

Where $\hat{u}_\rho, \hat{u}_\phi, and\ \hat{u}_t$ represent the unit vectors in cylindrical system. If the positional vectors of points (t, ϕ) and (t', ϕ') are $\bar{r}$ and $\bar{r}'$, respectively, then the relative positional vector $\bar{R}$ have the form:

$$|\bar{R}| = |\bar{r} - \bar{r}'| = [(\rho - \rho')^2 + (z - z')^2 + 4\rho\rho' sin^2\left(\frac{\phi - \phi'}{2}\right)]^{1/2} \tag{2-22}$$

For the wire case, as mentioned in the beginning of this chapter. It is one dimension but direction is determined by its location on the body (BOR). It may be the direction of the axis of rotation, of the BOR, then to be a trend toward the z-axis, or change its location on the rotation curve, without being part of it, and thus be either x-axis as depicted in Fig.(2-1) or y-axis direction. The positioned vector $\vec{R}$ between the field and source point on the wire segments can be written in Cartesian coordinates as:

$$\left|\vec{R}\right| = [\,(x-x')^2 + (y-y')^2 + (z-z')^2]^{1/2} \quad (2\text{-}23)$$

With the possibility to conversion the coordinate system from Cartesian to coincide with body coordinates , especially in the calculations of interaction matrices.

For the junction region as shown in Fig.(2-2), we are dealing with the first part (attachment segment S_a) as in the wire case. In the second part (disk region S_d) the detailed forms for the junction region by using the coordinate system approximated as flat disk of radius *b*. the radius *b* being much smaller than the local BOR curvature at the junction attachment point. The plane of the disk also determined with the wire direction, it may be located in yz-plane when the wire in x-axis direction see Fig.(2-2), and the positioned vector $\vec{R}$ can be written as follow:

$$\left|\vec{R}\right| = [\,r^2 + r'^2 - 2rr'\cos(\phi-\phi')]^{1/2} \quad (2\text{-}24)$$

2.2.3 Evaluation of matrix element

The expansion of the currents on the BOR surface, the wire segments, and the junction given in Eqs.(2-7) to (2-9) are substituted in Eq.(2-6). Now, following the MoM, the total current on the body is expressed as superposition of all the basis functions [117]

$$J = \sum_n \sum_i \left(I_{ni}^{st}\,\bar{J}_{ni}^{st} + I_{ni}^{s\phi}\bar{J}_{ni}^{s\phi} \right) + \sum_\ell I_\ell^w \bar{J}_\ell^w + \sum_j I^j\,\bar{J}^j \quad (2\text{-}25)$$

Where *n*, *i*, ℓ and *j* take on all possible values. The inner product of integral operators L(•), see appendix (B), in Eq. (2-6) are formed with testing functions $\overrightarrow{W}(=\bar{J}^*)$ via the Galerkin's approach, where the a asterisk denotes the conjugate operation. The testing operation is used to reduce the EFIE to a set of system of linear equations that can be written in matrix form as:

$$[Z][I] = [V] \quad (2\text{-}26a)$$

$$[\langle W, L(J)\rangle][I] = \left[\langle W, E^{inc}\rangle\right] \quad \text{(2-26b)}$$

The current vector I contains the unknown coefficients in the Eq. (2-25). Equations (2-26) are actually an infinite set of equations but can be reduced to a finite set by choosing a maximum value for *n* based on some convergence criteria. Since any given current must be tested with all weighting functions, nine distinct types of impedance elements results Z^{ss}, Z^{ww}, Z^{jj} represent the self -terms, and Z^{sw}, Z^{ws}, Z^{sj} , Z^{js}, Z^{wj}, Z^{jw} are represented the interaction terms. The superscripts *s*, *w*, and *j* refer to BOR surface, wire and junction, respectively.

The matrix Eq. (2-26a) can be rewritten as:

$$\begin{bmatrix} [Z^{ss}] & [Z^{sw}] & [Z^{sj}] \\ [Z^{ws}] & [Z^{ww}] & [Z^{wj}] \\ [Z^{js}] & [Z^{jw}] & [Z^{jj}] \end{bmatrix} \begin{bmatrix} [I^s] \\ [I^w] \\ [I^j] \end{bmatrix} = \begin{bmatrix} [V^s] \\ [V^w] \\ [V^j] \end{bmatrix} \quad \text{(2-27)}$$

In which the right column vectors above represents, a generalized voltage vectors, where $[V^s]$, $[V^w]$ and $[V^j]$ are the excitation voltage matrix of the BOR, the wire, and the junction region, respectively. In the left side of equation(2-27), the Z elements are the familiar impedance defining the EM interactions between various parts of BOR are represented by $[Z^{ss}]$ impedance matrix. Similarly, the BOR–wire, the BOR-junction, the wire – wire, the wire – junction and the junction–junction impedance matrices are denoted by $[Z^{sw}]$, $[Z^{sj}]$, $[Z^{ww}]$, $[Z^{wj}]$, and $[Z^{jj}]$, respectively. While $[I^s]$, $[I^w]$ and $[I^j]$ are the unknown coefficients of the electric current density on the BOR, wire and junction surfaces, respectively.

2.2.3.1 Evaluation of Z-sub matrices elements

The impedance blocks relating to the surfaces actually consist of several sub matrices, one for each mode number *n*. According to [76] the impedance matrix takes on the following block structure:-

$$Z = \begin{bmatrix} Z_N^{ss} & & & Z_N^{sw} & Z_N^{sj} \\ & Z_0^{ss} & & Z_0^{sw} & Z_0^{sj} \\ & & Z_{-N}^{ss} & Z_{-N}^{sw} & Z_{-N}^{sj} \\ Z_N^{ws} & Z_0^{ws} & Z_{-N}^{ws} & Z^{ww} & Z^{wj} \\ Z_N^{js} & Z_0^{js} & Z_{-N}^{js} & Z^{jw} & Z^{jj} \end{bmatrix} \quad (2\text{-}28)$$

Where N is the magnitude of highest mode number (i.e., n=0, ±1,....., ±N). Specific analytical expressions for the various sub matrices in Eq.(2-28) can be obtained by evaluating the inner products having the form:

$$Z = < \bar{W}, L(\bar{J}) > = \iint_S ds \iint_{\acute{s}} d\acute{s} \, . j\eta k \, [\bar{W}.\bar{J} - \frac{1}{K^2}(\nabla'.\bar{W})(\nabla.\bar{J})] \frac{e^{-jkR}}{4\pi R} \quad (2\text{-}29)$$

Where all superscripts and subscripts on $\bar{W}$ and $\bar{J}$ are omitted for simplicity and S and S' refers to surfaces containing the field and source points, respectively; $\omega\mu = k\eta$ and $\omega\epsilon = k/\eta$.

The detailing of the derivations for these sub-matrices are built here on two cases, which is junction – independent , and dependent.

2.2.3.1.1 Junction – Independent impedance elements

1-The BOR – BOR matrix elements Z^{ss}

This matrix represents the first element in Eq. (2-28), its partitioned into four parts corresponding to the t and ϕ directed current components. Since both basis and testing functions have components in t and ϕ direction, each element matrix in Z_{mn}^{ss} can be written as

$$Z_{mn}^{ss} = \begin{bmatrix} Z_{mn}^{sstt} & Z_{mn}^{sst\phi} \\ Z_{mn}^{ss\phi t} & Z_{mn}^{ss\phi\phi} \end{bmatrix} \quad (2\text{-}30)$$

The (i, j)$_{th}$ element of these sub-matrices is obtained from

$$Z_{mn,ij}^{ss\alpha\beta} = < \bar{W}_{mi}^{s\alpha}, L_s \left(\bar{J}_{nj}^{s\beta} \right) > \quad (2\text{-}31)$$

Where α, β are combination of t and ϕ, and m and n are mode numbers; $\bar{W}_{mi}^{s\alpha}$ and $\bar{J}_{nj}^{s\beta}$ are the i$_{th}$ testing and j$_{th}$ current basis functions, respectively, on

the BOR surface. Importantly, matrix elements for mode numbers $m \neq n$ are identically zero because of the orthogonality of testing function and operator therefore the inner product for Eq. (2-31) with applying of Eq. (2-29) yields to

$$Z_{mn,ij}^{ss\alpha\beta} = < \bar{W}_{ni}^{s\alpha}, L_s \left(\bar{J}_{nj}^{s\beta}\right) > = \iint_s ds \iint_{s'} ds' . j\eta k \left[\bar{W}_{ni}^{s\alpha} . \bar{J}_{nj}^{s\beta} - \frac{1}{k^2} (\nabla'_s . \bar{W}_{ni}^{s\alpha})(\nabla_s . \bar{J}_{nj}^{s\beta})\right] \frac{e^{-jkR}}{4\pi R} \quad (2\text{-}32)$$

Where R is the positioned vector and given by Eq.(2- 22). To calculate the four parts in Eq.(2-30), we must make some calculation in Eq. (2-32) by using the Eqs. (2-7) and (2-17) to get:

$$\begin{aligned}
\left(\bar{W}_{ni}^{s} . \bar{J}_{nj}^{s}\right)^{tt} &= f_i(t') f_j(t) e^{jn(\phi-\phi')} (\hat{u}_{t'} . \hat{u}_t) \\
\left(\bar{W}_{ni}^{s} . \vec{J}_{nj}^{s}\right)^{t\phi} &= f_i(t') f_j(t) e^{jn(\phi-\phi')} \left(\hat{u}_{t'} . \hat{u}_\phi\right) \\
\left(\bar{W}_{ni}^{s} . \vec{J}_{nj}^{s}\right)^{\phi t} &= f_i(t') f_j(t) e^{jn(\phi-\phi')} \left(\hat{u}_{\phi'} . \hat{u}_t\right) \\
\left(\bar{W}_{ni}^{s} . \vec{J}_{nj}^{s}\right)^{\phi\phi} &= f_i(t') f_j(t) e^{jn(\phi-\phi')} \left(\hat{u}_{\phi'} . \hat{u}_\phi\right)
\end{aligned} \quad (2\text{-}33)$$

From definition of ∇, the divergence of the two vectors $W_{ni}^{\alpha}(r')$and $J_{nj}^{\beta}(r)$ in the second term of the right side in Eq. (2-32) can be found as follow:

$$\nabla'_s . \bar{W}_{ni}^{s}(r') = \left[\frac{1}{\rho'} \frac{\partial}{\partial t'} (\rho' \hat{u}_{t'}) + \frac{1}{'\rho} \frac{\partial}{\partial \phi'} \left(\hat{u}_{\phi'}\right)\right] . \bar{W}_{ni}^{\alpha}(r') \quad (2\text{-}34)$$

$$\nabla_s . \bar{J}_{nj}^{\beta}(r) = \left[\frac{1}{\rho} \frac{\partial}{\partial t} (\rho \hat{u}_t) + \frac{1}{\rho} \frac{\partial}{\partial \phi} \left(\hat{u}_\phi\right)\right] . \bar{J}_{nj}^{\beta}(r) \quad (2\text{-}35)$$

By applying Eqs. (2-34) and (2-35) in Eq.(2-32), we get

$$\begin{aligned}
\left[(\bar{\nabla}'_s . \bar{W}_i)(\bar{\nabla}_s . \bar{J}_j)\right]^{tt} &= f'_i(t') f'_j(t) e^{jn(\phi-\phi')} \\
\left[(\bar{\nabla}'_s . \bar{W}_i)(\bar{\nabla}_s . \bar{J}_j)\right]^{t\phi} &= \frac{jn}{\rho} f'_i(t') f_j(t) e^{jn(\phi-\phi')} \\
\left[(\bar{\nabla}'_s . \bar{W}_i)(\bar{\nabla}_s . \bar{J}_j)\right]^{\phi t} &= \frac{-jn}{\rho} f_i(t') f'_j(t) e^{jn(\phi-\phi')} \\
\left[(\bar{\nabla}'_s . \bar{W}_i)(\bar{\nabla}_s . \bar{J}_j)\right]^{\phi\phi} &= \frac{n^2}{\rho\rho'} f_i(t') f_j(t') f_j(t) e^{jn(\phi-\phi')}
\end{aligned} \quad (2\text{-}36)$$

The complete form of the Eq. (2-32), is shown in appendix (C) and yields to

$$(Z_n^{tt})_{ij} = -jk\eta \sum_{p=1}^{4}\sum_{q=1}^{4}[T_pT_q\left\{\sin v_p \sin v_q \frac{G_{n+1}+G_{n-1}}{2} + \cos v_p \cos v_q\, G_n\right\} - GnK2T'pT'q]$$ (2-37a)

$$(Z_n^{t\phi})_{ij} = -k\eta \sum_{p=1}^{4}\sum_{q=1}^{4}[T_pT_q \sin v_p \frac{G_{n+1}-G_{n-1}}{2} + \frac{n}{K^2\rho_q} T_q T'_p G_n] \quad (2\text{-}37b)$$

$$(Z_n^{\phi t})_{ij} = k\eta \sum_{p=1}^{4}\sum_{q=1}^{4}[T_pT_q \sin v_q \frac{G_{n+1}-G_{n-1}}{2} - \frac{n}{K^2\rho_p} T_p T'_q G_n] \quad (2\text{-}37c)$$

$$(Z_n^{\phi\phi})_{ij} = -jk\eta \sum_{p=1}^{4}\sum_{q=1}^{4} T_pT_q[\frac{G_{n+1}+G_{n-1}}{2} - \frac{n^2}{K^2}\frac{G_n}{\rho_p\rho_q}] \quad (2\text{-}37d)$$

2-The BOR – wire interaction matrix Z^{sw}

The interaction matrix of body and wire, Z_n^{sw}, is also partitioned into *t* and ϕ component, therefore each element matrix in Z_n^{sw} has the form

$$Z_n^{sw} = \begin{bmatrix} Z_n^{sw,t} \\ Z_n^{sw,\phi} \end{bmatrix} \quad (2\text{-}38)$$

With the (i, ℓ)$_{th}$ element, these submatrices are defined as:

$$Z_{n,i\ell}^{sw,\alpha} = < \bar{W}_{ni}^{s\alpha}, L_w(\bar{J}_\ell^w) > \quad (2\text{-}39)$$

Where α=*t* or ϕ and $\bar{W}_{ni}^{s\alpha}$ is the i$_{th}$ BOR testing function and $\bar{J}_\ell^w$ is the ℓ$_{th}$ wire current basis function. This basis and testing functions can be expanded as in Eq.(2-29) to have the form:

$$Z_{n,i\ell}^{sw,\alpha} = \iint_s ds \int_\ell dh.jk\eta[\bar{W}_{ni}^{s\alpha}.\bar{J}_\ell^w - \frac{1}{k^2}(\nabla'_s.\bar{W}_{ni}^{s\alpha})(\nabla.\bar{J}_\ell^w)]\frac{e^{-jkR}}{4\pi R} \quad (2\text{-}40)$$

The dot product between basis function of wire in Eq.(2-8),(2-16) and testing function of BOR in Eq.(2-17) could have done to give

$$\bar{W}_{ni}^{st}.\bar{J}_\ell^w = f_i(t)f_\ell(h)e^{-jn\phi}(\hat{u}_t.\hat{u}_\ell^w) \quad (2\text{-}41a)$$

$$\bar{W}^{s\phi}.\bar{J}_\ell^w = f_i(t)f_\ell(h)e^{-jn\phi}(\hat{u}_\phi.\hat{u}_\ell^w) \quad (2\text{-}41b)$$

And the divergence of the two vectors $W_{ni}^{\alpha}(\acute{r})$ and $J_\ell^w(r)$ by using Eqs. (2-34) and (2-35), where the wire has one dimension, written as:

$$\nabla.\bar{J}_\ell^w = f'_\ell(h) \quad (2\text{-}42a)$$

$$\nabla.\bar{W}^{st} = f'_i(t)e^{-jn\phi} \quad (2\text{-}42b)$$

$$\nabla.\bar{W}^{s\phi} = \frac{jn}{\rho} f_i(t) e^{-jn\phi} \tag{2-42c}$$

For BOR [33]

$$\iint_s \; ds = \int_0^N dt \; \int_0^{2\pi} \rho d\phi \tag{2-43}$$

Substitute the last Eqs. (2-41), (2-42) and (2-43) into (2-40) this yields to

$$\left(Z_n^{sw,t}\right)_{i\ell} = \int_0^N dt \int_0^{2\pi} \rho d\phi \int_\ell dh.jk\eta[f_i(t)f_\ell(h)(\hat{u}_t.\hat{u}_\ell^w) - \frac{1}{k^2} f'_i(t) f'_\ell(h)\Big] e^{-jn\phi} \frac{e^{-jkR}}{4\pi R} \tag{2-44a}$$

$$\left(Z_n^{sw,\phi}\right)_{i\ell} = \int_0^N dt \int_0^{2\pi} \rho d\phi \int_\ell dh.jk\eta \left[f_i(t)f_\ell(h)\left(\hat{u}_\phi.\hat{u}_\ell^w\right) + \frac{jn}{k^2\rho} f_i(t) f'_\ell(h)\Big] e^{-jn\phi} \frac{e^{-jkR}}{4\pi R} \tag{2-44b}$$

For explicit solution to BOR and wire we must choose the $f_i(t)$ and $f_\ell(h)$, the *t* and *h* expansion functions by using Eqs. (2-11) and (2-16) in Eq. (2-44) to get:

$$\left(Z_n^{sw,t}\right)_{i\ell} = \frac{jk\eta}{4\pi} \int_0^N dt \int_0^{2\pi} \rho d\phi \int_\ell dh\,[T(t)T(h)(\hat{u}_t.\hat{u}_\ell^w) - \frac{1}{K^2} T'(t)T'(h)\Big] \frac{e^{-j(kR+n\phi)}}{R} \tag{2-45a}$$

$$\left(Z_n^{sw,\phi}\right)_{i\ell} = \frac{jk\eta}{4\pi} \int_0^N dt \int_0^{2\pi} \rho d\phi \int_\ell dh\left[T(t)T(h)\left(\hat{u}_\phi.\hat{u}_\ell^w\right) + \frac{jn}{k^2\rho} T(t)T'(h)\Big] \frac{e^{-j(kR+n\phi)}}{R} \tag{2-45b}$$

where *T* and *T'* is the triangle function and its derivative, respectively and is given in Eqs.(2-12),(2-13) and (2-14) for the BOR and wire for(*t*) and (*h*) integration, the *T* function is approximated by four pulses (*p*) for field point (BOR) and have a values of function and its derivative are $\frac{1}{8},\frac{3}{8},\frac{3}{8},\frac{1}{8}$ and $\frac{1}{2},\frac{1}{2},-\frac{1}{2},-\frac{1}{2}$, and (*q*) for source point (wire) and have values of function and its derivative are $\frac{1}{4},\frac{3}{4},\frac{3}{4},\frac{1}{4}$ and 1,1,-1,-1. Hence, the general relation for Z^{sw} can be written as

$$\left(Z_n^{sw,t}\right)_{i\ell} = \frac{jk\eta}{4\pi}\sum_{p=1}^{4}\sum_{q=1}^{4}\int_0^{2\pi} d\phi[T_p(t)T_q(h)\left(\hat{u}_t.\hat{u}_\ell^w\right) + \frac{1}{k^2}T'_p(t)T'_q(h)]\frac{e^{-j(kR_{pq}+n\phi)}}{R_{pq}} \quad (2\text{-}46a)$$

$$\left(Z_n^{sw,\phi}\right)_{i\ell} = \frac{jk\eta}{4\pi}\sum_{p=1}^{4}\sum_{q=1}^{4}\int_0^{2\pi} d\phi[T_p(t)T_q(h)\left(\hat{u}_\phi.\hat{u}_\ell^w\right) + \frac{jn}{k^2\rho_p}T_p(t)T'_q(h)]\frac{e^{-j(kR_{pq}+n\phi)}}{R_{pq}} \quad (2\text{-}46b)$$

Where $R_{pq}$is the position vector between BOR and wire, and take the form

$$R_{pq} = \left[\left(\rho_p\cos\phi - x_q\right)^2 + \left(\rho_p\sin\phi - y_q\right)^2 + \left(Z_p - Z_q\right)^2\right]^{1/2} \quad (2\text{-}47)$$

And the dot product between unit vectors $(\hat{u}_t.\hat{u}_\ell^w)$ and $(\hat{u}_\phi.\hat{u}_\ell^w)$ depends on the direction of wire where $\hat{u}_t$ and $\hat{u}_\phi$ are known, and the dot product processes are shown in table (2-1) for all possibilities of wire direction.

3-The wire – BOR Interaction matrix Z^{ws}

The submatrices Z_n^{ws}can be obtained from elements of Z_n^{sw}submatrices. According to the definition of basis and testing functions on the wire and on the BOR we have

$$Z_{n,\ell i}^{ws,\alpha} = < \bar{W}_\ell^w, L_s\left(\bar{J}_{nj}^{s\alpha}\right) > \quad (2\text{-}48)$$

Where α=*t* or ϕ, this equation could devolve into:

$(Z_n^{ws,\alpha})_{\ell i} = (Z_{-n}^{sw,\alpha})_{i\ell}$ or

$$(Z_n^{ws,\alpha})_{\ell i} = -(Z_n^{sw,\alpha})_{i\ell} \quad (2\text{-}49)$$

4-The wire-wire matrix elements Z^{ww}

According to definition of basis and testing functions on the wire itself, the *(ℓ, k)$_{th}$* wire-wire interaction matrix elements are defined as,

$$Z_{\ell k}^{ww} = < \bar{W}_k^w, L_w(\bar{J}_\ell^w) > \quad (2\text{-}50)$$

Where $\bar{W}_k^w$ is the k_{th} wire testing function and $\bar{J}_\ell^w$is the ℓ_{th} wire current basis function, and $L_w(\bar{J}_\ell^w)$ is one dimensional operator on the wire current density.

Expand Eq.(2-50) by using Eq. (2-29) to give :

$$Z_{\ell k}^{ww} = \int_{\ell} dh \int_{k} dh'.jk\eta \left[\left(\vec{W}_k^w . \vec{J}_\ell^w \right) - \frac{1}{k^2} \left(\nabla' . \vec{W}_k^w \right) \left(\nabla . \vec{J}_\ell^w \right) \right] \frac{e^{-jkR}}{4\pi R} \qquad (2\text{-}51)$$

The basis and testing functions are defined in Eqs. (2-8),(2-16) and (2-18), the using of these equations are related to

$$\left.\begin{aligned} \vec{W}_k^w . \vec{J}_\ell^w &= f_k(h') f_\ell(h) (\hat{u}_k^w . \hat{u}_\ell^w) \\ \nabla . \vec{W}_k^w &= f'_k(h') \\ \nabla . \vec{J}_\ell^w &= f'_\ell(h) \end{aligned}\right\} \qquad (2\text{-}52)$$

Now , applying Eq.(2-52) in Eq.(2-51) we get the general form of interaction matrix between wire-wire, as follow:

$$Z_{\ell k}^{ww} = \int_{\ell} dh \int_{k} dh'.jk\eta \left[f_k(h') f_\ell(h) (\hat{u}_k^w . \hat{u}_\ell^w) - \frac{1}{k^2} f'_k(h') f'_\ell(h) \right] \frac{e^{-jkR}}{4\pi R} \qquad (2\text{-}53)$$

Where $\hat{u}_\ell^w$ and $\hat{u}_k^w$ are unit vectors along ℓ_{th} and k_{th} segments on the wire. For (h) and (h') integrations, the T and T' functions are approximated by four pulses in source and field point by useful application of Eq. (2-16), the Eq. (2-53) becomes:

$$Z_{\ell k}^{ww} = \frac{jk\eta}{4\pi} \sum_{p=1}^{4} \sum_{q=1}^{4} [T_p(h) T_q(h') (\hat{u}_\ell^w . \hat{u}_k^w) - \frac{1}{k^2} T'_p(h) T'_q(h')] \frac{e^{-jkR_{pq}}}{R_{pq}} \qquad (2\text{-}54)$$

Where R_{pq} is the position vector between the source and field point on the wire segments, and have the general form:

$$R_{pq} = |r - r'| = [(x_p - x_q)^2 + (y_p - y_q)^2 + (z_p - z_q)^2]^{1/2} \qquad (2\text{-}55)$$

2.2.3.1.2 Junction – dependent impedance elements

1-The junction – junction matrix elements Z^{ij}

The junction element Z^{ij} is considered first. Referring to Eq. (2-9), the junction basis function consists of a disk term and wire attachment term. The planar annular disk patch S_d is assumed to approximate the BOR surface at

the junction point (Fig. (2-2)). This assumption is satisfactory when the disk radius b is much less than the BOR radius of curvature (ρ) at the attachment point, mean that $b<<\rho$, and the disk diameter is small compared to a wavelength. The self – impedance element at the wire / surface junction region Z^{jj} is described as follow:

$$Z^{jj} =< \bar{W}_a^j, L_j(\bar{J}_a^j) > +< \bar{W}_d^j, L_j(\bar{J}_d^j) > +< \bar{W}_d^j, L_j(\bar{J}_a^j) > +< \bar{W}_a^j, L_j(\bar{J}_d^j) > \quad (2\text{-}59)$$

This equation can be re-written in more details

$$\begin{aligned} Z^{jj} &= \int_0^{h0} dh' \int_0^{h0} dh.jk\eta\,[\bar{W}_a^j.\bar{J}_a^j - \tfrac{1}{k^2}(\nabla'.\bar{W}_a^j)(\nabla.\bar{J}_a^j)]\tfrac{e^{-jkR}}{4\pi R} + \\ &\int_{-\pi}^{\pi} d\varphi' \int_a^b dr' \int_{-\pi}^{\pi} d\varphi \int_a^b dr.jk\eta\left[\bar{W}_d^j.\bar{J}_d^j - \tfrac{1}{k^2}\left(\nabla'.\bar{W}_d^j\right)\left(\nabla.\bar{J}_d^j\right)\right]\tfrac{e^{-jkR}}{4\pi R} + \\ &\int_0^{h0} dh \int_a^b dr \int_{-\pi}^{\pi} d\varphi\,.jk\eta\,[\bar{W}_d^j.\bar{J}_a^j - \tfrac{1}{k^2}(\nabla'.\bar{W}_d^j)(\nabla.\bar{J}_a^j)]\,\tfrac{e^{-jkR}}{4\pi R} + \\ &\int_0^{h0} dh \int_a^b dr \int_{-\pi}^{\pi} d\varphi\,.jk\eta\,\left[\bar{W}_a^j.\bar{J}_d^j - \tfrac{1}{k^2}\left(\nabla'.\bar{W}_a^j\right)\left(\nabla.\bar{J}_d^j\right)\right]\tfrac{e^{-jkR}}{4\pi R} \end{aligned} \quad (2\text{-}60)$$

For simplicity and shorten the steps we will use here and in the rest of submatrices in junction – dependent, the concept of triangle functions in the definition of the basis and testing functions directly. From Eqs. (2-9)and (2-19) we get

$$\left.\begin{aligned} \bar{\mathrm{W}}_{\mathrm{a}}^{\mathrm{j}}.\bar{\mathrm{J}}_{\mathrm{a}}^{\mathrm{j}} &= \tfrac{1}{4\pi^2 aa'}\,T_a(h')T_a(h)(\hat{u}_{\acute{a}}.\hat{u}_a) \\ \bar{\mathrm{W}}_{\mathrm{d}}^{\mathrm{j}}.\bar{\mathrm{J}}_{\mathrm{d}}^{\mathrm{j}} &= \tfrac{1}{4\pi^2 rr'}\,\tfrac{1}{(b-a)^2}(b-r')(b-r)(\hat{u}_{\acute{r}}.\hat{u}_r) \\ \bar{\mathrm{W}}_{\mathrm{d}}^{\mathrm{j}}.\bar{\mathrm{J}}_{\mathrm{a}}^{\mathrm{j}} &= \tfrac{1}{4\pi^2 ar}T_a(h)\tfrac{(r-b)}{(b-a)}\,(\hat{u}_a.\hat{u}_r) \\ \bar{\mathrm{W}}_{\mathrm{a}}^{\mathrm{j}}.\bar{\mathrm{J}}_{\mathrm{d}}^{\mathrm{j}} &= \tfrac{1}{4\pi^2 ar}T_a(h)\tfrac{(r-b)}{(b-a)}(\hat{u}_a.\hat{u}_r) \end{aligned}\right\} \quad (2\text{-}61)$$

and

$$\left.\begin{aligned} \nabla'.\bar{\mathrm{W}}_{\mathrm{a}}^{\mathrm{j}} &= \tfrac{1}{2\pi a'}T'_a(h) \\ \nabla.\bar{\mathrm{J}}_{\mathrm{a}}^{\mathrm{j}} &= \tfrac{1}{2\pi a}T'_a(h) \\ \nabla'.\bar{\mathrm{W}}_{\mathrm{d}}^{\mathrm{j}} &= \tfrac{1}{2\pi r'}\tfrac{1}{(b-a)} \\ \nabla.\bar{\mathrm{J}}_{\mathrm{d}}^{\mathrm{j}} &= \tfrac{1}{2\pi r}\tfrac{1}{(b-a)} \end{aligned}\right\} \quad (2\text{-}62)$$

Where $\nabla.J_d^j = \frac{1}{r}\frac{d}{dr}(rJ^r)$ (2-63)

By substituted Eqs.(2-61) and (2-62) in Eq. (2-60), the general equation for junction region with vanishing conditions of currents at $r=a$ and $r=b$, lead to:

$$Z^{jj} = \frac{jk\eta}{4\pi}\int_0^{h0} dh' \int_0^{h0} dh \left[T_a(h')T_a(h)(\hat{u}_{\acute{a}}.\hat{u}_a) - \frac{1}{k^2}\, T_a(h')T_a(h)\right]\frac{e^{-jkR}}{R} + \frac{jk\eta}{16\pi^3(b-a)^2}\int_{-\pi}^{\pi} d\varphi' \int_a^b dr' \int_{-\pi}^{\pi} d\varphi \int_a^b dr \left[(b-r')\,(b-r)(\hat{u}_{\acute{r}}.\hat{u}_r) - \frac{1}{k^2}\right]\frac{e^{-jkR}}{R} + \frac{jk\eta}{8\pi^2(b-a)}\int_0^{h0} dh \int_a^b dr \int_{-\pi}^{\pi} d\varphi \left[T_a(h)(r-b)(\hat{u}_a.\hat{u}_r) - \frac{1}{k^2}T'_a(h)\right]\frac{e^{-jkR}}{R} + \frac{jk\eta}{8\pi^2(b-a)}\int_0^{h0} dh \int_a^b dr \int_{-\pi}^{\pi} d\varphi \left[T_a(h)(r-b)(\hat{u}_a.\hat{u}_r) - \frac{1}{k^2}T'_a(h)\right]\frac{e^{-jkR}}{R}$$

(2-64)

It can be seen the impedance Z^{jj} of the junction region is composed of four terms, the self-impedance between wire antennas the mutual – impedance between the wire and disk, and the self impedance between disks. The second term in Eq. (2-64) is the self – impedance element between disks, which is expressed as Z_{pp}^{jj}, there is a singularity in Z_{pp}^{jj} when $r' \rightarrow r$

$$Z_{pp}^{jj} = \frac{jk\eta}{16\pi^3(b-a)^2}\int_{-\pi}^{\pi} d\varphi' \int_a^b dr' \int_{-\pi}^{\pi} d\varphi \int_a^b dr \left[(b-r')\,(b-r)(\hat{u}_{\acute{r}}.\hat{u}_r) - \frac{1}{k^2}\right]\frac{e^{-jkR}}{R} \qquad (2\text{-}65)$$

Where $\hat{u}_{\acute{r}}.\hat{u}_r = \cos(\varphi - \varphi')$ and $\vec{R}$ the position vector is given by (2-24), good idea has been suggested by [85] to deal with solution of singularity.

In Eq. (2-65) , Let:

$\alpha = \varphi - \varphi', \quad d\alpha = d\varphi'$

$\beta = \varphi + \varphi', \quad d\beta = d\varphi$

According to the integral domain of Eq. (2-65), convert the integral domain φ and φ' to α and β, and suppose

$$\left.\begin{aligned} Z(r,r') &= \int_{-\pi}^{\pi} d\varphi' \int_{-\pi}^{\pi} d\varphi \left[(b-r')(b-r)\cos(\varphi-\varphi') - \frac{1}{k^2}\right]\frac{e^{-jkR}}{R} \\ &= \frac{1}{2}\int_{\alpha} d\alpha \int_{\beta} d\beta f(\alpha) \\ &= \frac{1}{2}\int_{-2\pi}^{0} f(\alpha)d\alpha \int_{-2\pi-\alpha}^{2\pi+\alpha} d\beta + \frac{1}{2}\int_{0}^{2\pi} f(\alpha)d\alpha \int_{-2\pi+\alpha}^{2\pi-\alpha} d\beta \\ &= \frac{8\pi}{2}\int_{0}^{\pi} f(\alpha)d\alpha - \int_{0}^{2\pi} f(\alpha)\alpha d\alpha + 4\pi\int_{0}^{\pi} f(\alpha)d\alpha - \int_{0}^{2\pi} f(\alpha)\alpha d\alpha \\ &= 8\pi\int_{0}^{\pi} f(\alpha)d\alpha - 2\int_{0}^{2\pi} f(\alpha)\alpha d\alpha \end{aligned}\right\} \quad (2\text{-}66)$$

Where

$$f(\alpha) = \left[(b-r')(b-r)\cos\alpha - \frac{1}{k^2}\right]\frac{e^{-jkR}}{R} \quad (2\text{-}67)$$

Suppose $\alpha = 2\pi - \delta$

$\cos\alpha = \cos\delta$, It can be obtain

$$\int_{0}^{2\pi} f(\alpha)\alpha d\alpha = \int_{0}^{2\pi} f(\delta)(2\pi-\delta)d\delta = 2\pi\int_{0}^{2\pi} f(\delta)d\delta - \int_{0}^{2\pi} f(\delta)d\delta \quad (2\text{-}68)$$

So ,

$$\int_{0}^{2\pi} f(\alpha)\alpha d\alpha = \pi\int_{0}^{2\pi} f(\alpha)d\alpha = 2\pi\int_{0}^{\pi} f(\alpha)d\alpha \quad (2\text{-}69)$$

Using Eq. (2-69) in (2-66) to get

$$Z(r,r') = 4\pi\int_{0}^{\pi} f(\alpha)d\alpha \quad (2\text{-}70)$$

So, the self-impedance term between disks

$$\begin{aligned} Z_{pp}^{jj} &= \frac{jk\eta}{16\pi^3(b-a)^2}\, 4\pi\int_{a}^{b} dr' \int_{a}^{b} dr\; Z(r,r') \\ &= \int_{a}^{b} dr' \int_{a}^{b} dr \left[(b-r')(b-r).g_1 - \frac{1}{k^2}h_1\right] \end{aligned} \quad (2\text{-}71)$$

Where

$$g_1 = \frac{1}{\pi}\int_{0}^{\pi} \frac{e^{-jkR}}{R}\cos\alpha\, d\alpha \quad (2\text{-}72a)$$

$$h_1 = \frac{1}{\pi}\int_{0}^{\pi} \frac{e^{-jkR}}{R} d\alpha \quad (2\text{-}72b)$$

and

$R = [R_0^2 - 2rr'\cos\alpha]^{1/2}$ where $R_0 = \sqrt{r'^2 + r^2}$ $(r,r')\epsilon[a,b]$

Using Watson's formula [31] deduced that

$$e^{-jkR} = e^{-jkR_0} + \sum_{m=1}^{\infty} \frac{(k^2 rr')^m h_{m-1}^2(KR_0)}{n!(KR_0)^{m-1}} cos^m\alpha \quad (2\text{-}73)$$

Where h_{m-1}^2 is the spherical Henkel function of the second kind of order $m-1$. Substituting Eq.(2-73) in Eq. (2-72) and making use of a recursion relation of spherical Henkel function, then:

$$G^n(r,r') = \delta_{n,0} \frac{e^{-jkR_0}}{R_0} - jk \sum_{m=1}^{\infty} A_m^n h_m^2(KR_0)(\frac{Krr'}{KR_0})^m \quad (2\text{-}74)$$

Where, $\delta_{n,0} = \begin{cases} 1 & for\ m = 0 \\ 0 & otherwise \end{cases}$ (2-75)

and, $A_m^n = \frac{1}{\pi m!}\int_0^{\pi} cos^m\alpha \cos(n\alpha)\, d\alpha$ (2-76)

The spherical Henkel function $h_m^2(KR_0)$ can be expanded as [118]:

$$h_m^2(KR_0) = j^{m+1} \frac{e^{-jkR_0}}{kR_0} \sum_{\ell=0}^{m} \frac{(m+\ell)!}{\ell!(m-\ell)!} \frac{1}{(j2KR_0)^{\ell}} \quad (2\text{-}77)$$

Form (2-77) and (2-74), we get:

$$G^n(r,r') = \frac{e^{-jkR_0}}{R_0} [\delta_{n,0} + \sum_{m=1}^{\infty} \sum_{\ell=0}^{m} B_{m,\ell}^n \frac{(K^2 rr')^m}{(KR_0)^{m+\ell}}] \quad (2\text{-}78)$$

Where $B_{m,\ell}^n = A_m^n \frac{(m+\ell)!}{\ell!(m-\ell)!} \frac{j^{m-\ell}}{(2)^{\ell}}$ (2-79)

For disk n=1 [85], then

$$G^n(r,r') = \frac{e^{-jkR_0}}{R_0} [1 + \sum_{m=1}^{\infty} (r.r')^m \sum_{\ell=0}^{m} \frac{(k^2)^m}{(kR_0)^{m+\ell}} \frac{(m+\ell)!}{\ell!(m-\ell)!} \frac{j^{m-\ell}}{(2)^{\ell}} \frac{1}{\pi m!} \int_0^{\pi} cos^m\alpha \cos\alpha d\alpha] \quad (2\text{-}80)$$

Therefore, Eq. (2-72) by using Eq. (2-80) becomes

$$g_1 = \frac{e^{-jkR_0}}{R_0} \left\{ \frac{1}{\pi} \int_0^{\pi} \cos\alpha\, d\alpha + \sum_{m=1}^{\infty} (r'.r)^m [\sum_{\ell=0}^{m} \frac{(m+\ell)!}{m!\ell!(m-\ell)!} \cdot 2^{-\ell}(jK)^{m-\ell} R_0^{-(m+\ell)}] \int_0^{\pi} \cos^{\mathrm{m}}\alpha \cos\alpha\, d\alpha \right\} \quad (2\text{-}81)$$

$$h_1 = \frac{e^{-jkR_0}}{R_0} \left\{ 1 + \sum_{m=1}^{\infty} (r'.r)^m \left[\sum_{\ell=0}^{m} \frac{(m+\ell)!}{m!\ell!(m-\ell)!} . 2^{-\ell}(jK)^{m-\ell} R_0^{-(m+\ell)} \right] \int_0^{\pi} \cos^{\mathrm{m}}\alpha\, d\alpha \right\} \quad (2\text{-}82)$$

So, the singularity in integral Eq. (2-64) can be extracted, and

$$Z^{jj} = \frac{jk\eta}{4\pi}\sum_{p=1}^{2}\sum_{q=1}^{2}[T_p(h)T_q(h') - \frac{1}{k^2}T'_p(h)T'_q(h')]\,h_1 + \frac{jk\eta}{4\pi(b-a)^2}\int_a^b dr'\int_a^b dr\,[(b-r')(b-r).g_1 - \frac{1}{k^2}h_1] + \frac{jk\eta}{4\pi(b-a)}\sum_{q=1}^{2} - \frac{T_p(h')}{k^2}\int_a^b dr\,h_1 \quad (2\text{-}84)$$

2-The BOR – junction matrix elements Z^{sj}

The BOR-junction impedance elements are given by

$$Z_{n,j}^{sj,\alpha} = < \bar{W}_{ni}^{s\alpha}, L_j(\bar{J}_a^j) > + < \bar{W}_{ni}^{s\alpha}, L_j(\bar{J}_d^j) > \quad (2\text{-}85)$$

and can take the form:

$$Z_{n,j}^{sj,\alpha} = \int_0^N dt\int_0^{2\pi}\rho d\phi\int_0^{h0} dh.jk\eta\left[W_{ni}^{s\alpha}.J_a^i - \frac{1}{k^2}(\nabla'.\bar{W}_{ni}^{s\alpha})(\nabla.\bar{J}_a^i)\right]\frac{e^{-jkR}}{4\pi R} + \int_0^N dt\int_0^{2\pi}\rho d\phi\int_{-\pi}^{\pi}d\varphi\int_a^b dr.jk\eta\,[W_{ni}^{s\alpha}.J_d^i - \frac{1}{k^2}(\nabla'.\bar{W}_{ni}^{s\alpha})(\nabla.\bar{J}_d^i)\frac{e^{-jkR}}{4\pi R} \quad (2\text{-}86)$$

Where α=t or ϕ, is the mode number, and $\bar{W}_{ni}^{s\alpha}$ is the testing function associated with the i_{th} BOR annulus. First simplification of the Eq. (2-86) is hold by the process of dot product and divergence of basis and testing functions for BOR and junction, which is given in Eqs. (2-17) and (2-9), as follow:

$$\left.\begin{aligned}
\bar{W}_{ni}^{st}.\bar{J}_a^i &= \frac{1}{2\pi a}T(t)T_a(h)e^{-jn\phi}(\hat{u}_t.\hat{u}_a)\\
\bar{W}_{ni}^{s\phi}.\bar{J}_a^i &= \frac{1}{2\pi a}T(t)T_a(h)e^{-jn\phi}(\hat{u}_\phi.\hat{u}_a)\\
\bar{W}_{ni}^{st}.\bar{J}_d^i &= \frac{1}{2\pi r}\frac{r-b}{b-a}T(t)e^{-jn\phi}(\hat{u}_t.\hat{u}_r)\\
\bar{W}_{ni}^{s\phi}.\bar{J}_d^i &= \frac{1}{2\pi r}\frac{r-b}{b-a}T(t)e^{-jn\phi}(\hat{u}_\phi.\hat{u}_r)
\end{aligned}\right\} \quad (2\text{-}87a)$$

$$\left.\begin{aligned}
\nabla.\bar{W}_{ni}^{st} &= T'(t)e^{-jn\phi}\\
\nabla.\bar{W}_{ni}^{s\varphi} &= -\frac{jn}{\rho}T(t)e^{-jn\phi}\\
\nabla.\bar{J}_a^i &= \frac{1}{2\pi a}T'_a(h)\\
\nabla.\bar{J}_d^i &= \frac{1}{2\pi r}\frac{1}{b-a}
\end{aligned}\right\} \quad (2\text{-}87b)$$

In order to get the same value of current for attachment part of junction in each annulus of the body, a new formula of $T_a(h)$ can be introduced as follow:

$$T_a = \frac{h_0 - h}{h_0} \quad and \quad T'_a = \frac{d}{dh} T_a(h) = \frac{1}{h_0} \tag{2-88}$$

Thus, the general form of Eq. (286) is taken by substituting of Eqs. (2-87) and (2-88) to give:

$$\begin{aligned}\left(Z_n^{sj,t}\right)_i = {} & \frac{jk\eta}{4\pi h_0} \sum_{p=1}^{4} \int_0^{2\pi} d\phi \int_0^{h0} dh \left[T_p(t)\,(h_0 - h)(\hat{u}_t . \hat{u}_a) - \frac{1}{k^2} T'_p(t)\right] \\ & \frac{e^{-j(kR_{pq1} + n\varphi)}}{R_{pq1}} + \frac{jk\eta}{8\pi^2 (b-a)} \sum_{p=1}^{4} \int_0^{2\pi} d\phi \int_{-\pi}^{\pi} d\varphi \int_a^b dr \\ & \left[T_p(t)\,(r-b)(\hat{u}_t . \hat{u}_r) - \frac{1}{k^2} T'_p(t)\right] \frac{e^{-j(kR_{pq2} + n\phi)}}{R_{pq2}}\end{aligned} \tag{2-89a}$$

$$\begin{aligned}\left(Z_n^{sj,\phi}\right)_i = {} & \frac{jk\eta}{4\pi h_0} \sum_{p=1}^{4} \int_0^{2\pi} d\phi \int_0^{h0} dh \left[T_p(t)(h_0 - h)\left(\hat{u}_\phi . \hat{u}_a\right) + \frac{jn}{k^2 \rho_p} T_p(t)\right] \\ & \frac{e^{-j(kR_{pq1} + n\phi)}}{R_{pq1}} + \frac{jk\eta}{8\pi^2 (b-a)} \sum_{p=1}^{4} \int_0^{2\pi} d\phi \int_{-\pi}^{\pi} d\varphi \int_a^b dr \\ & \left[T_p(t)\,(r-b)\left(\hat{u}_\phi . \hat{u}_r\right) - \frac{1}{k^2} T'_p(t)\right] \frac{e^{-j(kR_{pq2} + n\phi)}}{R_{pq2}}\end{aligned} \tag{2-89b}$$

Where R_{pq1} is the position vector between attachment part and BOR, R_{pq2} is the positions vetor between disk and BOR, which can be determined by using Eq. (2-24).

3-The junction – BOR interaction matrix Z^{js}

The junction – BOR matrix elements can be obtained from the submatricies of BOR – junction element as follow

$$Z_{n,i}^{js,\alpha} = < \bar{W}_a^j , L(\bar{J}_{ni}^{s\alpha}) > + < \bar{W}_d^j , L(\bar{J}_{ni}^{s\alpha}) > \tag{2-92}$$

$$(Z_n^{js,\alpha})_i = (Z_{-n}^{sj,\alpha})_i \tag{2-93}$$

Where α=t or ϕ with respect to BOR.

4-The wire – junction matrix Z^{wj}

The wire – junction matrix elements Z_ℓ^{wj} are defined from the interaction of testing function of wire $\bar{W}_\ell^w$ and the two parts of basis function region, $\bar{J}_a^i$ and $\bar{J}_d^i$, as follow

$$Z_\ell^{wj} =< \bar{W}_\ell^w, L_j(\bar{J}_a^i) > \; + < \bar{W}_\ell^w, L_j(\bar{J}_d^i) \qquad (2\text{-}94)$$

Where $\bar{J}_a^i$ and $\bar{J}_d^i$ is the basis function in attachment segment and disk region of junction, respectively. From the application of Eq. (2-29) the Eq. (2-94) have the form:

$$\begin{aligned} Z_\ell^{wj} = & \int_\ell dh' \int_0^{h0} dh.jk\eta \left[\bar{W}_\ell^w.\bar{J}_a^i - \frac{1}{k^2}(\nabla'.\bar{W}_\ell^w)(\nabla.\bar{J}_a^i)\right]\frac{e^{-jkR}}{4\pi R} + \\ & \int_\ell dh' \int_a^b dr \int_{-\pi}^{\pi} d\varphi\,.jk\eta \left[\bar{W}_\ell^w.\bar{J}_d^i - \frac{1}{k^2}(\nabla'.\bar{W}_\ell^w)(\nabla.\bar{J}_d^i)\right]\frac{e^{-jkR}}{4\pi R} \end{aligned} \qquad (2\text{-}95)$$

Implies the testing function of wire from Eqs. (2-16), (2-18) and the basis function from Eqs. (2-9) and (2-16) to reduce the first and second term of Eq. (2-95) to the following forms:

$$\left.\begin{aligned} \bar{W}_\ell^w.\bar{J}_a^i &= \frac{1}{2\pi a} f'_\ell(h') f_a(h)(\hat{u}_\ell^w.\hat{u}_a) \\ \bar{W}_\ell^w.\bar{J}_d^i &= \frac{1}{2\pi r}\frac{r-b}{b-a} f_\ell(h')(\hat{u}_\ell^w.\hat{u}_r) \end{aligned}\right\} \qquad (2\text{-}96a)$$

and,

$$\left.\begin{aligned} \nabla'.\bar{W}_\ell^w &= f'_\ell(h') \\ \nabla.\bar{J}_a^i &= \frac{1}{2\pi a} f'_a(h) \\ \nabla.\bar{J}_d^i &= \frac{1}{2\pi r}\frac{1}{b-a} \end{aligned}\right\} \qquad (2\text{-}96b)$$

Note that the divergence for $J^j = \bar{J}_d^i$ is expressed in terms of the coordinate system of planar disk and implies that in the disk region, the radial component of current J^r is much greater than the a azimuthal component J^φ.

By applying the Eqs. (2-96) with the advantage of triangle function formula, in Eq. (2-95), the general formula of wire – junction interaction matrix becomes:

$$Z_{\ell}^{wj} = \int_{\ell} dh' \int_{0}^{h0} dh.jk\eta \left[T_{\ell}(h')T_{a}(h)(\hat{u}_{\ell}^{w}.\hat{u}_{a}) - \frac{1}{k^2}T'_{\ell}(h')T'_{a}(h)\right]\frac{e^{-jkR}}{4\pi R} + \frac{1}{2\pi(b-a)}\int_{\ell} dh' \int_{a}^{b} dr \int_{-\pi}^{\pi} d\varphi.jk\eta \left[T_{\ell}(h')(r-b)(\hat{u}_{\ell}^{w}.\hat{u}_{r}) - \frac{1}{k^2}T'_{\ell}(h')\right]\frac{e^{-jkR}}{4\pi R} \quad (2\text{-}97)$$

Where the boundary condition at $r=b$ and $r=a$ imposed that neglected the $\frac{1}{r}$ and $\frac{1}{a}$ factors. Using the same concept defined previously for the reduction of the integral on *(h)* and *(h')* by triangle function *T* and its derivative *T'* pluses, the new form of Eq. (2-97) can be written as:

$$Z_{\ell}^{wj} = \frac{jk\eta}{4\pi}\sum_{p=1}^{4}\sum_{q=1}^{2}[T_{p}(h')T_{q}(h)\,(\hat{u}_{\ell}^{w}.\hat{u}_{a}) - \frac{1}{k^2}T'_{p}(h')T'_{q}(h)]\;\frac{e^{-jkR_{pq}}}{R_{pq}} - \frac{jk\eta}{8\pi^2(b-a)}\sum_{p=1}^{4}\int_{a}^{b} dr \int_{-\pi}^{\pi} d\varphi\,[T'_{p}(h')(r-b)(\hat{u}_{\ell}^{w}.\hat{u}_{r}) - \frac{1}{k^2}T'_{p}(h')]\frac{e^{-jkR_{pq}}}{R_{pq}} \quad (2\text{-}98)$$

5- The junction – wire matrix Z^{jw}

The junction – wire elements is equal to the transpose of wire-junction matrix elements, as follow:

$$Z^{jw} = transpose\ Z^{wj} \quad (2\text{-}99)$$

2.2.4 Evaluation of driving vector and far field components

The procedure of measurement matrix or linear measurement by J.R. Mautz and R.F. Harrington [8] is utilized to evaluate the driving and the far scattered fields for CBOR. Furthermore; components of the field at a point, voltage along given conductor and current crossing a given surface are linear measurements [59].

Note that the excitation matrix is resulting from induced current on body surface and measurement matrix is result from far scatted fields produced induced currents.

So, any linear measurement of the field from a current *J* on a body *S* can be expressed as a linear functional of *J*, that is

$$(V) = < \bar{J}, \bar{E}^{inc} > \quad (2\text{-}100)$$

According to the reciprocity theorem one can find radiation field $\bar{E}^r$at distance *r* from origin due to current *J* on *S*

$$\bar{E}^r . \hat{u}_r = -\frac{jw\mu}{4\pi r} e^{-jk_0 r} \int_s \bar{E}^r . \bar{J}(r') \quad (2\text{-}101)$$

Where $\hat{u}_r$ is the unit vector specifying the polarization of the incident wave.

$$\bar{E}^r = \hat{u}_r e^{j\hat{k}.\bar{r}_i} \quad (2\text{-}102)$$

Eq. (2-102) is arbitrary plane wave of superposition of two orthogonal components, E_θ and E_ϕ, and its unit vectors are

$$\hat{u}_r^\theta = \cos\theta_r \cos\phi_r \ \hat{x} + \cos\theta_r \sin\phi_r \ \hat{y} - \sin\theta_r \ \hat{z} \quad (2\text{-}103a)$$

$$\hat{u}_r^\phi = -\sin\phi_r \hat{x} + \cos\phi_r \ \hat{y} \quad (2\text{-}103b)$$

and $\hat{k} = k.k_0$ is the wave number unit vector in the direction of propagation $\bar{r}_i$ is the vector pointing from origin.

From MoM solution, the current is given by a superposition $J = \sum I_j J_j$, and Eq. (2-100) is reduced to be

$$Measurement = [\ R\ ][\ I\ ] \quad (2\text{-}104)$$

Where [*I*] is the matrix in (2-26) which has the form

$$[\ I\ ]=[\ Y\ ][\ V\ ] \quad (2\text{-}105a)$$

Where [*Y*]=1/[*Z*] is the inverse of the total [*Z*], and [*R*] is the measurement row matrix

$$[R]=\left[< \vec{J}_i, \bar{E}_u^r >\right] \ , \ u=\theta \text{ or } \phi \text{ polarization} \quad (2\text{-}105b)$$

By using Eqs. (2-101) and (2-102), we get

$$\bar{E}^i . \hat{u}_r = -\frac{jw\mu}{4\pi r} e^{-jk_0 r} [\ R\ ][\ I\ ] \quad (2\text{-}106)$$

So, for scattering problem (BOR – wire – junction) in the system matrix (2-27) the entire column voltage vector is full. Each element corresponds to the excitation caused by the electric field of the incident wave at each port is written as:

$$[V] =< \bar{W}, \bar{E}_u^r >] = [< \bar{J}^*, \bar{E}_u^r >] \quad (2\text{-}107)$$

Where $\bar{W}$ is the appropriate testing function corresponding to the BOR the wire, or the junction and $\bar{J}^*$ is the complex conjugate of the corresponding basis function. Therefore, the generalized voltage vector in (2-107) can be obtained from (2-105b) for BOR, wire, and junction as follow:

2.2.4.1 BOR

For BOR, the expansion for *J* can be separated into *t*– and ϕ- directed components, according to Eq. (2-105b) for θ-polarized $(\hat{u}_r = \hat{u}_r^{\theta})$ in Eq. (2-102), lead to:

$$(R_n^{\alpha\theta})_i =< \bar{J}_{ni}^{\alpha}, \bar{E}_{\theta}^r > \quad (2\text{-}108a)$$

and for ϕ-polarized , $\hat{u}_r = \hat{u}_r^{\phi}$

$$(R_n^{\alpha\phi})_i =< \bar{J}_{ni}^{\alpha}, \bar{E}_{\phi}^r > \quad (2\text{-}108b)$$

Where α=t or ϕ

From the required dot product of unit vectors $\hat{u}_t, \hat{u}_{\phi}, \hat{u}_{\theta}^r \, , and \, \hat{u}_{\phi}^r$, which is given in Eqs. (2-12) and (2-103) , as in appendix (D) one can get

$$\bar{k}.\bar{r} = k_0[\rho \sin\theta_r \cos\phi + z\cos\theta_r] \quad (2\text{-}109)$$

And from this result the electric field in Eq. (2-102) can be written as

$$\bar{E}_{\theta}^r = \hat{u}_{\theta}^r \, e^{-jk_0[\rho \sin\theta_r \cos\phi + z\cos\theta_r]} \quad (2\text{-}110a)$$

$$\bar{E}_{\phi}^r = \hat{u}_{\phi}^r e^{-jk_0[\rho \sin\theta_r \cos\phi + z\cos\theta_r]} \quad (2\text{-}110b)$$

By axisymmetric of BOR Eqs. (2-110) are given the form:

$$(R_n^{\alpha\theta})_i = \iint_s \bar{J}_{ni}^{\alpha}.\bar{E}_{\theta}^{r}\, ds \quad \text{.....}\theta\text{-polarized} \tag{2-111}$$

$$(R_n^{\alpha\phi})_i = \iint_s \bar{J}_{ni}^{\alpha}.\bar{E}_{\phi}^{r}\, ds \quad \text{.....}\phi\text{-polarized} \tag{2-112}$$

Eqs. (2-111) and (2-112) give four probabilities of *R* which can be written as in appendix (D), as follow:

$$\left.\begin{aligned}
(R_n^{t\theta})_i &= \sum_{q=1}^{4} C_q \left[\sin v_q \cos\theta_r \left(J_{n+1}(x) - J_{n-1}(x) + 2j\cos v_q \sin\theta_r J_n(x)\right)\right] \\
(R_n^{\phi\theta})_i &= \sum_{q=1}^{4} jC_q \cos\theta_r \left(J_{n+1}(x) - J_{n-1}(x)\right) \\
(R_n^{t\phi})_i &= \sum_{q=1}^{4} -jC_q \sin v_q \left(J_{n+1}(x) - J_{n-1}(x)\right) \\
(R_n^{\phi\phi})_i &= \sum_{q=1}^{4} C_q \left(J_{n+1}(x) - J_{n-1}(x)\right)
\end{aligned}\right\} \tag{2-113}$$

Where, $J_n(x) = J_n(k\rho_p \sin\theta_r)$ and $C_q = \pi j^{n+1} T_q e^{jkz_q \cos\theta_r}$.

In general , $R_n^{t\theta}$ and $R_n^{\phi\phi}$ are even in *n* , while $R^{t\phi}$ and $R^{\phi\theta}$ are odd in *n*. compare Eq. (2-7) and Eq.(2-17) the excitation matrix $[V_n]$ differ from the measurement matrix $[R_n]$ by the sign of *n*. for plane wave excitation with axially incident plane wave only *n=±1* mode are excited, and:

$$(V_n^{\alpha\beta})_j = (R_{-n}^{\alpha\beta}) \tag{2-114}$$

Where *αβ* represents *tθ*, *ϕθ*, *tϕ*, or *ϕϕ*.

2.2.4.2- Wire

The contribution to $\bar{R}^u$ from the wire is given by

$$R^{w,u} = < \bar{J}_{\ell}^{w}, \bar{E}_{u}^{r} > \tag{2-115}$$

Where u=θ or φ is the polarization, thus

$$E^r = E_{\theta}^{r} + E_{\phi}^{r} \tag{2-116}$$

by using Eq. (2-116) in Eq. (2-115) to get

$$R^{w,\theta} = < \bar{J}_{\ell}^{w}, \bar{E}_{\theta}^{r} > \tag{2-117a}$$

$$R^{w,\phi} = < \bar{J}_{\ell}^{w}, E_{\phi}^{r} > \tag{2-117b}$$

$\bar{E}_\theta^r$ and E_ϕ^r are defined in Eq. (2-110) and $\bar{J}_\ell^w$ in Eq. (2-8), by substituting these equations in (2-117), obtaining:

$$R^{w,\theta} = \int_\ell dh \int_0^{2\pi} d\phi \left[T_\ell(h) e^{jx\cos\phi}\, e^{jz\cos\theta_r}\right](\hat{u}_\ell^w \cdot \hat{u}_\theta^r) \quad (2\text{-}118)$$

$$R^{w,\phi} = \int_\ell dh \int_0^{2\pi} d\phi \left[T_\ell(h) e^{jx\cos\phi}\, e^{jz\cos\theta_r}\right](\hat{u}_\ell^w \cdot \hat{u}_\phi^r) \quad (2\text{-}119)$$

Eqs. (2-118) and (2-119) are the general formula in two components of polarization for wire matrix element, and the vectors dot product in last equations can be obtained when wire direction is determined ($\hat{u}_\ell^w$) and $\hat{u}_\theta^r, \hat{u}_\phi^r$ is given in Eq. (2-10). The voltage element $[V^w] = [R^w]$, because of the real value of basis function.

2.2.4.3 Junction

The contribution to R^u from the junction region is given by:

$$R^{j,u} = < \bar{J}_a^j, , \bar{E}_u^r > + < \bar{J}_d^j, \bar{E}_u^r > \quad (2\text{-}120)$$

And with two orthogonal components of polarization Eq. (2-120) becomes:

$$R^{j,\theta} = < \bar{J}_a^j, , \bar{E}_\theta^r > + < \bar{J}_d^j, \bar{E}_\theta^r > \quad (2\text{-}121a)$$

$$R^{j,\varphi} = < \bar{J}_a^j, , \bar{E}_\varphi^r > + < \bar{J}_d^j, \bar{E}_\varphi^r > \quad (2\text{-}121b)$$

In more details by using Eq. (2-110) and (2-7) , Eqs. (2-121) yields:

$$R^{j,\theta} = \int_0^{h0} dh \int_0^{2\pi} d\phi \left[T_a(h) e^{jx\cos\phi}\, e^{jz\cos\theta_r}\right](\hat{u}_a \cdot \hat{u}_\theta^r) + \frac{1}{2\pi(b-a)} \int_a^b dr \int_0^{2\pi} d\phi \left[(r-b) e^{jx\cos\phi}\, e^{jz\cos\theta_r}\right](\hat{u}_r \cdot \hat{u}_\theta^r) \quad (2\text{-}122a)$$

$$R^{j,\phi} = \int_0^{h0} dh \int_0^{2\pi} d\phi \left[T_a(h) e^{jx\cos\phi}\, e^{jz\cos\theta_r}\right](\hat{u}_a \cdot \hat{u}_\phi^r) + \frac{1}{2\pi(b-a)} \int_a^b dr \int_0^{2\pi} d\phi \left[(r-b) e^{jx\cos\phi}\, e^{jz\cos\theta_r}\right](\hat{u}_r \cdot \hat{u}_\phi^r) \quad (2\text{-}122b)$$

For the junction voltage element $\left[V^j\right]$, which basis function is real,

$\left[V^j\right] = \left[R^j\right]$.

So, the unknown coefficients in Eq. (2-105a) are given in compact from

$$\begin{bmatrix} I_n^t \\ I_n^\phi \\ I^w \\ I^j \end{bmatrix} = \begin{bmatrix} Y_n^{tt} & Y_n^{t\phi} \\ Y_n^{\varphi t} & Y_n^{\phi\phi} \end{bmatrix} \begin{bmatrix} V_n^t \\ V_n^\phi \end{bmatrix} + [Y^w][V^w] + \left[Y^j\right]\left[V^j\right] \quad (2\text{-}123)$$

Finally, the far scattered field components, E_θ and E_ϕ are given in the form

$$\begin{bmatrix} E_\theta^s \\ E_\phi^s \end{bmatrix} = \frac{-jw\mu}{4\pi r_0}\, e^{-jkr}\left[\sum_{i=1}^{N_s-1} \begin{bmatrix} R_{ni}^{t\theta} & R_{ni}^{\phi\theta} \\ R_{ni}^{t\phi} & R_{ni}^{\phi\phi} \end{bmatrix} \begin{bmatrix} I_{ni}^t \\ I_{ni}^t \end{bmatrix} + \sum_{i=1}^{N_w-1} \begin{bmatrix} R^{w,\theta} \\ R^{w,\phi} \end{bmatrix} [I^w] + \right.$$

$$\left. \sum_{i=1}^{N_a-1} \begin{bmatrix} R^{j,\theta} \\ R^{j,\phi} \end{bmatrix} \left[I^j\right] \right] \quad (2\text{-}124)$$

Where *r* is the distance from origin to the point of observation of E^S.

Table (2-1): The dot product representations of composite body ($\hat{u}_a$ take the same procedure of $\hat{u}_l$).

Disk plane	unit vector u_r, u_a, u_l representations	Wire dot product representations		Junction dot product representations	
YZ	$\hat{u}_r = \hat{y}\cos\varphi + \hat{z}\sin\varphi$ $\hat{u}_a = \hat{x}\,x$ $\hat{u}_l = \hat{x}\,x$	$\hat{u}_l \cdot \hat{u}_{\acute{l}}$	$x\acute{x}$	$\hat{u}_r \cdot \hat{u}_{\acute{r}}$	$\cos(\varphi - \acute{\varphi})$
		$\hat{u}_l \cdot \hat{u}_t$	$x\sin v\cos\phi$	$\hat{u}_r \cdot \hat{u}_t$	$\sin v\sin\phi\cos\varphi + \cos v\sin\varphi$
		$\hat{u}_l \cdot \hat{u}_\phi$	$-x\sin\phi$	$\hat{u}_r \cdot \hat{u}_\phi$	$\cos\varphi\cos\phi$
		$\hat{u}_l \cdot \hat{u}_r$	0	$\hat{u}_r \cdot \hat{u}_l$	0
		$\hat{u}_l \cdot \hat{u}_\theta^r$	$x\cos\theta_r\cos\phi_r$	$\hat{u}_r \cdot \hat{u}_\theta^r$	$\cos\varphi\cos\theta_r\sin\phi_r - \sin\theta_r\sin\varphi$
		$\hat{u}_l \cdot \hat{u}_\phi^r$	$-x\sin\phi_r$	$\hat{u}_r \cdot \hat{u}_\phi^r$	$\cos\varphi\cos\phi_r$
XY	$\hat{u}_r = \hat{x}\cos\varphi + \hat{y}\sin\varphi$ $\hat{u}_a = \hat{z}\,z$ $\hat{u}_l = \hat{z}\,z$	$\hat{u}_l \cdot \hat{u}_{\acute{l}}$	$z\acute{z}$	$\hat{u}_r \cdot \hat{u}_{\acute{r}}$	$\cos(\varphi - \acute{\varphi})$
		$\hat{u}_l \cdot \hat{u}_t$	$z\cos v$	$\hat{u}_r \cdot \hat{u}_t$	$\sin v\cos\phi\cos\varphi + \sin v\sin\phi\sin\varphi$
		$\hat{u}_l \cdot \hat{u}_\phi$	0	$\hat{u}_r \cdot \hat{u}_\phi$	$-\sin\phi\cos\varphi + \sin\varphi\cos\phi$
		$\hat{u}_l \cdot \hat{u}_r$	0	$\hat{u}_r \cdot \hat{u}_l$	0
		$\hat{u}_l \cdot \hat{u}_\theta^r$	$-z\sin\theta_r$	$\hat{u}_r \cdot \hat{u}_\theta^r$	$\cos\varphi\cos\theta_r\cos\phi_r + \cos\theta_r\sin\phi_r\sin\varphi$
		$\hat{u}_l \cdot \hat{u}_\phi^r$	0	$\hat{u}_r \cdot \hat{u}_\phi^r$	$-\cos\varphi\sin\phi_r + \sin\varphi\sin\phi_r$
XZ	$\hat{u}_r = \hat{x}\sin\varphi + \hat{z}\cos\varphi$ $\hat{u}_a = \hat{y}\,y$ $\hat{u}_l = \hat{y}\,y$	$\hat{u}_l \cdot \hat{u}_{\acute{l}}$	$y\acute{y}$	$\hat{u}_r \cdot \hat{u}_{\acute{r}}$	$\cos(\varphi - \acute{\varphi})$
		$\hat{u}_l \cdot \hat{u}_t$	$y\sin v\sin\phi$	$\hat{u}_r \cdot \hat{u}_t$	$\sin v\cos\phi\sin\varphi + \cos v\cos\varphi$
		$\hat{u}_l \cdot \hat{u}_\phi$	$y\cos\phi$	$\hat{u}_r \cdot \hat{u}_\phi$	$\sin\varphi\sin\phi$
		$\hat{u}_l \cdot \hat{u}_r$	0	$\hat{u}_r \cdot \hat{u}_l$	0
		$\hat{u}_l \cdot \hat{u}_\theta^r$	$x\cos\theta_r\sin\phi_r$	$\hat{u}_r \cdot \hat{u}_\theta^r$	$\sin\varphi\cos\theta_r\cos\phi_r - \sin\theta_r\cos\varphi$
		$\hat{u}_l \cdot \hat{u}_\phi^r$	$y\cos\phi_r$	$\hat{u}_r \cdot \hat{u}_\phi^r$	$-\sin\varphi\sin\phi_r$

2.2.5 The radar cross section evaluation

In general the superposition of the two orthogonal components of incident wave, E_θ^i and E_φ^i, and the far – zone scattered wave , E_θ^s and E_ϕ^s , are related by the scattering matrix [41], according to:

$$\begin{bmatrix} E_\theta^s \\ E_\phi^s \end{bmatrix} = \frac{e^{-jkr}}{r} \begin{bmatrix} S^{\theta\theta} & S^{\theta\phi} \\ S^{\phi\theta} & S^{\phi\phi} \end{bmatrix} \begin{bmatrix} E_\theta^i \\ E_\phi^i \end{bmatrix} \tag{2-125}$$

The elements of scattering matrix can be expressed as a summation over the modal components as:

$$S^{pq} = \sum_n S_n^{pq} \tag{2-126}$$

Where pq denotes $\theta\theta$, $\theta\phi$, $\phi\theta$, $\phi\phi$.

The RCS is defined in the standard way for large r as:

$$\sigma = 4\pi R^2 \frac{|E^s|^2}{|E^i|^2} \tag{2-127}$$

Substituting (2-125) in (2-127), to get

$$\sigma^{pq} = 4\pi |S^{pq}|^2 \tag{2-128}$$

The scattered field is given by

$$\bar{E}^r . u = \frac{-j\omega\mu}{4\pi r} e^{-jkr} \begin{bmatrix} R^s & R^w & R^j \end{bmatrix} \begin{bmatrix} I^s \\ I^w \\ I^j \end{bmatrix} \tag{2-129}$$

Hence,

$$S^{pq} = \frac{-jw\mu}{4\pi} \begin{bmatrix} \left\{ \begin{bmatrix} [R_n^{tp}] & [R_n^{\phi p}] \end{bmatrix} \begin{bmatrix} Y_n^{tt} & Y_n^{t\phi} \\ Y_n^{\phi t} & Y_n^{\phi\phi} \end{bmatrix} \begin{bmatrix} V_n^{tq} \\ V_n^{\phi q} \end{bmatrix} + \right. \\ \left. [[R^{wp}]\,[Y^{wq}]\,[V^{wq}]] + \left[[R^{jp}] \left[Y^{jq} \right] \left[V^{jq} \right] \right] \right\} \end{bmatrix} \tag{2-130}$$

Therefore, the RCS normalized to wave length is given by substituting (2-130) in (2-128), and has the form:

$$\frac{\sigma^{pq}}{\lambda^2} = \frac{\eta^2 k^4}{16\,\pi^3}\left|\sum_{-n}^{n}\left(R_n^{tp} I^{tq} + R_n^{\phi p} I_n^{\phi q}\right) + R^{wp} I^{wq} + R^{jp} I^{jq}\right|^2, \qquad (2\text{-}131)$$

where the received and incident polarization are $p=\theta$ and $q=\theta$ or ϕ, respectively.

For example $\sigma^{\theta\theta}$ denote that the RCS measured in the θ-polarized receiver with ϕ=0 plane , while $\sigma^{\phi\theta}$ represent the plane of ϕ =90 and RCS measured by ϕ -polarized receiver. For the axially incident plane only $n=\pm 1$ modes are excited, therefore the RCS components in the horizontal polarization (HP) are given by [8]:

$$\sigma^{\theta\theta} = 16\pi \left|S_1^{\theta\theta}\right|^2 \cos^2\phi_r \qquad (2\text{-}132)$$

and the vertical polarization (VP)

$$\sigma^{\phi\theta} = 16\pi \left|S_1^{\phi\theta}\right|^2 \sin^2\phi_r \qquad (2\text{-}132)$$

And the scattered field components may be written as

$$E_\theta^s = 2\left(\frac{e^{-jkr}}{r}\right) S_1^{\theta\theta} \cos\phi_r \qquad (2\text{-}133)$$

$$E_\phi^s = 2j\left(\frac{e^{-jkr}}{r}\right) S_1^{\phi\theta} \sin\phi_r \qquad (2\text{-}134)$$

Note that in the bistatic case, RCS represented in both terms of illumination and scattering angles, i.e., $\sigma^{pq}(\theta_s, \phi_s, \theta_i, \phi_i)$ and all polarization cases, $\sigma^{\theta\theta}$, $\sigma^{\theta\phi}, \sigma^{\phi\theta}, and\ \sigma^{\phi\phi}$ are satisfying. For monostatic case, the angles of illumination and scattering are the same, i.e., $\theta_s = \theta_i$ and $\phi_s = \phi_i$ [14], hence only two component of polarization, $\sigma^{\theta\theta}$ and $\sigma^{\phi\phi}$, are computed [11]. In the same comparison, bistatic RCS computations require *R* to be computed twice, while for monostatic case, *R* needs to be computed only once [77] where *R* is the measurement matrix.

2.3 Computed Results

There are proven RCS prediction methods that can accurately approximate bistatic RCS as well as monostatic RCS for certain shapes. The exact analytical solutions are distinct and important for most researchers in scattering problems of EM waves from PEC, and is known for a specific number of regular shapes. In this research, the boundary conditions with the MoM were used to develop the numerical method of effective and simple to address these problems, where the accuracy of the solutions used in this method is very suitable for the PEC and corresponding BOR [3][119].

In this section, scattering data for several configurations were calculated. The results were compared with the results that are currently available in the literature. These results were found to be relied mainly on the validity and accuracy of EFIE formulation for scattering problem, and this advantage proved by the good results for PEC [67].

The computational technique of solving the EFIE by the MoM for the class of problems described as wires attached to a BOR, (Fig.(2-1), is shown here in scattering problems. This method was presented to determine the effect of surface electric currents $\bar{J}$ generated on the surface of the body with neglected influence of the magnetic surface currents $\bar{M}$. Each part of the composite body; the BOR, the wires, and the junctions region has its own unique class of current expansion function [76], as in Eqs.(2-7) to (2-9).

The preceding sections of this chapter deal with the processes account of both surface current and RCS of the composite body (irregular shape). To confirm the credibility of these formulations, they have been applied to a set of regular geometric shapes (BORs) beneficiaries of the processing speed of digital computers in the implementation of a set of software, where the application domain and the comparison with a group of researchers who touched these shapes being available.

After obtaining the results, which confirm the findings, the first deal with the important application, the composite body, where the RCS was obtained and compared with measurement results from [77]. Among these results , the case of the sphere with one or two wires, as well as a flat-faced cylinder with the same number of wires, while the case of cylinder with rounded ends was taken with wire-loop fins. Comparison of these results with the measurements and with good convergence leads to the proposed model of applications. This model was one of the military applications in the possession of the U.S.Air Force representative in one of its rockets.

Compared RCS of the rocket with the forms close to him in the study was by changing the body shape, and specifically changing the dimensions of the wings of the rocket while the body of the rocket was unchanged.

2.3.1 Examples

Computer programs have been written to calculate the square matrices and measurements vectors needed to calculate the far scattered fields and then RCS. To demonstrate the validity of the formulation, where the length of wire approach to 0.0000001λ, the numerical results are presented for some represented examples of CBORs by solving the EFIE with MoM technique as outlined. There are four cases of perfect conducting bodies are considered: (1) sphere, (2) cone-sphere, (3) cylinder rod with rounded ends, and (4) flat-faced cylinder, whose axis of symmetry coincides with the Z-axis illuminated by axially incident plane wave (i.e., $\theta_i = 180^o$).

To examine the results as a function of angle for both bistatic and monostatic RCS alternately, the bistatic scattering from a perfectly conducting spheres of radius a=0.1λ, 0.2λ, and 1.0λ, will be presented first and calculated for $\theta\theta$-polarized by using Eq.(2-131) without including wires or junction. The

distance and frequency are scaled, so, the segments on the generated curve are unified. The result of the computer program perfectly agrees with the MoM [59] and with the exact solution of Mie series results [63] as shown for three different radii in Fig.(2-6).

The bistatic ($\sigma^{\theta\theta}$ and $\sigma^{\phi\theta}$) and monostatic or backscatter ($\sigma^{\theta\theta}$ and $\sigma^{\phi\phi}$) cross section, for conducting cone-sphere of cone angle α=20^o with sphere of radius *ka*=1.21 and *kb*=7.28 as shown in Fig.(2-7), are computed and compared with other analytical results of Harrington and Mautz [11]. The results are depicted in Fig.(2-8) and (2-9), and the agreement between the two cases with other results are excellent.

The calculated cross section σ for cylinder with rounded ends of total length $L = 2.6\lambda$ and radius of the rod *ka*=2.16, as the configuration of fig. (2-10), are compared with the experimental data of [77]. Figure (2-11) shows the horizontal polarization $\sigma^{\theta\theta}$ and vertical polarization $\sigma^{\phi\phi}$ for monostatic scattering from cylinder, respectively. A good agreement was found between measured data and the calculated from MoM are achieved.

To illustrate the bistatic and monostatic scattering cross section for the last example, consider the flat-faced cylinder of length $l_c = 6\lambda$ and radius a= 1.2675λ in the bistatic case, and the other cylinder has the dimensions of $l_c = 1.98\lambda$ and a=0.343λ for the backscattering case. The resultant data, depicted in Fig.(2- 12), are excellent in agreement with the exact solutions of [65]. Also, according to Fig.(2-13), it can be shown that the results obtained from MoM are more accurate than (PO+PTD) [6] in comparison with experimental data of [77]. Experimental results are normalized to σ_o=0.0052, and the measurement frequency is 2.6 GHz. Thus, the output of the computer program is also normalized to the same value.

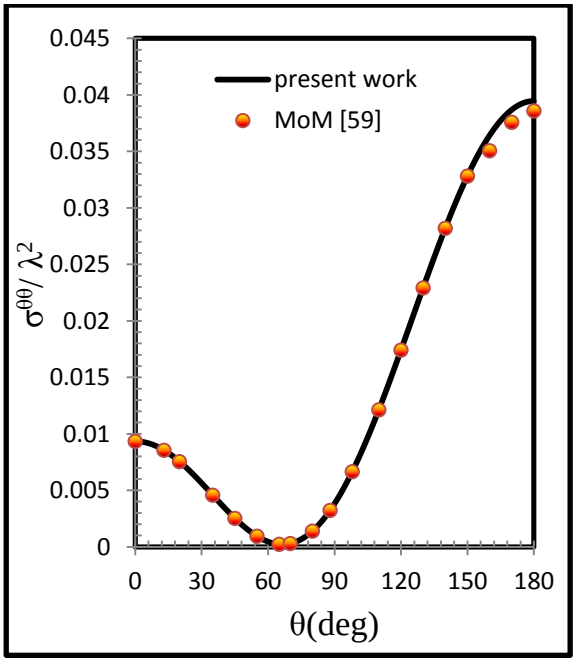

(a)

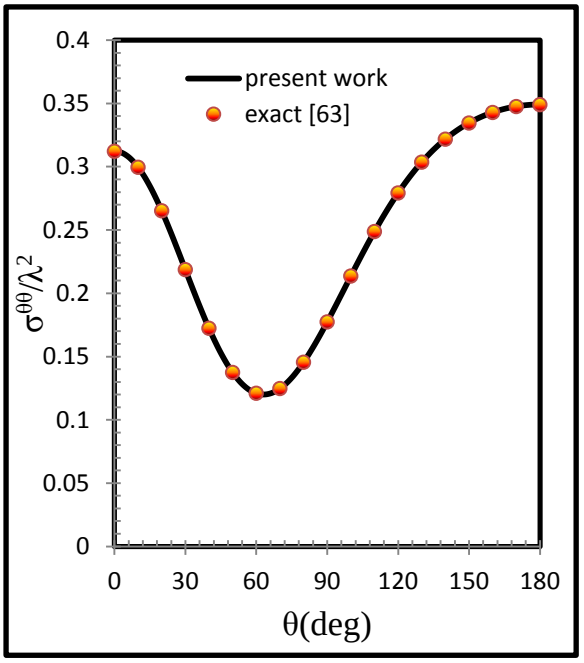

(b)

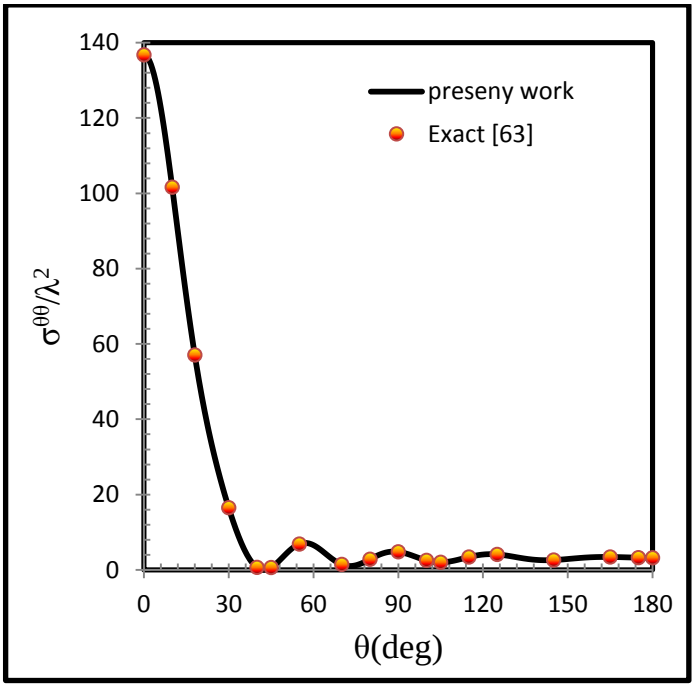

(c)

Fig.(2-6): Bistatic RCS for conducting sphere with axially incident plane wave and various radius of:(a) a=0.1 λ (b) a=0.2 λ (c) a=1.0 λ

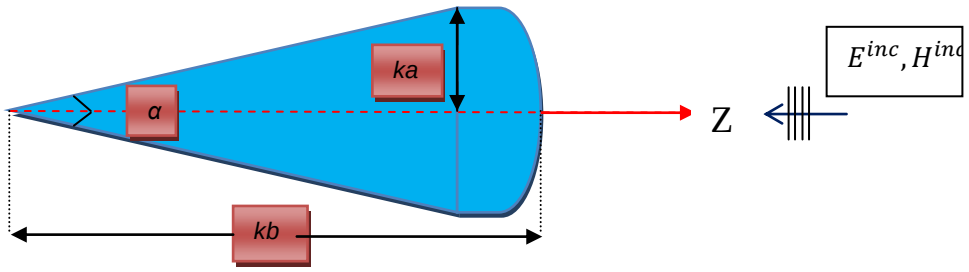

Fig.(2- 7): Dimensions of conducting cone-sphere.

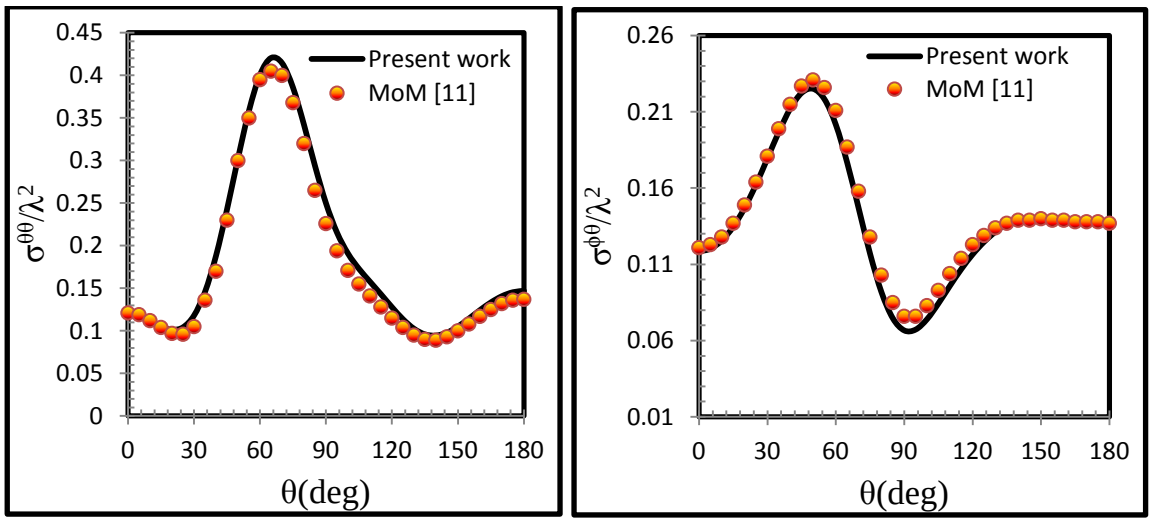

(a) (b)

Fig.(2-8): Computed bistatic RCS for conducting cone sphere($\alpha=20^o$, ka=1.21 and kb=7.28), (a) θθ-polarized. (b) ϕθ-polarized.

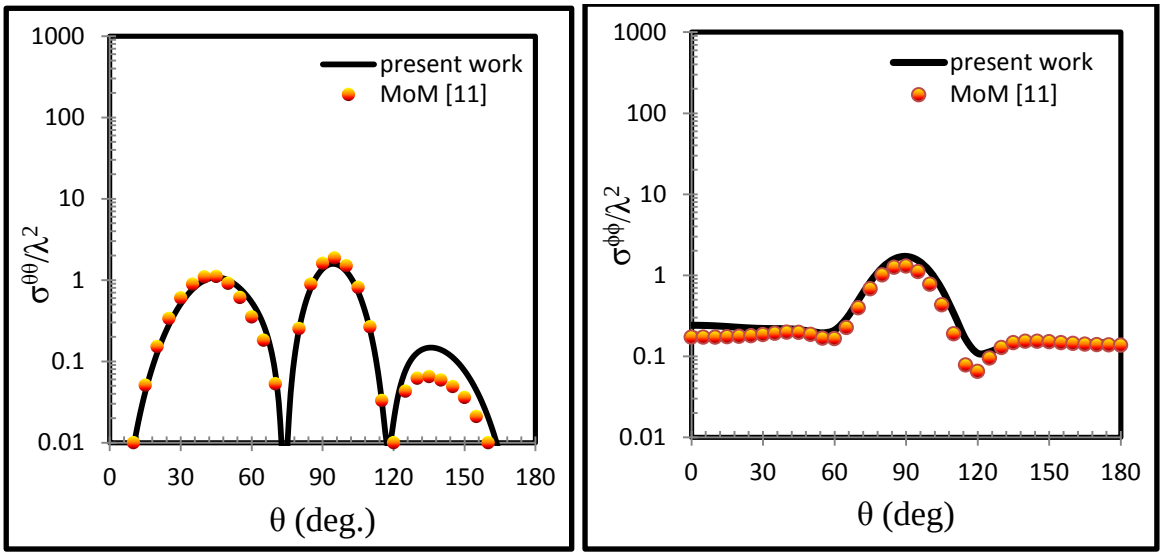

(a) (b)

Fig.(2-9): Computed Monostatic RCS for conducting cone sphere ($\alpha=20^o$, ka=1.21 and *kb=7.28), (a) θθ-polarized. (b) ϕϕ-polarized.*

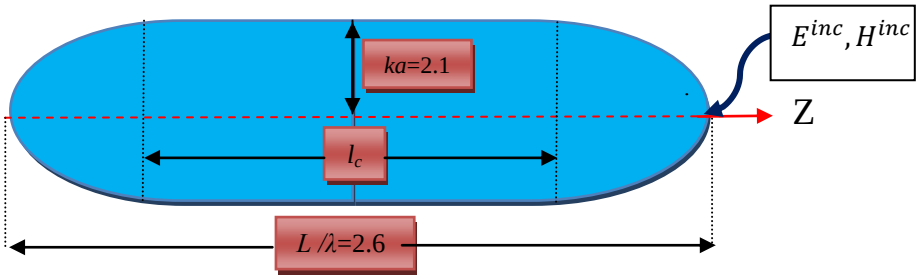

Fig.(2-10): Conducting cylinder with rounded ends.

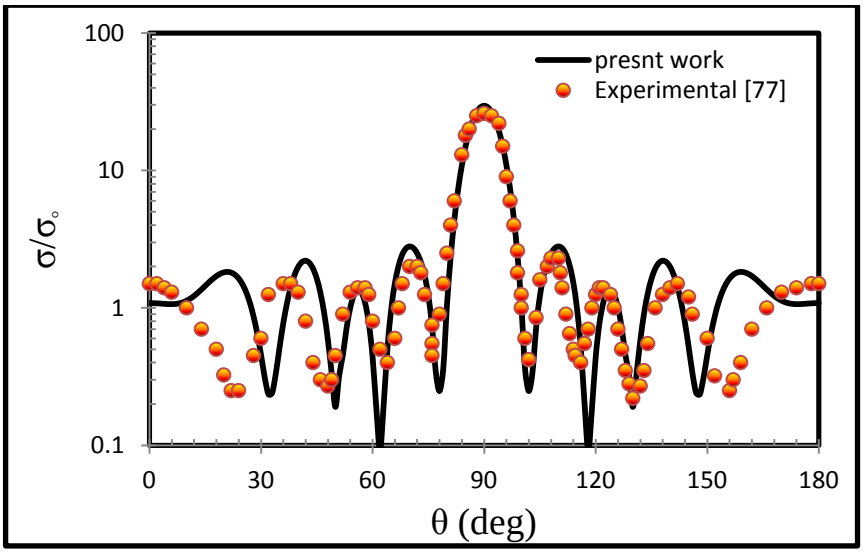

(a)

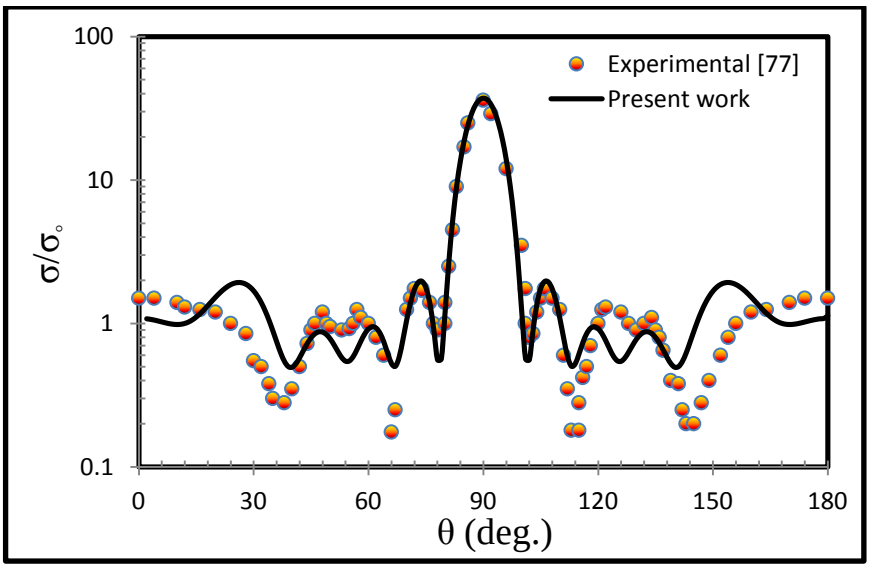

(b)

Fig.(2-11): Backscattering cross section of a perfect cylinder with hemisphere endcaps. (a) θθ-polarized. (b) ϕϕ-polarized.

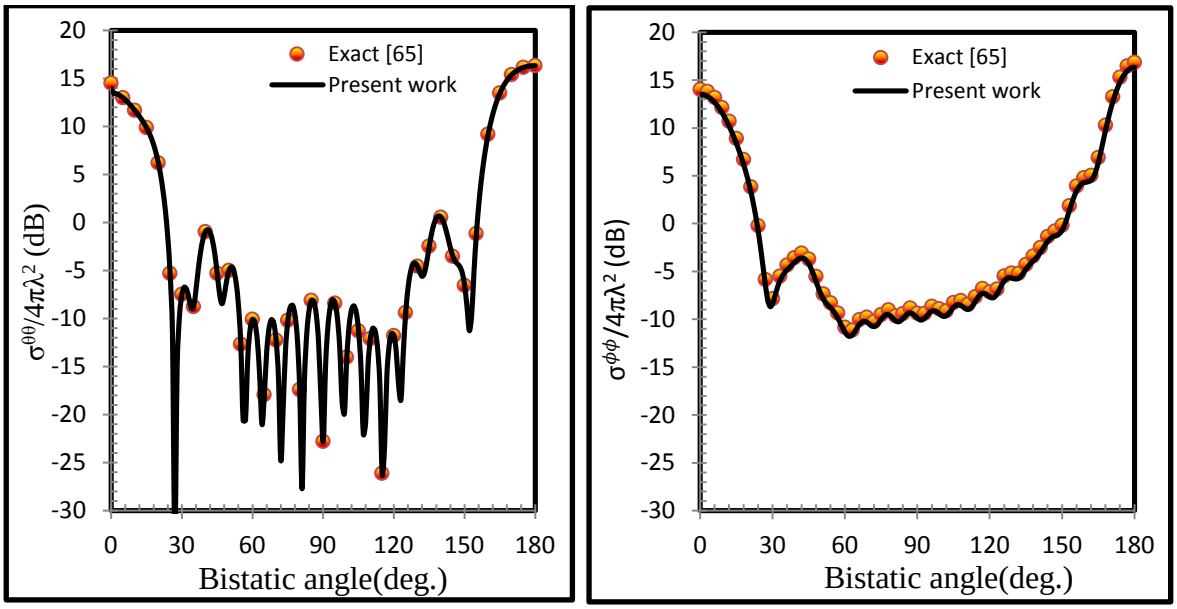

(a) (b)

Fig.(2-12): RCS versus bistatic angle of a perfectly conducting cylinder of $a = 1.2675\lambda$ *and* $l_c = 6\lambda$ *. (a) HP (b) VP.*

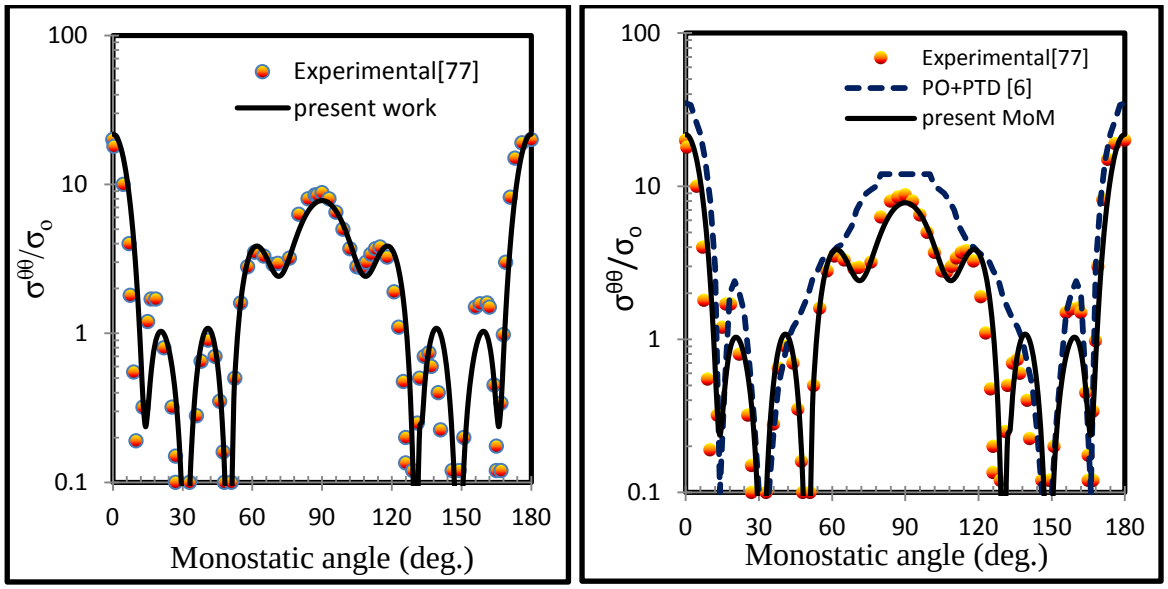

(a) (b)

Fig.(2-13): RCS versus monostatic angle of a perfectly conducting cylinder of $a = 0.343\lambda$ *and* $l_c = 1.98\lambda$*, in comparison with (a) Experimental (b) Experimental and combining (PO+PTD).*

2.3.2 Applications

2.3.2.1 Determining the outer radius of disk in junction region

The mathematical analysis using the junction region coordinate system, approximated as flat disk of the outer radius *b*, the inner radius of the disk corresponds to the wire radius *a* as shown in Fig.(2-2). This approximation is based on the disk radius *b* being much smaller than the local body curvature at the junction attachment point. The outer radius *b* is usually chosen to be between 0.1λ to 0.25λ, which has an effect on the impedance characteristic, especially on the impedance value of the resonance frequency point, 2.6 GHz, [85]. By using Eq.(2-84), the admittance versus *b* is calculated in the resonance frequency, as shown in Fig.(2-14). It can be seen that the admittance converges when the outer radius *b* is greater than 0.1λ. So the appropriate value of *b*=0.107λ was used in the computed results.

2.3.2.2 The utility applications

In this section the results shown here exhibited some of the applications depend on the utility of the BOR-Wire-Junction scattering algorithm. The computed results are compared with measured monostatic RCS obtained by [77] and normalized to the cross sections of a sphere, σ_o=0.00525m^2, which was computed using the Mie series solution for a perfect conducting sphere.

To test the validity of the analysis method on the composite body, the main goal is devoted to the results of the cross section RCS by using Eq.(2-131). The first results are computed for the conducting sphere of radius *a*=0.444λ (*ka*=2.79), with one attached wire of length ($l_w = 0.444\lambda$), Fig.(2-15), and with two attached wires of the same length ($l_{w1} = l_{w2} = 0.444\lambda$, Fig.(2-16). It can be seen that the computation results obtained using the MoM is in a good agreement with the measured, and the RCS of a sphere does not change for a body of radial symmetry alone. The addition of wires produces a result

that has twofold symmetry in the case of one wire, and has fourfold in the case of two wires. Note that when the incident polarization is normal, no effect at incident angles of 0^o and 180^o and the RCS is that of sphere alone. For backside incident $\theta>90^o$ of single wire, where the wire is partially shielded by sphere, the results show nulls that are less deep than on the front illuminated side.

The scattering cross section from the flat-faced cylinder of radius a=0.344λ and length $l_c = 1.98\lambda$ with attached wires of length $l_w = 0.880\lambda$, configuration depicted in Fig.(2-17), is also computed for horizontal polarization and comparison with experimental data as second application. The results are presented in Fig.(2-18) with one attached wire and Fig. (2-19) with two attached wires. The effect of thin wires and junction to the total backscattered RCS is noticeable. It is noted the scattering pattern for the cylinder remains the same for $\theta>140^o$. Because, the region where $\theta>140^o$ (see Fig.(2-17a)) is shadowed by the cylinder itself, whereas at broadside, θ=0^o and 180^o, the incident polarization is normal to the wire such that the resulting cross section is that of the cylinder alone. The cylinder RCS without attachments, in Fig.(2-13), has fourfold symmetry, where for one attached wire at the cylinder center with twofold symmetry. The addition of two attached wires opposite each other at the cylinder center, produces a result with fourfold symmetry.

In general for all applications, the addition of attached wires significantly alters the constant cross section of the BOR. Figure (2-20) shows the effect of wires, which have the same length, located at the center of cylinder with hemisphere ends (total length $L = 2.6\lambda$, hemisphere radius ka=2.16, and $kl_w = 5.18$) for the cases of bistatic and monostatic RCS.

The important part of the applications is to determine the efficacy of the composite body scattering to more complicated and practical geometries. The

calculations of RCS for missile configuration with wings modeled as wire-loops, shown in Fig.(2-21) with dimensions are $l_{w1}=l_1+l_2+l_3$, $l_{w2}=l_4+l_5+l_6$, $l_1=l_3=l_4=l_6$, $l_2=l_5$, *and* $v_1=v_2=v_3=v_4$, was obtained and compared with other measurements. The graph between the distance of point from the Z-axis, ρ_α, and distance of the point on the Z-axis, Z_α, is considered one of the most important tests that can be made on the form to give an accurate description of the missile, as shown in Fig.(2-22), where $\alpha=p$ or q and knowledge previously. This modeling approach is an extension of the stick representation used by [74], but the only difference here is that the body represented by a BOR. The body was a cylinder with hemisphere endcaps of diameter d/λ=0.688 (ka=2.16) and total length $L = 2.6\lambda$, the wire-loop wing of length $l_{w1} = l_{w2} = 0.826\lambda$ and $l_2 = 0.76l_1$with slant angle of wings v_i=45^o (i=1,...,4). The computed and measured results are in a good agreement for horizontal polarization of wire-loops representing the wing and shown in Fig.(2-23), whereas the wings do not contribute to the RCS for vertical polarization because the wings are normal to the incident electric vector, as confirmed by Fig.(2-24)

2.3.2.3 The accuracy of numerical method

To demonstrate the accuracy of the numerical method (MoM), the results were compared to the case of the cylinder with one wire, shown in Fig.(2-17a), and with the results calculated by the (PO+PTD) as shown in the Fig.(2-25). Note through the great convergence and obviously with the practical consequences for the results calculated by MoM with respect to other methods (PO+PTD) calculated by [6].

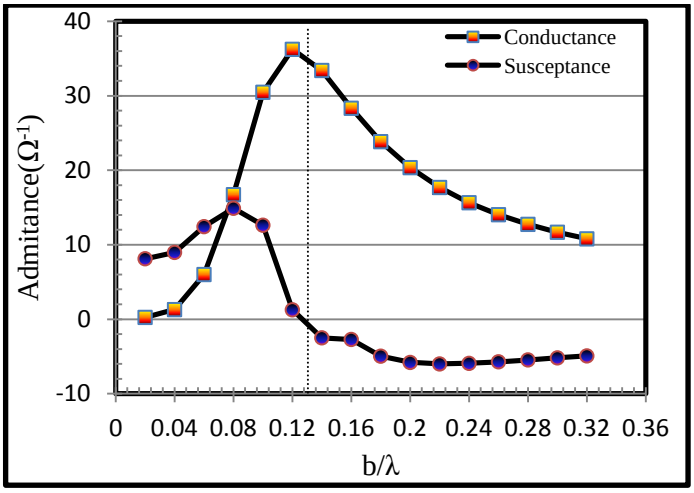

Fig.(2-14): Input admittance of the junction point versus disk radius b.

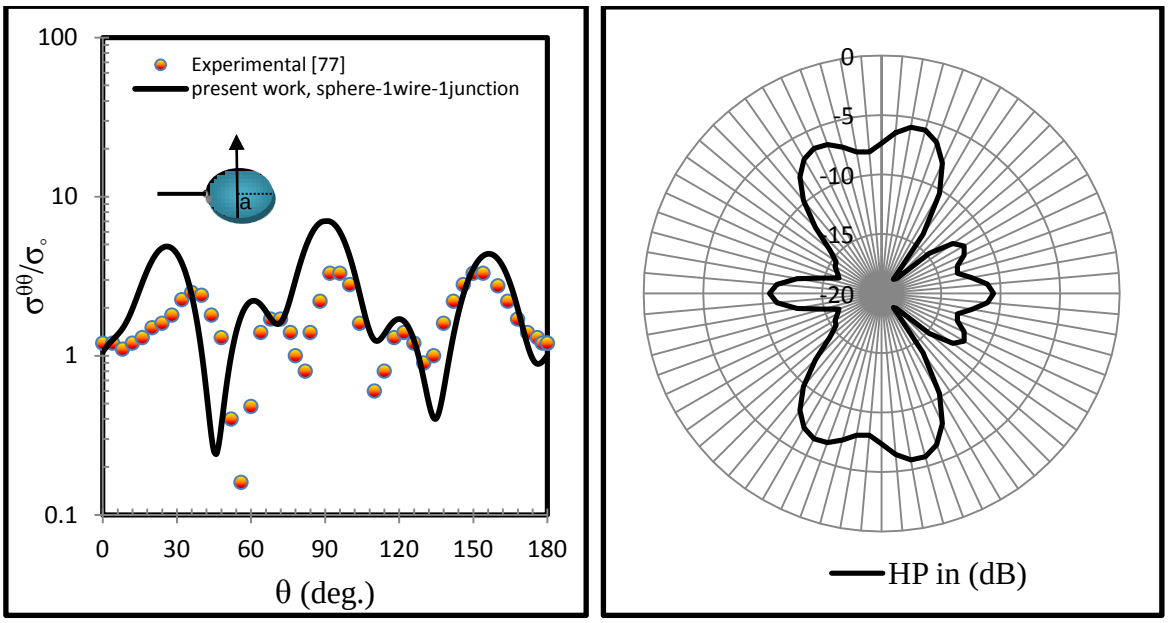

(a) (b)

Fig.(2-15): (a) Backscattering RCS in HP from PEC sphere (a=0.444λ) with one attached wire ($l_w = 0.444\lambda$). (b)HP present work with radar graph representation.

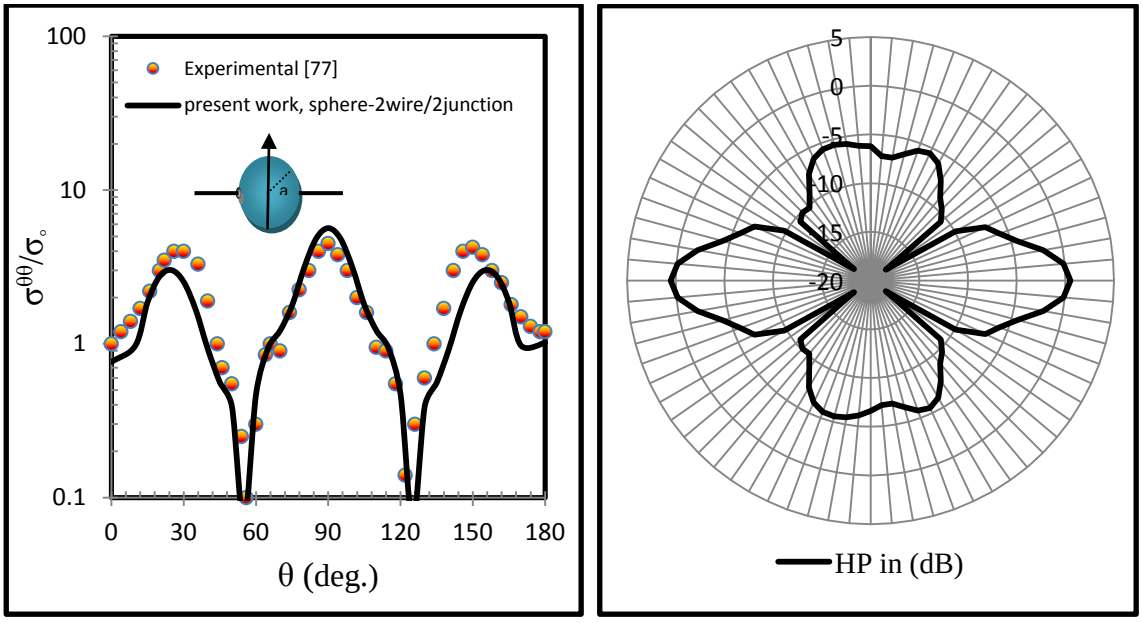

(a) (b)

Fig.(2-16): (a) Backscattering RCS in HP from PEC sphere (a=0.444λ) with two attached wires ($l_{w1} = l_{w2} = 0.444\lambda$). (b)HP present work with radar graph representation.

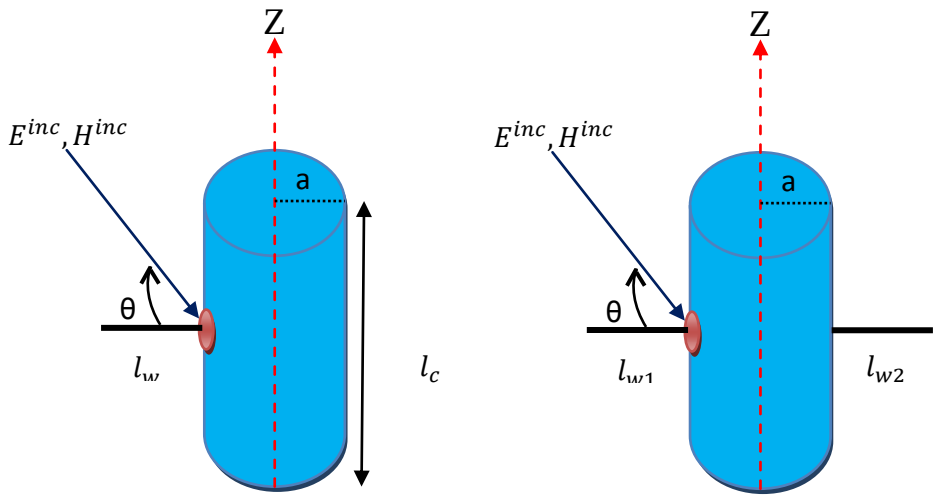

(a) (b)

Fig.(2-17): Flat-faced cylinder configuration ($a=0.344\lambda$, $l_c = 1.98\lambda$ and $l_{w1} = l_{w2} = 0.880\lambda$: (a) one attached wire (b) two attached wires.

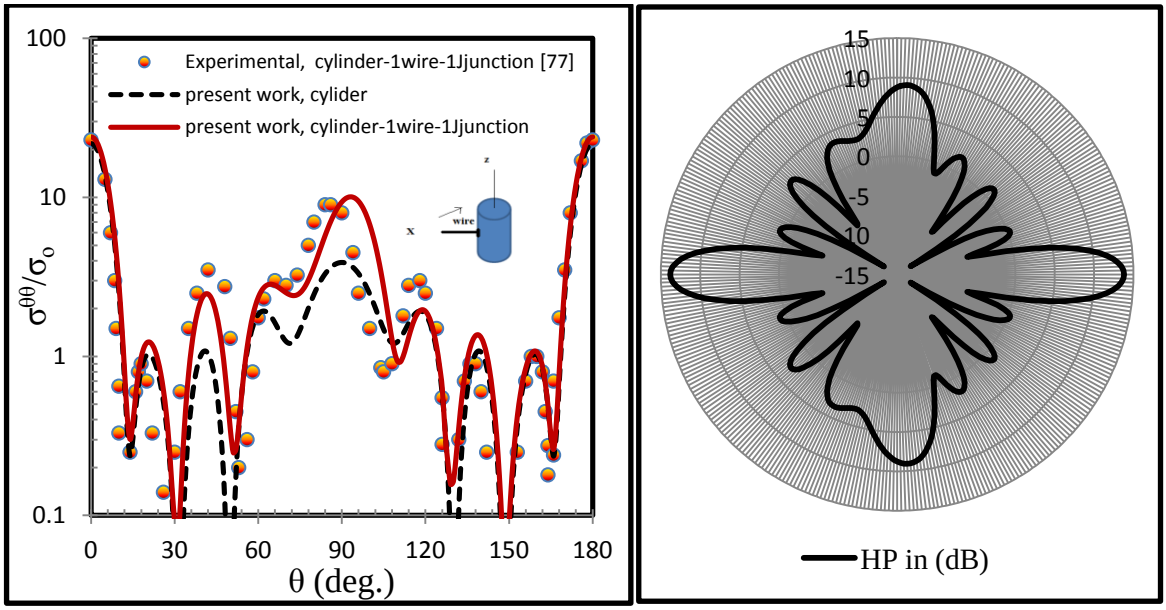

(a) (b)

Fig.(2-18): (a) Monostatic RCS in HP from PEC cylinder ($a=0.344\lambda$, $l_c = 1.98\lambda$) with one attached wire ($l_w = 0.880\lambda$) (b)HP present work with radar graph representation.

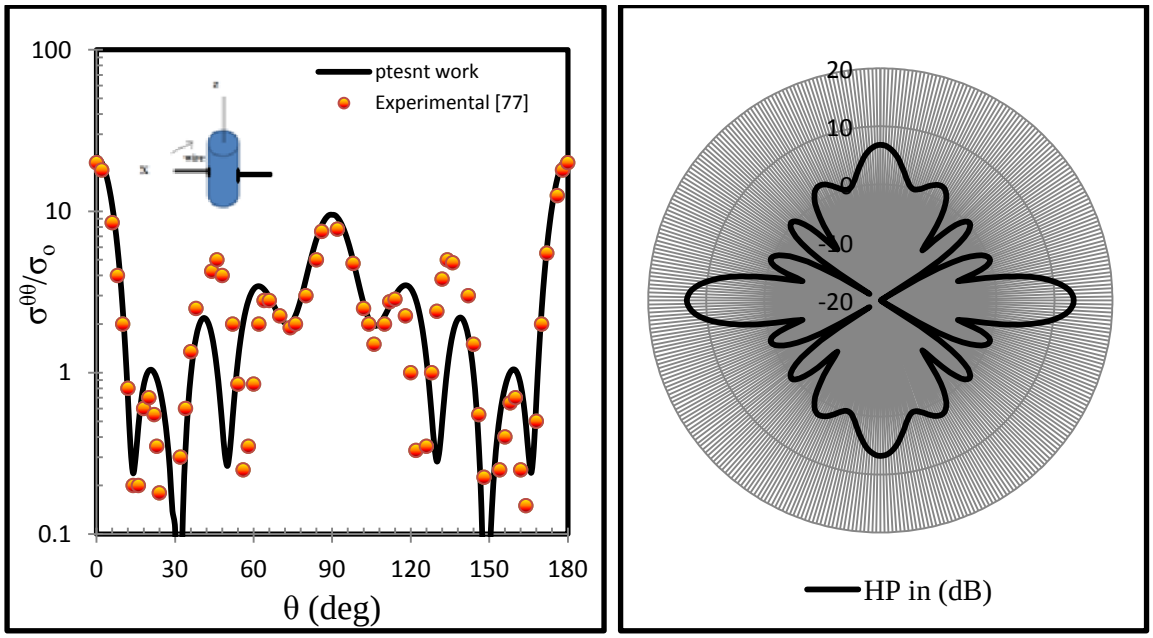

(a) (b)

Fig.(2-19): (a) Monostatic RCS in HP from PEC cylinder ($a=0.344\lambda$, $l_c = 1.98\lambda$) with two attached wire ($l_{w1} = l_{w2} = 0.880\lambda$) (b)HP present work with radar graph representation.

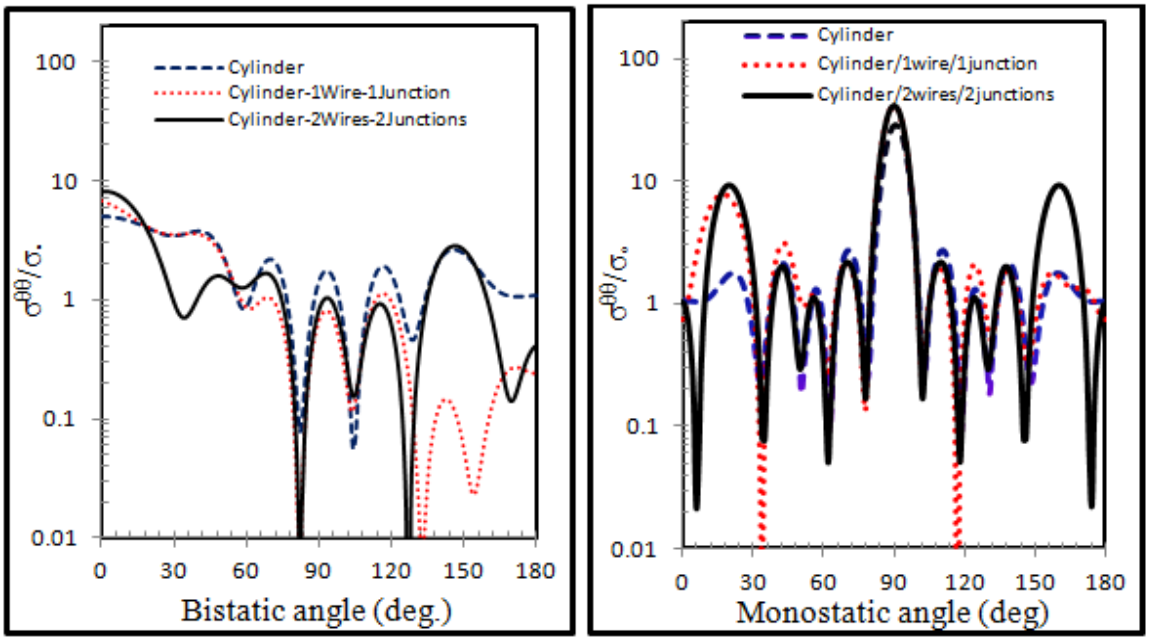

(a) (b)

Fig.(2-20): Computed RCS in HP for cylinder with hemisphere (ka=2.16, $L = 2.6\lambda$ and $kl_w = 5.18$) : (a) Bistatic case (b) Monostatic case.

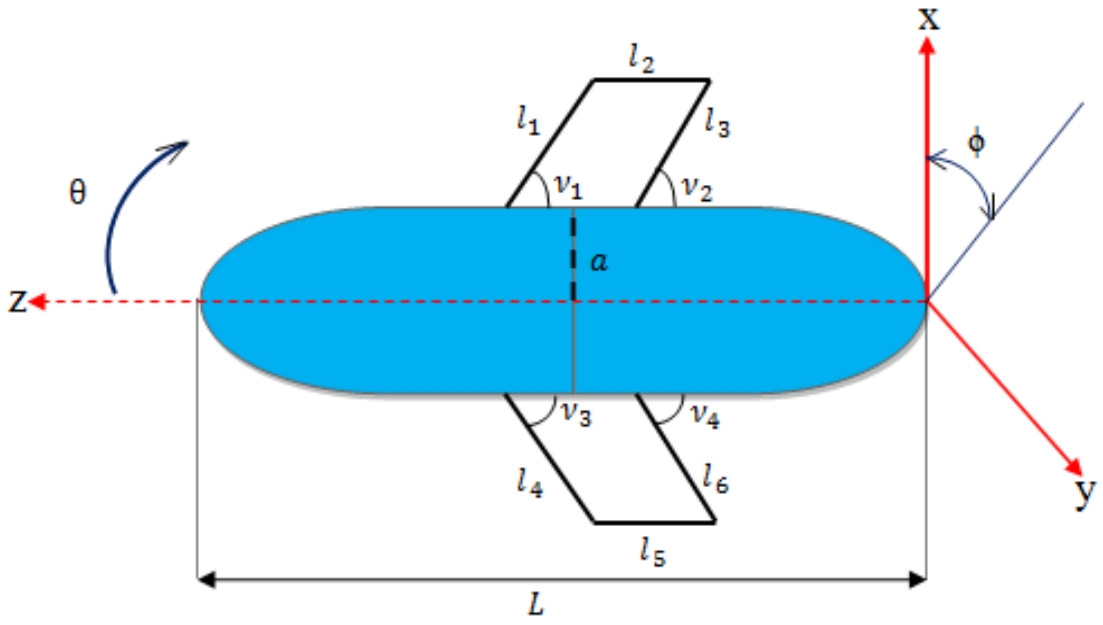

Fig.(2-21): Geometric shape for missile configuration with wings model, ($l_{w1}=l_1+l_2+l_3$, $l_{w2}=l_4+l_5+l_6$, $l_1=l_3=l_4=l_6$, $l_2=l_5$ and $v_1=v_2=v_3=v_4$).

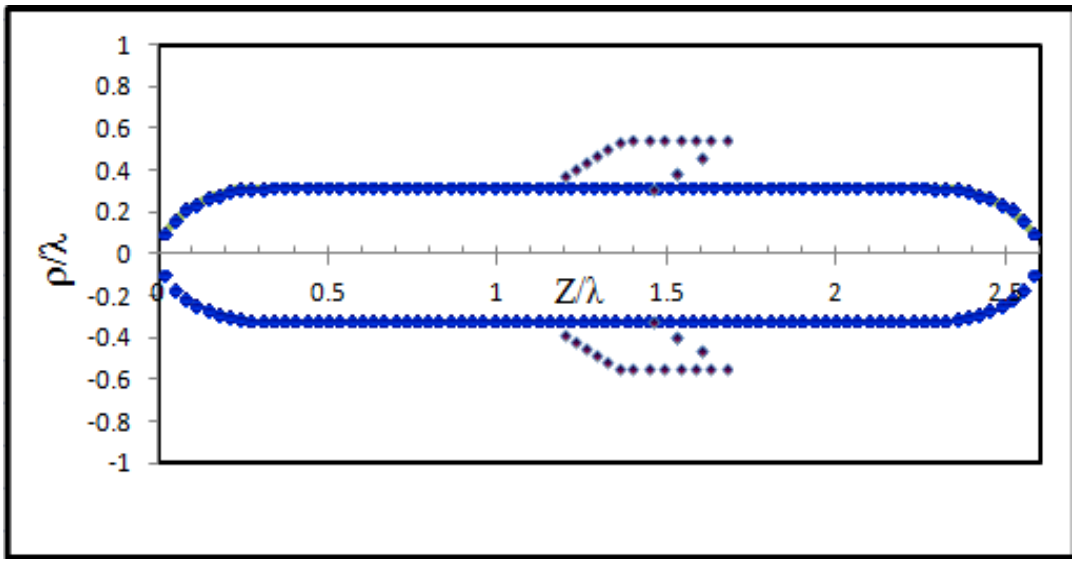

Fig.(2- 22): The precise shape of missile with two wings of slant angle 45^o.

($ka=2.16$, $L = 2.6\lambda$, $l_{w1}= l_{w2}=0.826\lambda$, $l_2=0.76\ l_1$ and $v_1=45^o$)

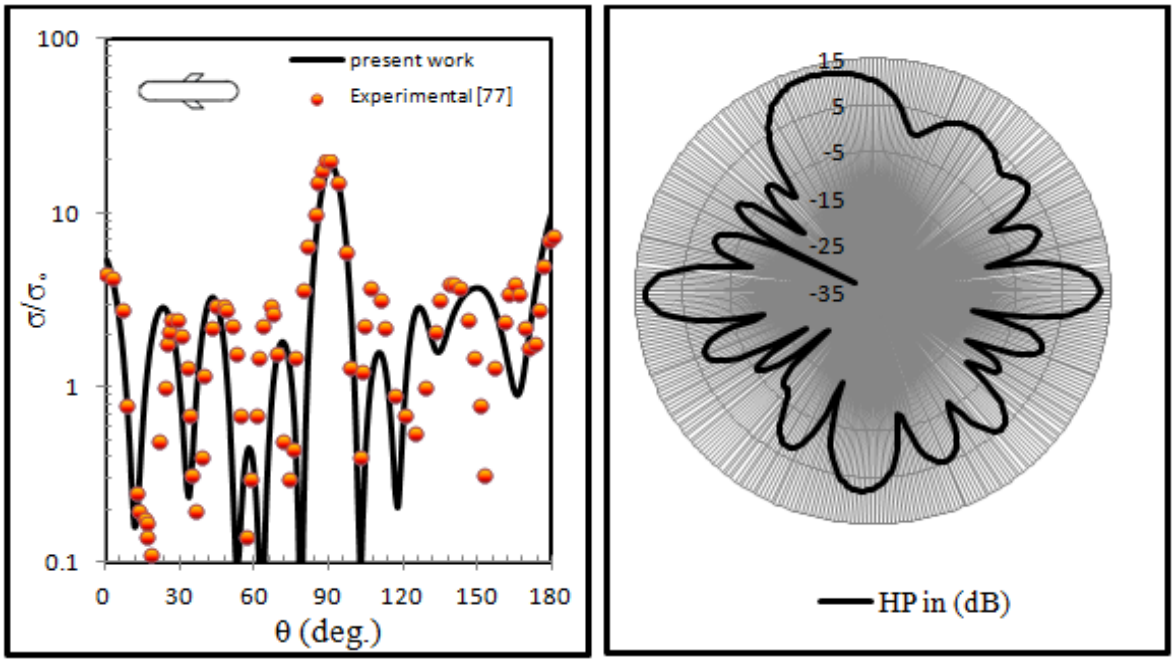

(a) (b)

Fig.(2-23):(a)Monostatic RCS in HP from cylinder with hemisphere endcaps and wire-loop wings ($ka=2.16$, $L = 2.6\lambda$, $l_{w1}= l_{w2}=0.826\lambda$, $l_2=0.76\ l_1$ and $v_1=45^o$). (b)HP present work with radar graph representation.

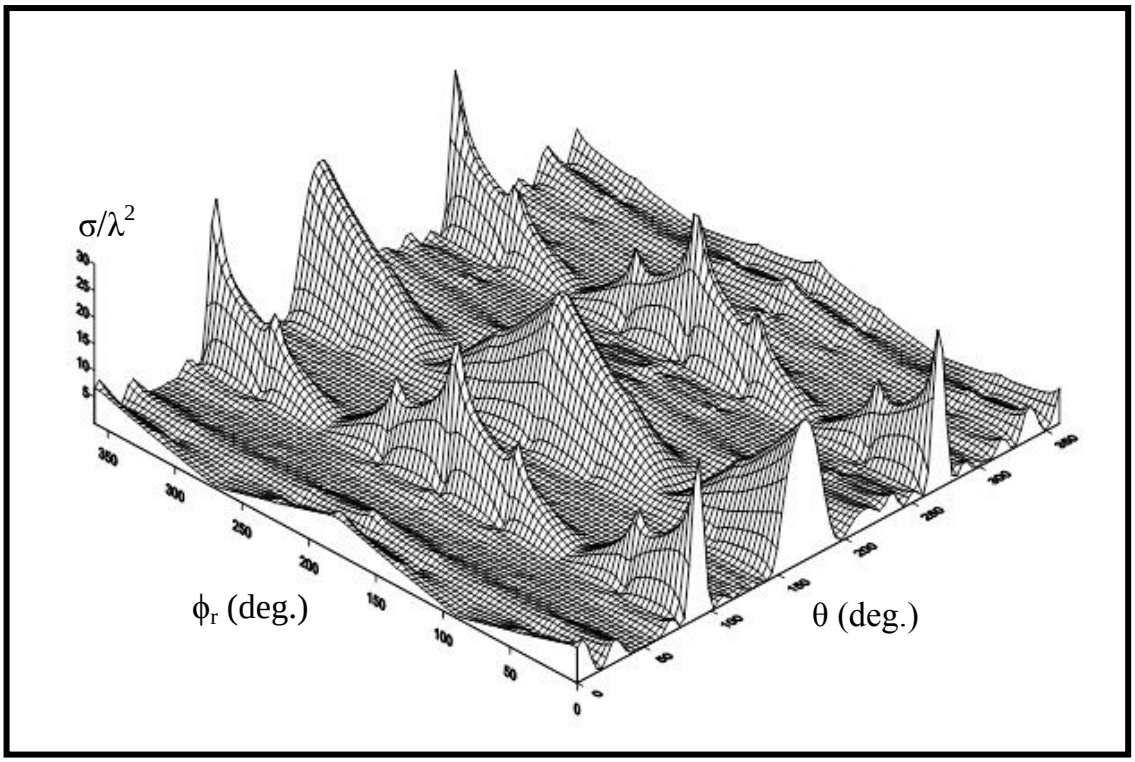

Fig.(2-24): Backscattering RCS in three-dimensional form.

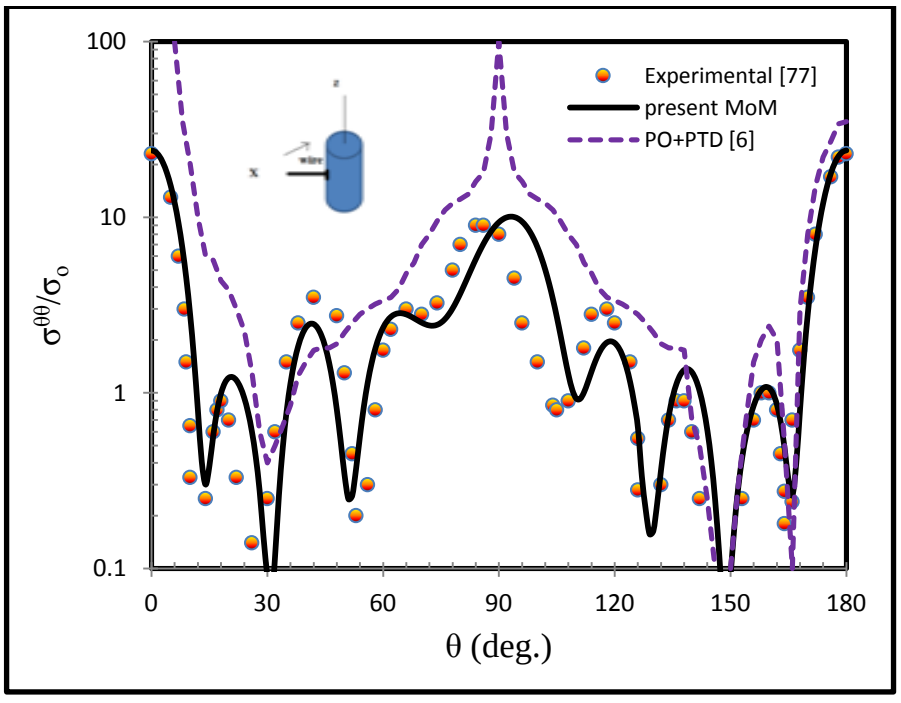

Fig.(2-25): Backscattering RCS, $\sigma^{\theta\theta}$, of the structure shown in figure (2-17a).

2.3.3 The Proposed Model

The study of complex irregular shapes are difficult to handle, because of the difficulty to get RCS account. The military targets is considered the most important of these forms. The difficulty of obtaining RCS for military targets invited us to resort to RCS of known shapes that approached the target, as adopted for a specific length of these forms**.**

Previous studies [67][71] that dealt extensively with the subject of the complex conducting bodies, represented by the CBOR, taking into account the change in the parts of the body and its impact on the RCS, being a regular body during the rotation process.

In the current study within this chapter, we used a complex composite body, the BOR, wires, and junction, further complicated to the problem by the presence status of no regularity to this body**.** It should be noted that we have avoided the study of the influence of conducting BOR parts, and we focused on the other side, represented by the wings, being one of the shape features that help to change in the RCS as a new and important aspect in dealing with complex objects.

We have adopted in the proposed model, a rocket that is used by US air force, which carries four wings like engineering scheme in Fig.(2- 26). From this scheme, we find that the rocket body without wings (BOR) consisting of three cylinders and three conical parts, in addition to the spherical front end of the rocket. All these parts have a total length fixed 2.6λ, where it can be compared to the results that we get with the results in previous studies of the same length bodies approach. Basic dimensions of the rocket shown in Fig.(2-26) and adopted here are as follows**:**

r_o - the radius of the rocket front end

L_{oi}- the length of cone on z-axis, i=1, 2, 3.

L_{zi}- the length of cylinder on z-axis, i=1, 2, 3.

r_{ai}- the cylinder high from z-axis, i=1, 2, 3.

$\left.\begin{matrix} h_1 = h_5 \\ h_2 = h_6 \end{matrix}\right\}$ the large wings high

$\left.\begin{matrix} h_3 = h_7 \\ h_4 = h_8 \end{matrix}\right\}$ the small wings high

$l_{w1} = l_1 + l_2 + l_3 = l_{w3} = l_7 + l_8 + l_9$ = the total wires length on the large wings.

$l_{w2} = l_4 + l_5 + l_6 = l_{w4} = l_{10} + l_{11} + l_{12}$ = the total wires length on the small wings.

ν_i = the wings slant angle (i=1,.....,8), where the slant angles of the lower wings is similar to those of upper wings but with opposite sign.

For the BOR we have the following structural formula:

R=2.6λ=9.2*a+27.5*L

Where, a=0.118λ

And the BOR parts have the Measurements insert in table (2-2).

Table (2-2): Dimensions of BOR parts in term of reference ratio a, and L.

Dimensions	$\mathbf{r_o}$	$\mathbf{r_{a1}}$	$\mathbf{r_{a2}}$	$\mathbf{r_{a3}}$	$\mathbf{L_{z1}}$	$\mathbf{L_{z2}}$	$\mathbf{L_{z3}}$	$\mathbf{L_{o1}}$	$\mathbf{L_{o2}}$	$\mathbf{L_{o3}}$
value	2.7*a	2.7*a	1.8*a	1.0*a	22.4*L	4.3*L	0.8*L	4.1*a	0.6*a	1.8*a

These measurements give a perfect shape for a rocket BOR by choosing the value of ***a*** and ***L*** as a reference ratio. As for choosing the ideal measurements of the wings will come later.

In order to conduct a comprehensive study, we will be testing the following:

2.3.3.1 The comparison with known RCS

To generalize the formulation for a proposed model, there are some comparisons with known RCS for the BOR and missile, that have been used to test the convergence with this model, and to verify the formulation suggested in the previous section. To compare with the BOR, the body dimensions are selected to make the BOR of rocket looks like the cylinder with hemisphere of Fig.(2-11). It is shown in Fig.(2-27) that our formulation on this conducting rocket without wings (BOR), approximated to cylinder, was correct by comparing the result with that in Fig.(2-11) with the appearance of some variation of the HP and VP and this difference in the curves is due to the flat end of the rocket. While Fig.(2-28) shows the RCS result for the rocket BOR without approximations and without wings in comparison with cylinder of Fig.(2-11) and it indicates the effect of changing the shape of the rocket on the RCS in both HP and VP-polarization.

As comparison with composite body, that was represented by a missile with two identical slant wings of Fig.(2-23), the RCS for the rocket approximate to this body depicted in Fig.(2-29a) and from through it a convergence in HP except some difference which also comes from the flat end of the rocket body. But this difference appears in more details in Fig.(2-29b) when we used the real BOR of the rocket, where its BOR parts are more effected on the RCS result, and one concludes that the body shape can be predicated for the number of oscillation of the current distribution on the conducting BOR.

2.3.3.2 The ideal wings dimensions

One of the most important measures of the composite body are those that determine the ideal dimensions of the wings to get the right shape and then scattering cross section area. This procedure is possible to be achieved to build relationships linking the dimensions of the wings with the dimensions of the body, as in the following table:

Table (2-3): Dimensions of wings in term of large parts of BOR.

Case	Large wing Dimensions			Small wing Dimensions		
	$l_1 = l_7$	$l_2 = l_8$	$l_3 = l_9$	$l_4 = l_{10}$	$l_5 = l_{11}$	$l_6 = l_{12}$
In term of large radius	4.*r_o	0.78* r_o	3.815* r_o	1.555* r_o	0.35* r_o	1.444* r_o
In term of large cylinder	1.034*L_{z1}	0.2* L_{z1}	0.986*L_{z1}	0.402*L_{z1}	0.0935*L_{z1}	0.373*L_{z1}
In term of large radius and cylinder	4.* r_o	0.2*L_{z1}	3.815* r_o	1.555* r_o	0.0935*L_{z1}	1.444* r_o

This was coupled with the relationships determine the height and length of wings depending on the slant angles, as follows:

$$h_1 = l_1 sin v_1 \quad and \quad h_5 = h_1$$
$$h_2 = l_3 sin v_2 \quad and \quad h_6 = h_2$$
$$h_3 = l_4 sin v_3 \quad and \quad h_7 = h_3$$
$$h_4 = l_6 sin v_4 \quad and \quad h_8 = h_4$$

According to the definition of the BOR the planar curve that generates the body must be satisfied during the scanning process, the relationship between ρ_α and z_α is shown in Fig.(2-30), which give the same real shape to the rocket, where the wings inclined at angles of the values: $v_1 = v_3 = 70^o$ and $v_2 = v_4 = 75^o$. As a result, Fig.(2-31) shows the ideal case which illustrates the RCS in HP-polarization of the rocket, calculated using Eq.(2-131), in which three possibilities are found without wings and two wings and finally four wings in monostatic case. The bistatic case has characterized in the rocket with four wings as in Fig(2-32). Results proved that the effect of the reflection waves is due to the wings and clear in the last two cases and also the number of oscillation of the current distribution on all parts of composite body.

2.3.3.3 The effect of wings parameters

There are many parameters of wings, like length, width, high, and the slant angles, that will be studied to make sense about the contribution of the composite body to the RCS. To understand the effect of these parameters, as shown in Fig.(2-26), on the RCS calculated, its classified into many test cases

and arrangement in table (2-4). All studied cases have been taken to monostatic RCS in HP and comparison with ideal case of Fig.(2-31), while the wings do not contribute to the RCS for VP because the wings are normal to the incident electric vector, as confirmed by figure (2-33). The scheme inside the Figs. (2-34) to (2-39) represent the precise shape of rocket.

The first test: the effect of small wing lengths l_4 and l_6 are studied for length equal to half length of large wings, i.e., $l_4 = \frac{l_1}{2}$ and $l_6 = \frac{l_3}{2}$, whereas other parameters remained in the same value of ideal case. Fig.(2-34a) shows the RCS result of increasing the length of small wings. The increasing of small wings length gave decreasing in the reflected and effected waves on the angles between 0^o to 90^o in front of large wings and increasing to waves interference after the large wings.

The second test: the effect of large wing lengths l_1 and l_3 are studied by taking h_1 and h_2 values to make increasing in large wings parameters l_1 and l_3, where h_1 increased by $\frac{h_3}{2}$ and h_2 by $\frac{h_4}{2}$, when other parameters stayed in ideal values. The Fig.(2-34b) illustrates the result of the RCS for increasing in large wings length. The effects of large wings length is strong in contrast with small wings, where the increasing to the waves interference appears in front of large wings and simple effect of small wings. It may come from size of large wings with respect to small wings, and then small current on small wings.

The third test: the effect of large wing widths are dealt with constant values of large wings angles, ν_1=85^o and ν_2=90^o, and changing the l_2 and l_8 values with suggested increasing equal to $l_5/2$ for l_2 and $l_{11}/2$ for l_8. Fig.(2-35) shows the RCS component in the HP (ϕ=0^o), where we find the contributions to the RCS are coming from the interference of waves in large and small wings together, and the increasing in width of large wings give a chance for incident waves to induced large current on the small wings.

The fourth test: the effect of large wing locations are included the changing in the location of large wings by using multi values of angles ν_1 and ν_2. As a result a new modification, the large width for wings have considerable effect for those parameters are shown in Fig.(2-36), where we find high effect in some peaks of the RCS. The extending in width gave new location and then arising different amount of generated current in calculating result of RCS.

The fifth test: the effect of angle ν_2 is made an approximate shapes for other known complex body, like aircraft, in order to arrive to useful treatment with these shapes, beneficiaries from the rocket application in future. This can be satisfied by changing the value of angle ν_2 (ν_6 taken the same value and opposite sign of ν_2) for large wings with controlling on the l_3 and l_9 values. The effect of ν_2 and ν_6 on RCS result was illustrated in Fig.(2-37), especially at value of ν_2=115^o, the large wings are completely approached with small wings. It has a new incident wave which generates a new induced current on total surface.

The sixth test: (the effect of angles ν_1 and ν_2) studied the effect of changing large wings angles together. This was implemented for two probabilities of angles value, as shown in Fig.(2-38), where the effect has appeared with clear form in the region in front of the large wings by increasing the RCS value. This may come from changing the shape of large wings to be similar to the shape of flat wings.

The seventh test: (the effect of flat wings) is special case for all wings when the angles υ_1, υ_2, υ_3, υ_4, take the same value equal to 90, which means that the wings are transformed exactly to be a flat shape. the RCS result for this case is depicted in Fig.(2-39) , where we find oscillation in the side peaks of RCS shape, toward increasing in front of large wings and decreasing toward the small wings.

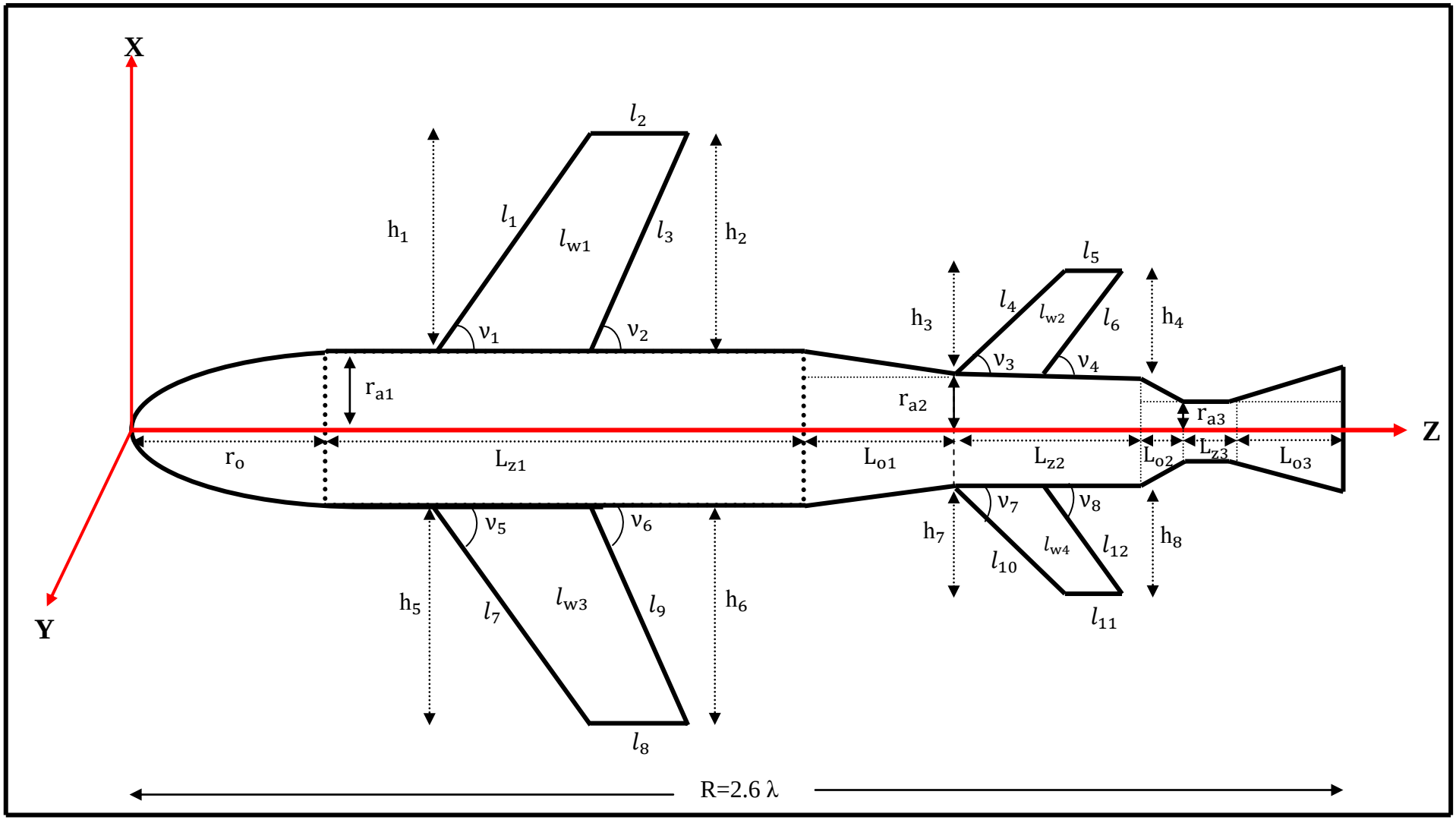

Fig.(2-26): Geometric scheme to parts of the proposed model.

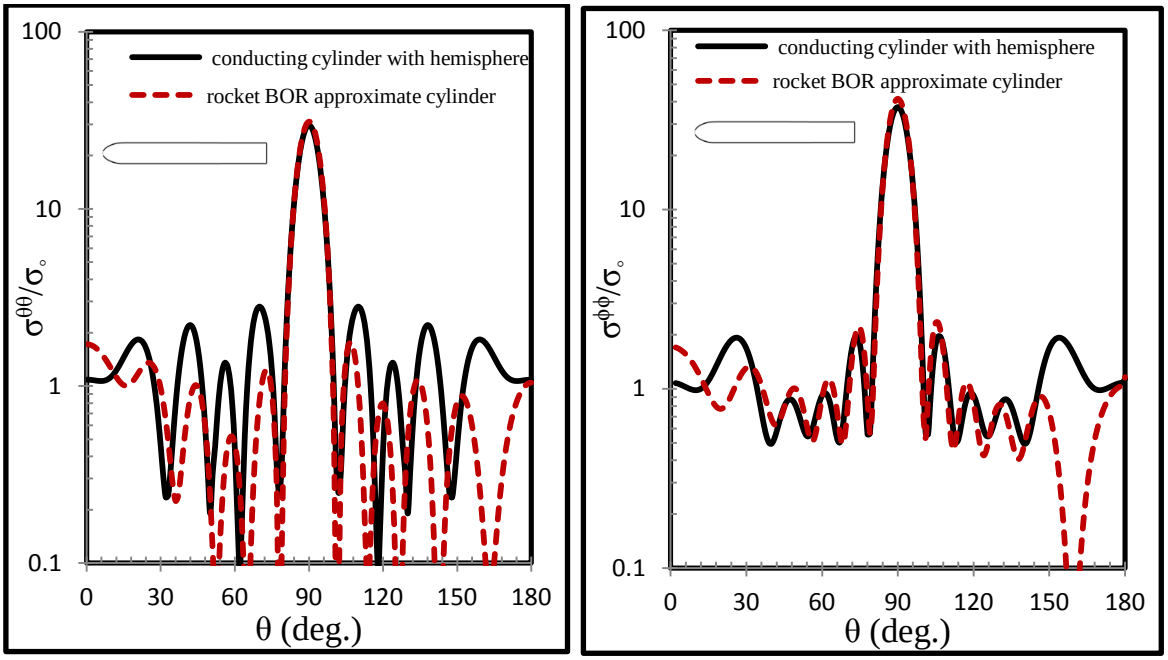

(a) HP (b)VP

Fig.(2-27): Monostatic RCS for the body (BOR) of Fig.(2-26) compared with that of Fig.(2-11).

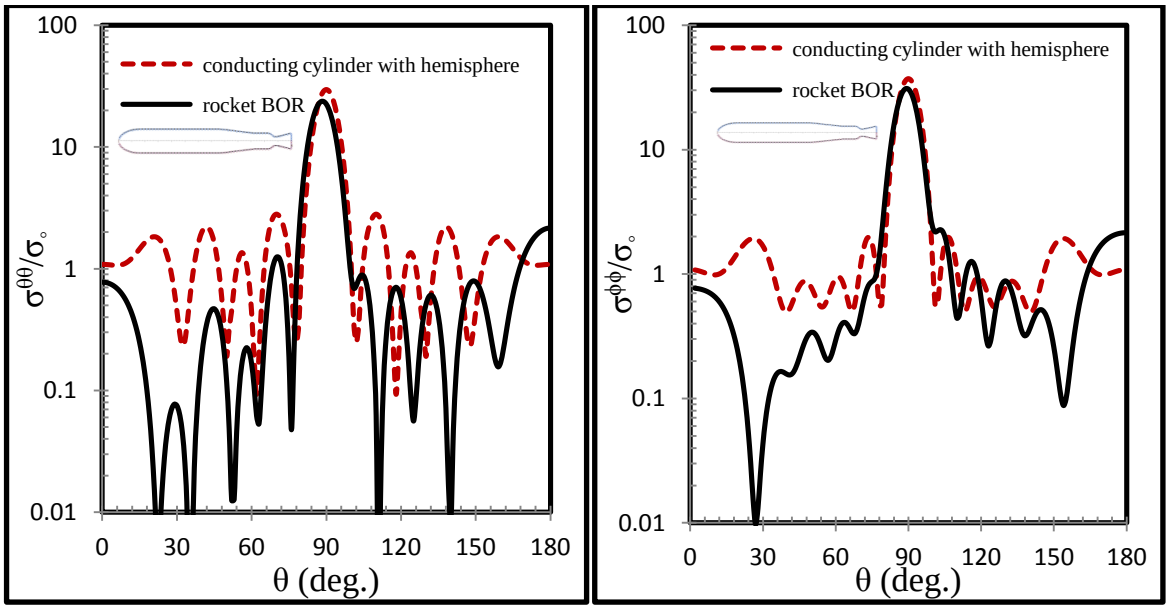

(a) HP (b) VP

Fig.(2-28): Monostatic RCS for the body (BOR) of Fig.(2-26) compared with that of Fig.(2-11).

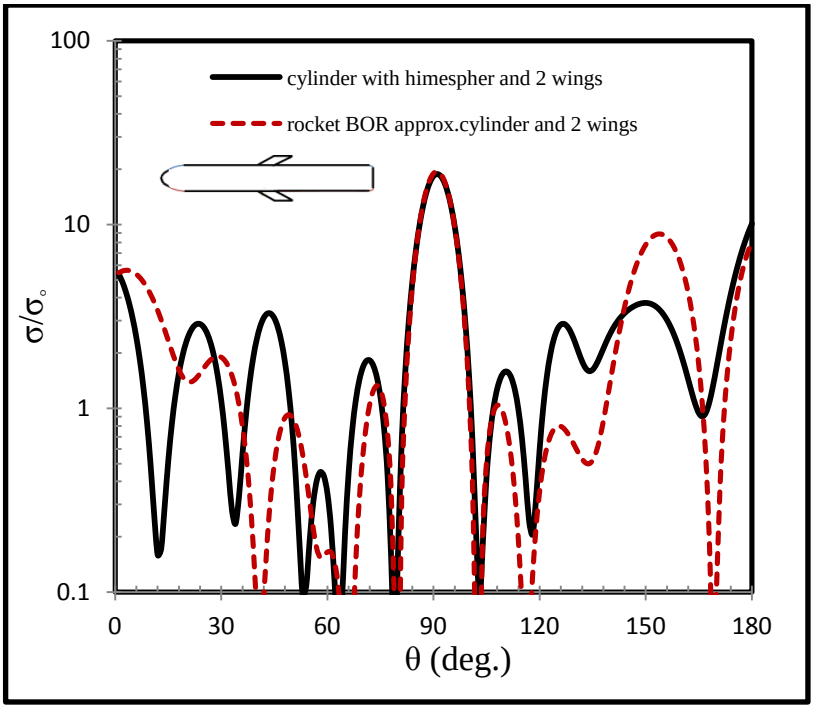

(a)

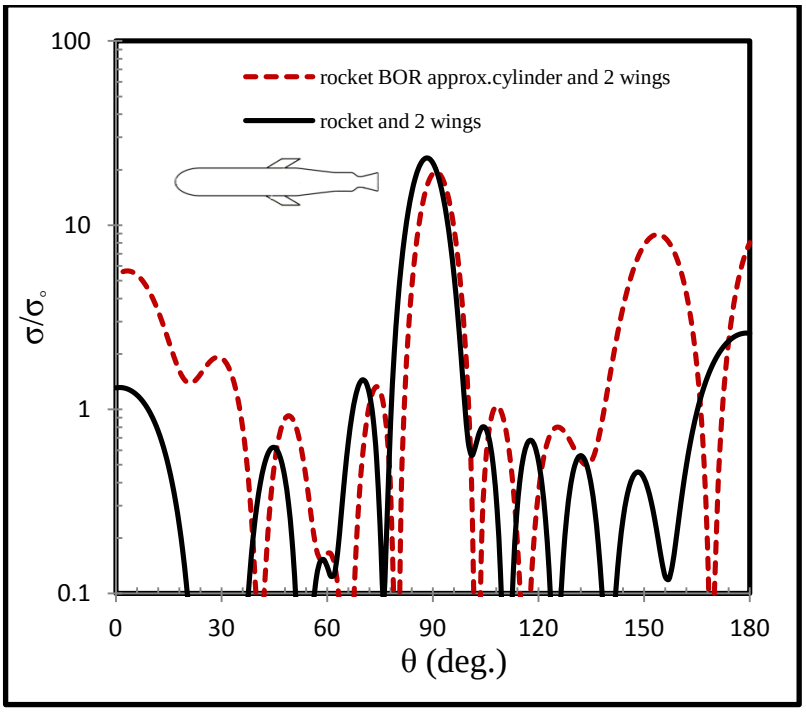

(b)

Fig.(2-29): Monostatic RCS in HP for the body of Fig.(2-26)with two wings compared with that of Fig.(2-23). (a) rocket BOR approximate cylinder. (b) rocket BOR has a real shape of Fig.(2-26).

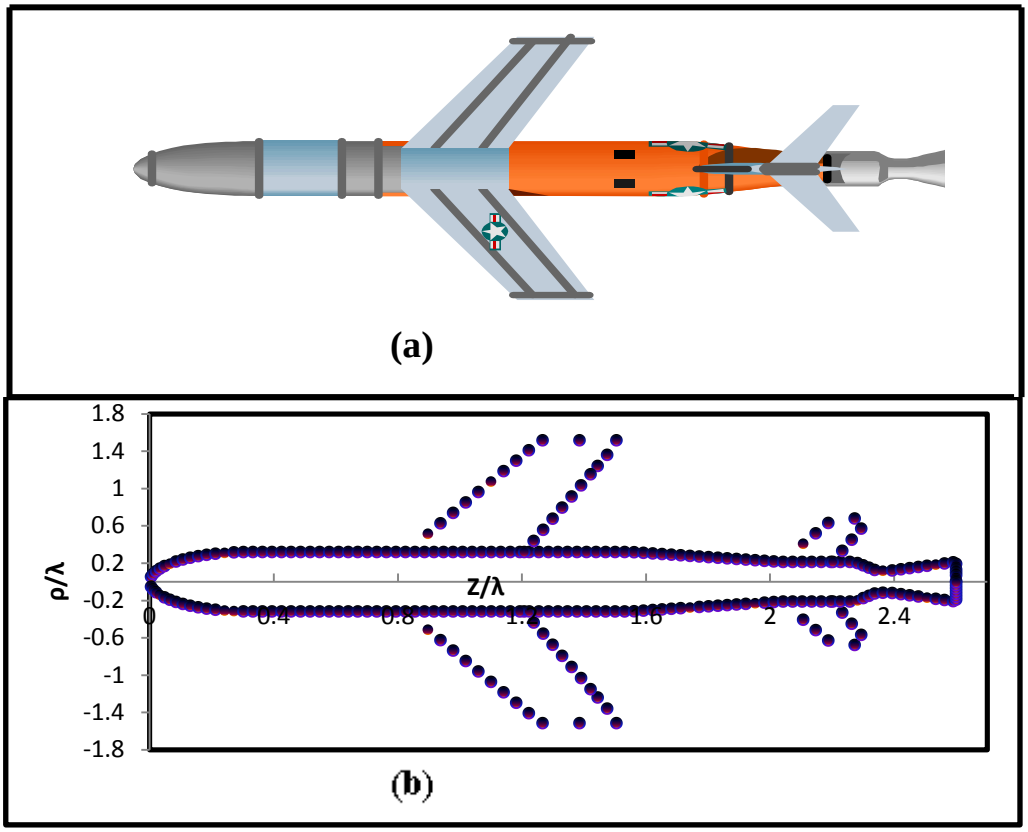

Fig.(2-30): (a) The real shape of model. (b) The precise shape of the model.

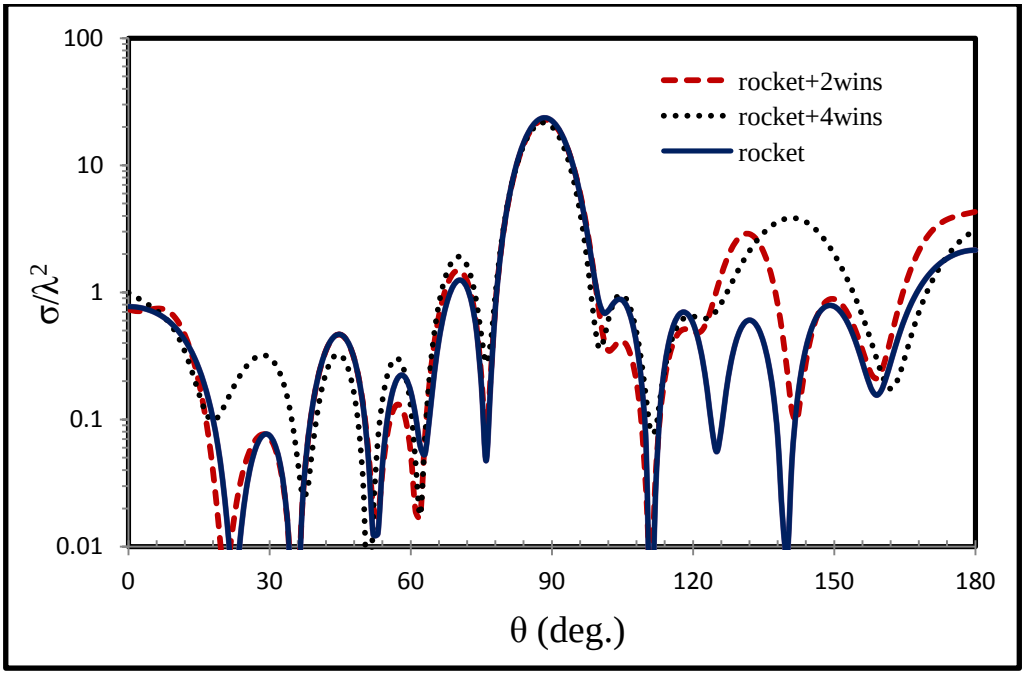

Fig.(2-31): Monostatic RCS in HP-polarization for three possibilities of model with ideal dimensions.

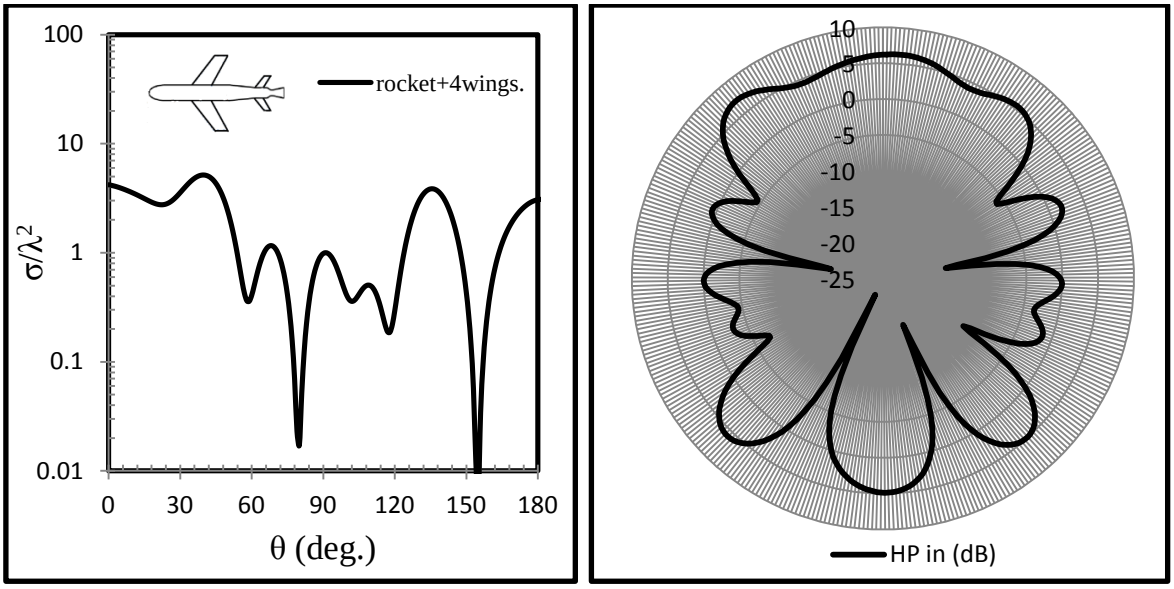

(a) (b)

Fig.(2-32): (a)Bistatic RCS in HP for the four wings case with ideal dimensions of Fig.(2-26). (b)HP of model with radar graph representation.

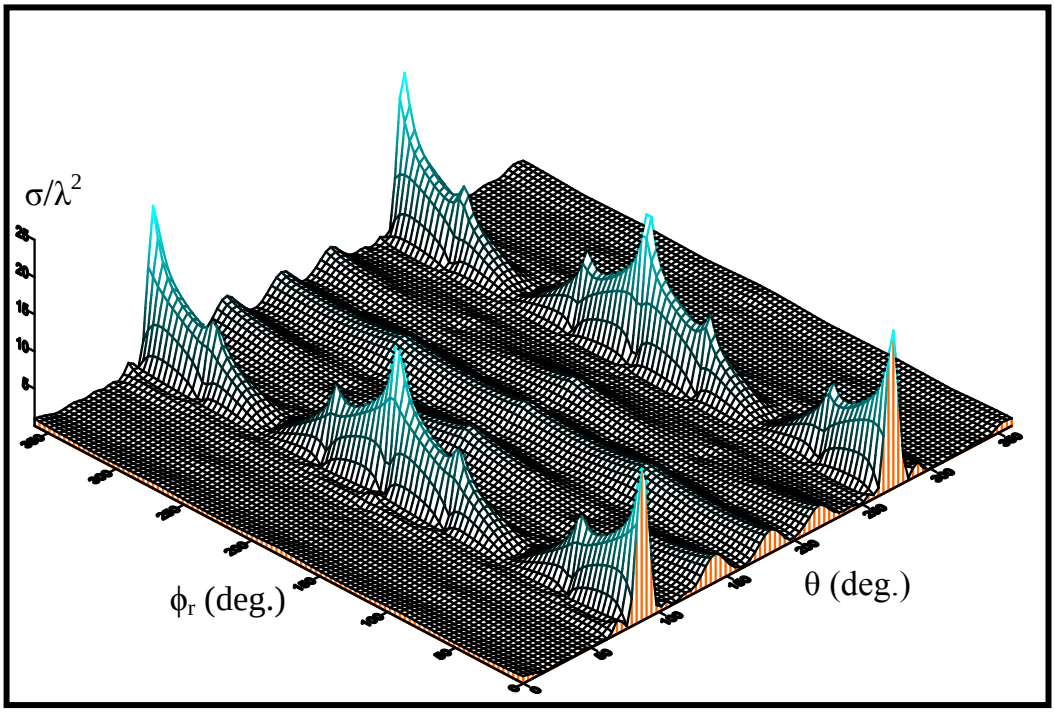

Fig.(2-33): *Monostatic RCS for proposed model in three-dimensional form.*

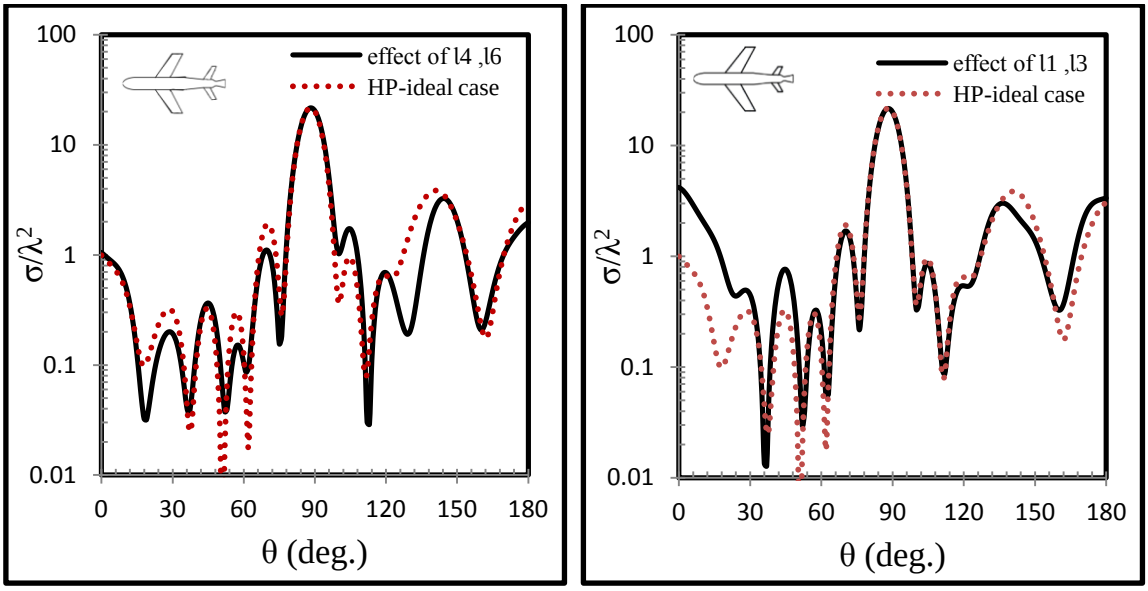

(a) (b)

Fig.(2-34): Computed backscatter cross section in HP for body of Fig.(2-26) with respect to: (a) small wings length. (b) large wings length.

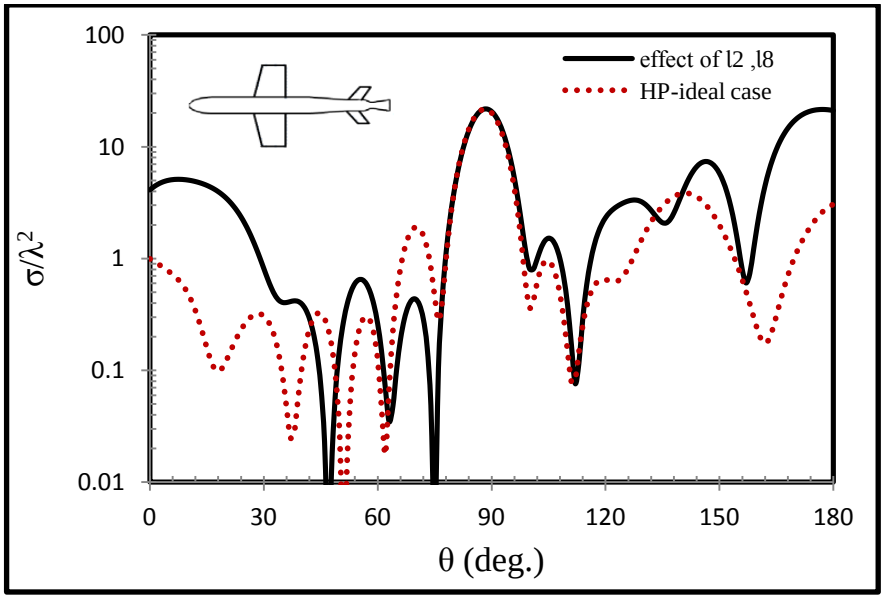

Fig.(2-35): Computed backscatter cross section in HP for body of Fig.(2-26) with respect to large wings width.

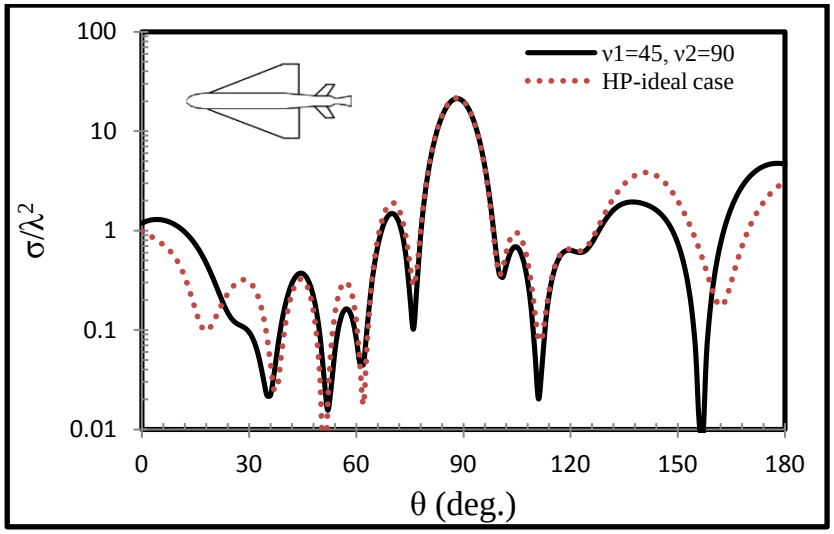

(a)

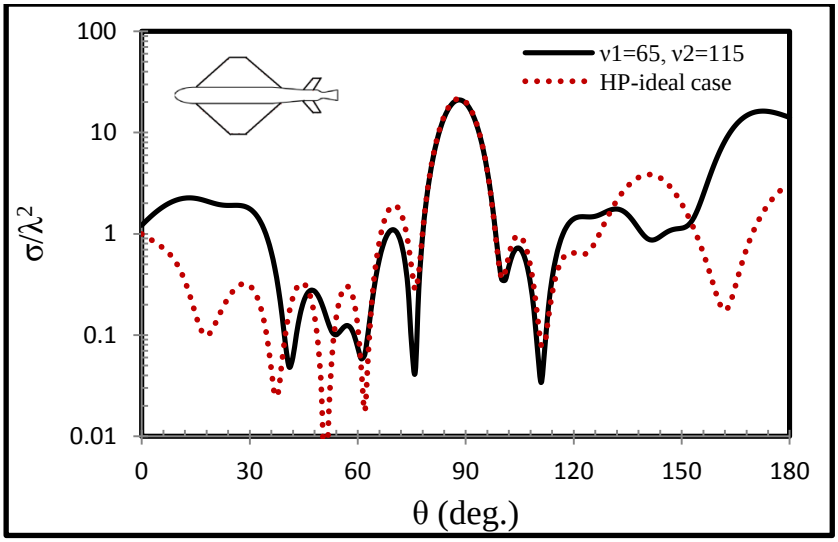

(b)

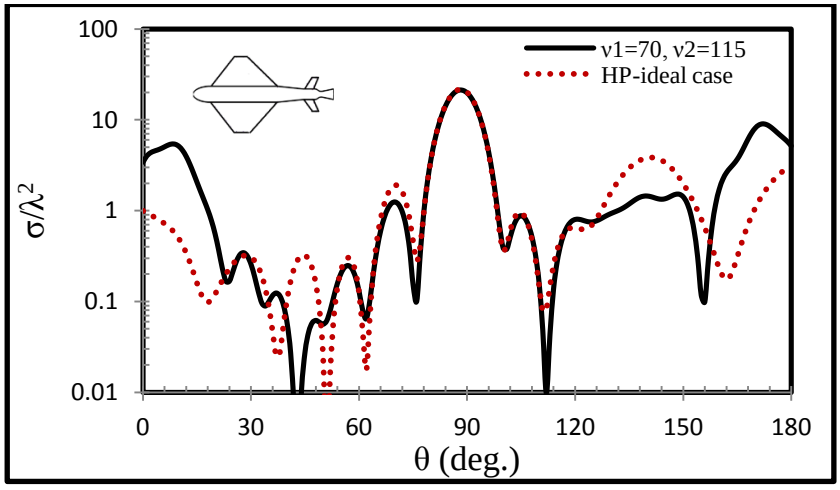

(c)

Fig.(2-36): Computed backscatter cross section in HP for body of Fig.(2-26) with respect to large wings location from through of put: (a) $v_1=45^o$, $v_2=90^o$. (b) $v_1=65^o$, $v_2=115^o$. (c) $v_1=70^o$, $v_2=115^o$.

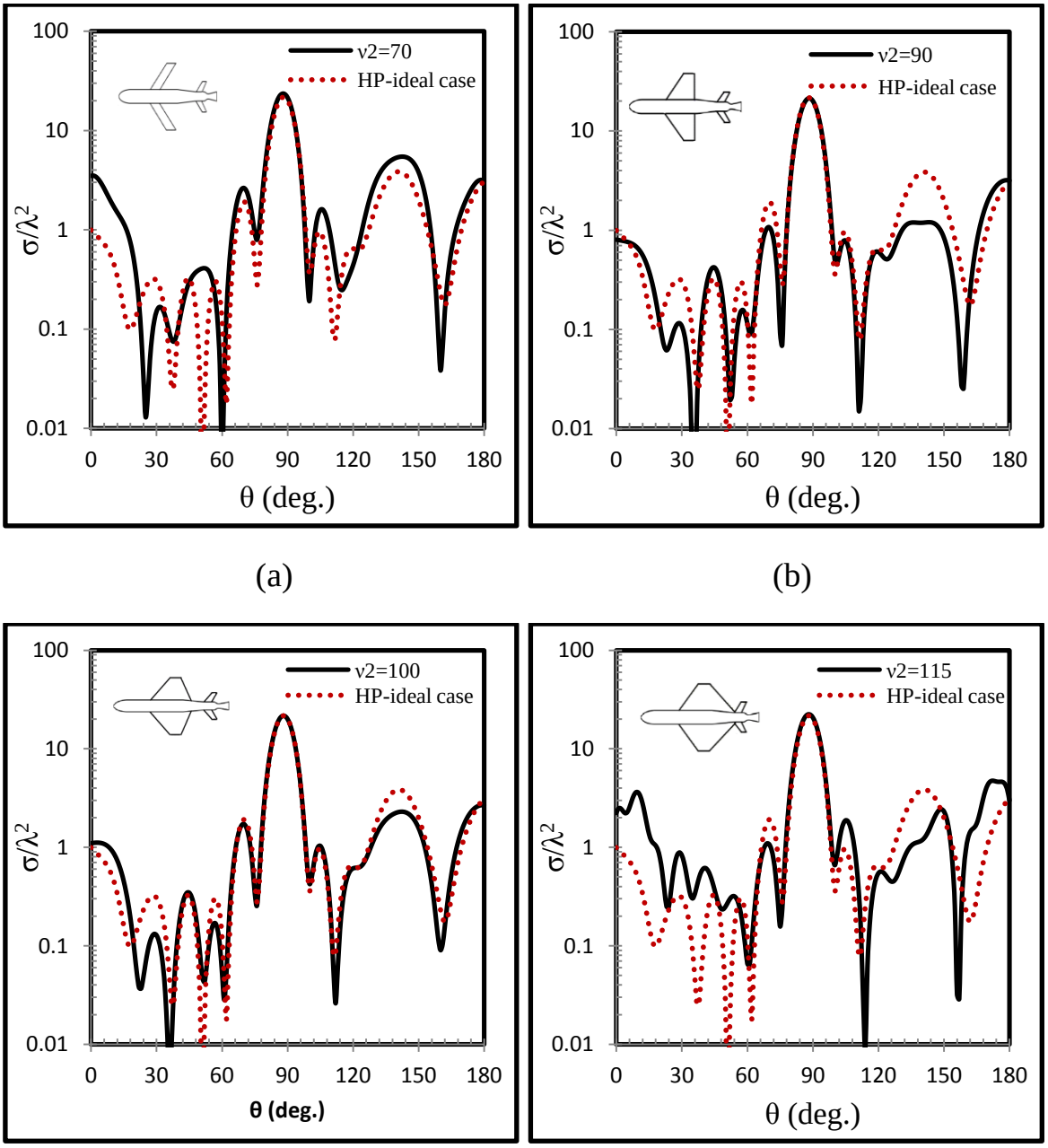

Fig.(2-37): Computed backscatter cross section in HP for body of Fig.(2-26) with respect to v_2 (v_6 =- v_2) angles in large wings location from through of put: (a) v_2=70°. (b) v_2=90°. (c) v_2=100°. (d) v_2=115°.

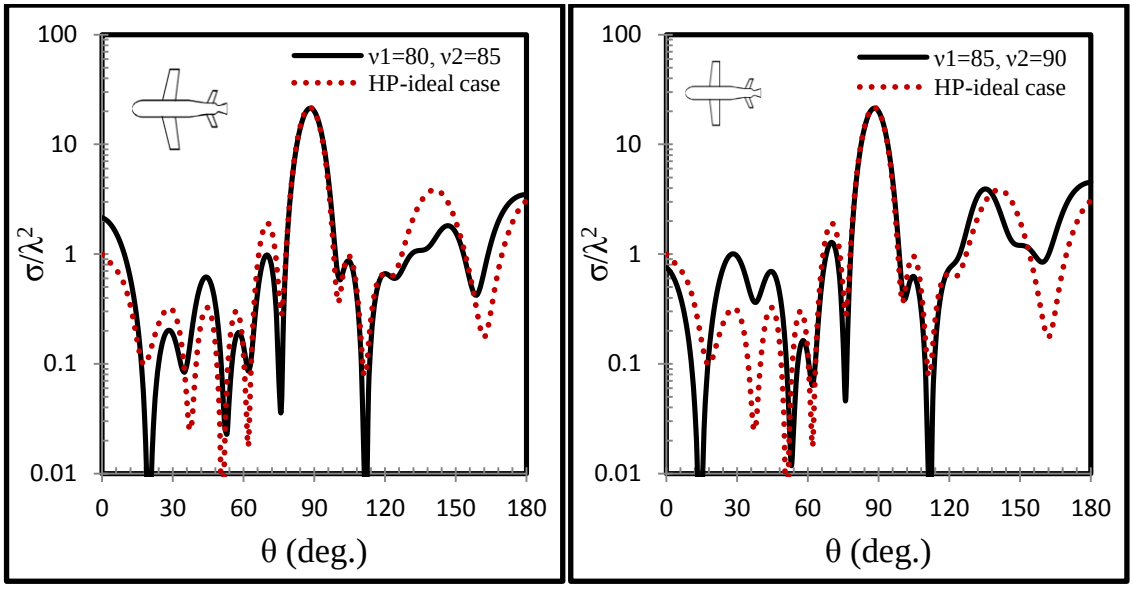

(a) *(b)*

Fig.(2-38): Computed backscatter cross section in HP for body of Fig.(2-26) with respect to large wings angles from through of put: (a) $v_1=80^o$, $v_2=85^o$. (b) $v_1=85^o$, $v_2=90^o$.

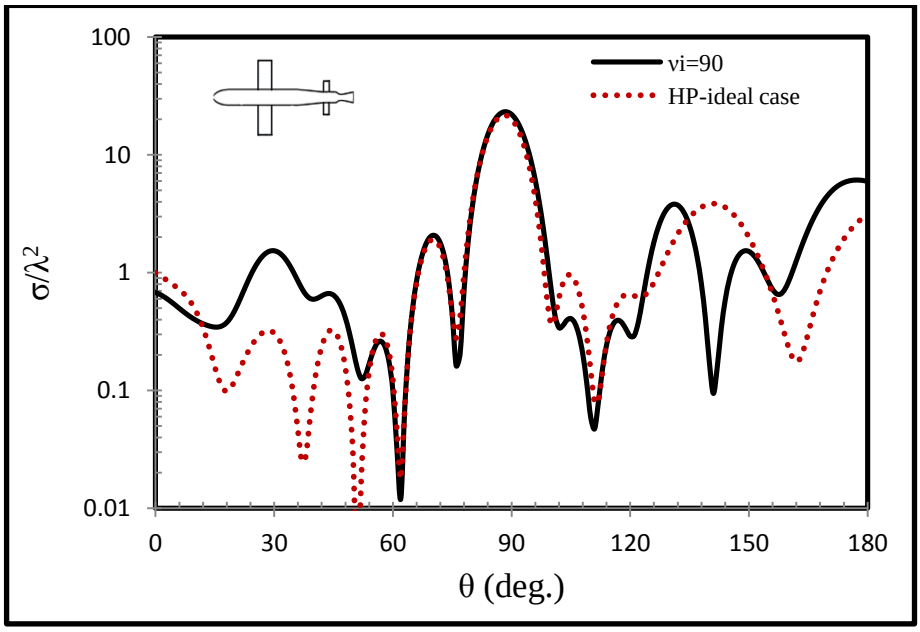

Fig.(2-39): Computed backscatter cross section in HP for body of Fig.(2-26) with respect to same values of all angles, $v_i=90^o$.

Table (2-4): The wings parameters in the study cases.

case	Large wings angles		Large Wings Dimensions						Small wings angles		Small Wings Dimensions					
	ν_1	ν_2	l_1/λ	l_2/λ	l_3/λ	h_1/λ	h_3/λ	N_{w1}	ν_3	ν_4	l_4/λ	l_5/λ	l_6/λ	h_4/λ	h_6/λ	N_{w2}
ideal	70	75	1.2743	0.2485	1.2154	1.1976	1.1772	23	70	75	0.4954	0.1115	0.4600	0.4656	0.4456	9
1	70	75	1.2743	0.2485	1.2154	1.1976	1.1772	23	70	75	0.6372	0.1115	0.6053	0.4931	0.2347	11
2	70	75	1.5221	0.2485	1.4558	1.4304	1.4100	27	70	75	0.4954	0.1115	0.4600	0.4656	0.4456	9
3	85	90	1.2020	0.3042	1.1772	1.1976	1.1772	23	70	75	0.4954	0.1115	0.4600	0.4656	0.4456	9
4	70	115	1.2743	0.2485	1.3011	1.1976	1.1772	23	70	75	0.4954	0.1115	0.4600	0.4656	0.4456	9
	65	115	1.3236	0.2485	1.3011	1.1976	1.1772	24	70	75	0.4954	0.1115	0.4600	0.4656	0.4456	9
	45	90	1.6937	0.2485	1.1772	1.1976	1.1772	26	70	75	0.4954	0.1115	0.4600	0.4656	0.4456	9
5	70	70	1.2743	0.2485	1.2526	1.1976	1.1772	23	70	75	0.4954	0.1115	0.4600	0.4656	0.4456	9
	70	90	1.2743	0.2485	1.1772	1.1976	1.1772	23	70	75	0.4954	0.1115	0.4600	0.4656	0.4456	9
	70	100	1.2743	0.2485	1.1198	1.1976	1.1772	23	70	75	0.4954	0.1115	0.4600	0.4656	0.4456	9
	70	115	1.2743	0.2485	1.3011	1.1976	1.1772	23	70	75	0.4954	0.1115	0.4600	0.4656	0.4456	9
6	80	85	1.2158	0.2485	1.1815	1.1976	1.1772	23	70	75	0.4954	0.1115	0.4600	0.4656	0.4456	9
	85	90	1.2020	0.2485	1.1772	1.1976	1.1772	23	70	75	0.4954	0.1115	0.4600	0.4656	0.4456	9
7	90	90	1.1976	0.2485	1.1772	1.1976	1.1772	23	90	90	0.4656	0.1115	0.4456	0.4656	0.4456	9

Chapter Three

Scattering from dielectric BOR with attached wires

3.1 Introduction

Electromagnetic scattering from conducting, dielectric and composite bodies is an important and challenging problem in the field of computational electromagnetic. Furthermore, composite structures of metallic and homogeneous dielectric materials have many important applications e.g., in the radar technology, antenna design and microwave engineering. Analytical solutions are available for only very limited geometries. For bodies having an arbitrary shape, one has to resort to some approximate numerical technique. A variety of approaches have been developed to study this problem, which includes the MoM, the FEM, and the FDTD method. When the bodies are homogeneous, MoM is preferred because the problem can be formulated in terms of surface integrals over the conducting and dielectric surfaces [103]. In special for BORs the problem is formulated in terms of integrals over generatrixes [48] [96]. For perfectly conducting BOR the problem has been exhaustively studied and the most accurate formulations are EFIE and CFIE (that is a linear combination of EFIE and MFIE) for opened and closed conducting bodies, respectively [46]. For dielectric BOR, many combinations of EFIE and MFIE have been investigated [48] [101].

EFIE-PMCHWT is the usual formulation for general composite structures [94] and [103]. In this formulation EFIE is applied on metallic surfaces and the Poggio-Miller- Chang-Harrington-Wu-Tsai (PMCHWT) formulation [48] is applied on the dielectric interfaces, but it is not sufficient for removing the interior resonances if the structure includes closed metallic surfaces. In that case, in addition, on those surfaces the CFIE must be applied [46].

Such solutions (or combinations of them) can be used in the analysis of scattering by composite body (DBOR -wire-junction) as they are shown in

Fig. (3-1). However, the problem of DBOR-wire was formulated in a system of wire radiators coupled to DBOR [99], based on MoM and deals with this problem in the same way of conducting bodies [76].

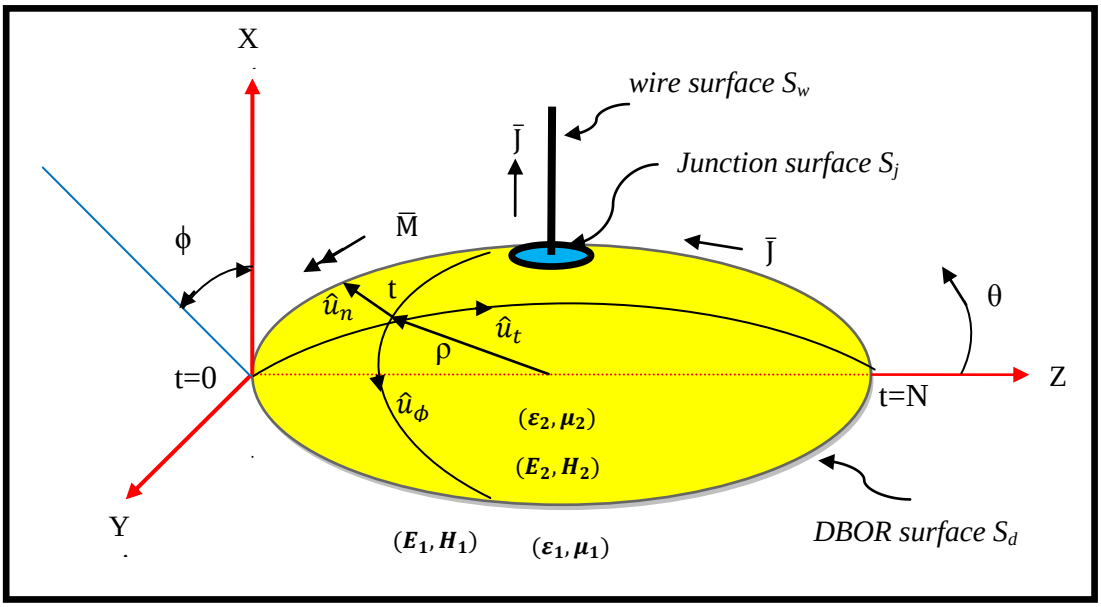

Fig.(3-1): Homogeneous dielectric object $(\varepsilon_2\ , \mu_2)$ embedded in a homogenous medium $(\varepsilon_1\ , \mu_1)$ with electric attached wire. $\bar{J}$ and $\bar{M}$ are the equivalent surface currents for the exterior region.

3.2 Formulation of the boundary value problem

In this section, wires attached to DBORs are considered. The geometry of Fig.(3-2a) is typical of the EM boundary value problem of a structure consist of DBOR-wire-junction. The DBOR is represented as the cross section of a surface revolution, S_{de}. Moreover, the DBOR is composed of a homogeneous material with constituent parameters ϵ_d and μ_d, where ϵ_d and μ_d are the permittivity and permeability of the material, respectively. On the other hand , the region exterior to the DBOR is composed of a homogeneous medium of constituent parameters ϵ_e and μ_e. The thin conductor wire can be represented as one dimensional structure, in like manner with well developed thin wire theory [35], and represented by S_{wd} and S_{we} where the subscripts

"wd" and "we" refer to wire elements interior and exterior to the DBOR, respectively. Likewise, attachment region at the wire/DBOR surface (junction region) represented by S_{jd} and S_{je} where the subscripts "jd" and "je" refer to junction elements interior and exterior to the DBOR, respectively. The electric and magnetic field vectors are represented by the symbols $\bar{E}$ and $\bar{H}$ with superscripts "dt" and "et" refer to the total field interior and exterior to the DBOR, respectively. The field vectors $\bar{E}$ and $\bar{H}$ with superscript "d" and "e" refer to the fields which arise from the equivalent currents which reside on the surfaces in the interior and exterior problems. The superscript "i" refers to the known field. The equivalent electric and magnetic surface currents which arise from application of the field equivalence principle are represented by the symbols $\bar{J}$ and $\bar{M}$, respectively.

The original problem of Fig.(3-2a) can be divided into two problems: one of the interior region, and the other for the exterior region. For this purpose, the equivalence principle [38] is used and the two equivalent problems are illustrated in Figs.(3-2b) and (3-2c). The field components in each region of Fig.(3-2a) can be constructed readily from the equivalent currents. The boundary conditions to be satisfied are:

$$\hat{n}\times\bar{E}^{et}=0 \qquad (3\text{-}1a)$$

$$\hat{n}\times\bar{H}^{et}=0 \qquad (3\text{-}1b)$$

$$\hat{n}\times\bar{E}^{dt}=0 \qquad (3\text{-}1c)$$

$$\hat{n}\times\bar{H}^{dt}=0 \qquad (3\text{-}1d)$$

and the surface equivalent currents are:

$$\bar{J}_{we}=\hat{n}\times\bar{H}^{e} \quad \text{, on } S_{we} \qquad (3\text{-}2a)$$

$$\bar{J}_{wd}=\hat{n}\times\bar{H}^{d} \quad \text{, on } S_{wd} \qquad (3\text{-}2b)$$

$$\bar{J}_{je}=\hat{n}\times\bar{H}^{e} \quad \text{, on } S_{je} \qquad (3\text{-}2c)$$

$$\bar{J}_{jd}=\hat{n}\times\bar{H}^{d} \quad \text{, on } S_{jd} \qquad (3\text{-}2d)$$

$\bar{J}_{de} = \hat{n} \times \bar{H}^e$, on S_{de} (3-2e)

$\bar{M}_{de} = -\hat{n} \times \bar{E}^e$, on S_{de} (3-2f)

Eqs.(3-1) form a set of four equations in the two unknowns $\bar{J}$ and $\bar{M}$. The method of solution is applied only when the number of equations is equal to the number of unknowns. In accordance with Miller [36] and PMCHWT [48] the four equations are reduced to two equations by defining the form of linear combination as follow:

$$-\hat{n} \times (E^e + \alpha E^d) = \hat{n} \times E^{ie} \quad (3\text{-}3)$$

$$-\hat{n} \times (H^e + \beta H^d) = \hat{n} \times H^{ie} \quad (3\text{-}4)$$

Where α and β are linear combination and given by [48]

$$\alpha = -\epsilon_d / \epsilon_e \quad (3\text{-}5)$$

$$\beta = -\mu_d / \mu_e \quad (3\text{-}6)$$

By enforcing the boundary conditions that the tangential component of the electric field must vanish at the conductor surface, and that the tangential components of both electric and magnetic fields must be continuous across the dielectric surface, a system of integro-differential equations is obtained from which the unknowns J_{wd}, J_{we} , J_{jd} , J_{je} , J_{de} and M_{de} can be determined. This system of equations can be written in operator form [100] as the following:

$\bar{E}^d_{\tan}(\bar{J}_{de} + \bar{J}_{wd} + \bar{J}_{jd}, \bar{M}_{de}) = \bar{E}^{id}_{\tan}$, on S_{wd} and S_{jd} (3-7a)

$\bar{E}^e_{\tan}(\bar{J}_{de} + \bar{J}_{we} + \bar{J}_{je}, \bar{M}_{de}) = -\bar{E}^{ie}_{\tan}$, on S_{we} and S_{je} (3-7b)

$\bar{E}^e_{\tan}(\bar{J}_{de} + \bar{J}_{we} + \bar{J}_{je}, \bar{M}_{de}) + \bar{E}^d_{\tan}(\bar{J}_{de} + \bar{J}_{wd} + \bar{J}_{jd}, \bar{M}_{de}) = \bar{E}^{id}_{\tan} - \bar{E}^{ie}_{\tan}$, on S_{de} (3-7c)

$\bar{H}^e_{\tan}(\bar{J}_{de} + \bar{J}_{we} + \bar{J}_{je}, \bar{M}_{de}) + \bar{H}^d_{\tan}(\bar{J}_{de} + \bar{J}_{wd} + \bar{J}_{jd}, \bar{M}_{de}) = \bar{H}^{id}_{\tan} - \bar{H}^{ie}_{\tan}$, on S_{de} (3-7d)

The above system of equations consists of the EFIE on the conductor surfaces, and both the EFIE and the MFIE on the DBOR surface. This formulation is referred to as the EFIE-PMCHWT [101].

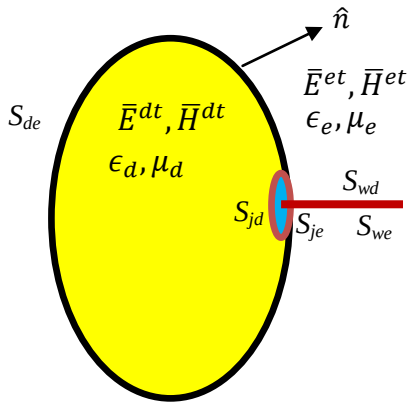

(a)

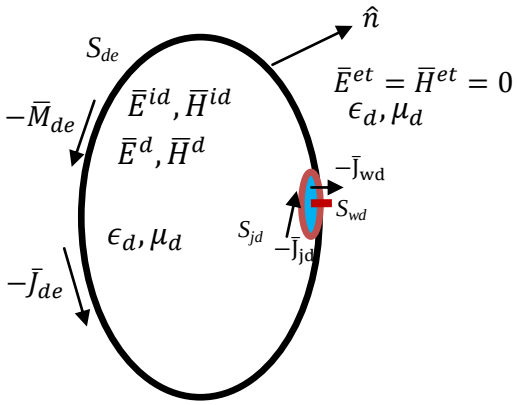

(b)

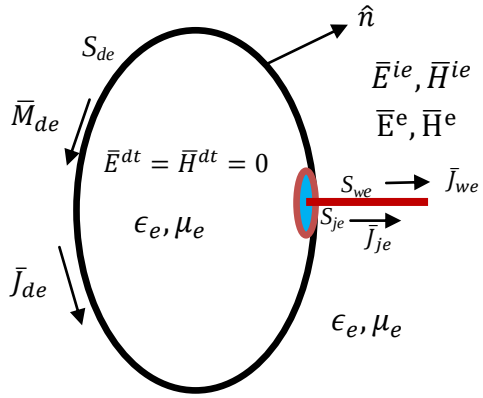

(c)

Fig.(3-2): (a) The original problem, (b) The interior and (c) The exterior problem.

3.3 The potential integrals

The fields $\bar{E}(J,M)$ and $\bar{H}(J,M)$ of Eqs.(3-7), which represent the integro-differential operators, are defined in terms of magnetic and electric vector and scalar potential functions represented by $\bar{A},\bar{F},\Phi,\text{and}\,\Psi$, respectively. These field vectors are given by [92], as follow

$$\bar{E}^a(\bar{J},\bar{M}) = -j\omega\bar{A}^a(\bar{J}) - \nabla\Phi^a(\bar{J}) - \frac{1}{\varepsilon_a}\nabla\times\bar{F}^a(\bar{M}) \tag{3-8}$$

$$\bar{H}^a(\bar{J},\bar{M}) = -j\omega\bar{F}^a(\bar{M}) - \nabla\psi^a(\bar{M}) + \frac{1}{\mu_a}\nabla\times\bar{A}^a(\bar{J}) \tag{3-9}$$

Where the potential functions are defined by [91] as:

$$\bar{A}^a(\bar{r}) = \mu_a\iint_{s'}\bar{J}(\bar{r}')\,G^a(\bar{r},\bar{r}')\,ds' \tag{3-10}$$

$$\bar{F}^a(\bar{r}) = \varepsilon_a\iint_{s'}\bar{M}(\bar{r}')\,G^a(\bar{r},\bar{r}')\,ds' \tag{3-11}$$

$$\Phi^a(\bar{r}) = \frac{1}{\varepsilon_a}\iint_{s'}\rho_e(\bar{r}')\,G^a(\bar{r},\bar{r}')\,ds' \tag{3-12}$$

$$\psi^a(\bar{r}) = \frac{1}{\mu_a}\iint_{s'}\rho_m(\bar{r}')\,G^a(\bar{r},\bar{r}')\,ds' \tag{3-13}$$

And S is a surface that includes all surfaces ,DBOR, wire, and junction, that contributes to the field in region (a). The superscript (a) represents (e) or (d). The surface charge density ρ_e and ρ_m are related to the current sources through the equation of continuity

$$\bar{\nabla}'_s\cdot\bar{J}(\bar{r}') = -j\omega\rho_e(\bar{r}') \tag{3-14}$$

$$\bar{\nabla}'_s\cdot\bar{M}(\bar{r}') = -j\omega\rho_m(\bar{r}') \tag{3-15}$$

The function $G^a(\bar{r},\bar{r}')$ is the scalar free space Green's function and is a function of $\bar{r}\;and\;\bar{r}'$, the position vectors of field and source coordinates, respectively.

3.4 PMCHWT integral equation for DBOR object.

Surface IE methods are popular in solving EM scattering containing homogeneous dielectric materials. The scattering of EM waves from a homogeneous object having permittivity ϵ_2 and permeability μ_2 in a homogeneous background medium (ϵ_1, μ_1), as shown in Fig.(3-1), can be solved by PMCHWT integral equations [51], as follow:

$$\hat{n} \times \bar{E}^{inc} = \hat{n} \times [L_1(\bar{J}) + L_2(\bar{J})] - \hat{n} \times [K_1(\bar{M}) + K_2(\bar{M})] \quad (3\text{-}17)$$

$$\hat{n} \times \bar{H}^{inc} = \hat{n} \times [K_1(\bar{J}) + K_2(\bar{J})] + \hat{n} \times \left[\frac{1}{\eta_1^2} L_1(\bar{M}) + \frac{1}{\eta_2^2} L_2(\bar{M})\right] \quad (3\text{-}18)$$

Where J and M are the incident electric and magnetic current densities, $\eta_i = \sqrt{\mu_i/\epsilon_i}$ is the wave impedance for region i (i=1,2), $\bar{E}^{inc}$ and $\bar{H}^{inc}$ are the incident electric and magnetic field, respectively. The operators L_i and K_i are defined as [39]:

$$L_i(X) = j\omega\mu_i \int_s \left[XG_i + \frac{1}{\omega^2\mu_i\epsilon_i} \nabla\acute{V}.XG_i\right] ds \quad (3\text{-}19a)$$

$$K_i(X) = \int_s X \times \nabla G_i \, ds \quad (3\text{-}19b)$$

Where S is the surface of the scatterer, and G_i is the scalar Green's function of background medium (i=1) or dielectric region (i=2) expressed as:

$$G_i(r, \acute{r}) = \frac{e^{-jk_i|r-\acute{r}|}}{4\pi|r-\acute{r}|} \quad (3\text{-}20)$$

with $k_i = \omega\sqrt{\mu_i\epsilon_i}$

3.5 Moment Method Solution

The surface integral Eqs.(3-7) are solved by MoM. The described problem can be solved in an efficient manner by a judicious choice of basis and testing functions. First, consider the DBOR of Fig.(3-1). Due to the axial symmetry, two components of electric and magnetic current can be identified: one directed along the generating arc $(\hat{u}_t)$, and the other in the

circumferential direction ($\hat{u}_\phi$). In order to solve PMCHWT IEs (3-17) and (3-18), the unknown surface current densities are first expanded in terms of Fourier modes [88]

$$\bar{J}_s(t,\phi) = \bar{J}^t(t,\phi) + \bar{J}^\phi(t,\phi)$$
$$= \sum_{n=-\infty}^{\infty}\left[\bar{J}_n^t(t) + \bar{J}_n^\phi(t)\right]e^{jn\phi} \quad (3\text{-}21a)$$

$$\bar{M}_s(t,\phi) = \eta_a(\bar{M}^t(t,\phi) + \bar{M}^\phi(t,\phi))$$
$$= \eta_a \sum_{n=-\infty}^{\infty}\left[\bar{M}_n^t(t) + \bar{M}_n^\phi(t)\right]e^{jn\phi} \quad (3\text{-}21b)$$

Where η_a is the wave impedance for interior or exterior regions.

These components can be further expanded on the generating arc in terms of sub-domain basis functions f_i as

$$\left.\begin{aligned}\bar{J}_n^t(t) &= \hat{u}_t \sum_{i=1}^{N_d-1} I_{ni}^t f_i(t)\\ \bar{J}_n^\phi(t) &= \hat{u}_\phi \sum_{i=1}^{N_d-1} I_{ni}^\phi f_i(t)\end{aligned}\right\} \quad (3\text{-}22a)$$

$$\left.\begin{aligned}\bar{M}_n^t(t) &= \hat{u}_t \sum_{i=1}^{N_d-1} k_{ni}^t f_i(t)\\ \bar{M}_n^\phi(t) &= \hat{u}_\phi \sum_{i=1}^{N_d-1} k_{ni}^\phi f_i(t)\end{aligned}\right\} \quad (3\text{-}22b)$$

Where the $f_i(t) = \frac{1}{\rho}T_i(t)$ and T_i is the triangular function, introduced in Eq.(2-12). The testing function is

$$\bar{W}_{mi}^\alpha = \hat{u}_\alpha f_i(t) e^{-jm\phi} \text{ , } \alpha=t \text{ or } \phi \quad (3\text{-}23)$$

For wire and junction, the basis and testing functions are introduced in the chapter two by Eqs.(2-8), (2-9), (2-18), and (2-19).

The unknown current coefficients (I_{ni}^t, I_{ni}^ϕ, k_{ni}^t, k_{ni}^ϕ, I^w, I^j) can be determine via the MoM by forming the inner product via the Galerkin technique. So, the PMCHWT IEs for DBOR (3-17) and (3-18) can be written [98] as:

$$(P_1 + P_2)[J] - (Q_1 + Q_2)[M] = b^{TE} \quad (3\text{-}24)$$

$$(Q_1 + Q_2)[J] - \left(\frac{1}{\eta_1^2}P_1 + \frac{1}{\eta_2^2}P_2\right)[M] = b^{TH} \quad (3\text{-}25)$$

$$(P_i)_{mn} = \langle f_m, L_i(f_n)\rangle \quad (3\text{-}26)$$

$$(Q_i)_{mn} = \langle f_m, K_i(f_n) \rangle \quad (3\text{-}27)$$

$$b_m^{TE} = \langle f_m, E^{inc} \rangle \quad (3\text{-}28)$$

$$b_m^{TH} = \langle f_m, H^{inc} \rangle \quad (3\text{-}29)$$

Where f_n is the basis function and f_m is the testing function. The testing functions are orthogonal to operators *L(J)* and *K(M)* when $m \neq n$. So, all impedance elements are zero except for those $m=n$, and each mode can be treated separately. For each mode, we have to solve the following matrix equation

$$\begin{bmatrix} Z_n^{EE} & Z_n^{EH} \\ Z_n^{HE} & Z_n^{HH} \end{bmatrix} \begin{bmatrix} I_n \\ M_n \end{bmatrix} = \begin{bmatrix} V_n^E \\ V_n^H \end{bmatrix} \quad (3\text{-}30)$$

In order to balance the impedance elements [98], the matrix equation can be written as

$$\begin{bmatrix} Z_n^{EE} & Z_n^{EH} \\ \eta_1 Z_n^{HE} & \eta_1^2 Z_n^{HH} \end{bmatrix} \begin{bmatrix} I_n \\ \eta_1 M_n \end{bmatrix} = \begin{bmatrix} V_n^E \\ \eta_1 V_n^H \end{bmatrix} \quad (3\text{-}31)$$

Now the composite body (DBOR/wire/junction) have a system of equations by substituting Eqs.(3-21), (2-8), and (2-9) , from chapter tow, into Eqs.(3-7) and using the linearity of the operators, yield:

$$\sum_{n=-\infty}^{\infty} \left[\sum_{j=1}^{N_d-1} I_{nj}^d \overline{E}_{\tan}^d \left(\overline{J}_{nj}^d, 0 \right) + \sum_{l=1}^{N_w-1} I_l^{wd} \overline{E}_{\tan}^d \left(\overline{J}_w^d, 0 \right) + \sum_{j=1}^{Na-1} I_j^{jd} \overline{E}_{\tan}^d \left(\overline{J}_j^d, 0 \right) + \eta_d \sum_{j=1}^{N_d-1} K_{nj} \overline{E}_{\tan}^d \left(0, \overline{M}_{nj} \right) \right] = \overline{E}_{\tan}^{id} \left(\overline{J}^d \right)$$

on S_{wd} and S_{jd} (3-32a)

$$\sum_{n=-\infty}^{\infty} \left[\sum_{j=1}^{N_d-1} I_{nj}^e \overline{E}_{\tan}^e \left(\overline{J}_{nj}^e, 0 \right) + \sum_{l=1}^{N_w-1} I_l^{we} \overline{E}_{\tan}^e \left(\overline{J}_w^e, 0 \right) + \sum_{j=1}^{N_a-1} I_j^{je} \overline{E}_{\tan}^e \left(\overline{J}_j^e, 0 \right) + \eta_e \sum_{j=1}^{N_d-1} K_{nj} \overline{E}_{\tan}^e \left(0, \overline{M}_{nj} \right) \right] = \overline{E}_{\tan}^{ie} \left(\overline{J}^e \right)$$

, on S_{we} and S_{je} (3-32b)

$$\left.\begin{aligned}&\sum_{n=-\infty}^{\infty}\left[\sum_{j=1}^{N_d-1}I_{nj}\left\{\bar{E}^{d}_{\tan}\left(\bar{J}^{d}_{nj},0\right)+\bar{E}^{e}_{\tan}\left(\bar{J}^{e}_{nj},0\right)\right\}+\sum_{j=1}^{N_w-1}\left\{I^{wd}_{l}\bar{E}^{d}_{\tan}\left(\bar{J}^{d}_{w},0\right)+\right.\right.\\&I^{we}_{l}\bar{E}^{e}_{\tan}\left(\bar{J}^{e}_{w},0\right)\Big\}+\sum_{j=1}^{Na-1}\left\{I^{jd}_{j}\bar{E}^{d}_{\tan}\left(\bar{J}^{d}_{j},0\right)+I^{je}_{j}\bar{E}^{e}_{\tan}\left(\bar{J}^{e}_{j},0\right)\right\}+\\&\left.\sum_{j=1}^{N_d-1}K_{nj}\left\{\eta_d\bar{E}^{d}_{\tan}\left(0,\bar{M}_{nj}\right)+\eta_e\bar{E}^{e}_{\tan}\left(0,\bar{M}_{nj}\right)\right\}\right]=\bar{E}^{id}_{\tan}\left(\bar{J}^{d}\right)-\bar{E}^{ie}_{\tan}\left(\bar{J}^{e}\right)\end{aligned}\right\}\quad\text{, on } S_{de}\qquad(3\text{-}32c)$$

$$\left.\begin{aligned}&\sum_{n=-\infty}^{\infty}\left[\sum_{j=1}^{N_d-1}I_{nj}\left\{\bar{H}^{d}_{\tan}\left(\bar{J}^{d}_{nj},0\right)+\bar{H}^{e}_{\tan}\left(\bar{J}^{e}_{nj},0\right)\right\}+\sum_{j=1}^{N_w-1}\left\{I^{wd}_{l}\bar{H}^{d}_{\tan}\left(\bar{J}^{d}_{w},0\right)+\right.\right.\\&I^{we}_{l}\bar{H}^{e}_{\tan}\left(\bar{J}^{e}_{w},0\right)\Big\}+\sum_{j=1}^{Na-1}\left\{I^{jd}_{j}\bar{H}^{d}_{\tan}\left(\bar{J}^{d}_{j},0\right)+I^{je}_{j}\bar{H}^{e}_{\tan}\left(\bar{J}^{e}_{j},0\right)\right\}+\\&\left.\sum_{j=1}^{N_d-1}K_{nj}\left\{\eta_d\bar{H}^{d}_{\tan}\left(0,\bar{M}_{nj}\right)+\eta_e\bar{H}^{e}_{\tan}\left(0,\bar{M}_{nj}\right)\right\}\right]=\bar{H}^{id}_{\tan}\left(\bar{J}^{d}\right)-\bar{H}^{ie}_{\tan}\left(\bar{J}^{e}\right)\end{aligned}\right\}\quad\text{, on } S_{de}\qquad(3\text{-}32d)$$

An advantage of the Galerkin's procedure is the resulting symmetry in the inner products when the coordinates of the testing and basis functions are interchanged.

Therefore, the Eqs.(3-32) have a system of new equations which may be expressed in matrix form as follow:

$$\begin{bmatrix} ([Z^{e}_{de,de}]_n + \eta_r[Z^{d}_{de,de}]_n) & ([Y^{e}_{de,de}]_n + [Y^{d}_{de,de}]_n) & \eta_r[Z^{d}_{de,wd}]_n & [Z^{e}_{de,we}]_n & \eta_r[Z^{d}_{de,jd}]_n & [Z^{e}_{de,je}]_n \\ ([Y^{e}_{de,de}]_n + [Y^{d}_{de,de}]_n) & (-[Z^{e}_{de,de}]_n + \frac{1}{\eta_r}[Z^{d}_{de,de}]_n) & [Y^{d}_{de,wd}]_n & [Y^{e}_{de,we}]_n & [Y^{d}_{de,jd}]_n & [Y^{e}_{de,je}]_n \\ \eta_r[Z^{d}_{wd,de}]_n & [Y^{d}_{wd,de}]_n & [Z^{d}_{wd,wd}] & [0] & [Z^{d}_{wd,jd}] & [0] \\ [Z^{e}_{we,de}]_n & [Y^{e}_{we,de}]_n & [0] & [Z^{e}_{we,we}] & [0] & [Z^{e}_{we,je}] \\ \eta_r[Z^{d}_{jd,de}]_n & [Y^{d}_{jd,de}]_n & [Z^{d}_{jd,wd}] & [0] & [Z^{d}_{jd,jd}] & [0] \\ [Z^{e}_{je,de}]_n & [Y^{e}_{je,de}]_n & [0] & [Z^{e}_{je,we}] & [0] & [Z^{e}_{je,je}] \end{bmatrix} \begin{bmatrix} [I^{\alpha}]_n \\ [k^{\alpha}]_n \\ [I^{wd}] \\ [I^{we}] \\ [I^{jd}] \\ [I^{je}] \end{bmatrix} = \begin{bmatrix} [V^{\alpha}_{de}]^{E}_{n} \\ [V^{\alpha}_{de}]^{H}_{n} \\ [V^{wd}] \\ [V^{we}] \\ [V^{jd}] \\ [V^{je}] \end{bmatrix}$$

.....(3-33)

where $\eta_r = \sqrt{\mu_a/\epsilon_a}$, and α = t or ϕ

3.5.1 Evaluation of Z-submatrices elements

The interaction matrices between DBOR-wire (Z^{sw}),wire-DBOR (Z^{ws}), DBOR-junction (Z^{sj}), junction-DBOR (Z^{js}), wire-wire (Z^{ww}), wire-junction (Z^{wj}), junction-wire (Z^{jw}), and junction-junction (Z^{jj}), are in fact similarly to those of conductor part in chapter two, except the equations of those sub-matrices can be re-written in terms of the symbols (*e*) or (*d*) which denoted by subscript (*a*) related to the equivalence regions . Specifically, for the factors ϵ_a, μ_a , η_a and k_a, where the model Greens function (MGF) may be changed. Furthermore, all matrices are classified in the same way of conductor part, by junction-independent and dependent impedance elements, respectively.

3.5.1.1 Junction-independent impedance elements

To avoid repetition in matrix equations, Z^{sw}, Z^{ws}, and Z^{ww}, because it described the same Eqs.(2-46), (2-49), and (2-54) in chapter two. We use the same formulas with the exception of these equations represent the region (*e*) or (*d*) as described in the beginning of the section (3.5.1). While the body-body matrix elements summarizes as follow:

The impedance matrix elements of DBOR between source element (*i*) and field element (*j*) are found from electric field produced from electric current density $\bar{J}$

$$\left(Z_{mn}^{\alpha\beta}\right)_{ij}^{JE} = \left\langle \overline{W}_{mi}^{\alpha}, \overline{E}^{a}\left(\bar{J}_{nj}^{\beta}, 0\right)\right\rangle \tag{3-34a}$$

or from magnetic field produced from magnetic current density $\bar{M}$, as:

$$\left(Z_{mn}^{\alpha\beta}\right)_{ij}^{MH} = \left\langle \overline{W}_{mi}^{\alpha}, \overline{H}^{a}\left(0, \overline{M}_{nj}^{\beta}\right)\right\rangle \tag{3-34b}$$

Eqs.(3-34) can be expressed in terms of the vector and scalar potential from Eqs.(3-8) and (3-9), respectively, to get

$$\left(Z_{mn}^{\alpha\beta}\right)_{ij}^{JE} = \left\langle \overline{W}_{mi}^{\alpha}, \left(-j\omega\overline{A}^{a}\left(\overline{J}_{nj}^{\beta}\right) - \nabla\phi^{a}\left(\overline{J}_{nj}^{\beta}\right)\right)\right\rangle \tag{3-35a}$$

$$\left(Z_{mn}^{\alpha\beta}\right)_{ij}^{MH} = \left\langle \overline{W}_{mi}^{\alpha}, \left(-j\omega\overline{F}^{a}\left(\overline{M}_{nj}^{\beta}\right) - \nabla\psi^{a}\left(\overline{M}_{nj}^{\beta}\right)\right)\right\rangle \tag{3-35b}$$

where α and β are either *t*- or ϕ- direction. The superscripts (*a*) denotes the either (*e*) or (*d*). The relationship between impedance matrices is

$$\left(Z_{n}^{\alpha\beta}\right)_{ij}^{MH} = \frac{1}{\eta_a^2}\left(Z_{n}^{\alpha\beta}\right)_{ij}^{JE} \tag{3-36}$$

Where $\eta_a = \sqrt{\mu_a / \varepsilon_a}$

The inner product of the electric field with the weighting function $\overline{W}_{mi}^{\alpha}$, (Eq.(3-35a)), is shown in Appendix (C) and yields to :-

$$\left(Z_{n}^{tt}\right)_{ij}^{JE} = -jK_a\eta_a\sum_{p=1}^{4}\sum_{q=1}^{4}\left[T_pT_q\left\{\sin\nu_p\sin\nu_qG_2 + \cos\nu_p\cos\nu_qG_1\right\} - \frac{G_1}{K_a^2}T_p'T_q'\right] \tag{3-37a}$$

$$\left(Z_{n}^{t\phi}\right)_{ij}^{JE} = -K_a\eta_a\sum_{p=1}^{4}\sum_{q=1}^{4}\left[T_pT_q\sin\nu_pG_3 + \frac{n}{K_a^2\rho_q}T_p'T_qG_1\right] \tag{3-37b}$$

$$\left(Z_{n}^{\phi t}\right)_{ij}^{JE} = K_a\eta_a\sum_{p=1}^{4}\sum_{q=1}^{4}\left[T_pT_q\sin\nu_qG_3 + \frac{n}{K_a^2\rho_p}T_pT_q'G_1\right] \tag{3-37c}$$

$$\left(Z_{n}^{\phi\phi}\right)_{ij}^{JE} = -jK_a\eta_a\sum_{p=1}^{4}\sum_{q=1}^{4}T_pT_q\left[G_2 - \frac{n^2}{K_a^2\rho_p\rho_q}G_1\right] \tag{3-37d}$$

G_1, G_2 and G_3 are defined in Eqs.(B-25) as:-

$$G_1 = \int_0^{\pi}\frac{e^{-jK_aR}}{R}\cos(n\phi)\,d\phi \tag{3-38a}$$

$$G_2 = \int_0^{\pi}\frac{e^{-jK_aR}}{R}\cos(n\phi)\cos\phi d\phi \tag{3-38b}$$

$$G_3 = \int_0^{\pi}\frac{e^{-jK_aR}}{R}\sin(n\phi)\sin\phi d\phi \tag{3-38c}$$

$$R = \sqrt{\left(\frac{\rho_p}{4}\right)^2 + 4\rho_p^2\sin^2\left(\frac{\phi}{2}\right)} \tag{3-38d}$$

The Gaussian quadrature technique is used to calculate these integrals. Eq.(3-38d), represents approximation for *R* when $t=t'$. ρ_p , ρ_q , ν_p and ν_q are the ρ and ν evaluated in t_p and t_q , respectively, where t_p and t_q are given in Eq.(C-20b).

3.5.1.2 Junction-dependent impedance elements

In same manner of independent part, the matrices Z^{jj}, Z^{sj}, Z^{js}, Z^{wj}, and Z^{jw} was described in Eqs.(2-84), (2-89), (2-93), (2-98), and (2-99) , based on the same concepts above.

3.5.2 Evaluation of Y-submatrices elements

3.5.2.1 DBOR-DBOR admittance elements

The admittance matrix elements of DBOR between source element (*i*) and field element (*j*) is found from magnetic field produced from electric current density $\bar{J}$, as follow:

$$\left(Y_{mn}^{\alpha\beta}\right)_{ij}^{JH} = \left\langle \overline{W}_{mi}^{\alpha}, \overline{H}^{a}\left(\bar{J}_{nj}^{\beta},0\right)\right\rangle \tag{3-39a}$$

or from electric field produced from magnetic current density $\bar{M}$, as follow:

$$\left(Y_{mn}^{\alpha\beta}\right)_{ij}^{ME} = \left\langle \overline{W}_{mi}^{\alpha}, \overline{E}^{a}\left(0,\overline{M}_{nj}^{\beta}\right)\right\rangle \tag{3-39b}$$

Eqs.(3-39) can be expressed in terms of the vector potential from Eqs.(3-8) and (3-9), respectively, to get

$$\left(Y_{mn}^{\alpha\beta}\right)_{ij}^{JH} = \left\langle \overline{W}_{mi}^{\alpha}, \left(\frac{1}{\mu_a}\nabla\times\overline{A}^{a}\left(\bar{J}_{nj}^{\beta}\right)\right)\right\rangle \tag{3-40a}$$

$$\left(Y_{mn}^{\alpha\beta}\right)_{ij}^{ME} = \left\langle \overline{W}_{mi}^{\alpha}, \left(-\frac{1}{\varepsilon_a}\nabla\times\overline{F}^{a}\left(\overline{M}_{nj}^{\beta}\right)\right)\right\rangle \tag{3-40b}$$

The relationship between these admittance matrices is proved here as :-

$$\left(Y_{n}^{\alpha\beta}\right)_{ij}^{ME} = -\left(Y_{n}^{\alpha\beta}\right)_{ij}^{JH} \tag{3-41}$$

The inner product of the magnetic field with the weighting function $\overline{W}_{mi}^{\alpha}$, (Eq.(3-40a)), is shown in Appendix (E) and yields to :-

$$\left(Y_n^{tt}\right)_{ij}^{JH} = j\sum_{p=1}^{4}\sum_{q=1}^{4} T_p T_q G_6\left[\rho_q \cos\nu_q \sin\nu_p + \sin\nu_q\left\{\sin\nu_p(z_p - z_q) - \rho_p \cos\nu_p\right\}\right] \quad (3\text{-}42a)$$

$$\left(Y_n^{t\phi}\right)_{ij}^{JH} = \sum_{p=1}^{4}\sum_{q=1}^{4} T_p T_q\left[\rho_q \cos\nu_p G_4 + \left\{\sin\nu_p(z_p - z_q) - \rho_p \cos\nu_p\right\} G_5\right] \quad (3\text{-}42b)$$

$$\left(Y_n^{\phi t}\right)_{ij}^{JH} = \sum_{p=1}^{4}\sum_{q=1}^{4} T_p T_q\left[\rho_p \cos\nu_q G_4 - \left\{\sin\nu_q(z_p - z_q) + \rho_q \cos\nu_q\right\} G_5\right] \quad (3\text{-}42c)$$

$$\left(Y_n^{\phi\phi}\right)_{ij}^{JH} = j\sum_{p=1}^{4}\sum_{q=1}^{4} T_p T_q\left(z_p - z_q\right) G_6 \quad (3\text{-}42d)$$

Where,

$$G_4 = \int_0^{\pi} \cos(n\phi)\frac{(1 + jK_a R)}{R^3} e^{-jK_a R} d\phi \quad (3\text{-}43a)$$

$$G_5 = \int_0^{\pi} \cos(n\phi)\cos\phi\frac{(1 + jK_a R)}{R^3} e^{-jK_a R} d\phi \quad (3\text{-}43b)$$

$$G_6 = \int_0^{\pi} \sin(n\phi)\sin\phi\frac{(1 + jK_a R)}{R^3} e^{-jK_a R} d\phi \quad (3\text{-}43c)$$

Again, the Gaussian quadrature technique is used to calculate these integrals.

3.5.2.2 DBOR-Wire admittance elements

The mutual admittance between the DBOR-wire, Y^{sw}, is found from:

$$\left(Y_n^{sw,\alpha}\right)_{il}^{JH} = \left\langle \overline{W}_{ni}^{s\alpha}, \overline{H}^{a}\left(\bar{J}_l^{w}, 0\right)\right\rangle = \int_s \overline{W}_{ni}^{s\alpha} \cdot \overline{H}^{a}\left(\bar{J}_l^{w}, 0\right) ds \quad (3\text{-}44)$$

Where the testing function $\overline{W}_{ni}^{s\alpha}$ is defined in Eq.(3- 23) and the basis function $\bar{J}_l^{w}$ is defined in Eq.(2-8). The magnetic field can be written, according to Appendix (E), as follow:

$$\overline{H}^{a}\left(\bar{J}_l^{w}, 0\right) = \int_s G_o^{a}\left(\bar{r}, \bar{r}'\right)\left(\overline{R} \times \bar{J}_l^{w}\left(\bar{r}\right)\right) ds \quad (3\text{-}45a)$$

Where G_o^a and $\bar{R}$ is given by

$$G_o^a(\bar{r},\bar{r}') = -\left(\frac{1+jK_aR}{R^2}\right) G^a(\bar{r},\bar{r}') \tag{3-45b}$$

$$\bar{R} = \hat{x}(x-x') + \hat{y}(y-y') + \hat{z}(z-z') \tag{3-45c}$$

Therefore, by using Eqs.(3-23), (2-8), and (3-45) in Eq.(3-44), integral expressions for the matrix elements can be written as:

$$\begin{aligned}\left(Y_n^{sw,t}\right)_{il}^{JH} &= \frac{1}{4\pi}\int_0^N dt \int_0^{2\pi} d\phi \int_l dh\, T(t)T_l(h)\, \hat{u}_t \cdot (\hat{u}_l^w \times \bar{R}) \frac{1+jk_aR}{R^3} e^{-j(k_aR+n\phi)} \\ &= \frac{1}{4\pi}\sum_{p=1}^{4}\sum_{q=1}^{4}\int_0^{2\pi} d\phi \left[T_p(t)T_q(h)\, \hat{u}_t \cdot (\hat{u}_l^w \times \bar{R}) \frac{1+jk_aR}{R^3} e^{-j(k_aR+n\phi)} \right]\end{aligned} \tag{3-46a}$$

$$\begin{aligned}\left(Y_n^{sw,\phi}\right)_{il}^{JH} &= \frac{1}{4\pi}\int_0^N dt \int_0^{2\pi} d\phi \int_l dh\, T(t)T_l(h)\, \hat{u}_\phi \cdot (\hat{u}_l^w \times \bar{R}) \frac{1+jk_aR}{R^3} e^{-j(k_aR+n\phi)} \\ &= \frac{1}{4\pi}\sum_{p=1}^{4}\sum_{q=1}^{4}\int_0^{2\pi} d\phi \left[T_p(t)T_q(h)\, \hat{u}_\phi \cdot (\hat{u}_l^w \times \bar{R}) \frac{1+jk_aR}{R^3} e^{-j(k_aR+n\phi)} \right]\end{aligned} \tag{3-46b}$$

Where $\hat{u}_t$ and $\hat{u}_\phi$ is the surface unit vectors of DBOR and given by

$$\hat{u}_t = \hat{x}\sin\theta\cos\phi + \hat{y}\sin\theta\sin\phi + \hat{z}\cos\theta$$
$$\hat{u}_\phi = -\hat{x}\sin\phi + \hat{y}\cos\phi$$

$T(t)$ is the *ith* surface triangle function ,given in Eq.(2-12), $\hat{u}_l^w$ is unit vector along the *lth* segment of wire, and given to any expectation direction as in table (2-1), $T_l(h)$ denotes a triangle function as in Eq.(2-18), while R is given by

$$R = \sqrt{(\rho_p\cos\phi - x_q)^2 + (\rho_p\sin\phi - y_q)^2 + (z_p - z_q)^2}$$

However, to get expression for one direction of wire, it should be recalled the Coordinates in Table (2-1).

3.5.2.3 DBOR-Junction admittance elements

The mutual admittance between the DBOR-junction, Y^{sj}, is found from:

$$\begin{aligned}\left(Y_n^{sj,\alpha}\right)_i^{JH} &= \left\langle \overline{W}_{ni}^{s\alpha}, \overline{H}^{a}\left(\overline{J}_a^{j},0\right)\right\rangle + \left\langle \overline{W}_{ni}^{s\alpha}, \overline{H}^{a}\left(\overline{J}_d^{j},0\right)\right\rangle \\ &= \int_s \overline{W}_{ni}^{s\alpha}\cdot\overline{H}^{a}\left(\overline{J}_a^{j},0\right)ds + \int_s \overline{W}_{ni}^{s\alpha}\cdot\overline{H}^{a}\left(\overline{J}_d^{j},0\right)ds \end{aligned} \quad (3\text{-}47)$$

Where the testing function $\overline{W}_{ni}^{s\alpha}$ is defined in Eq.(3- 23) and the basis functions $\overline{J}_a^{j}$ and $\overline{J}_d^{j}$ is defined in Eq.(2-9). The magnetic field can be written, according to Appendix (E), as follow:

$$\overline{H}^{a}\left(\overline{J}_a^{j},0\right)=\int_s G_o^{a}\left(\overline{r},\overline{r}'\right)\left(\overline{R}\times\overline{J}_a^{j}\left(\overline{r}\right)\right)ds$$

(3-48a)

$$\overline{H}^{a}\left(\overline{J}_d^{j},0\right)=\int_s G_o^{a}\left(\overline{r},\overline{r}'\right)\left(\overline{R}\times\overline{J}_d^{j}\left(\overline{r}\right)\right)ds \quad (3\text{-}48b)$$

Where G_o^{a} and $\overline{R}$ defined in Eqs.(3-45).

Integral expressions for the matrix elements can be found by using Eqs.(3-23), (2-9), and (3-48) in Eq.(3-47) to be obtained:

$$\begin{aligned}\left(Y_n^{sj,t}\right)_i^{JH} &= \frac{1}{4\pi h_\circ}\int_0^N dt\int_0^{2\pi}d\phi\int_0^{h_\circ}dh\left(h_\circ-h\right)T(t)T_l(h)\,\hat{u}_{\mathrm{t}}\cdot(\hat{u}_a\times\overline{R})\frac{1+jk_aR}{R^3}e^{-j(k_aR+n\phi)} \\ &+\frac{1}{4\pi(b-a)}\int_0^N dt\int_0^{2\pi}d\phi\int_0^{2\pi}d\varphi\int_a^b dr\left[T(t)(r-b)\,\hat{u}_{\mathrm{t}}\cdot(\hat{u}_r\times\overline{R})\right]\frac{1+jk_aR}{R^3}e^{-j(k_aR+n\phi)}\end{aligned} \quad (3\text{-}49a)$$

$$\begin{aligned}\left(Y_n^{sj,\phi}\right)_i^{JH} &= \frac{1}{4\pi h_\circ}\int_0^N dt\int_0^{2\pi}d\phi\int_0^{h_\circ}dh\left(h_\circ-h\right)T(t)T_l(h)\,\hat{u}_{\phi}\cdot(\hat{u}_a\times\overline{R})\frac{1+jk_aR}{R^3}e^{-j(k_aR+n\phi)} \\ &+\frac{1}{4\pi(b-a)}\int_0^N dt\int_0^{2\pi}d\phi\int_0^{2\pi}d\varphi\int_a^b dr\left[T(t)(r-b)\,\hat{u}_{\phi}\cdot(\hat{u}_r\times\overline{R})\right]\frac{1+jk_aR}{R^3}e^{-j(k_aR+n\phi)}\end{aligned} \quad (3\text{-}49b)$$

Where $\hat{u}_a$ is an outward-directed unit vector on the attachment segment of junction region, $\hat{u}_r$ is an unit vector on the disk surface a way from wire. For more details we can use the information in table (2-1) for complete solutions to any expectation direction in the Eqs.(3-49).

3.5.3 Deriving the excitation matrix

Measurement vectors are used to obtain the far field of the equivalent surface currents *J* and *M* radiating in medium outside surface *S*. Furthermore, to evaluate the excitation matrix. This far field is scattered by structure of DBOR-wire-junction. For plane wave excitation, and through the reciprocity theorem [88] one may find the radiation field $\bar{E}^s$ at a distance *r* from the origin is due to the surface currents *J* and *M* on *S* as,

$$\bar{\mathrm{E}}^s \cdot \hat{u}^r = \iint_s (\bar{J}(\bar{r}) \cdot \bar{E}^r - \bar{M}(\bar{r}) \cdot \bar{H}^r)\, ds \tag{3-50}$$

Where $\hat{u}^r$ is a unit vector specifying the polarization , $\hat{u}_\theta^r$ or $\hat{u}_\phi^r$, of the wave, $\bar{E}^r$ and $\bar{H}^r$ is the electric and magnetic field is due to $\hat{u}^r$, respectively, and given by:

$$\bar{\mathrm{E}}^{\mathrm{r}} = -\frac{jk\eta}{4\pi r} e^{-jk r_r}\, \hat{u}^r\, e^{-j\bar{k}_r \cdot \bar{r}} \tag{3-51a}$$

$$\bar{\mathrm{H}}^{\mathrm{r}} = -\frac{j}{4\pi r} e^{-jk r_r} (\bar{\mathrm{k}}_{\mathrm{r}} \times \hat{u}^r)\, e^{-j\bar{k}_r \cdot \bar{r}} \tag{3-51b}$$

where r_r is the distance between measurement point and the origin in the vicinity of *S*. Also, k_r is the propagation vector of the plane wave, *k* is the propagation constant and η is the intrinsic impedance of the medium outside *S*.

In addition, it is assumed that the incident EM field $\bar{E}^i$ and $\bar{H}^i$ is either a θ-polarized field defined by [48] as:

$$\begin{aligned} \bar{\mathrm{E}}^{\mathrm{i}} &= k\eta\, \hat{u}_\theta^t\, e^{-j\bar{k}_t \cdot \bar{r}} \\ \bar{\mathrm{H}}^{\mathrm{i}} &= k\, \hat{u}_y\, e^{-j\bar{k}_t \cdot \bar{r}} \end{aligned} \tag{3-52a}$$

or a ϕ-polarized defined by

$$\overline{\mathrm{E}}^{\mathrm{i}} = k\eta\,\hat{u}_y\, e^{-j\bar{k}_t\cdot\bar{r}}$$
$$\overline{\mathrm{H}}^{\mathrm{i}} = k\,\hat{u}_\theta^t\, e^{-j\bar{k}_t\cdot\bar{r}} \qquad (3\text{-}52b)$$

where k_t is the propagation vector and, as shown in Fig.(3-3), $\hat{u}_\theta^t$ and $\hat{u}_y$ are unit vectors in the θ_t -and y-direction, respectively.

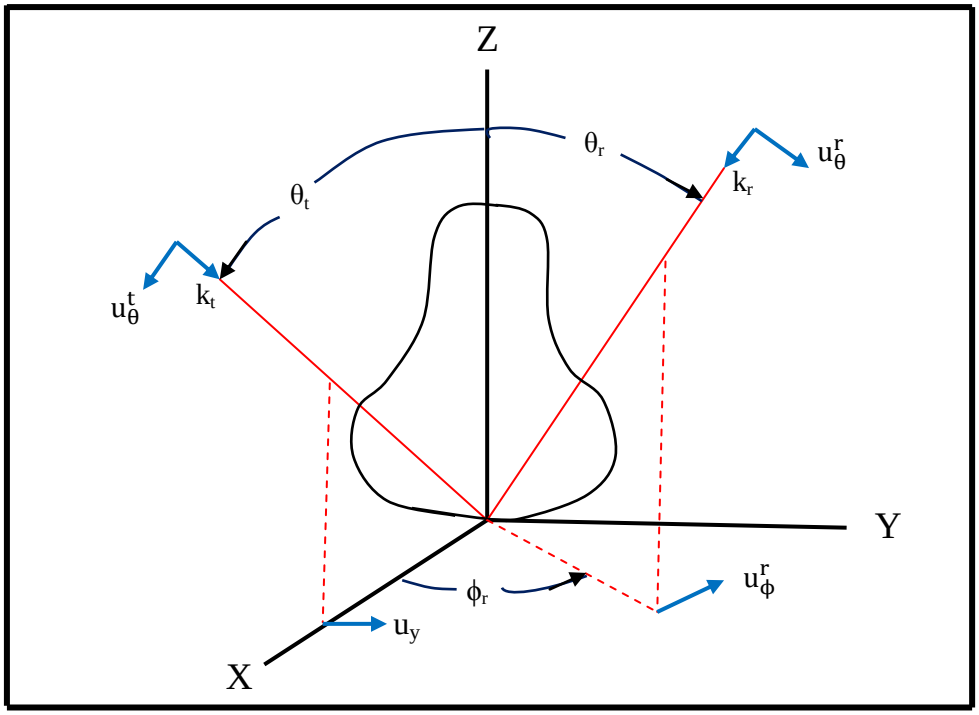

Fig.(3-3): Plane wave scattering by a DBOR.

For DBOR, substituting Eq.(3-21) in (3-50) with nth mode only, one obtains

$$\bar{E}^s \cdot \hat{u}^r = (-\frac{jk\eta}{4\pi r})e^{-jk_r r}[R][I] \qquad (3\text{-}53)$$

Where [I] is the unknown coefficients

$$[I] = \left[[I_n^t], \left[I_n^\varphi\right], [k_n^t], \left[k_n^\varphi\right]\right]^T \qquad (3\text{-}54)$$

and,

$$[R] = \left[[R_n^t], \left[R_n^\phi\right], [\mathcal{R}_n^t], \left[\mathcal{R}_n^\phi\right]\right] \qquad (3\text{-}55)$$

with,

$$
\begin{aligned}
(R_n^t)_i &= \langle \bar{E}^r, \bar{J}_{ni}^t \rangle \\
(R_n^\phi)_i &= \langle \bar{E}^r, \bar{J}_{ni}^\phi \rangle \\
(\mathcal{R}_n^t)_i &= \langle \bar{H}^r, \bar{M}_{ni}^t \rangle \\
(\mathcal{R}_n^\phi)_i &= \langle \bar{H}^r, \bar{M}_{ni}^\phi \rangle
\end{aligned}
\tag{3-56}
$$

The radiated field consists of the two orthogonal components E_θ and E_ϕ with its unit vectors $\hat{u}_\theta^r$, $\hat{u}_\phi^r$ as

$$
\begin{aligned}
\hat{u}_\theta^r &= \hat{x}\cos\theta_r\cos\phi_r + \hat{y}\cos\theta_r\sin\phi_r - \hat{z}\sin\theta_r \\
\hat{u}_\phi^r &= -\hat{x}\sin\phi_r + \hat{y}\cos\phi_r
\end{aligned}
\tag{3-57}
$$

For θ-polarized plane wave , $\hat{u}^r = \hat{u}_\theta^r$, one obtains

$$
\begin{aligned}
(R_n^{t\theta})_i &= \langle \bar{E}_\theta^r, \bar{J}_{ni}^t \rangle \\
(R_n^{\phi\theta})_i &= \langle \bar{E}_\theta^r, \bar{J}_{ni}^\phi \rangle \\
(\mathcal{R}_n^{t\phi})_i &= \langle \bar{H}_\phi^r, \bar{M}_{ni}^t \rangle \\
(\mathcal{R}_n^{\phi\phi})_i &= \langle \bar{H}_\phi^r, \bar{M}_{ni}^\phi \rangle
\end{aligned}
\tag{3-58}
$$

And for the ϕ-polarized plan wave , $\hat{u}^r = \hat{u}_\phi^r$, to obtain

$$
\begin{aligned}
(R_n^{t\phi})_i &= \langle \bar{E}_\phi^r, \bar{J}_{ni}^t \rangle \\
(R_n^{\phi\phi})_i &= \langle \bar{E}_\phi^r, \bar{J}_{ni}^\phi \rangle \\
(\mathcal{R}_n^{t\theta})_i &= -\langle \bar{H}_\theta^r, \bar{M}_{ni}^t \rangle \\
(\mathcal{R}_n^{\phi\theta})_i &= -\langle \bar{H}_\theta^r, \bar{M}_{ni}^\phi \rangle
\end{aligned}
\tag{3-59}
$$

The details of these inner products can be found elsewhere [46] and Appendix (D). The driving vector [*V*] differs from the measurement vector [*R*] by the sign of *n* in comparing between Eq.(3-21) and (3-22), therefore

$$
\begin{aligned}
\left(\mathrm{V}_{\mathrm{n}}^{\mathrm{pq}}\right)_i^E &= \left(\mathrm{R}_{-\mathrm{n}}^{\mathrm{pq}}\right)_i \\
\left(\mathrm{V}_{\mathrm{n}}^{\mathrm{pq}}\right)_i^H &= -\left(\mathcal{R}_{-\mathrm{n}}^{\mathrm{pq}}\right)_i
\end{aligned}
\tag{3-60}
$$

Where *pq* represents *tθ*, *φθ*, *tφ*, or *φφ*.

In other hand side, the contribution to R^w from the wire in both θ-and ϕ-polarized can be written in the form:

$$R^{w,\theta} = \langle \bar{E}_{\theta}^{r}, \bar{J}_{l}^{w} \rangle$$
$$R^{w,\phi} = \langle \bar{E}_{\phi}^{r}, \bar{J}_{l}^{w} \rangle \quad (3\text{-}61)$$

Where $\bar{J}_l^w$ is defined by equation (2-8). Moreover, the driving vector is equal to measurement vector because the basic functions and the weight functions are real, and then

$$V^w = R^w \quad (3\text{-}62)$$

Similarly, the contribution to R^j from the junction are

$$R^{j,\theta} = \langle \bar{E}_{\theta}^{r}, \bar{J}_{a}^{j} \rangle + \langle \bar{E}_{\theta}^{r}, \bar{J}_{d}^{j} \rangle$$
$$R^{j,\phi} = \langle \bar{E}_{\phi}^{r}, \bar{J}_{a}^{j} \rangle + \langle \bar{E}_{\phi}^{r}, \bar{J}_{d}^{j} \rangle \quad (3\text{-}63)$$

Where $\bar{J}_a^j$ and $\bar{J}_d^j$ are defined by equation (2-9). Also, for the same reason in the wire part, we have

$$V^j = R^j \quad (3\text{-}64)$$

3.5.4 The radar cross section evaluation

The scattering cross section σ^{pq} is defined by

$$\sigma^{pq} = 4\pi r^2 \frac{\left|\bar{E}_{pq}^{s}\right|^2}{\left|\bar{E}^{i}\right|^2} \quad (3\text{-}65)$$

Where p is either θ or ϕ and q is either θ or ϕ, E^i and E^s is the incident and scattered field. For large r the relation between scattering matrix of Eq.(2-125) and (3-65) can be written as:

$$\sigma^{pq} = 4\pi |S^{pq}|^2 \quad (3\text{-}66)$$

Where

$$S^{pq} = \frac{-j\omega\mu}{4\pi}\left\{\left[\left[R_n^{tp}\right]\left[R_n^{\phi p}\right]\left[\mathcal{R}_n^{tq}\right]\left[\mathcal{R}_n^{\phi q}\right]\right]\cdot\left[I_n\right]^T + \left[\left[R^{wp}\right]\left[I^{wq}\right]\right] + \left[\left[R^{jp}\right]\left[I^{jq}\right]\right]\right\} \quad (3\text{-}67)$$

So, the RCS normalized to wavelength is given by substituting (3-67) in (3-66), to obtain:

$$\frac{\sigma^{pq}}{\lambda^2} = \frac{\eta^2 k^4}{16\pi^3}\left|\sum_{-n}^{n}\left(R_n^{tp}I_n^{tq} + R_n^{\phi p}I_n^{\varphi q} + \mathcal{R}_n^{tp}k_n^{tq} + \mathcal{R}_n^{\phi p}k_n^{\varphi q}\right) + R^{wp}I^{wq} + R^{jp}I^{jq}\right|^2 \quad (3\text{-}68)$$

The last relation may be written for horizontal polarization (HP), $\phi_r = 0$, as follow [8]:

$$\sigma^{\theta\theta} = 16\pi\left|S^{\theta\theta}\right|^2 cos^2\phi_r \quad (3\text{-}69)$$

And for vertical polarization (VP), $\phi_r = 90$:

$$\sigma^{\phi\theta} = 16\pi\left|S^{\phi\theta}\right|^2 sin^2\phi_r \quad (3\text{-}70)$$

3.6 Computed results

The equations of the previous sections have been solved numerically on a digital computer to investigate the dependence of scattering cross section of DBOR and the composed body (DBOR-wire-junction) on the size, shape, and dielectric constant of the scattering object. This comes with the advantage of accuracy in the solution of SIE formulation. Recent studies have shown that SIE formulations may have very different accuracy [51][94]. In particular, the choice of a formulation is important if the surface is irregular or material contrast is changed [120]. Next the solution of EFIE-PMCHWT formulations for EM scattering by composite body with irregular shape using the MoM with Galerkin's test procedure has been presented.

3.6.1 Validity of evaluation

To demonstrate the validity of the formulation, numerical results are presented for a homogeneous DBOR illuminated by a plane wave, for which the PMCHWT is known.

The first example is a lossy dielectric sphere, whose radius are set to be ka=1,and the values of dielectric constant are ε_r=1.44 and ε_r=4. The bistatic RCS computed by the PMCHWT integral equation methods, are shown in Figs.(3-4) and (3-5), respectively. It can be seen from figures that the HP and VP results are in agreement with [88]. Moreover, the matrix elements integrals are computed numerically by using 20 point Gaussian quadrature.

The second example considered is a plane wave scattering from finite dielectric cylinder of radius a=0.25λ and high 2a, with ε_r=4. Figure (3-6) shows the computed bistatic RCS for homogeneous dielectric cylinder based on the equivalent surface electric and magnetic currents. The RCS results are shown as a function of θ in the horizontal plane $\sigma^{\theta\theta}$ and vertical plane $\sigma^{\phi\theta}$. It can be seen that the results of the solution is in good convergence with the PMCHWT results in [48]. In addition, the numerical integrals used in computing the matrix elements by using 48 point Gaussian quadrature.

A closed cylindrical rod with rounded ends of radius a=0.2 λ and length $l_c = 1.1\lambda$ is next examined by SIE. It is chosen as another test to illustrate the validity of formulation and MoM to complex bodies, as depicted in Fig.(3-7). Figure (3-7) shows that the solution accuracy of PMCHWT results in the two polarizations (HP and VP) in agreement with that of EFIE with ε_r=1. However, the agreement represented by the coincided with conductor part of [61].

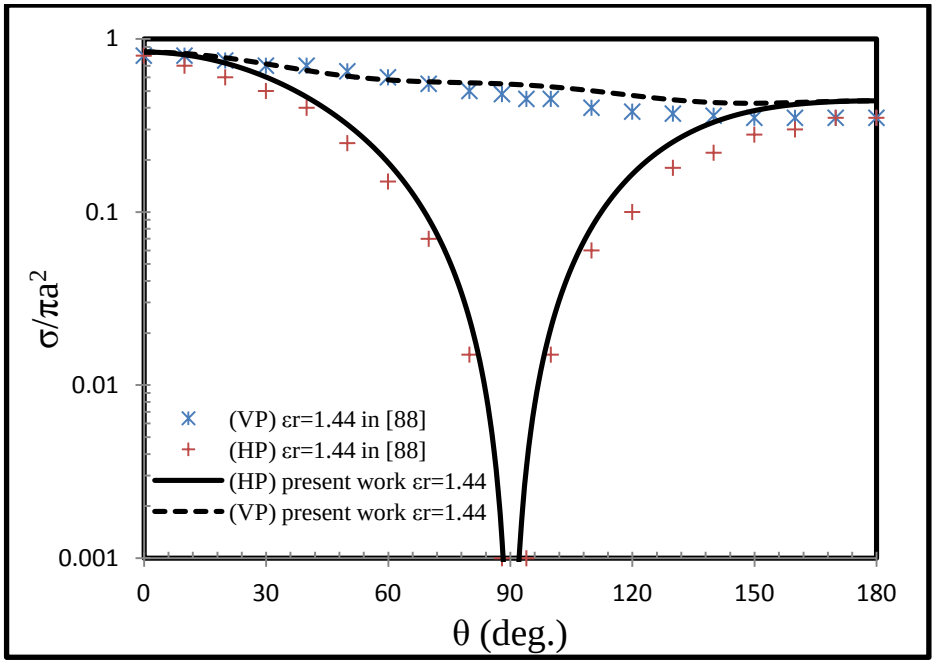

Fig.(3-4): Bistatic RCS of dielectric sphere (ε_r=1.44 and radius a=0.159λ).

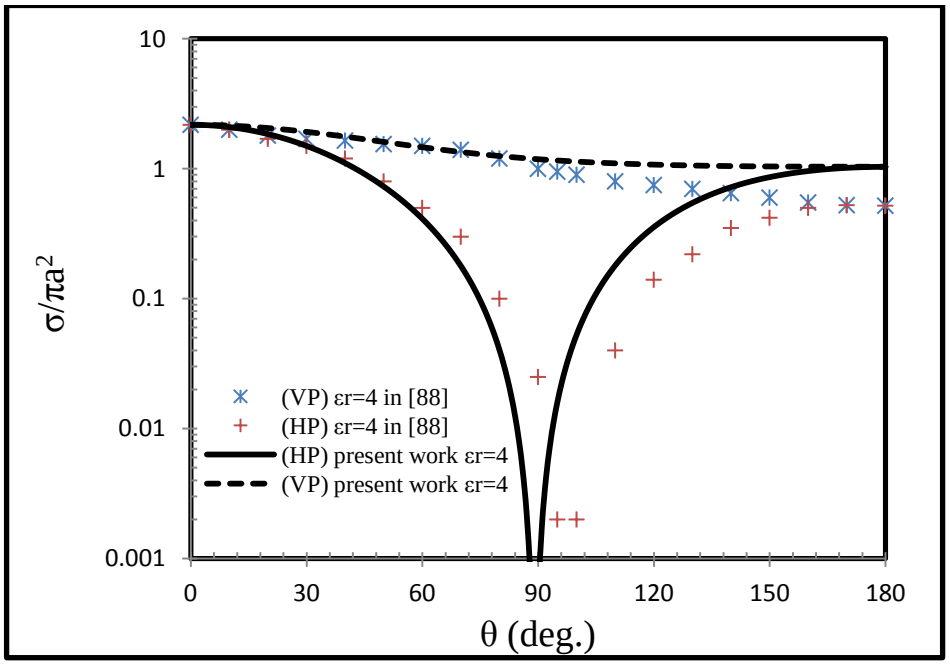

Fig.(3-5): Bistatic RCS of dielectric sphere (ε_r=4 and radius a=0.159λ).

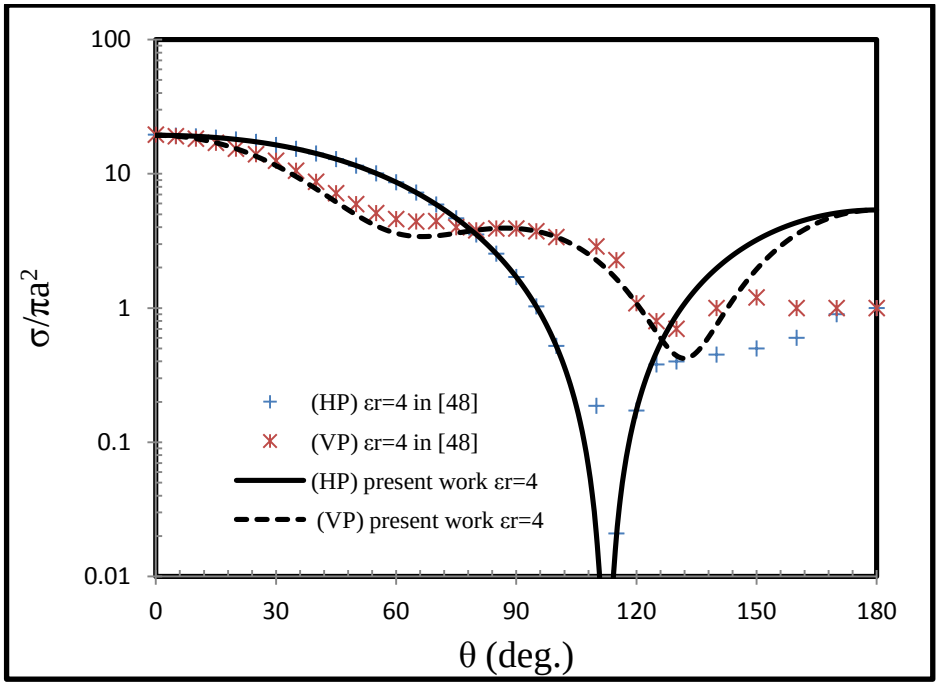

Fig.(3-6): Bistatic plane wave scattering pattern for finite dielectric cylinder, PMCHWT solution (radius a=0.25λ , high 2a and ε_r=4).

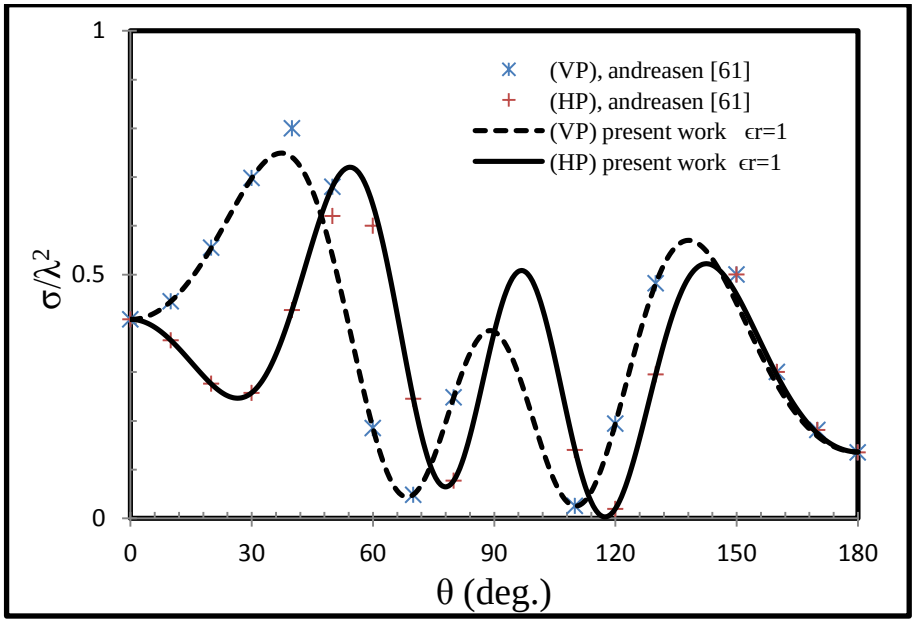

Fig.(3-7): Bistatic RCS for the dielectric cylindrical rod with rounded ends (radius a=0.2 λ , length $l_c = 1.1\lambda$ and ε_r = 1)in comparison with conducting case.

3.6.2 Applications

In this section, some numerical results are presented to generalize the EFIE-PMCHWT on a selected applications consist of DBOR-wire-junction. Furthermore, the method of numerical solution for a particular scattering problem consists of choosing a value for ε_r and the number of attached wires. The first results are computed for the a dielectric sphere with ε_r=4 and radius such that *ka*=2.79, with one attached wire of length $l_w = 0.444\lambda$. Figure(3-8) shows the backscattered RCS in horizontal polarization by applying Eq.(3-68) in the case of dielectric sphere with single wire. In comparing the results with the conductor case, the addition of wire produces a result that has less than number of lobe and no lobe symmetry. This result may be explained by the fact that the effect of single wire and dielectric constant appears for backside incident $\theta>90^o$, where the wire is partially shielded by sphere. Moreover, the null is less deep than on the front illuminated side with sharp decreased in RCS between $\theta=30^o$ to $\theta=150^o$ as a common effect of wire and dielectric constant.

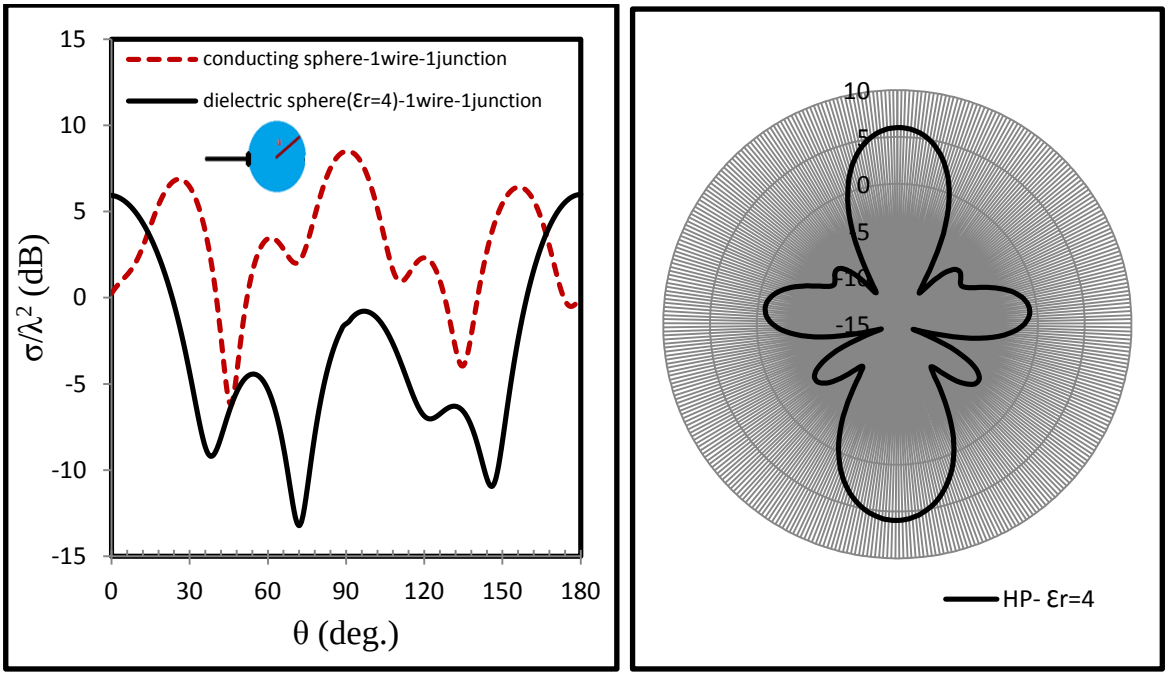

(a) (b)

Fig.(3-8): (a) Backscattered RCS in HP of EFIE-PMCHWT formulation for a homogeneous dielectric sphere with one attached wire (radius a=0.444λ , ε_r=4 and l_w=0.444λ), (b) radar graph representation.

To explain the effect of two attached wires, another important application is applied by taking a dielectric flat-faced cylinder with ε_r=4 and radius a=0.344λ and length $l_c = 1.98\lambda$, where anyone of the two wires has a length of $l_w = 0.880\lambda$. A similar phenomenon has been observed previously in the case of conducting bodies with two attached wires, but the result here shows that the effect of ε_r and thin wires on total RCS is noticeable. It can be seen that the results show the same effect for the two wires, located at cylinder center, on the RCS, whereas the common effect with ε_r is changed the total backscattered RCS between angles $\theta=10^o$ to $\theta=170^o$ from that in the conductor case as shown in Fig.(3-9).

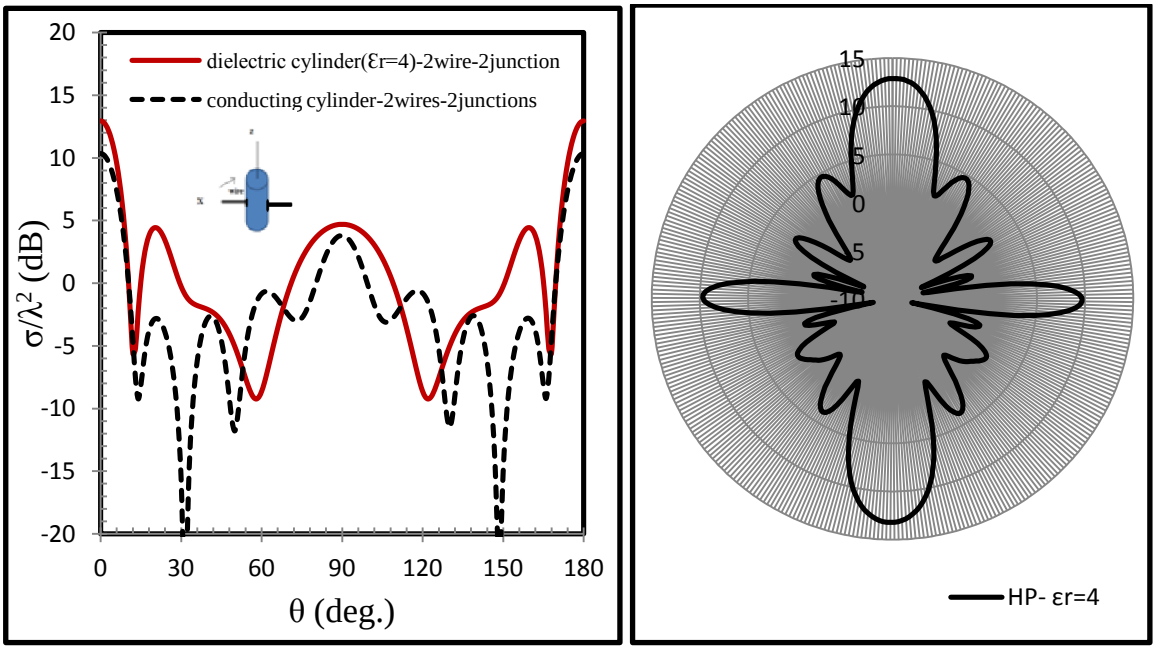

(a) (b)

Fig.(3-9): (a) Backscattered RCS in HP of EFIE-PMCHWT formulation for finite homogeneous dielectric cylinder with two attached wires (radius $a=0.344\lambda$, $\varepsilon_r=4$, $l_c=1.98\lambda$ and $l_w=0.880\lambda$), (b) radar graph representation.

It is interesting to note that in the last two applications the effect of single value for dielectric constant were appearing in total RCS. Another important application finding were that for several possible value of ε_r. it is represented by a missile consisting of a dielectric cylindrical rod with rounded ends of radius a=0.32λ and total length $l_c = 2.6\lambda$, and ε_r = 2,4, and 6, with wire-loop wings of length $l_w = 0.826\lambda$. Figure(3-10) shows the monostatic cross section for the horizontal polarization for different values of ε_r. However, this result has not previously been described, in addition to the last applications. It should be noted that the effect of changing ε_r will be disparate among these values as shown in Fig.(3-10).

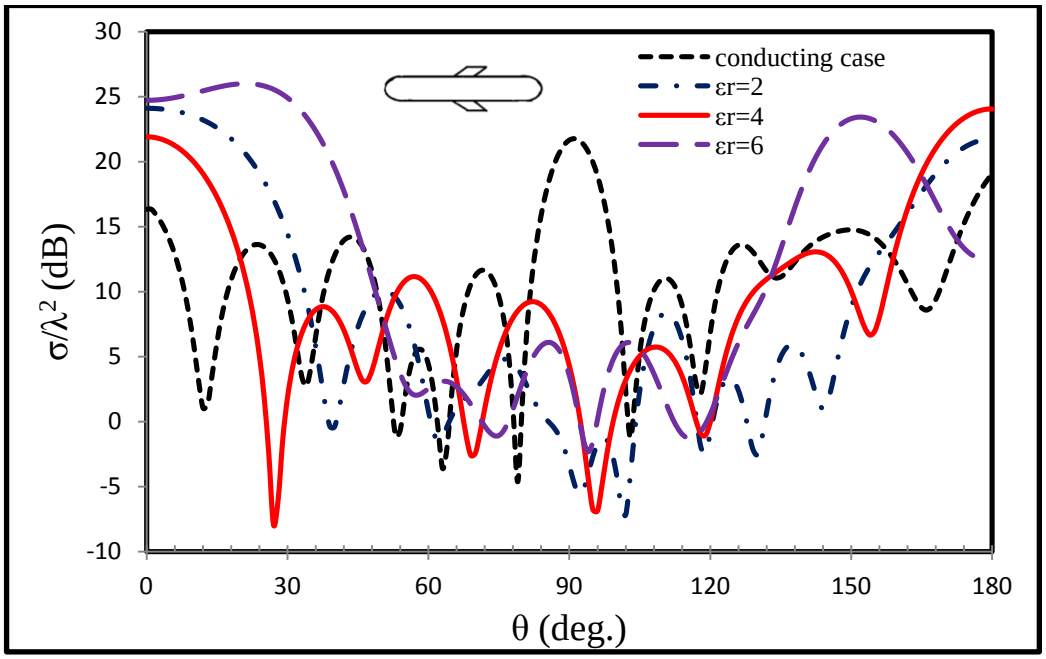

Fig.(3-10): Backscattered RCS in HP of EFIE-PMCHWT formulation for homogeneous dielectric cylindrical rod with rounded ends of different values of ε_r , with two wire-loop wings (radius $a=0.32\lambda$, $l_c=2.6\lambda$, and $l_w=0.826\lambda$).

The most interesting finding was the effect of high loosy dielectric material on total radar cross section, where complex permittivity of the dielectric ε written in the form $\varepsilon = \varepsilon_r \varepsilon_o - j\frac{\sigma}{\omega}$, ε_r is relative permittivity of the dielectric, σ represents the conductivity of dielectric, ω is the angular frequency, and the propagation constant is $k = k_o(\varepsilon_r/\varepsilon_o)^{1/2}$. This test was applied on the last application (missile) with the same values of ε_r . Fig.(3-11) and (3-12) show the monostatic cross section for the horizontal polarization for different values of ε_r and two probabilities of σ, where the increasing in σ was accompanied by a decrease in the value of RCS.

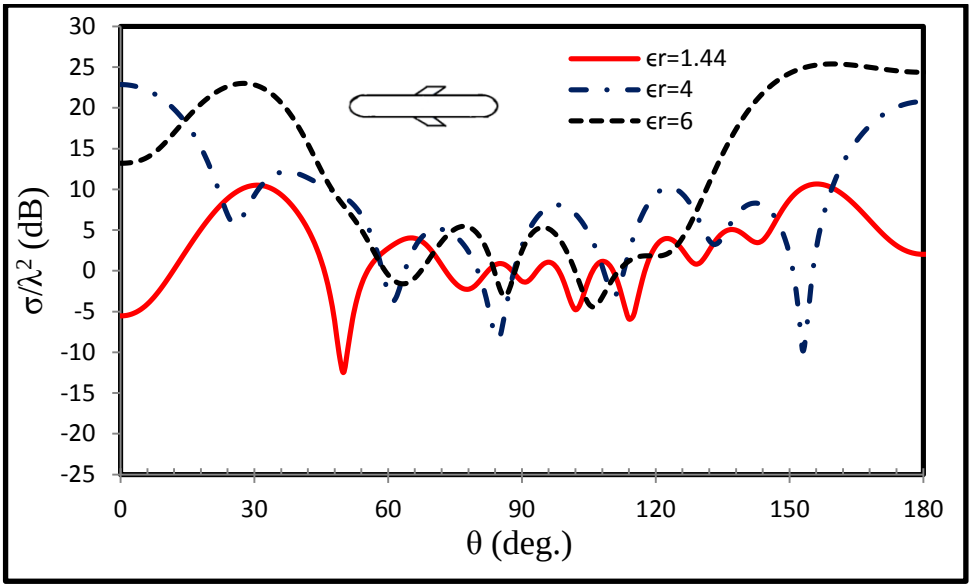

Fig.(3-11): Monostatic RCS for HP of EFIE-PMCHWT formulation for high lossy dielectric cylindrical rod with rounded ends of different values of ε_r , with two wire-loop wings with $\sigma = 10^3 mho/m$, radius $a=0.32\lambda$, $l_c=2.6\lambda$, and $l_w=0.826\lambda$.

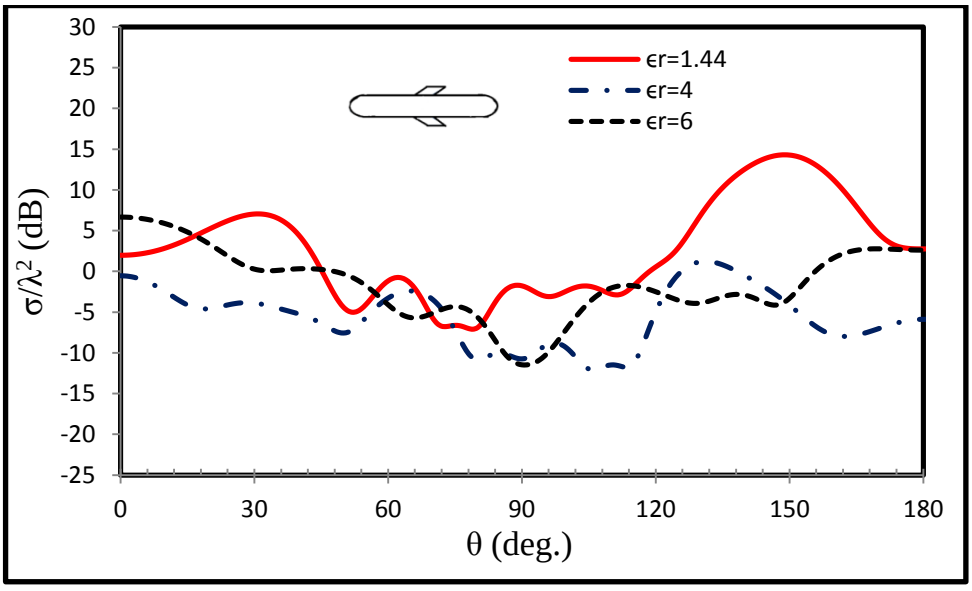

Fig.(3-12): Monostatic RCS for HP of EFIE-PMCHWT formulation for high lossy dielectric cylindrical rod with rounded ends of different values of ε_r, with two wire-loop wings with $\sigma = 10^1 mho/m$, radius $a=0.32\lambda$, $l_c=2.6\lambda$, and $l_w=0.826\lambda$.

Chapter Four

Scattering from dielectrically coated BOR with attached wires

4.1 Introduction

The problem of EM scattering from conducting objects coated by the dielectrics has been studied extensively and many publications are available for this problem. These studies have been motivated not solely by academic interest but by many engineering applications as well. The coated considerations interest are of practical importance, for example, in radar camouflage, where the coating might be used to minimize or maximize the scattering, and in scattering measurement, where the coating can reduce the influence of the supports on the test object [105]. However, most of earlier techniques have been utilized to solve 2D structures and three-dimensional BOR [101][104].

Recently, the study of the EM scattering from conducting objects coated with thin electric or magnetic materials has been the subject of intense investigation. Proper selection of the coating material can be used to reduce significantly RCS of the coated objects [110]. It is known that the RCS of a conducting body can be reduced if it is coated with absorbing materials especially with anisotropic RAM [111]. Moreover, coated by thin-layer material has received much attention because these composite dielectric and conductor structures are used in many applications, such as the evaluation of echo from stealth aircraft [112].

Various numerical techniques MoM, FDTD, and FEM and formulations of SIEs have been used to treat the problem of conducting objects coated with electric and/or magnetic materials. The general SIE formulations are valid for arbitrary coating thicknesses and these formulations have been used to treat conducting objects with thin or thick coatings. These

formulations require careful calculation of the matrix elements when the coating thickness approaches zero [110**]**. Also the use of these formulations requires a large matrix size. The integral equation used in [103] for the analysis of arbitrarily shaped 3D coated structure is the combination of the EFIE and the PMCHWT formulation. Kishk and Shafai [101] developed five different formulations, including a CFIE formulation in which the electric and magnetic fields have been used, for multi BORs. In general, imposition of the tangential boundary condition on both the electric and magnetic fields on the coating and on the conducting surface ensures a well-posed formulation. The PMCHWT approach addresses the coating, while the CFIE formulation in [46] is a satisfactory remedy at the conductor.

In this study a new and complicated structure was used. The composite dielectric and conductor structures with attached thin electric wires are presented here, where the junction region located between the wires and DBOR surface as shown in Fig.(4-1). By observing the shape regions, we find that the EFIE-PMCHWT formulations are possible to apply between DBOR and wires. correspondingly, the CFIE-PMCHWT formulations are possible to apply between the composite dielectric and conductor structures.

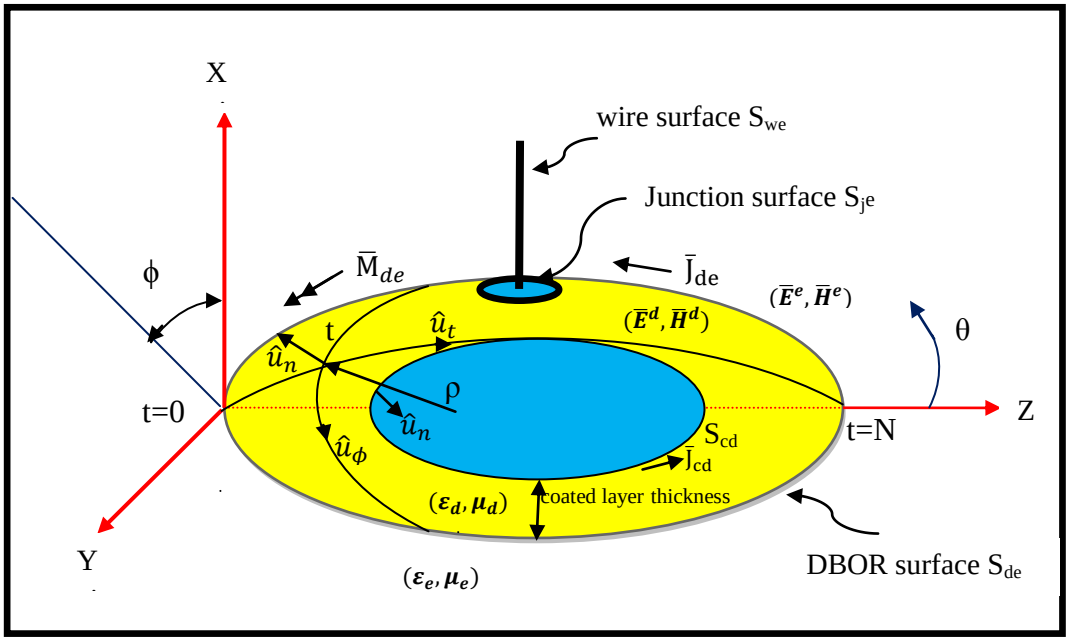

Fig.(4-1): Composite problem with attached thin electric wire, homogeneous dielectric object (ε_d, μ_d) embedded in a homogenous medium (ε_e, μ_e) enclosing a conductor. $\bar{J}_{de}$ and $\bar{M}_{de}$ are the equivalent currents for the interior and exterior region.

4.2 Formulation of the boundary value problem

In this section, we present formulations by using SIEs to analyze the dielectrically coated BOR (DCBOR) with attached thin electric wire and junction at the wire/DBOR surface. For the purpose of presentation, we assume that the conducting body enclosed by a homogeneous dielectric material. The DCBOR are represented as the cross section of a surface of revolution, S_{de} and S_{cd}, respectively. The regions on the exterior and interior of the dielectric body, enclosing a conductor, are characterized by constitutive parameters (ε_e, μ_e) and (ε_d, μ_d), respectively. The thin electric wire can be represented by one dimensional structure, on compliance with the well-known thin wire theory [35], and the wire elements are characterized by S_{wd} and S_{we} with respect to the interior and exterior to the DBOR. The same concept applies to the junction region, which is represented by S_{jd} and S_{je}. The

complex structure (DCBOR-wire-junction) is illuminated by an incident plane wave, of which the electric and magnetic fields are denoted by $\mathbf{E}^i$ and $\mathbf{H}^i$. The equivalent electric and magnetic surface currents ,which arise from application of the field equivalence principle [38] on the exterior and interior region of Fig.(4-2a), are represented by the symbols $\bar{J}$ and $\bar{M}$, respectively. From this principle two equivalent problems, interior and exterior, are illustrated in Figs.(4-2b) and (4-2c), respectively. The field components in each region can therefore be found readily from these equivalent currents, these equivalent currents are still unknown and can be determined by enforcing the boundary conditions for the field vectors in Fig.(4-2a). The boundary conditions to be satisfied are:-

$$\hat{n}\times\bar{E}^{et}=0 \qquad (4\text{-}1a)$$

$$\hat{n}\times\bar{H}^{et}=0 \qquad (4\text{-}1b)$$

$$\hat{n}\times\bar{E}^{dt}=0 \qquad (4\text{-}1c)$$

$$\hat{n}\times\bar{H}^{dt}=0 \qquad (4\text{-}1d)$$

The electric and magnetic field vectors are represented by the symbols $\bar{E}$ and $\bar{H}$ with superscripts "*dt*" and "*et*" refer to the total field interior and exterior to the DCBOR, respectively.

The surface equivalent currents are:

$$\bar{J}_{we}=\hat{n}\times\bar{H}^{e} \quad \text{, on } S_{we} \qquad (4\text{-}2a)$$

$$\bar{J}_{wd}=\hat{n}\times\bar{H}^{d} \quad \text{, on } S_{wd} \qquad (4\text{-}2b)$$

$$\bar{J}_{je}=\hat{n}\times\bar{H}^{e} \quad \text{, on } S_{je} \qquad (4\text{-}2c)$$

$$\bar{J}_{jd}=\hat{n}\times\bar{H}^{d} \quad \text{, on } S_{jd} \qquad (4\text{-}2d)$$

$$\bar{J}_{cd}=\hat{n}\times\bar{H}^{d} \quad \text{, on } S_{cd} \qquad (4\text{-}2e)$$

$$\bar{J}_{de}=\hat{n}\times\bar{H}^{e} \quad \text{, on } S_{de} \qquad (4\text{-}2f)$$

$$\overline{M}_{de} = -\hat{n} \times \overline{E}^{e} \quad \text{, on } S_{de} \qquad (4\text{-}2g)$$

By enforcing the continuity of the tangential components of the total electric and magnetic fields on S_{cd} , S_{de} , S_{we} , S_{wd} , S_{je} , and S_{jd} regions, from which the unknown $\overline{J}_{wd}, \overline{J}_{we}, \overline{J}_{jd}, \overline{J}_{je}, \overline{J}_{cd}, \overline{J}_{de}$ and $\overline{M}_{de}$ can be determined. A system of integro-differential equations can be obtained and written in operator form as [100][101]:

$$\overline{E}^{d}_{\tan}(\overline{J}_{de} + \overline{J}_{cd} + \overline{J}_{wd} + \overline{J}_{jd}, \overline{M}_{de}) = \overline{E}^{id}_{\tan} \quad \text{, on } S_{wd} \text{ and } S_{jd} \qquad (4\text{-}3a)$$

$$\overline{E}^{e}_{\tan}(\overline{J}_{de} + \overline{J}_{we} + \overline{J}_{je}, \overline{M}_{de}) = -\overline{E}^{ie}_{\tan} \quad \text{, on } S_{we} \text{ and } S_{je} \qquad (4\text{-}3b)$$

$$\overline{E}^{d}_{\tan}(\overline{J}_{de} + \overline{J}_{cd}, \overline{M}_{de}) = \overline{E}^{id}_{\tan} \quad \text{, on } S_{cd} \qquad (4\text{-}3c)$$

$$\overline{E}^{e}_{\tan}(\overline{J}_{de} + \overline{J}_{we} + \overline{J}_{je}, \overline{M}_{de}) + \overline{E}^{d}_{\tan}(\overline{J}_{de} + \overline{J}_{cd} + \overline{J}_{wd} + \overline{J}_{jd}, \overline{M}_{de}) = \overline{E}^{id}_{\tan} - \overline{E}^{ie}_{\tan} \quad \text{, on } S_{de} \qquad (4\text{-}3d)$$

$$\overline{H}^{e}_{\tan}(\overline{J}_{de} + \overline{J}_{we} + \overline{J}_{je}, \overline{M}_{de}) + \overline{H}^{d}_{\tan}(\overline{J}_{de} + \overline{J}_{cd} + \overline{J}_{wd} + \overline{J}_{jd}, \overline{M}_{de}) = \overline{H}^{id}_{\tan} - \overline{H}^{ie}_{\tan} \quad \text{, on } S_{de} \qquad (4\text{-}3e)$$

The subscript (tan) denotes the tangential components of the fields on the surface in equation. $\overline{E}^{a}(\overline{J}, \overline{M})$ and $\overline{H}^{a}(\overline{J}, \overline{M})$ are the electric and magnetic fields due to the equivalent electric and magnetic currents $\overline{J}$ and $\overline{M}$ radiating in the homogeneous medium characterized by μ_a and ε_a everywhere. The superscripts (a) represents (e) or (d).

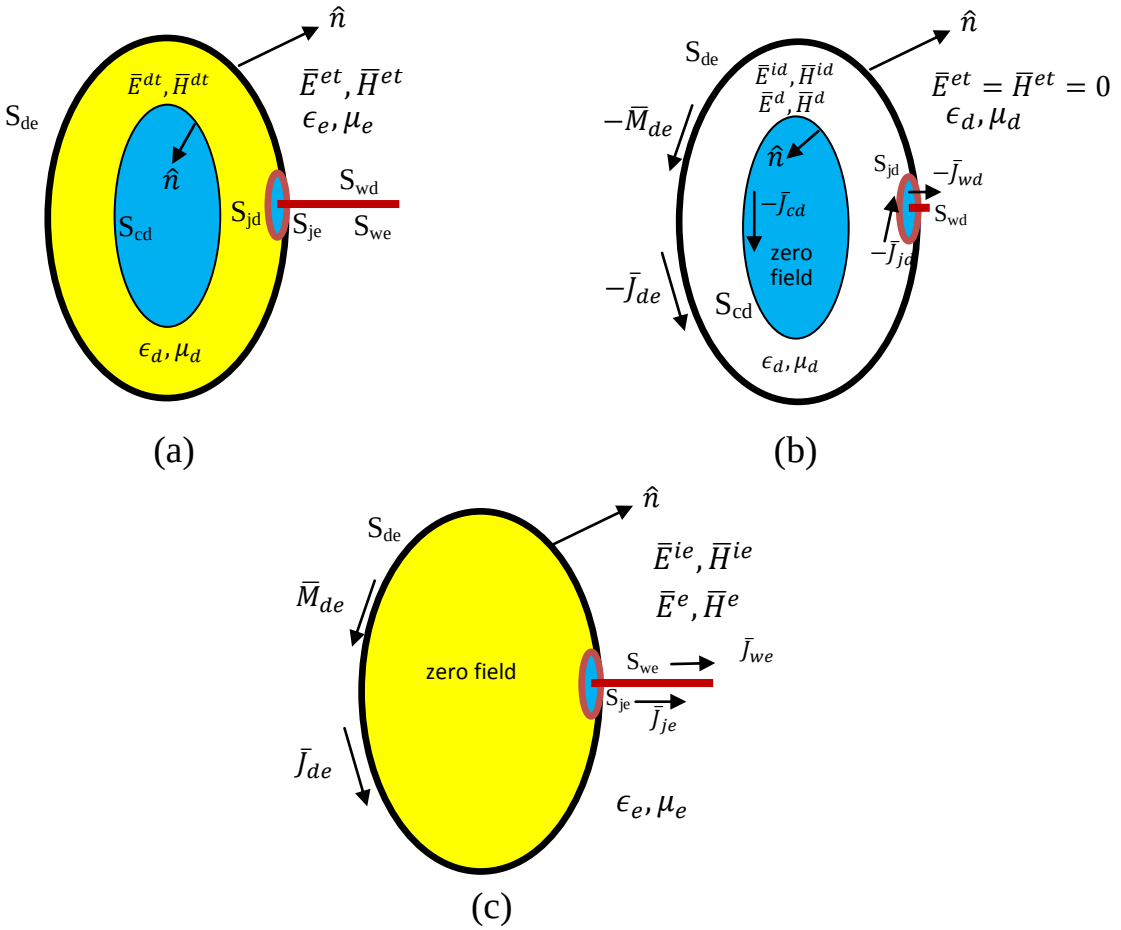

Fig.(4-2): (a) The original problem, (b) The interior problem and (c) The exterior problem.

As mentioned the CFIE-PMCHWT formulations can be applied between the composite dielectric and conductor structures, and EFIE-PMCHWT formulations can be applied between DBOR and wires. These formulas are possible to explain briefly by place of application. The combined of E- and H-field formulations suffer from the resonance problem, similar to the formulations for the conducting bodies [46]. To overcome the problem in the composite dielectric and conductor structures, a linear combination of the E- and H-field formulations may be obtained to give [101]:

$$\hat{n} \times \bar{H}^d(\bar{J}_{cd} + \bar{J}_{de}, \bar{M}_{de}) - \frac{\alpha^d}{\eta_d} \bar{E}^d_{tan}(\bar{J}_{cd} + \bar{J}_{de}, \bar{M}_{de}) = 0 \qquad \text{just outside } S_{cd} \quad (4\text{-}4)$$

$$\hat{n} \times \bar{H}^d(\bar{J}_{cd} + \bar{J}_{de}, \bar{M}_{de}) - \frac{\alpha^d}{\eta_d} \bar{E}^d_{tan}(\bar{J}_{cd} + \bar{J}_{de}, \bar{M}_{de}) = 0 \qquad \text{just outside } S_{de} \quad (4\text{-}5)$$

$$\hat{n} \times \bar{H}^e(\bar{J}_{de}, \bar{M}_{de}) - \frac{\alpha^e}{\eta_e} \bar{E}^e_{tan}(\bar{J}_{de}, \bar{M}_{de}) = \hat{n} \times \bar{H}^e(\bar{J}^{ie}, \bar{M}^{ie}) - \frac{\alpha^e}{\eta_e} \bar{E}^e_{tan}(\bar{J}^{ie}, \bar{M}^{ie})$$

just inside S_{de} (4-6)

Kishk and Shafai [101] proved that the results , EFIE-PMCHWT and combined field formulations for coated conductors, are very closed in comparison with exact analytical solutions (Mie series). So, in the present work, for coated conductors, we define "EFIE-PMCHWT" the formulation that utilizes an E-field on the conductor and a PMCHWT on the dielectric consistent with DBOR-wires. This was confirmed by the Eq.(4-3), where α=β=1 in Eqs.(3-3) and (3-4).

The scattering of EM waves from coated conductors object having permeability ϵ_d and permeability μ_d with a homogeneous background medium (ϵ_e, μ_e) as shown in Fig.(4-1), can be expressed in terms of integro-differential operator according to PMCHWT formulation [102], the boundary condition on S_{de} imply:

$$\bar{E}^{inc}_{tan} = [L_1\bar{J}_1 - K_1\bar{M}_1 - L_2\bar{J}_2 + K_2\bar{M}_2]_{tan} \quad (4\text{-}7)$$

$$\bar{H}^{inc}_{tan} = \left[K_1\bar{J}_1 + \frac{1}{\eta_1^2} L_1\bar{M}_1 - K_2\bar{J}_2 - \frac{1}{\eta_2^2} L_2\bar{M}_2\right]_{tan} \quad (4\text{-}8)$$

Where $\bar{J}_i$ and $\bar{M}_i$ are the incident electric and magnetic current densities for region *i* (*i*=1,2), also the wave impedance $\eta_i = \sqrt{\mu_i/\epsilon_i}$, $\bar{E}^{inc}$ and $\bar{H}^{inc}$ are the incident electric and magnetic field, respectively.

The integro-differential operators L_i and K_i are defined as [68]:

$$L_i\bar{X}(\bar{r}) = j\omega\mu_i \int_s \left[\bar{X}(\bar{r}') + \frac{1}{\omega^2\mu_i\epsilon_i} \nabla\acute{V}.\bar{X}(\bar{r}')\right] G_i(|\bar{r} - \bar{r}'|) d\acute{s} \quad (4\text{-}9)$$

$$K_i\bar{X}(\bar{r}) = \int_s \bar{X}(\bar{r}') \times \nabla G_i(|\bar{r} - \bar{r}'|)\, d\acute{s} \quad (4\text{-}10)$$

where $\epsilon_{i=}\epsilon_\circ\epsilon_{ir}$, $\mu_{i=}\mu_\circ\mu_{ir}$, and $\eta_i = \eta_\circ(\frac{\mu_{ir}}{\epsilon_{ir}})^{1/2}$; $\epsilon_\circ$ and $\mu_\circ$ are the permittivity and permeability of free space, respectively; and the subscript ***r*** denotes the

relative constitutive quantity. The Green's function for an unbounded medium is denoted by G_i, with the constitutive parameters ϵ_i and μ_i .

4.3 Moment Method Solution

Consider the general geometry of a scatterer made of coated conductors with attached wire as illustrated in Fig.(4-1). In the numerical approach the scattering problem is formulated in terms of the equivalent currents on the surface of the scatterer, leading to a set of integral equations which are solved using the MoM. The Galerkin procedure is carried out to test boundary integral equations and reduce the functional form of the equations to a partitioned matrix equation.

The DCBOR with attached wires have a system of unknown currents, which defined with basis function in Eqs.(3-12), (2-8), and (2-9), all these unknowns are Possible to give Eq.(4-3) the following forms:

$$\left.\begin{aligned}\sum_{n=-\infty}^{\infty}\Bigg[\sum_{j=1}^{N_d-1} I_{nj}\overline{E}^{d}_{\tan}\left(\overline{J}^{d}_{nj},0\right)+\sum_{j=1}^{N_c-1} I^{c}_{nj}\overline{E}^{d}_{\tan}\left(\overline{J}^{c}_{nj},0\right)+\sum_{l=1}^{N_w-1} I^{wd}_{l}\overline{E}^{d}_{\tan}\left(\overline{J}^{d}_{w},0\right)+\\ \sum_{j=1}^{Na-1} I^{jd}_{j}\overline{E}^{d}_{\tan}\left(\overline{J}^{d}_{j},0\right)+\eta_d\sum_{j=1}^{N_d-1} K_{nj}\overline{E}^{d}_{\tan}\left(0,\overline{M}_{nj}\right)\Bigg]=\overline{E}^{id}_{\tan}\left(\overline{J}^{d}\right)\end{aligned}\right\} \quad \text{on } S_{wd} \text{ and } S_{jd} \quad (4\text{-}11a)$$

$$\left.\begin{aligned}\sum_{n=-\infty}^{\infty}\Bigg[\sum_{j=1}^{N_d-1} I_{nj}\overline{E}^{e}_{\tan}\left(\overline{J}^{e}_{nj},0\right)+\sum_{l=1}^{N_w-1} I^{we}_{l}\overline{E}^{e}_{\tan}\left(\overline{J}^{e}_{w},0\right)\\ +\sum_{j=1}^{N_a-1} I^{je}_{j}\overline{E}^{e}_{\tan}\left(\overline{J}^{e}_{j},0\right)+\eta_e\sum_{j=1}^{N_d-1} K_{nj}\overline{E}^{e}_{\tan}\left(0,\overline{M}_{nj}\right)\Bigg]=\overline{E}^{ie}_{\tan}\left(\overline{J}^{e}\right)\end{aligned}\right\} \quad \text{on } S_{we} \text{ and } S_{je} \quad (4\text{-}11b)$$

$$\sum_{n=-\infty}^{\infty}\Bigg[\sum_{j=1}^{N_d-1} I_{nj}\overline{E}^{d}_{\tan}\left(\overline{J}^{d}_{nj},0\right)+\sum_{j=1}^{N_c-1} I^{c}_{nj}\overline{E}^{d}_{\tan}\left(\overline{J}^{c}_{nj},0\right)+\eta_d\sum_{j=1}^{N_d-1} K_{nj}\overline{E}^{d}_{\tan}\left(0,\overline{M}_{nj}\right)\Bigg]=\overline{E}^{id}_{\tan}\left(\overline{J}^{d}\right)$$

$$\text{on } S_{cd} \quad (411c)$$

$$\left.\begin{aligned}&\sum_{n=-\infty}^{\infty}\Bigg[\sum_{j=1}^{N_d-1}I_{nj}\left\{\overline{E}^{d}_{\tan}\left(\overline{J}^{d}_{nj},0\right)+\overline{E}^{e}_{\tan}\left(\overline{J}^{e}_{nj},0\right)\right\}+\sum_{j=1}^{N_c-1}I_{nj}\overline{E}^{d}_{\tan}\left(\overline{J}^{c}_{nj},0\right)+\\&\sum_{l=1}^{N_w-1}\left\{I_l^{wd}\overline{E}^{d}_{\tan}\left(\overline{J}^{d}_{w},0\right)+I_l^{we}\overline{E}^{e}_{\tan}\left(\overline{J}^{e}_{w},0\right)\right\}+\sum_{j=1}^{Na-1}\left\{I_j^{jd}\overline{E}^{d}_{\tan}\left(\overline{J}^{d}_{j},0\right)+I_j^{je}\overline{E}^{e}_{\tan}\left(\overline{J}^{e}_{j},0\right)\right\}\\&+\sum_{j=1}^{N_d-1}K_{nj}\left\{\eta_d\overline{E}^{d}_{\tan}\left(0,\overline{M}_{nj}\right)+\eta_e\overline{E}^{e}_{\tan}\left(0,\overline{M}_{nj}\right)\right\}\Bigg]=\overline{E}^{id}_{\tan}\left(\overline{J}^{d}\right)-\overline{E}^{ie}_{\tan}\left(\overline{J}^{e}\right)\end{aligned}\right\}\text{ on } S_{de} \quad (4\text{-}11d)$$

$$\left.\begin{aligned}&\sum_{n=-\infty}^{\infty}\Bigg[\sum_{j=1}^{N_d-1}I_{nj}\left\{\overline{H}^{d}_{\tan}\left(\overline{J}^{d}_{nj},0\right)+\overline{H}^{e}_{\tan}\left(\overline{J}^{e}_{nj},0\right)\right\}+\sum_{j=1}^{N_c-1}I_{nj}\overline{H}^{d}_{\tan}\left(\overline{J}^{c}_{nj},0\right)\\&+\sum_{l=1}^{N_w-1}\left\{I_l^{wd}\overline{H}^{d}_{\tan}\left(\overline{J}^{d}_{w},0\right)+I_l^{we}\overline{H}^{e}_{\tan}\left(\overline{J}^{e}_{w},0\right)\right\}\sum_{j=1}^{Na-1}\left\{I_j^{jd}\overline{H}^{d}_{\tan}\left(\overline{J}^{d}_{j},0\right)+I_j^{je}\overline{H}^{e}_{\tan}\left(\overline{J}^{e}_{j},0\right)\right\}\\&+\sum_{j=1}^{N_d-1}K_{nj}\left\{\eta_d\overline{H}^{d}_{\tan}\left(0,\overline{M}_{nj}\right)+\eta_e\overline{H}^{e}_{\tan}\left(0,\overline{M}_{nj}\right)\right\}\Bigg]=\overline{H}^{id}_{\tan}\left(\overline{J}^{d}\right)-\overline{H}^{ie}_{\tan}\left(\overline{J}^{e}\right)\end{aligned}\right\}\text{ on } S_{de} \quad (4\text{-}11e)$$

The dot product between Eq.(4-11) and the weighting functions, Galerkin approach, in Eqs.(2- 18), (2-19), and (3-23), and this gives a system of linear equation has the form:

$$[\,I\,]\,[\,Z\,]=[\,V\,] \qquad (4\text{-}12)$$

and in more details it can be written in matrix form as follow:

$$\begin{bmatrix} [Z^{c}_{cd,cd}]_n & [Z^{c}_{cd,de}]_n & \eta_r[Y^{c}_{cd,de}]_n & [0] & [0] & [0] & [0] \\ [Z^{d}_{de,cd}]_n & ([Z^{e}_{de,de}]_n + \eta_r[Z^{d}_{de,de}]_n) & ([Y^{e}_{de,de}]_n + [Y^{d}_{de,de}]_n) & \eta_r[Z^{d}_{de,wd}]_n & [Z^{e}_{de,we}]_n & \eta_r[Z^{d}_{de,jd}]_n & [Z^{e}_{de,je}]_n \\ \eta_r[Y^{d}_{de,cd}]_n & ([Y^{e}_{de,de}]_n + [Y^{d}_{de,de}]_n) & (-[Z^{e}_{de,de}]_n + \frac{1}{\eta_r}[Z^{d}_{de,de}]_n) & [Y^{d}_{de,wd}]_n & [Y^{e}_{de,we}]_n & [Y^{d}_{de,jd}]_n & [Y^{e}_{de,je}]_n \\ [0] & \eta_r[Z^{d}_{wd,de}]_n & [Y^{d}_{wd,de}]_n & [Z^{d}_{wd,wd}] & [0] & [Z^{d}_{wd,jd}] & [0] \\ [0] & [Z^{e}_{we,de}]_n & [Y^{e}_{we,de}]_n & [0] & [Z^{e}_{we,we}] & [0] & [Z^{e}_{we,je}] \\ [0] & \eta_r[Z^{d}_{jd,de}]_n & [Y^{d}_{jd,de}]_n & [Z^{d}_{jd,wd}] & [0] & [Z^{d}_{jd,jd}] & [0] \\ [0] & [Z^{e}_{je,de}]_n & [Y^{e}_{je,de}]_n & [0] & [Z^{e}_{je,we}] & [0] & [Z^{e}_{je,je}] \end{bmatrix} \begin{bmatrix} [I^{\alpha}]_n \\ [I^{\alpha}]_n \\ [k^{\alpha}]_n \\ [I^{wd}] \\ [I^{we}] \\ [I^{jd}] \\ [I^{je}] \end{bmatrix} = \begin{bmatrix} [V^{\alpha}_{cd}]^{E}_{n} \\ [V^{\alpha}_{de}]^{E}_{n} \\ [V^{\alpha}_{de}]^{H}_{n} \\ [V^{wd}] \\ [V^{we}] \\ [V^{jd}] \\ [V^{je}] \end{bmatrix}$$

.....(4-13)

where $\eta_r = \sqrt{\mu_a/\epsilon_a}$, and α = t or ϕ

To avoid repetition, all solutions of Z-and Y-submatricies in the matrix equation (4-13) and also driving vector (R) are the same that suggested in chapter two in case of CBOR, and chapter three in case of DBOR.

4.4 The radar cross section evaluation

The problem of scattering in radars include plane waves falling on the scatterer, as well as measurements of scattered field in far field region. The assembly in the RCS pattern is depending on:

1- The incident and scattered fields, $\bar{E}^{inc}, \bar{E}^{sca}$ or $\bar{H}^{inc}, \bar{H}^{sca}$.

2- The contribution of electric current $\bar{J}$ and magnetic current $\bar{M}$ with respect to BOR, and also wire and junction regions, to find the excitation matrices.

3- The finding of the unknown current coefficients of DCBOR, where DBOR coefficients intervention in the equation account for the final RCS.

4- The finding of the unknown current coefficients of wire and junction regions, which have only electric current $\bar{J}$.

5- The final relation of RCS is the sum of all regions with their currents and measurement matrices .$\mathcal{R}$

In general, the scattered wave in far-zone is the result of two orthogonal components, E_θ and E_ϕ. After finding the unknown current coefficients for all regions of composed structures (coated conductor) with attached wire in the present of junction region between the wire and DBOR, the RCS in both θ- and ϕ-polarized scattered fields can be computed according to [102][76] by:

$$\sigma^{\theta\beta}=\frac{\eta^2k^4}{16\pi^3}\left|\left\{\sum_{-\infty}^{\infty}e^{-jn\phi_s}\sum_{i=1}^{N_s-1}\left[\left[R_{ni}^{t\theta}\right]\ \left[-R_{ni}^{\phi\theta}\right]\ \left[\mathrm{R}_{ni}^{t\phi}\right]\ \left[-\mathrm{R}_{ni}^{\phi\phi}\right]\right]\left[\begin{bmatrix}I_i^{t\beta}\\I_i^{\phi\beta}\\K_i^{t\beta}\\K_i^{\phi\beta}\end{bmatrix}\right]\right\}+\sum_{i=1}^{N_w-1}\left[R_i^{w\theta}\right]\left[I_i^{w\beta}\right]++\sum_{i=1}^{N_a-1}\left[R_i^{j\theta}\right]\left[I_i^{j\beta}\right]\right|^2 \quad (4\text{-}14)$$

$$\sigma^{\phi\beta}=\frac{\eta^2k^4}{16\pi^3}\left|\left\{\sum_{-\infty}^{\infty}e^{-jn\phi_s}\sum_{i=1}^{N_s-1}\left[\left[R_{ni}^{t\phi}\right]\ \left[-R_{ni}^{\phi\phi}\right]\ \left[-\mathrm{R}_{ni}^{t\theta}\right]\ \left[\mathrm{R}_{ni}^{\phi\theta}\right]\right]\left[\begin{bmatrix}I_i^{t\beta}\\I_i^{\phi\beta}\\K_i^{t\beta}\\K_i^{\phi\beta}\end{bmatrix}\right]\right\}+\sum_{i=1}^{N_w-1}\left[R_i^{w\phi}\right]\left[I_i^{w\beta}\right]++\sum_{i=1}^{N_a-1}\left[R_i^{j\phi}\right]\left[I_i^{j\beta}\right]\right|^2 \quad (4\text{-}15)$$

Where $\beta=\theta\ or\ \phi$

4.5 Computed results

In the domain of EMs, studies of EM scattering problems are of common interest. DCBOR with attached electrical wires is chosen here as the scatterer to be discussed, because it is a most representative model for applications used in this chapter . Moreover, a series of computer programs will be advantageous to the study of influence of different dielectric coatings to RCS. Our work comprise establishing appropriate IEs, solving the equations for surface currents using MoMs, compiling computer programs which are effective for DCBOR of arbitrary cross-sectional shapes with attached wires can be conveniently used for different coating materials, and presenting some examples to show the validity and versatility of the method.

4.5.1 Validity of the formulation

The validity of the computational procedure was first verified. The numerical solution using the present method is compared with the exact solution for the coated sphere, where the analytic solutions are possible for a few geometries and can only be generated easily for spheres, using Mei series [102]. Figure (4-3) shows the bistatic RCS in θθ-and ϕϕ-polarized of coated conducting sphere for radius a_1 = 0.394 λ, a_2 = 0.311λ, where the excitation is due to a plane wave incident from the direction of θ = 180°. It was shown from this figure that the agreement between both solutions, CFIE and EFIE-PMCHW, is very good with exact solution [102] for a coating thickness equal to 0.083λ and ε_r = 2. Another test for the validity of numerical solution was found for new value of dielectric constant, ε_r =4, also in θθ-and ϕϕ-polarized are computed. Figure (4-4) shows the bistatic RCS of coated conducting sphere for radius a_1 = 0.477 λ, a_2 = 0.119λ, and dielectric layer thickness t=0.358 λ. Where we find agreement with exact result [68] is very clear.

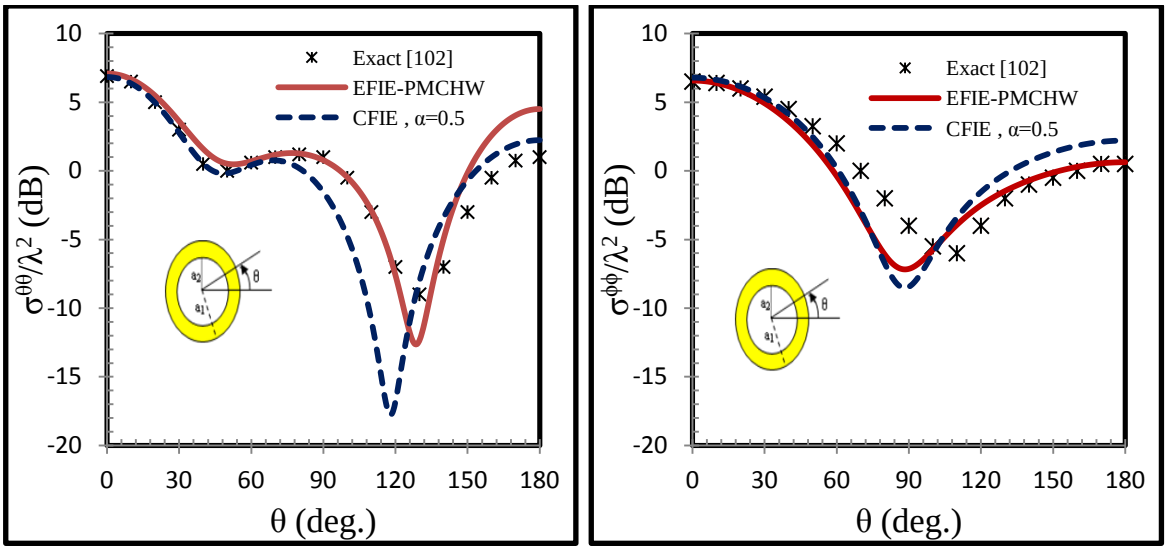

(a) θθ- polarized *(b) ϕϕ-polarized*

Fig.(4-3): computed bistatic cross section for conducting sphere (a_2=0.311λ) coated with homogeneous dielectric (a_1 = 0.394 λ, and ε_r =2.): comparison of the generalized CFIE, EFIC-PMCHWT, and Mie solutions.

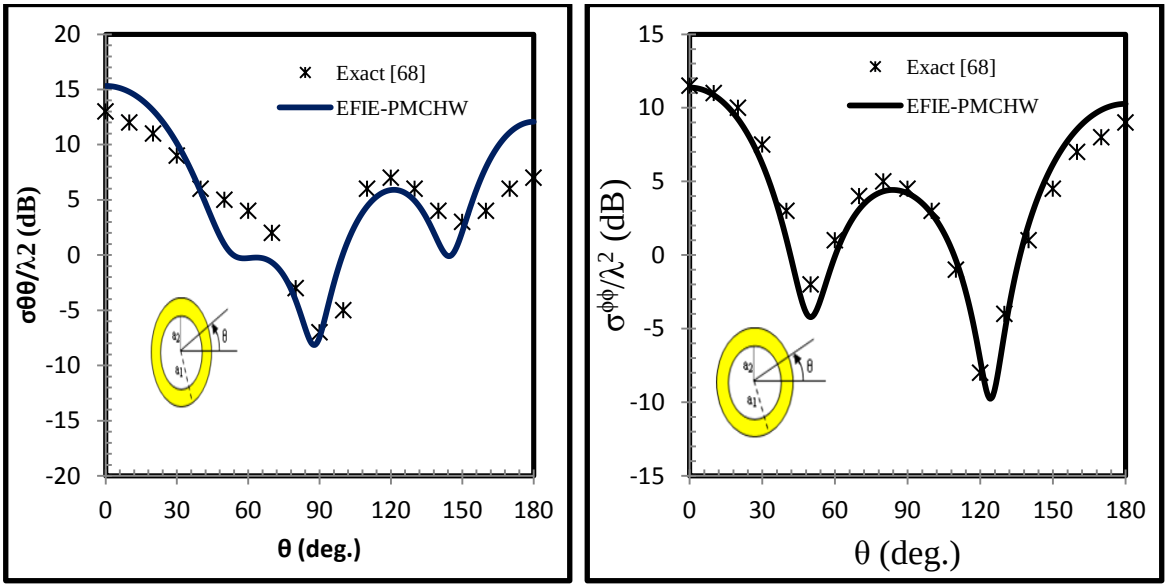

(a) θθ- polarized *(b) ϕϕ-polarized*

Fig.(4-4): computed bistatic cross section for conducting sphere (a_2 = 0.119λ) coated with homogeneous dielectric (a_1 = 0.477 λ, and ε_r =4.): comparison of the generalized EFIC-PMCHWT, and Mie solutions.

4.5.2 Applications

To illustrate the properties and behavior of the present generalized EFIE-PMCHWT formulations, next some results for perfectly conducting scatterers coated with a single homogeneous layer of dielectric material with attached wires are presented. Three applications are considered: (a) coated sphere with one attached wire, (b) coated flat-faced cylinder with two attached wires, and (c) coated rocket with four electric wings (partially coated for irregular object), the coated just for BOR. Because of the results has no previously been described, all applications depend on the comparisons of the results of conductor BOR with attached wires found in chapter two to demonstrate the effected of coated technique on the total RCS pattern. Note, the junction dimensions are that of chapter two.

The first application, conducting sphere of radius a=0.444λ, enclosed by a single layer of dielectric material with thickness t=0.083λ and ε_r=4. coated sphere attached with electric wire of length l_w=0.444λ. The HP backscattered cross sections for this complex structure are depicted in Fig.(4-5), Where we find that the decline in RCS can be very clear in comparison with the case of the conductor body. Furthermore, the effect of wire stays at angles $\theta > 90^{\circ}$ and the number of folds are in decreased.

To identify the second application, Fig.(4-6) shows the HP monostatic RCS of a conducting flat-faced cylinder coated with dielectric material of thickness t=0.083λ and ε_r=4, where the cylinder radius a=0.344λ and length lc=1.98λ. coated cylinder attached with two electric wires located at the center of cylinder and have equal length l_{w1}= $l_{w2=}$0.880λ. It is clear in Fig.(4-6) that the decline in RCS will be at the ends of the pattern, and in main lobe, and equal effect for both wires at the pattern sides of total RCS .

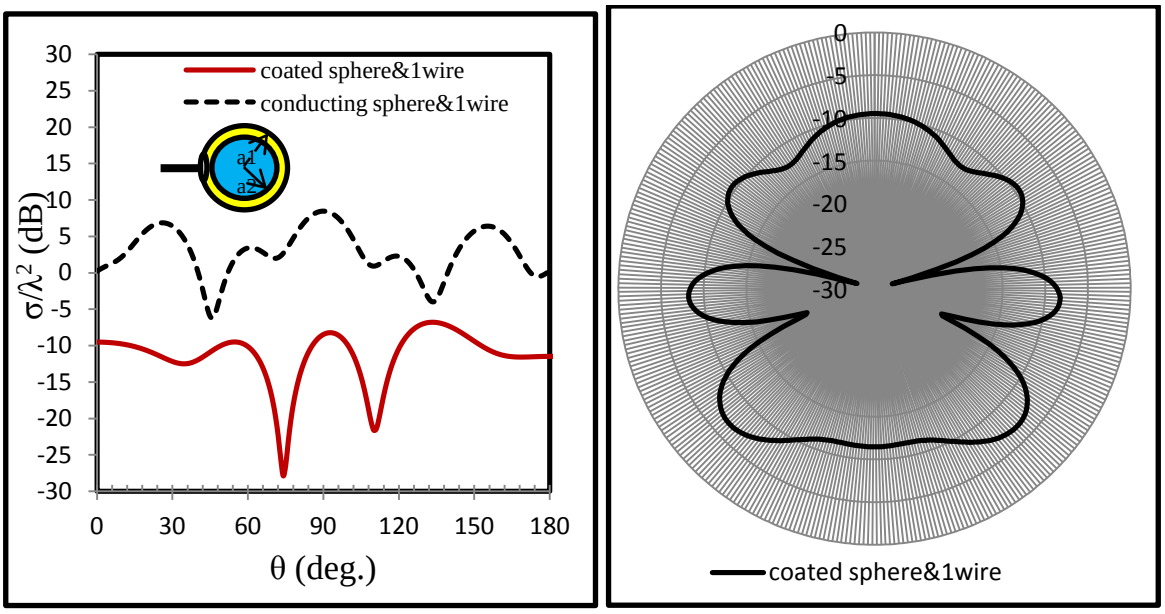

(a) (b)

Fig.(4-5): (a) Monostatic RCS in HP ($\phi=0^o$) for coated sphere with single attached electric wire: comparison with result of conductor case, $a_1= 0.444\lambda$, $a_2=0.361\lambda$, $l_w=0.444\lambda$, $\varepsilon_r=4$. (b) radar graph representation .

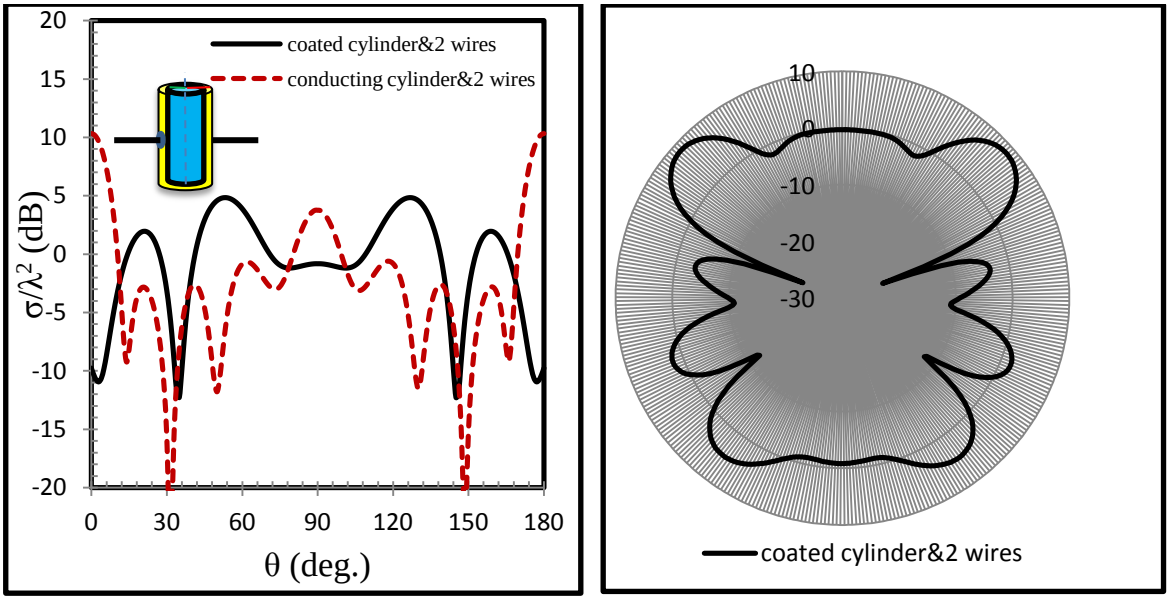

(a) (b)

Fig.(4-6): (a) Monostatic RCS in HP ($\phi=0^o$) for coated cylinder with two attached electric wire: comparison with result of conductor case, $a_1= 0.344\lambda$, $a_2=0.261\lambda$, $l_w=0.880\lambda$, $\varepsilon_r=4$. (b) radar graph representation for coated cylinder and two wires.

Third application involves the, complex irregular shapes structure with complex geometry, previously described in the chapter two as a proposed model of the conducting BOR with attached wires. In this chapter, DCBOR (rocket) with four electric wings is used with same ideal dimensions in chapter two, where the engineering scheme depicted in Fig.(4- 7). According to the definition of the BOR the planar curve that generates the body must be satisfied during the scanning process, the relationship between ρ_α and z_α as shown in Fig.(4-8), which gave the same real shape to the rocket with single dielectric layer of thickness (t). Third application includes several effects for coated parameters on total RCS, which means loss mechanisms of RAM parameters, and can be incorporated as follows:

4.5.2.1 The effect of dielectric constant

The HP monostatic cross section of the geometry in Fig.(4-7) is considered for the effect of dielectric constant. Figure (4-9) shows the effect of the dielectric constant, with single layer of constant thickness (t=0.083λ), on the RCS pattern. It can be shown that the effect of this parameter (ε_r) is very clear on RCS pattern when the dielectric constant varied, comparing with that of the conducting rocket of Fig.(2-25).

4.5.2.2 The effect of dielectric layer thickness

The thickness of dielectric layer is taken as an effective variable parameters for reducing RCS pattern of Fig.(4-7). Figure(4-10) illustrates monostatic RCS results as a function of different layer thickness and constant ε_r. It was shown from this figure that the dielectric layer thickness (t) can be verifying to get results for decreasing in most parts and increasing in some parts, $\theta > 90^\circ$, of RCS in comparison with conducting case.

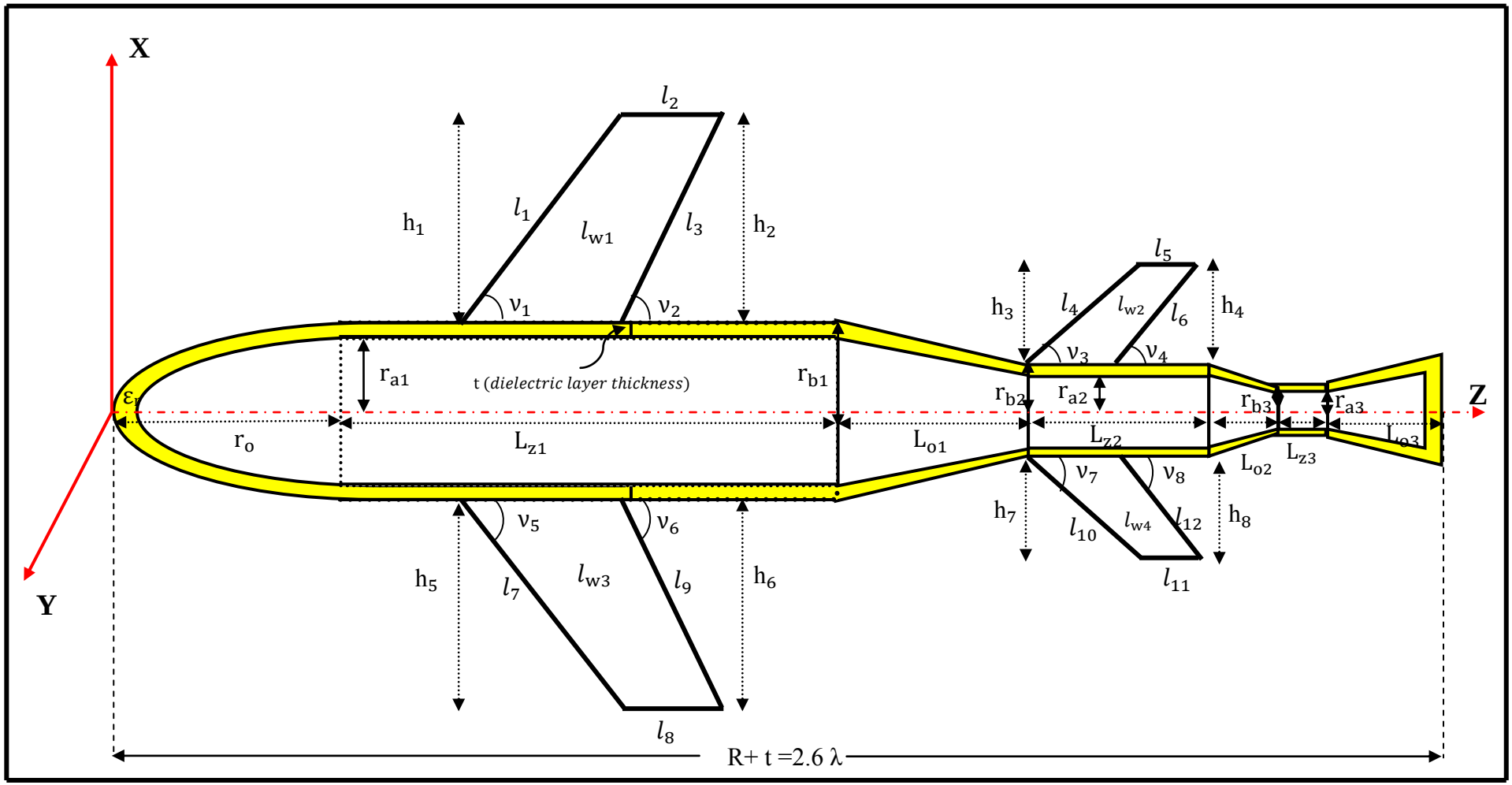

Fig.(4-7): Geometric scheme to parts of the DC-BOR (rocket) with four conducting wings as proposed model.

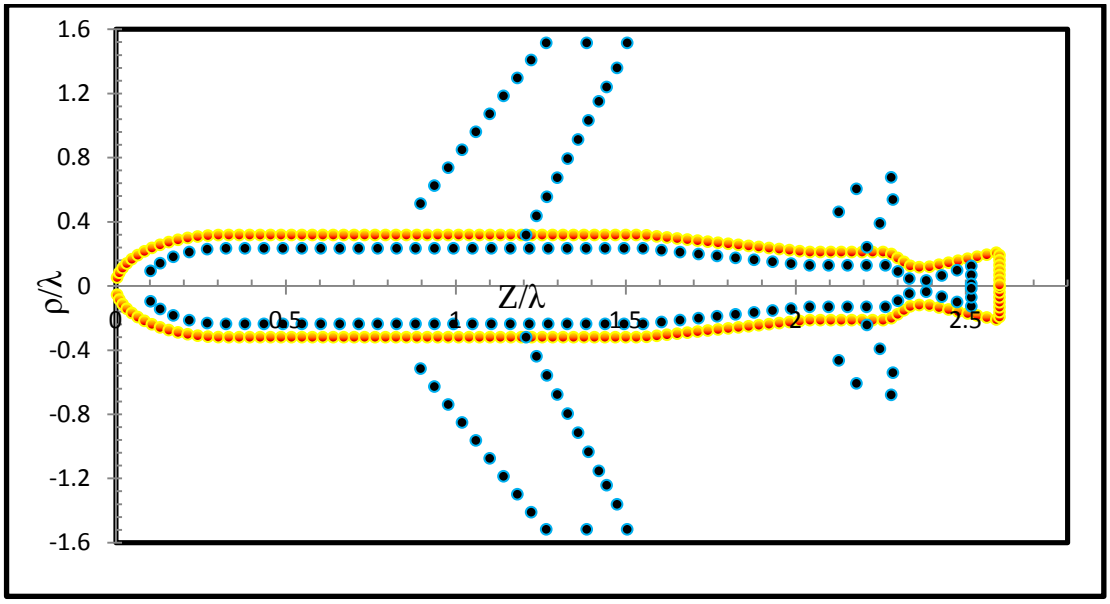

Fig.(4-8): The precise shape of the model in Fig.(4-7)

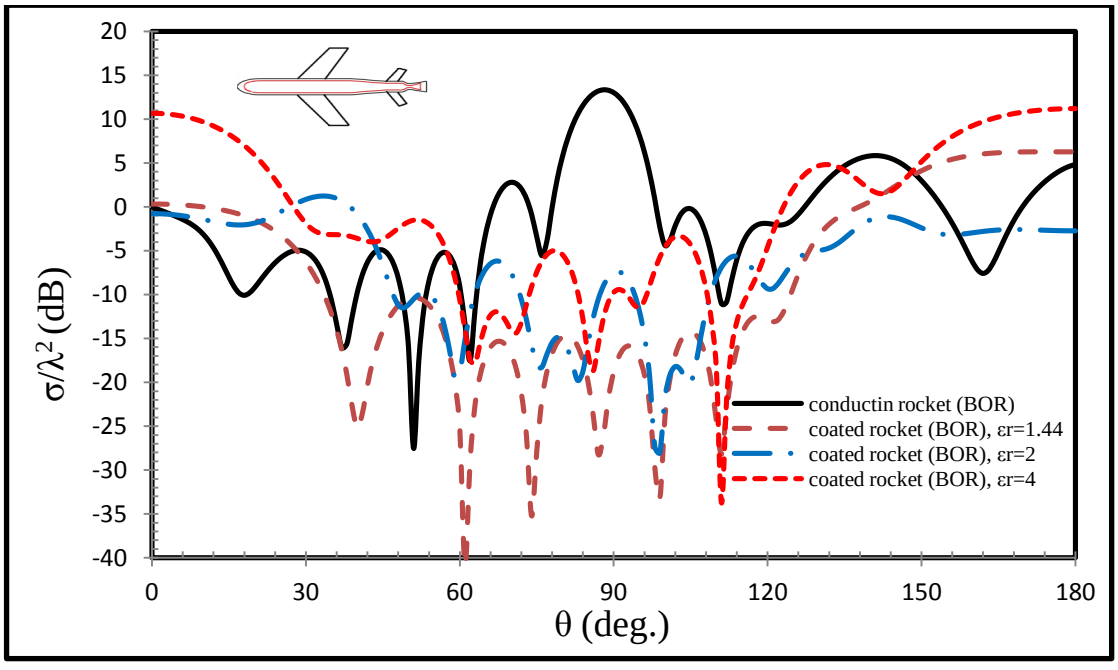

Fig.(4-9): Monostatic RCS in HP ($\phi=0^o$) of Fig.(4-7) of dielectric layer thickness, $t=0.083\lambda$, as a function of dielectric constant ε_r, in comparison with the result of conductor case.

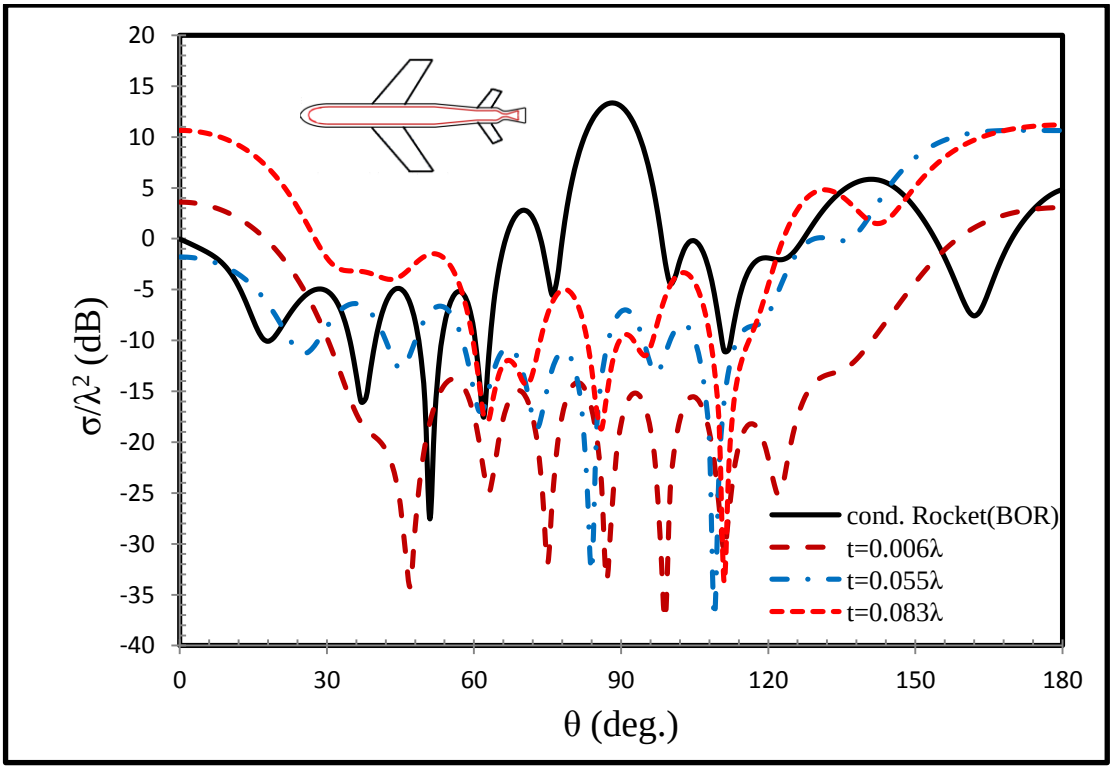

Fig.(4-10): Monostatic RCS in HP ($\phi=0^o$) of Fig.(4-7) of dielectric constant $\varepsilon_r=4$, as a function of layer thickness (t), in comparison with the result of conductor case.

4.5.2.3 The effect of lossy dielectric materials

As it is noted in chapter one there are many ways for reducing the RCS, such that the RAM. One of the most important parameters of RAM is the mechanism loss for electric absorbing material and magnetic absorbing material. To examine the scattering from the structure of Fig.(4-7) by using lossy dielectric materials, Figs.(4-11) shows the effect of lossy dielectric material, with single layer of constant thickness (t=0.083λ), on the total RCS , in comparison with conductor body in Fig.(2-25). It can be shown that the effect of imaginary component ,causes the loss in the material , and the effect of real component with varied values, is very clear by reducing the RCS pattern.

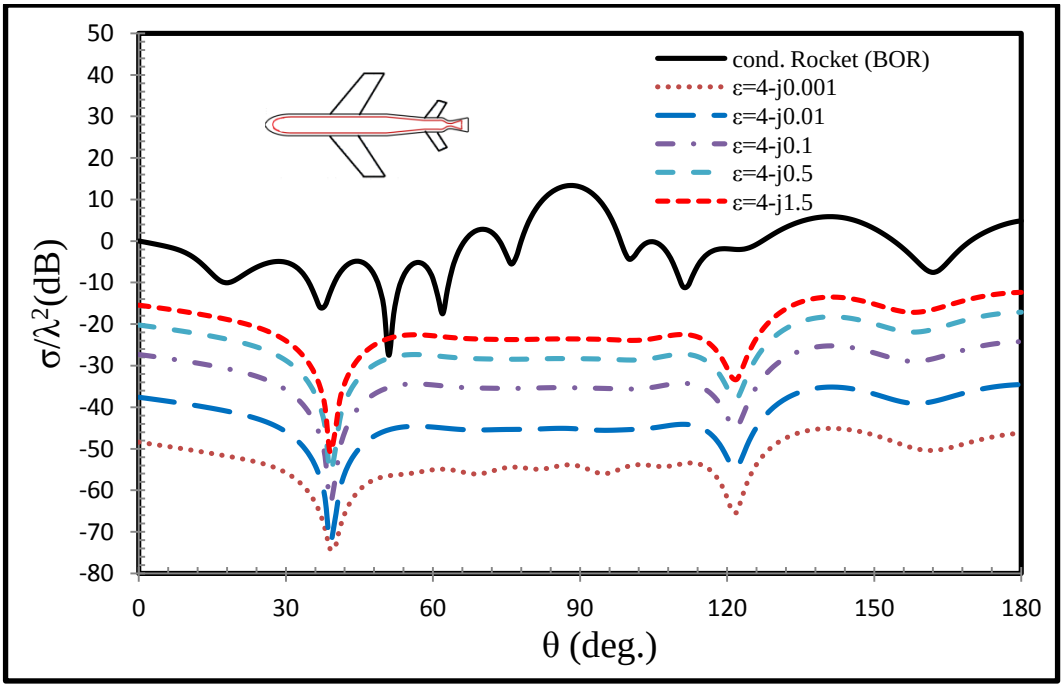

(a)

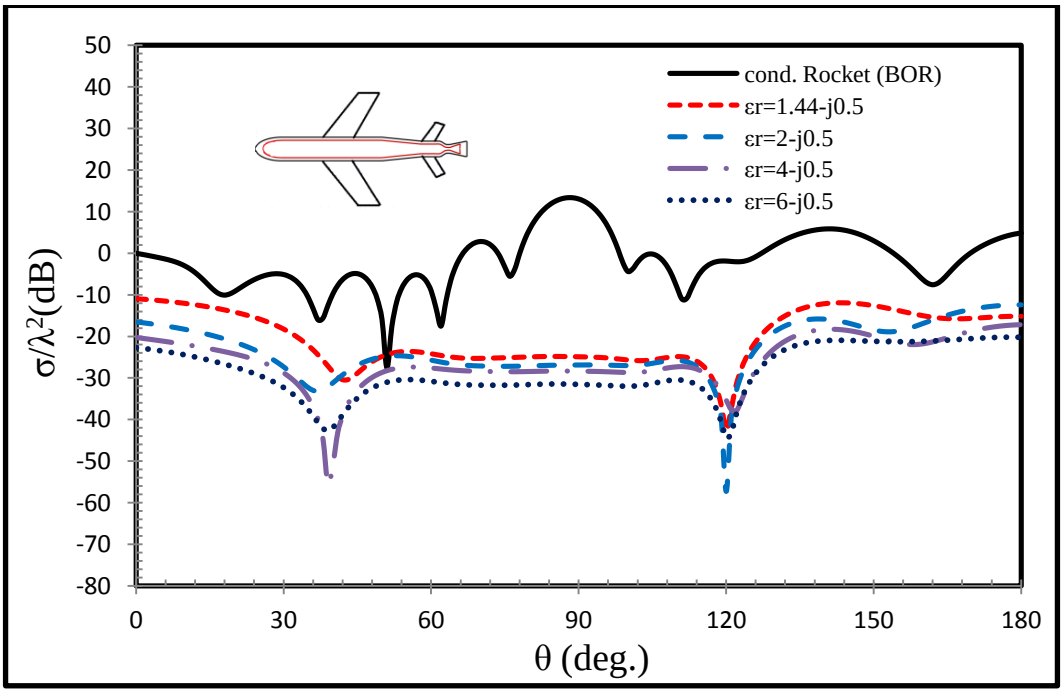

(b)

Fig.(4-11): Monostatic RCS in HP ($\phi=0^o$) of Fig.(4-7) of dielectric layer thickness, $t=0.083\lambda$, as a function of complex lossy dielectric constant , in comparison with the result of conductor case. (a) the effect of imaginary part. (b) the effect of real part.

4.5.2.4 The effect of electric and magnetic absorbing materials

An application of RAM coated aircraft was used by [14], and later used in partial coated by [26]. For a new application the RAM include electric and magnetic absorbing material, which is defined in Eqs.(1-35) and (1-36). Three values of normalized complex permittivity and permeability values ε_r and μ_r were applied on Fig.(4-7). Each value tested to illustrate the impact on RCS as shown in the Fig.(4-12), in which we find a good check for RCSR.

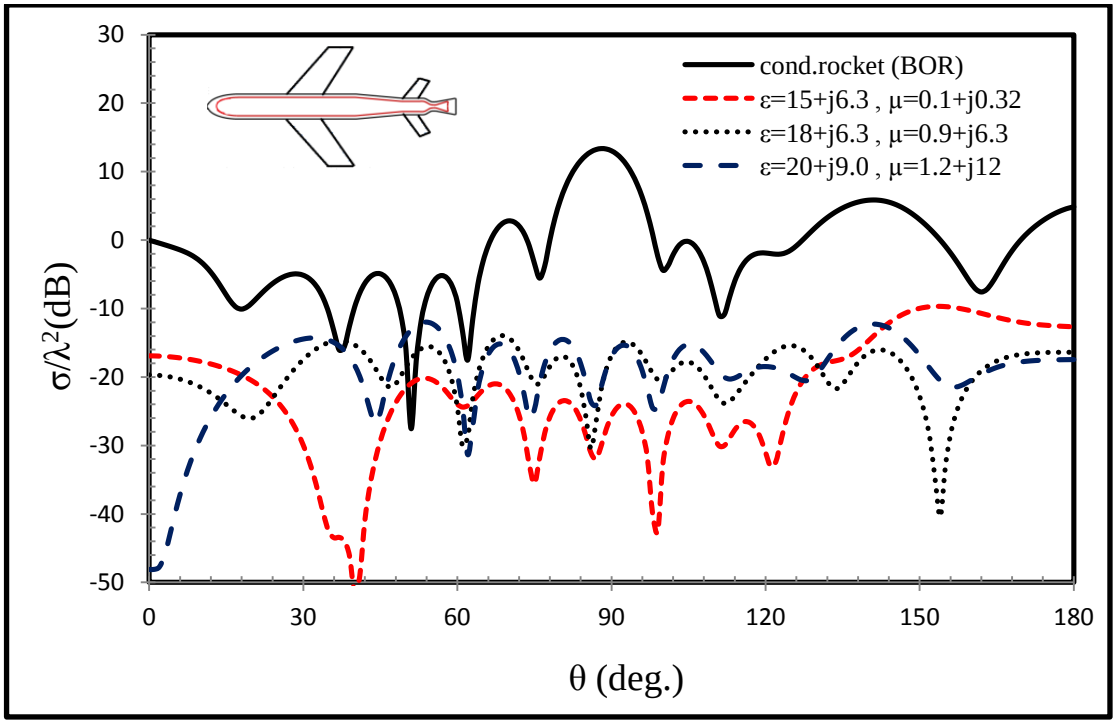

Fig.(4-12): Comparison of Monostatic RCS in HP (ϕ=0^o) for geometry in Fig.(4-7) of dielectric layer thickness, t=0.083λ, as a function of complex lossy dielectric constant in which has electric and magnetic RAM , comparison with the result of conductor case

Chapter Five

General conclusions and future works

5.1 Introduction

The current study was based on proper handling of the body (CBOR, DBOR, and DCBOR) in terms of finding an appropriate method to solve the IEs arising from surface currents, and then solve the problem of scattering from the body (scatterer). After that was a new application, the focus of the study, with attached wires and the existence of the junction between the wire and body surface. This resulted in the application model study. The model is irregular and complex represented a rocket with four wings, which added great importance for the study of where to find the RCS pattern for this rocket compared with known RCS of other structure , and then find a way to reduce RCS of this model. This way was to study the effect of shape and study the effect of dielectrically coated, RAM, as in chapters two and four.

5.2 General conclusions

From the results of this work, we sum up the following conclusion:

1- The method discussed and applied in our thesis is one of the most commonly used methods of solving BOR problems using the method of moments (MoM) technique with Galerkin's approach . This method has the treatments which are more effective than other methods, such as PO + PTD, as evidenced by comparisons in Fig.(2-13b).

2- Using EFIE formulation with MoM is best and efficient for CBOR, whereas CFIE, and PMCHWT formulations are the best and efficient for DBOR and DCBOR.

3- The sound theoretical framework developed in chapters two through four was validated by comparison of our results for various BORs with exact results and existing numerical and measured results whenever available, and

we have demonstrated the health of our results with those available through the figures contained in Chapters.

4- The addition of attached wires significantly alters the constant CBOR, DBOR, and DC-BOR cross-section.

5- Each part of the composite body, the BOR, the wires, and the junction region has its own unique class of current expansion functions. The presence of the effect of the junction is important to ensure continuity of current, and this is indicated by the research [76] and [85] and the results achieved by the present theory compared with experimental results and theoretical results, Fig.(2-25), which calculated in PO+PTD method.

6- The integral transform is introduced and the computation formula of the self-impedance Z^{jj} element at the junction region between the metal wire and the BOR surface is carefully derived to extract the singularity and a relatively accurate solution is obtained, and the results were accurate and efficient. Furthermore, according to the theoretical treatment in the calculation of the matrix Z^{jj} the disk radius as value fixed in all chapters are $a=0.005\lambda$, $b=0.107\lambda$.

7-The computational technique of solving the EFIE by the MoM, for the class of problems described as wires attached to a BOR, is shown here to be applicable to scattering problems. They gave excellent results compared with the experimental results available in the case of the conductor body with attached wires.

8- The calculations compare with available measurements for a missile configuration with wings modeled as wire loops were used to determine the efficacy of the BOR-wire-junction scattering to more complicated and practical geometries, where the results were very convincing. This modeling approach is an extension of the wire sticks representation used by Lin and Richmond [74] , except now the body is represented by a BOR.

9- The study of the subject of the influence of CBOR with attached wires, the proposed model, in calculating of RCS gave a broad idea and explained that the shape component to any object in space has a significant impact and very effective in calculating of RCS. This reason has given engineers and designers of spacecraft considerable attention in the industry of those vehicles, especially military ones, in order to reduce or change the shape of the RCS, making it difficult to identify them through the received radar signal reflected from them.

10- The study of scattering and RCS calculation for the proposed model, which represented by the rocket with four wings as in Fig.(2-26), came on the basis of comparisons with known RCS of the body has asymptotic shape like him a missile symmetrically own body is a cylinder with spherical ends and two wings as in Fig.(2-21). The comparative stages began body without wings (BOR), two wings, and then down to four wings and this is what appeared in the Figs.(2-23), (2-28), (2-29) and (2-31), as we find similarity to a large extent in the form of RCS in spite of the differences caused by minor differences in body shape and the number of wings.

11- The Study of shape effect on the RCS pattern focused on the wings in terms of length, width and height. The tests proved that this effect will be evident on the side lobes of the RCS pattern.

12- The best dimensions of the rocket, which gives the form conforms to the real shape, has the selection of dimensions in terms of large radius r_o referred to as in Fig.(2-26), and the angles of declined is ideal for both ends of the four wings ,which in the values of 70^o and 75^o, and a fixed-length is the same for the body comparative him, R=2.6λ. In addition the changing of angles ν_2 and ν_6 is made an approximate shapes for other known complex body, like aircraft, in order to arrive to useful treatment with these shapes, beneficiaries from the rocket application in future.

13- In the case of DBOR-wire-junction, the moment matrix for DBOR is twice as moment matrix of CBOR. The EFIE-PMCHWT formulations with MoM of Galerkin's approach give largely reasonable results compared with that of CBOR-wire-junction, and the complex lossy DBOR-wire-junction, which is constructed from many parts, is treated efficiently with these formulations.

14- Down to a new application, the DBOR-wire-junction is considered an important entrance to the DCBOR-wire-junction adopted the method of analysis where the same, EFIE-PMCHWT formulations, except that the number of regions has increased.

15- Thickness of the coating layer is an important factor for the attenuation of EM waves, and it showed in the reduce of RCS for different values of thickness.

16- Coated with single layer of complex lossy dielectric in proposed model, DCBOR-wire-junction, is treated efficiently with that formulations, where the reducing in RCS pattern has appeared clearly.

17- The using of RAM include complex parameters ,ϵ and μ, for electric and magnetic absorbing materials, with single layer of constant thickness ($t=0.083\lambda$), was a good check for RCSR in partial coated in complex proposed model. Where this method has proven its efficiency in reducing and distortion the RCS pattern.

18- Adoption of the comparative results of CBOR-wire-junction with cases of DBOR-wire-junction and DCBOR-wire-junction was due to the lack of available results, the fact that the two subjects in the new application.

19- To finalize, having demonstrated that the computer program gives correct data for a variety of target shapes presented in this thesis, we have confidence that the program will perform equally well with other targets using the programming language Fortran Power Station 90.

5.3 Future work suggestion

The previous formulations of the problems that presented in this work is concentrated on the either simple or complex BORs with attached wires. To develop this study to treat another problems we suggest the following future works with abbreviated ideas:

1- By using multi-layers dielectric coated conduction BOR with the structure of Fig.(4-7), one can find the RCS for this model and then trying EFIE-PMCHWT formulations on many coated regions.

2- This model can be developed into fully coated CBOR-wire-junction, coated BOR and wings together, and study this case to see the reduce in RCS.

3- Study of scattering problem to another sample of conducting rockets include:

* Four fins in addition to wings, as shown in Fig.(5-1).

* Four coated fins in addition to partially coated BOR , as shown in Fig.(5-2).

To determine RCS, in this case we dealing with fins with the wire format in two separate directions.

4- Application of BOR-wire-junction may be develops to include the most important shapes, with different mathematical treatments , including:

*Coated RAM aircraft, Fig.(5-3a), by using the wire sticks representation.
*Coated RAM aircraft, Fig.(5-3b), by using the wire grid model.

5- The application of the idea of chiral BOR, which is partially covered by a thin conducting shield, to develop the system of BOR-wire-junction and then its applications under title " partially shielded chiral BOR with attached wires".

6- The study of EM scattering from BOR with attached wires and non-planar disk as junction region.

7-The study of radiation from wire antenna attached to BOR.

8- Electromagnetic scattering from BOT with attached wires.

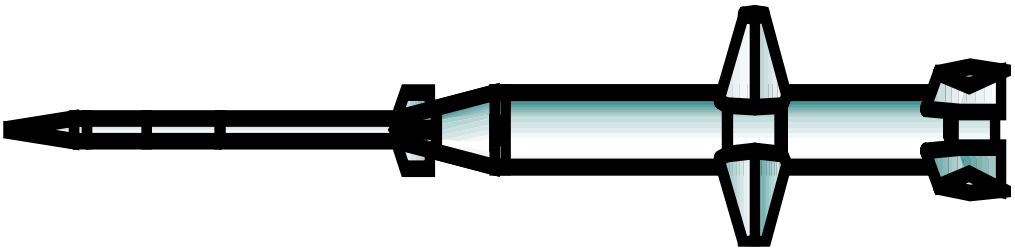

Fig.(5-1): Sample of rocket (BOR) include fins and wings.

Fig.(5-2): Sample of rocket include coated fins and partially coated BOR.

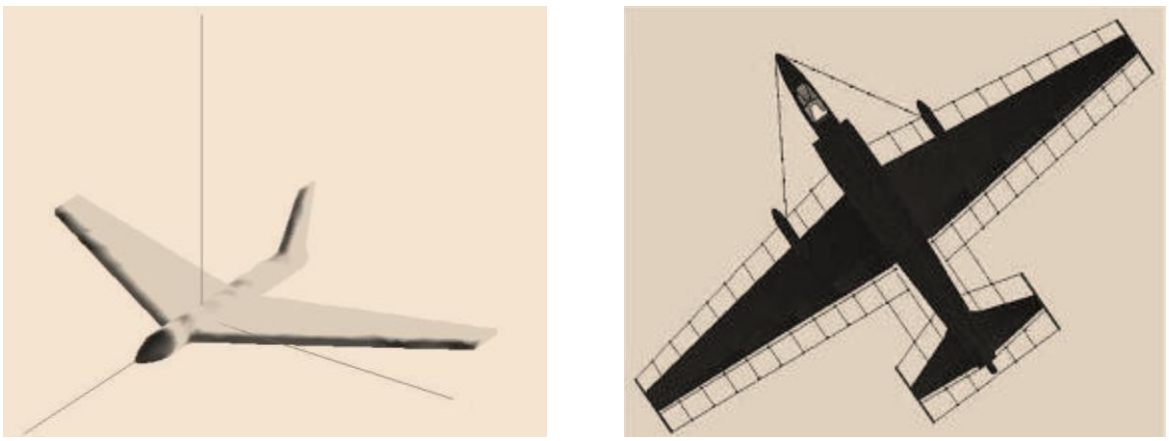

(a) (b)

Fig.(5-3):(a) coated RAM aircraft dealing with the wire sticks representation.

(b) coated RAM aircraft dealing with the wire grid model.

References

[1] Vinoy, K. J., and Jha, R. M., "***Radar absorbing materials from theory to design and characterization***", Kluwer Academic publishers, Boston/London, 1996.

[2] Davidson, D. B., "***Computational electromagnetic for RF and microwave engineering, 2nd edition***", Cambridge University press, 2010.

[3] Sebaq, A. M., "***Studies on the Scattering of Study State and Transient Electromagnetic Wave by Imperfectly Conducting and Coated Structures*** ", Ph. D. Thesis submitted to the faculty of graduate studies, the university of Manitoba, Canada, 1984.

[4] Peterson, A., Ray, S., and Mittra, R., " ***Computational Methods for Electromagnetics"***, IEEE Press, 1998.

[5] Blake, L. V., "***Radar range performance analysis***", Artech House, ISBN 0-89006-224-2, Norwood, USA, 1986.

[6] Ozturk, A. K., "***Implementation of physical theory of diffraction for radar cross section calculations***", M. Sc. Elec.Eng. Thesis submitted to the Institute of Engineering and Sciences of Bilkant University, 2002.

[7] Knott, E. F., Shaeffer, J. F., and Tuley, M. T.," ***Radar cross section: Its prediction, measurement and reduction*** ", Artech House, Inc., USA, 1985.

[8] Mautz, J. R., and Harrington, R. F.,**"*Radiation and scattering from bodies of revolution*",** Appli. Sci. Res., Vol.20, pp.405-435, 1969.

[9] Skolnick, M. I., "***Introduction to radar system***", Mc Graw-hill, book company, New York, 1980.

[10]James, A. S., and James, L. K., "***Coherent radar performance***", Academic Journal, ch2, 1996.

[11] Harrington, R. F. and Mautz, j. r. "***Radiation and scattering from bodies of revolution*** ", Rep.. AFCRL-69-0305, Syracuse Univ., Syracuse. NY**,** 1969.

[12] Sarabandi, K. and Nashashibi, A., "***A novel bistatic scattering matrix measurements technique using a monostatic radar***", IEEE Trans. Antennas propaga., Vol. 44, No. 1, 1996.

[13] Christopher, J. B. and Peter, J. C., "***An investigation of bistatic calibration objects***", IEEE trans. Geosc. And remote sensing, vol. 43, no. 10, 2005.

[14] Knott, E .F., Shaeffer, J. F., and Tuley, M.T., ***"Radar Cross Section, 2nd Edition***", Sci.Tech Publishing, Inc. 2004.

[15] Uslenghi, P.L.E.," ***Electromagnetic Scattering***", Academic Press, Inc., New York, NY., USA, 1978.

[16] Rodriques, V., Elsherbeni, A. Z., and Smith, C. E., "***A body of revolution finite difference time domain method***", Prog. Elec. research, PIER 24, 257-277, 1999.

[17] Jin, J., "***The finite element method in electromagnetics***", John wiely and sons, 1993.

[18]Volakis, J. L., Chattererjee, A., and Kempel, L. C., "***Finite element for electromagnetics***" IEEE press., 1998.

[19] Taflove, A., and Hagness, S. C., "***Computational electromagnetics: The finite difference time-domain method***", Artech House, 3d ed, 2005.

[20] Kosanovich, S., and Mittra, R., "***Comparison of scattering parameter calculations using touchston and a full-wave electromagnetic solver based upon the Finite-Difference Time-Domain Method",*** Microwave Opt. Techn. Letters., Vol. 15, No. 6, 1997.

[21] Mcnamara, D. A., Pistorius, C. W., and Malherbe, J. A., "***Introduction to the uniform geometrical theory of diffraction***", Artech House, Boston, 1990.

[22] Miller, E. K., "***A selective survey of computational electromagnetcs***", IEEE Trans. Antennas propagat., Vol.36, No.9, pp.1281-1305, 1988.

[23] Michaeli, A., "***Equivalent edge currents for arbitrary aspects of observation***", IEEE Trans. Antennas propagat., Vol.23, pp.252-258, 1984.

[24] Zhahe, L., Huang, P., Gao, X., Ying, L., and Jinzu, J., "***Multi-frequency RCS reduction characteristics of shape stealth with MLFMA with improved MMN***", Chinese Journal of Aeronautics, Vol.23, pp.327-33, 2010.

[25] Zhao, S. C., Wang, B.Z., and He, Q. Q., "***Broadband radar cross section reduction of a rectangular patch antenna***", prog. Elec. Research, PIER 79, pp.263-275, 2008.

[26] Mauro, A. A., Rafael, J. P., and Mirabel, C. R., "***Simulations of the radar cross section of stealth aircraft***", SBMO/IEEE MTT-S International Microwave & optoelectronics Conference, pp.409-412, IMOC 2007.

[27] Yeo, J., and Kim, D., "***Novel tapered AMC structures for backscattered RCS reduction***", J. Electromagn. waves and Appl., Vol.23, pp.697-709, 2009.

[28] Miacci, M. A., and Rezende, M. C., "***Basic on radar cross section reduction measurements of simple and complex targets using microwave absorbers***", Applied measurements systems http:/www.intechopen.com, , 2012.

[29] Saville, P., "***Review of radar absorbing materials***", A technical Report, Defencs & D Canada, 2005.

[30] Jiming, S., Lu, C., and Cho, C., "***Multilevel fast multipole algorithm for electromagnetic scattering by complex objects***", IEEE trans. Antennas propagat., Vol.45, No.10, 1997.

[31] Abdelmageed, A. K., "***Efficient evaluation of modal Green's functions arising in EM scattering by bodies of revolution***", Progress In Electromagnetics Research, PIER 27, pp. 337-356, 2000.

[32] Wen, M. Y., Da Gang, F., and Tie, J. C., "***Closed form modal Greens functions for accelerated computation of bodies of revolution***", IEEE Trans. Antennas propagat., Vol. 56, No. 11, 2008.

[33] Godaymi, W. A., "***Electromagnetic radiation from circular-shaped microstrip antennas as bodies of revolution***", Thesis submitted to University of Basrah, 2007.

[34] Werner, D. H., Werner, P. L., Huffman, J. A., Ferraro, A. J., and Breakall, J. K., "***An exact solution of the generalized exponential integral and its application to moment method formulations***", IEEE Trans. Antennas propagat., Vol.41, pp.1716-1719,1993.

[35] Harrington, R. F., "***Field Computation by Moment Methods***", Macmillan, New York, 1968.

[36] Miller, E. K., Medgyesi-Mitschang, L., Newman, E. H., "***Computational electromagnetics: frequency-domain method of moments***", New York: IEEE press, 1992.

[37] Resende, U. C., and Fernando, J. S., "***Numerical convergence of method of moments in the analysis of bodies of revolution***",

[38] Stutzman, W. L., and Thiele, G. A., "***Antenna theory and design***", John Wiely & Sons, Inc., New York, 1981.

[39] Medgyesi-Mitschang, L., and Putnam, J. M., "***Integral equation formulation for imperfectly conducting scatterer***", IEEE trans. Antennas propagat., Vol.AP-33, No.2, pp.206-214,1985.

[40] Paolo, B., "***Integral representations of the electromagnetic field and boundary integral equations***", Dept. of Electronic Eng., School of Eng., University of Rome, Rome, 2003.

[41] Gibson, W. C., "***The method of moments in electromagnetics***", Chapman & Hall/CRC,2008.

[42] Yeh, C. and Shimabukuro, F. I., "***A new proof on boundary conditions in electromagnetic theory***", prog. Elect.Research symp. proc.,Taipei, 25-28, 2013.

[43] Kong, J. A., *"**Electromagnetic Wave Theory***", Wiley, New York, 1986.

[44] Yeh, C., and Shimabukuro, F. I., "***The Essence of Dielectric Waveguides***", Springer, New York, 2008.

[45] Medgyesi-Mitschange, L. N., and Wang, D., "***Hybrid methods for analysis of complex scatterers***", proc. IEEE, Vol.77, No.5, 1989.

[46] Mautz, J. R., and Harrington, R. F., "***H-field, E-field, and combined field solutions for bodies of revolution***", Interim Technical Report, RADC-TR-77-109, 1977.

[47] Yeung, M. S., "***Single integral equation for electromagnetic scattering by three-dimensional homogeneous dielectric objects***", IEEE Trans. Antennas propagat., Vol.47, No.10, 1999.

[48] Mautz, J. R., and Harrington, R. F., "***Electromagnetic scattering from a homogeneous material body of revolution***", AEU-Int. Journal of Electronics communication,Vol.33, pp.71-80, 1979.

[49]Umashankar, K., Taflove, A., and Rao, S. M., " ***Electromagnetic scattering by arbitrary shaped three-dimensional homogeneous lossy dielectric objects***", IEEE Trans. Antennas propagat., Vol.AP-34, pp.758-766, 1986.

[50] Resende, U. C., Moreira, F. J., and Odilon, M. C., "***EMFIE and MEFIE formulations for the analysis of scattering from dielectric and composite bodies of revolution***", Microwave Opt.Techn.Letters., Vol. 53, No. 2, pp. 398-402, 2011.

[51] Yla-Oijala, P., "***Numerical analysis of combined field integral equation formulations for electromagnetic scattering by dielectric and composite objects***", Prog.Electr.Resea.C, Vol.3, 19-43, 2008.

[52] Hwu, S. U., Wilton, D. R.,"***Electromagnetic scattering and radiation by arbitrary configurations of conducting bodies and wires***" San Diego State University, Tech. Rep., No.87-17, 1988.

[53] Crispin, J. W. JR., and Maffet, A. L., "***Radar cross section estimation for simple shapes***", proc. IEEE, Vol.53, No.8, pp.833-848, 1965.

[54] Gaylor, K., "***Radar absorbing materials-mechanism and materials***", MRL Tech. Rep., AR No.005-686, common wealth of Australia, 1989.

[55] Kittel, C., "***Introduction to solid state physics, 6th ed***", wiely, 1986.

[56] Dybdal, R. B., "***Radar cross section measurements***", IEEE, pp.498-516, 1987.

[57] Gama, A. M., and Rezende, M. C., "***Complex permeability and permittivity variation of radar absorbing materials based on MnZn ferrite in microwave frequencies***", Material Research, Vol.16, No.5, pp.997-1001, 2013.

[58] Yao, j. J., He, Si-Y., Chen, H. T., and Zhu, G. Q., "***A RCS reduction design of object with anisotropic impedance surface using genetic algorithm***", PIER symposium Research, Xian, china, march 22-26, 2010.

[59] Qutubudding, K., "***Partially shielded chiral bodies of revolution***", Ph.D. Eng. Thesis submitted to Graduate school of syracuse University, 2012.

[60] Guire, T., Varadan, V. V., and Varadan, V. K., "***Influence of chirality on the reflection of EM waves by planar dielectric slabs***", IEE Trans. Electromagn. Compat., Vol.32, No.4, pp.300-303, 1990.

[61] Andreasen, M. G., "***Scattering from bodies of revolution***", *IEEE Trans. Antennas Propagat.,* vol. AP-13, pp. 303 310, 1965.

[62] Bornholdt, J. M., and Medgyesi-Mitschange, L. N., "***Mixed-domain Galerkin expansions in scattering problems***", IEEE Trans. Antennas. Propagat., Vol. 36, No. 2, 1988.

[63] Yehuda, L., Amir, B. and Alona, B., "***Generalized Formulations for Electromagnetic Scattering from Perfectly Conducting and Homogenous Material Bodies-Theory and Numerical Solution*** ", IEEE Trans. Antennas. Propagat. Vol. 36, No. 12, pp. 1722-1735, 1988.

[64] Hurst, M. P., and Medgyesi-Mitschange, L. N., "***Scattering from partial bodies of revolution***", IEEE Trans. Antennas. Propagat., Vol. 38, No. 1, 1990.

[65] Schmitz, J. L., "***Dual-surface magnetic-field integral equation solution for bodies of revolution***", RL-TR-91-139, Hanscom AFB, MA, ADA 260725, 1991.

[66] Datthanasombat, S., and Prata, A., "***A compact moment method for determining the electromagnetic scattering of bodies of revolution***", Proc IEEE, 1999.

[67] Hashim A. A., "***Electromagnetic Scattering and Radiation from Bodies of Revolution (BoR)***", Ph. D. Thesis Submitted to the College of Science of Basrah Univ., Iraq, 2002.

[68] Medgysi-Mitschang, L. N. and Putnam, J. M., "***Electromagnetic scattering from axially inhomogeneous bodies of revolution***", IEEE Trans. Antennas Propag., vol. AP-32, No.8, 1984.

[69] Maclennan, J. M., "***Verification and limitations of the monostatic-bistatic radar cross section derived by kell***", MSc. Thesis submitted to the faculty of the school of engineering of the airforce institute of technology, Air University, 1988.

[70] Burkholder, R. J., Gupta, I. J., and Johnson, J. T., "***Comparison of monostatic and bistatic radar images***", IEEE Trans. Antennas Propag., vol.45, No.3, 2003.

[71] AL-Assdi, R. A., "***Studying the Effect of Conducting of Revolution (BoR) Shape on Computing Radar Cross Section (RCS)***", MSc. Thesis Submitted to the College of Science of Basrah Univ., Iraq, 2006.

[72] Cakir, C., and Sevgi, L., "***Radar cross-section (RCS) analysis of high frequency surface wave radar targets***", Turk J Elec Eng & Comp Sci, Vol.18, No.3, 2010.

[73] Mackenzie, A. I., Rao, S. M., and Baginski, M. E., "***Method of moments solution of electromagnetic scattering problems involving arbitrarily-shaped conducting/dielectric bodies using triangular patches and pulse basis functions***", IEEE Trans. Antennas Propag., vol.58, No.2, 2010.

[74] Lin, Y. T., and Richmond, J. H., "***EM modeling of aircraft at low frequency***", IEEE Trans. Antennas Propagat., Vol.AP-23, No.1, Jan., 1975.

[75] Newman, E. H., and Pozar, D. M., "***Electromagnetic modeling of composite wire and surface geometries***", IEEE Trans. Antennas Propagat., Vol.AP-26, No.6, 1978.

[76] Shaeffer, J. F. and Medgysi-Mitschang, L. N., "***Radiation from wire antennas attached to bodies of revolution: the junction problem***", IEEE Trans. Antennas Propagat., Vol. AP-29, No. 3 , 1981.

[77] Shaeffer, J. F., "***EM scattering from bodies of revolution attached wires***", IEEE Trans. Antennas Propagat., Vol. AP-30, No. 3,1982.

[78] Medgyesi-Mitschang, L. N., and Eftimiu, C., "***Scattering from wires and open circular cylinders of finite length using entire domain Galerkin expansions***", IEEE Trans. Antennas Propagat., Vol. AP-30, No. 4, pp. 628 636, 1982.

[79] Perez-Leal, R., and Catedra, M. F., "***Input impedance of wire antennas attached on-axis to conducting bodies of revolution*** ", IEEE Trans. Antennas Propagat., Vol.36, No.9, 1988.

[80] Qiu, Z., and Butler, C. M., "***Analysis of a wire in the presence of an open body of revolution*** ", Prog. Electromagn. Research., PIER 15, 1-26, 1988.

[81] Tekin, I., and Newman, E. H., "***Method of moments solution for a wire attached to an arbitrary faceted surface***", IEEE Trans. Antennas Propagat., Vol.46, No.4, 1998.

[82] Young, J., and Butler, C. M., "***Efficient analysis of a thin-wire antenna attached to a body***", Proceedings of the XXVIIth General Assembly of URSI, p. 1397, Maastricht, The Netherlands, 2002.

[83] Taboada, J. M.,Rodriguez, J. L., and Obelleiro, F., "***Comparison of moment-method solutions for wire antennas attached to arbitrarily shaped bodies***", Microwave Opt.Techn.Letter., Vol. 26, No. 6 , 2000.

[84] Young, J., and Butler, C. M., "***An efficient method for the analysis of a structure comprising an appendage attached to a planar surface of a conducting body***", IEEE Trans. Antennas Propagat., Vol.53, No.9, 2005.

[85] Cao, X., and Gao, J., "***The singularity problem at the wire/surface junction region for antenna and arrays with bodies of revolution***", Prog. Electromagn. Research B., Vol.10, 117-130, 2008.

[86] Poggio, A. J., and Miller, E. K., "***Integral equations of three-dimensional scattering problems***", Chap.4 of Computer Techniques for Electromagnetics, edited by R.Mittra, Pergamon Press, 1973.

[87] Chang, Y., and Harrington, R. F., "***A surface formulation for characteristic modes of material bodies***", Report TR-74-7, Dept. of Electrical and Computer Engineering, Syracuse University. Syracuse, N.Y., 1974.

[88] Wu, T. K., and Tsai, L. L., "***Scattering from arbitrarily-shaped lossy dielectric bodies of revolution***", Radio Science,Vol.12, No.5, pp.709-718, 1977.

[89] Fowler, B. W., and Sung, C. C., "***Scattering of an electromagnetic wave from dielectric bodies of irregular shape***", J.Opt.Soc.Am., Vol.69, No.5, 1979.

[90] Gong, Z., and Glisson, A. W., "***A hybrid equation approach for the solution of electromagnetic scattering problems involving two-dimensional inhomogeneous dielectric cylinders***", IEEE Trans. Antennas Propagat., Vol. 35, No. 1, 1990.

[91] Yeung, M. S., "***Single integral equation for Electromagnetic scattering by three-dimensional homogeneous dielectric bodies***", IEEE Trans. Antennas Propagat., Vol.47, No. 10, 1999.

[92] Yeung, M. S., "***Solution of electromagnetic scattering problems involving three-dimensional homogeneous dielectric objects by the single integral equation method*** ", Jour. Scien. Comput., Vol.15, No.1, 2000.

[93] Kucharski, A., "***A method of moments solution for electromagnetic scattering by inhomogeneous dielectric bodies of revolution***", IEEE Trans. Antennas Propagat., Vol. 48, No. 8, 2000.

[94] Yla-Oijala, P., Taskinen, M., and Sarvas, J., "***Surface integral equation method for general composite metallic and dielectric structures with junctions***", Prog. Electr. Resea., PIER 52, 81-108, 2005.

[95] Kucharski, A. "***Electromagnetic scattering by partially inhomogeneous dielectric bodies of revolution***", Microwave Opt. Techn. Letters., Vol. 44, No. 3, 2005.

[96] Resende, U. C., and Fernando, J. S., Odilon, M. C., and Joao, A. V., "***Optimal number of basis functions in the MoM solutions for bodies of revolution***", Jour. Microwave and Optoele., Vol.6, No.1, 2007.

[97] Necmi, S. T., "***A new formulation and solution method of electromagnetic scattering from arbitrary shaped dielectric objects***", Microwave Opt. Techn. Letters., Vol. 50, No. 11, 2008.

[98] Rui, X., Hu, J., and Liu, Q. H., "***Fast inhomogeneous plane wave algorithm for homogeneous dielectric body of revolution***", Commun. omput. phys., vol. 8, No.8, pp.917-932, 2010.

[99] Junker, G. P., Kishk, A. A., and Glisson, A. W., "***MoM solution of wire radiators coupled to dielectric bodies of revolution***", IEEE Antennas. Propag. Society Int. Symp., pp.40-43, Ann Arbor, MI, 1993.

[100] Junker, G. P., Kishk, A. A., Glisson, A. W.,and Kajfez, D."***Dielectric disk radiating elements***", Rome Lab., Technical Report, RL-TR-95-149, University of Mississippi, 1995.

[101] Kishk, A. A., and Shafai, L., "***Numerical solution of scattering from coated bodies of revolution using different integral equation formulations***", IEE Proc. Vol. 133, Pt. H, No. 3, pp. 227-232, 1986.

[102] Huddleston, P. L., Medgyesi-Mitschang, L. N., and Putnam, J. M., "***Combined field integral equation formulation for scattering by dielectrically coated conducting bodies***", IEEE Trans. Antennas Propaga., Vol.Ap-34, No. 4, pp. 510-520, 1986.

[103] Rao, S. M., Chung, C. C., Cravey, L. R., and Wilkes, D. L., "***Electromagnetic scattering from arbitrary shaped conducting bodies coated with lossy materials of arbitrary thickness***", IEEE Trans. Antennas Propaga., Vol. 39, No. 5, 1991.

[104] Putnam, J. M., and Medgyesi-Mitschang, L. N., "***Combined field integral equation formulation for inhomogeneous two-and three-dimensional bodies: the junction problem***", IEEE Trans. Antennas Propaga., Vol.39, No. 5, 1991.

[105] Yehuda, L., Amir, B. and Alona, B., "***Analysis of electromagnetic scattering from dielectrically coated conducting cylinders using a multifilament current model*** ", IEEE Trans. Antennas. Propagat. Vol. 36, No. 11, 1988.

[106] Antar, Y. M., Kishk, A. A., Shafai, L., and Allan, L. E., "***Radar backscattering from partially coated targets with axial symmetry***", IEEE Trans. Antennas Propaga., Vol. 37, No. 5, 1989.

[107] Arvas, E., and Sarkar, T. K., "***RCS of two-dimensional structures consisting of both dielectrics and conductors of arbitrary cross section***", IEEE Trans. Antennas Propaga., Vol. 37, No. 5, 1989.

[108] Yiqun, J., and Zhangquan, G., "***Research on electromagnetic scattering from partially coated conducting cylinders***", Jour. Elec., Vol. 8, No. 4, 1991.

[109] Kishk, A. A., Bridges, G. E., Sebak, A., and Shafai, L., "***Integral equation solution of scattering from partially coated conducting bodies of revolution***", IEEE Trans. on Magnetics, Vol. 27, No. 5, 1991.

[110] Kishk, A. A., and Gordon, R. K., " ***Electromagnetic scattering from conducting bodies of revolution coated with thin magnetic materials*** ", IEEE Trans. on Magnetics, Vol. 30, No. 5, 1994.

[111] Yang, H., Xia, Y., Shu, L. and Wu, L., " ***Electromagnetic scattering from conducting flat plates coated with thin RAM*** ", Wuhan University Journal of Natural sciences, Vol. 7, No. 2, pp.185-188, 2002.

[112] Lei, L., Hu, J., and Hu, H., " ***Solving scattering from conducting body coated by thin-layer material by hybrid shell vector element with boundary integral method*** ", Int. Jour. Antennas Propaga., Research Article, Artical ID 854647, 2012.

[113] Jung, B. H., Sarkar, T. K. and Palma, M. S., "***Combined field integral equation formulation for the analysis of scattering from 3D conducting bodies coated with a dielectric material*** ", Microwave Opt.Techn.Letters., Vol. 40, No. 6, pp. 511-516, 2004.

[114] He, S., Nie, Z., and Hu, J., "***Numerical solution of scattering from thin dielectric-coated conductors based on TDS approximation and EM boundary conditions* ",** Progr. Electromag. Resa., PIER 93, 339-354, 2009.

[115] Yuyuan, A., Zhu, J., and Chen, R., "***Electromagnetic scattering of conducting bodies of revolution coated with chiral material***", Proc. IEEE, 2010.

[116] Mautz, J. R., "***Scattering from loaded wire objects near a loaded surface of revolution***", Syracuse Univ. Research Corp., Rep. No. SURC TN 74-030, 1974.

[117] Jenn, D. C., and Rusch, W. V., " ***An E-field integral equation solution for the radiation from reflector antennas with strust***", IEEE Trans. Anten. and Propag. Vol. 37, No. 6, pp. 683-689, 1989.

[118] Arfken, G. B., Weber, H. J., and Harris, F.E.," ***Mathematical methods for physicists***", Academic press, British library cataloging, 2013.

[119] Mittra, R., and Gordon, R. K., " ***Radar Scattering from Bodies of Revolution Using an Efficient Partial Differential Equation Algorithm***", IEEE Trans. Anten. and Propag. Vol. 37, No. 5, pp. 538-545, 1989.

[120] Yl¨a-Oijala, P., and Taskinen, M., "***Improving conditioning of the electromagnetic surface integral equations using normalized field quantities***", *IEEE Trans. Antennas Propag.*, Vol. 55, No. 1, 178–185, 2007.

Appendix (A)

The Method of Moments

The method of moments (MoM) is a numerical computational method of solving linear partial differential equations which have been formulated as integral equations, in boundary integral form [35].

The MoM has been applied to the matrix solution of the EM integral equation (IE). The problems solved by MoM include wires, two-dimensional and three- dimensional surfaces using surface patches, BOR, and bodies of translation (BOT). The solution goal, whether viewed as the end itself or as a necessary step for obtaining the scattered fields, is to determine the currents include on the scattering body [46,62].

A brief overview of the MoM described by Harrington and Gibson [35,41] is given below:

1- Linear operator equations: The numerical solutions of EM field problems are usually classified into two groups. The first one attacks directly EM fields, and the second one attacks the field sources. In both cases, the equations that are to be solved are linear operator equations in terms of the unknowns. However, in the first case the equations are differential, whereas in the second case they are integral. Both classes of equations belong to the general class of linear operator equations, which have the common form:

$$L(f) = g \qquad \text{(A-1)}$$

where L is the operator, g is the source or excitation, which is assumed to be a known function, and f is the field or response, which is the unknown function to be determined.

2- Basic steps of the MoM: The basic idea of the MoM is as follows. The unknown quantity (f) is expended in terms of a set of linearly independent known functions, f_n , by the following finite series:

$$f = \sum_{n=1}^{N} \alpha_n f_n \quad \text{(A-2)}$$

where α_n are unknown coefficients yet to be determine. The expansion functions should be chosen, usually based on experience, so that reasonable approximation of f is obtained with small number of terms, *N*. when Eq.(A-2) is substituted into (A-1). one obtains

$$L(\sum_{n=1}^{N} \alpha_n f_n) = g \quad \text{(A-3)}$$

due to the linearity of the operator. we can re write equation(A- 3) as

$$\sum_{n=1}^{N} \alpha_n \, L(f_n) = g \quad \text{(A-4)}$$

the unknown coefficients (α_n) should now be determined such that Eq.(A-4) is satisfied in a sense. Hence, a measure is needed describing the degree of accuracy to which the left side and the right side of Eq.(A-4) match. This measure is obtained by multiplied both sides of Eq.(A-4) by a known, properly selected function, referred to as the weighting function, W_m , and the results integrated over a spatial region. The choice of the weighting functions and inner product is, a gain, based on experience. Now we have

$$\sum_{n=1}^{N} \alpha_n \, \langle W_m \, , L(f_n) \rangle = \langle W_m \, , g \rangle \quad \text{(A-5)}$$

To obtain a determined system of linear equations for the coefficients α_n, the weighting procedure is done for a linearly independent set of *N* functions, yielding

$$\sum_{n=1}^{N} \alpha_n \, \langle W_m \, , L(f_n) \rangle = \langle W_m \, , g \rangle \, , \; m = 1, \ldots \ldots, N \quad \text{(A-6)}$$

Equation (A-6) represents a system of *N* ordinary linear equations in N unknowns, and it can be solved using various techniques. These techniques depend on the choosing the weight (testing) function. Galerkin's approach is popular method used to determine the testing function, which consists in choosing the same testing functions as the basis functions, that is, $W_m = f_n^{\,*}$ where * denote a complex conjugate. The system of linear equations from Eq.(A-6) can be written in matrix form as:

$$[L_{mn}] \, [\alpha_n] = [g_m] \quad \text{(A-7)}$$

Where

$$\begin{bmatrix} \langle W_1, L(f_1)\rangle & \langle W_1, L(f_2)\rangle & \cdots & \langle W_1, L(f_N)\rangle \\ \langle W_2, L(f_1)\rangle & \langle W_2, L(f_2)\rangle & \cdots & \langle W_2, L(f_N)\rangle \\ \vdots & \vdots & & \vdots \\ \langle W_N, L(f_1)\rangle & \langle W_N, L(f_2)\rangle & \ldots & \langle W_N, L(f_N)\rangle \end{bmatrix} \begin{bmatrix} \alpha_1 \\ \alpha_2 \\ \vdots \\ \alpha_N \end{bmatrix} = \begin{bmatrix} \langle W_1, g\rangle \\ \langle W_2, g\rangle \\ \vdots \\ \langle W_N, g\rangle \end{bmatrix} \quad \text{(A-8)}$$

Where the two indices *m* and *n* represents the field and source point, respectively. The unknown coefficients α_n can now be found using a matrix inversion technique.

Appendix (B)

The numerical solution of EFIE

In this appendix, the main steps for solving EFIE by numerical solution MoM [35,41] will be formalized.

The integral equation is formulated in the conventional way when denoted impressed field E^i and scattered field due to currents on the body E^s are founded. The total electric field is

$$\vec{E} = \vec{E}^i + \vec{E}^s \quad \text{(B-1)}$$

The scattered field can be expressed in terms of vector potential $\vec{A}$ and a scalar potential ϕ as:

$$\vec{E}^s = -j\omega\vec{A}(r) - \nabla\phi(\mathrm{r}) \quad \text{(B-2)}$$

The boundary condition requires that the tangential component of total *E* vanish on *S*, hence

$$\vec{E}^i_{tan} = -\vec{E}^s_{tan} \quad \text{(B-3)}$$

Where the subscript "tan" denotes tangential components on *S*.

problem can now be stated succinctly as:

$$L(\vec{J}) = \vec{E}^i_{tan} \quad \text{(B-4)}$$

Where L is the integro-differential operator

$$L(\vec{J}) = \left[j\omega\vec{A}(r) - \nabla\phi(\mathrm{r})\right]_{tan} \quad \text{(B-5)}$$

to solve (B-5) by MoM [8], let the inner product be defined as:

$$\langle \vec{W}, \vec{J} \rangle = \iint_s \vec{W}.\vec{J}\, ds \qquad \text{(B-6)}$$

Where W and J are tangential vectors on *S*. A set of expansion functions [J_j] is next defined, and the current on *S* approximated by

$$J = \sum_j I_j J_j \qquad \text{(B-7)}$$

Where I_j are components to be determined. from (B-7) and (B-4), which, because of the linearity of *L*, reduces to

$$\sum_j I_j J_j = \vec{E}^i_{tan} \qquad \text{(B-8)}$$

using testing functions (W_i), the inner product of (B-8) with each W_i is taken, then

$$\sum_j I_j \langle W_i, LJ_j \rangle = \langle W_i, E^i \rangle \quad , i = 1,2,3, ... \qquad \text{(B-9)}$$

The generalized network matrices, where the inner product involves only tangential components, are

$$[Z] = \left[\langle W_i, LJ_j \rangle\right] \qquad \text{(B-10)}$$

$$[V] = \left[\langle W_i, E^i \rangle\right] \qquad \text{(B-11)}$$

Appendix (C)

The calculation of the Z-submatrices elements

The general procedure for calculating the impedance submatrices elements equation can be found from the electric field and the current density which denoted *JE*, or from the magnetic field and the magnetic current density, denoted by *MH*. The relationship between these impedance matrices [33] is

$$\left(Z_n^{\alpha\beta}\right)_{ij}^{MH} = \frac{1}{\eta_a^2}\left(Z_n^{\alpha\beta}\right)_{ij}^{JE} \qquad \text{(C-1)}$$

Where $\eta_a = \sqrt{\mu_a / \varepsilon_a}$, α and β are either t- or ϕ-direction, the letter (a) referred

to the medium. The mutual impedance between a source element i and field element j with using of Eq.(3-34), is of the form

$$\left(Z_n^{\alpha\beta}\right)_{ij}^{JE} = \left\langle \overline{W}_{ni}^{\alpha}, \overline{E}^{a}\left(\overline{J}_{nj}^{\beta},0\right)\right\rangle \tag{C-2}$$

the electric field $\overline{E}\left(\overline{J}_{nj},0\right)$ in Eq.(C-2) can be expressed by rewriting eq.(B-2), then

$$\overline{E}^{a}\left(\overline{J}_{nj},0\right) = -j\omega\overline{A}^{a}\left(\overline{J}_{nj}\right) - \nabla\Phi^{a}\left(\overline{J}_{nj}\right) \tag{C-3}$$

$$\overline{A}^{a}\left(\overline{J}_{nj}\right) = \mu_a \int_s \overline{J}_{nj}\left(\overline{r}\right) G^{a}\left(\overline{r},\overline{r}'\right)\, ds \tag{C-4}$$

$$\Phi^{a}\left(\overline{J}_{nj}\right) = \frac{1}{\varepsilon_a}\int_s \sigma_{nj}\left(\overline{r}\right) G^{a}\left(\overline{r},\overline{r}'\right)\, ds \tag{C-5}$$

where $\overline{r}$ and $\overline{r}'$ are vectors from the origin point to the field and source points, respectively. $\overline{J}_{nj}(\overline{r})$ is the electric surface current on S , $\sigma_{nj}(\overline{r})$ is the surface charge given by:

$$\sigma_{nj}\left(\overline{r}\right) = \frac{j}{\omega}\nabla_s \cdot \overline{J}_{nj}\left(\overline{r}\right) \tag{C-6}$$

and, $G^{a}\left(\overline{r},\overline{r}'\right) = \dfrac{e^{-jK_a\left|\overline{r}-\overline{r}'\right|}}{4\pi\left|\overline{r}-\overline{r}'\right|}$ (C-7)

is the scalar Greens function.

The elements of the Z-submatrices which are defined by Substitution of Eq.(C-3) into Eq.(B-2), gives

$$\left(Z_n^{\alpha\beta}\right)_{ij}^{JE} = -\int_s \overline{W}_{ni}^{\alpha} \cdot \left\{ j\omega\overline{A}^{a}\left(\overline{J}_{nj}^{\beta}\right) + \nabla\Phi^{a}\left(\overline{J}_{nj}^{\beta}\right)\right\} ds \tag{C-8}$$

to transfer the differential operator on $\nabla_s \cdot \left(\Phi^{a}\overline{W}_{ni}^{\alpha}\right)$, this by using the vector identity[33] to the second term in Eq.(C-8) to obtain

$$\nabla_s \cdot \left(\Phi^{a}\overline{W}_{ni}^{\alpha}\right) = \overline{W}_{ni}^{\alpha} \cdot \left(\nabla_s\Phi^{a}\right) + \Phi^{a}\left(\nabla_s \cdot \overline{W}_{ni}^{\alpha}\right) \tag{C-9}$$

Hence

$$\int_s \nabla_s \cdot \left(\Phi^{a}\overline{W}_{ni}^{\alpha}\right) ds = \int_s \overline{W}_{ni}^{\alpha} \cdot \left(\nabla_s\Phi^{a}\right) ds + \int_s \Phi^{a}\left(\nabla_s \cdot \overline{W}_{ni}^{\alpha}\right) ds \tag{C-10}$$

from the application of two-dimensional divergence theorem on closed surface, we have $\int_s \nabla_s \cdot \left(\Phi^a \overline{W}_{ni}^{\alpha}\right) ds = 0$, and Eq.(C-10) becomes:

$$\int_s \overline{W}_{ni}^{\alpha} \cdot \nabla_s \Phi^a \; ds = -\int_s \Phi^a \left(\nabla_s \cdot \overline{W}_{ni}^{\alpha}\right) ds \tag{C-11}$$

Substituting the above equation into Eq.(C-8) to get

$$\left(Z_n^{\alpha\beta}\right)_{ij}^{JE} = -j\omega \int_s \overline{W}_{ni}^{\alpha} \cdot \overline{A}^a \left(\bar{J}_{nj}^{\beta}\right) ds + \int_s \Phi^a \left(\bar{J}_{nj}^{\beta}\right)\left(\nabla_s \cdot \overline{W}_{ni}^{\alpha}\right) ds$$

Substituting $\overline{A}^a$ and Φ^a from Eqs.(C-4) and (C-5) in the last equation, gives

$$\left(Z_n^{\alpha\beta}\right)_{ij}^{JE} = -j\omega\mu_a \int_{s'}\int_s \overline{W}_{ni}^{\alpha}(\bar{r}') \cdot \bar{J}_{nj}^{\beta}(\bar{r}) G^a(\bar{r},\bar{r}') \; ds\, ds' + \frac{j}{\omega\varepsilon_a} \int_{s'}\int_s \left(\nabla_s \cdot \bar{J}_{nj}^{\beta}(\bar{r})\right)$$

$$\left(\nabla'_s \cdot \overline{W}_{ni}^{\alpha}(\bar{r}')\right) G^a(\bar{r},\bar{r}') \; ds\, ds' \tag{C-12}$$

Eq. (C-12) represents the generalized impedance for a body in greater details, which have four types of impedances.

Going back to the relationship, we find the expansion functions given by:

$$\bar{J}_{nj}^{\beta}(\bar{r}) = \hat{u}_{\beta'} f_i(t)\, e^{jn\phi} \tag{C-13}$$

and the weighting function, which defined as the conjugate of Eq.(C-13), written as :

$$\overline{W}_{ni}^{\alpha}(\bar{r}') = \hat{u}_{\alpha} f_i(t')\, e^{-jn\phi'} \tag{C-14}$$

To evaluate the four types of impedances in Eq.(C-12), one must be obtained the $\overline{W} \cdot \bar{J}$, where the mode orthogonality in axis symmetric was taken early, i.e. (n=m), then we have:

$$\overline{W}_{ni}^{\beta} \cdot \bar{J}_{nj}^{\alpha} = \hat{u}_{\alpha} \cdot \hat{u}_{\beta'} f_i(t') f_j(t)\, e^{jn(\phi-\phi')} \tag{C-15}$$

The unit vector dot products, in terms of the body coordinates defined by Eqs.(2-21), are:-

$$\hat{u}_{t'} \cdot \hat{u}_t = \sin\nu \sin\nu' \cos(\phi-\phi') + \cos\nu \cos\nu' \tag{C-16a}$$

$$\hat{u}_{\phi'} \cdot \hat{u}_t = \sin\nu \sin(\phi - \phi') \tag{C-16b}$$

$$\hat{u}_{t'} \cdot \hat{u}_\phi = -\sin\nu' \sin(\phi - \phi') \tag{C-16c}$$

$$\hat{u}_{\phi'} \cdot \hat{u}_\phi = \cos(\phi - \phi') \tag{C-16d}$$

Here ν is the angle between the t direction and the z-axis.

Now, to find the surface divergence of the two vectors $\bar{J}_{nj}^{\beta}(\bar{r})$ and $\bar{W}_{ni}^{\alpha}(\bar{r}')$ in the second term of Eq.(C-12), as follow:-

$$\nabla_s \cdot \bar{J}_{nj}^{\beta}(\bar{r}) = \left(\frac{1}{\rho(t)} \frac{\partial}{\partial t}\left(\rho(t)\, \hat{u}_t \right) + \frac{1}{\rho(t)} \frac{\partial}{\partial \phi}\left(\hat{u}_\phi \right) \right) \cdot \bar{J}_{nj}^{\beta}(\bar{r}) \tag{B-17a}$$

$$\nabla'_s \cdot \bar{W}_{ni}^{\alpha}(\bar{r}') = \left(\frac{1}{\rho'(t')} \frac{\partial}{\partial t'}\left(\rho'(t')\, \hat{u}_{t'} \right) + \frac{1}{\rho'(t')} \frac{\partial}{\partial \phi'}\left(\hat{u}_{\phi'} \right) \right) \cdot \bar{W}_{ni}^{\alpha}(\bar{r}') \tag{B-17b}$$

Substituting Eqs.(C-15) and (C-17) into Eq.(C-12), and for an explicit solution we choose the $\rho(t) f_i(t)$ and $\frac{\partial}{\partial t}(\rho(t) f_i(t))$ as the triangle functions and the derivative of a triangle functions, respectively. For bodies of revolution [8]:-

$$\iint_s ds = \int_0^N dt \int_0^{2\pi} \rho(t)\, d\phi$$

$$\iint_{s'} ds' = \int_0^N dt' \int_0^{2\pi} \rho'(t')\, d\phi'$$

changing $\phi - \phi'$ to a new variable, and expressing the sine and cosine terms of (C-16) as exponentials, one ϕ integration in (C-12) can be performed as follow [61]

$$\int_0^{2\pi}\int_0^{2\pi} e^{jn(\phi-\phi')} \frac{e^{-jK_a R}}{4\pi R}\, d\phi' d\phi = \int_0^{2\pi} d\phi' \int_0^{2\pi} e^{jn\phi} \frac{e^{-jK_a R}}{4\pi R}\, d\phi$$

$$= \frac{1}{2} \int_0^{2\pi} [\cos(n\phi) + j\sin(n\phi)]\, \frac{e^{-jK_a R}}{R}\, d\phi$$

since the cosine and sine functions are even and odd functions, respectively, the remaining ϕ integration defines the Green function [61]

$$g_n = \int_0^{\pi} \cos(n\phi) \frac{e^{-jK_a R_\circ}}{R_\circ} d\phi \tag{C-18a}$$

where $R_\circ$ is given by (2-) with $\phi' = 0$, in the same way

$$\int_0^{2\pi}\int_0^{2\pi} \cos(\phi - \phi') e^{jn(\phi-\phi')} \frac{e^{-jK_a R}}{4\pi R} d\phi d\phi'$$

$$= \frac{1}{2}\left[\int_0^{\pi} \cos[(n+1)\phi] \frac{e^{-jK_a R_\circ}}{R_\circ} + \int_0^{\pi} \cos[(n-1)\phi] \frac{e^{-jK_a R_\circ}}{R_\circ}\right] d\phi = \frac{g_{n+1} + g_{n-1}}{2} \tag{C-18b}$$

and

$$\int_0^{2\pi}\int_0^{2\pi} \sin(\phi - \phi') e^{jn(\phi-\phi')} \frac{e^{-jK_a R}}{4\pi R} d\phi d\phi'$$

$$= \frac{1}{2j}\left[\int_0^{\pi} \cos[(n+1)\phi] \frac{e^{-jK_a R_\circ}}{R_\circ} - \int_0^{\pi} \cos[(n-1)\phi] \frac{e^{-jK_a R_\circ}}{R_\circ}\right] d\phi = \frac{g_{n+1} - g_{n-1}}{2j} \tag{C-18c}$$

Therefore, Eq.(C-12) becomes:-

$$\left(Z_n^{tt}\right)_{ij}^{JE} = \int_0^N dt' \int_0^N dt \left[j\omega\mu_a T(t'-t_i') T(t-t_j) \left(\sin\upsilon \sin\upsilon' \frac{g_{n+1} + g_{n-1}}{2} + \cos\upsilon \cos\upsilon' g_n \right) + \right.$$

$$\left. \frac{1}{j\omega\varepsilon_a} T'(t'-t_i') T'(t-t_j)\, g_n \right]$$

$$\left(Z_n^{t\phi}\right)_{ij}^{JE} = \int_0^N dt' \int_0^N dt \left[-\omega\mu_a T(t'-t_i') T(t-t_j) \sin\upsilon' \frac{g_{n+1} - g_{n-1}}{2} + \frac{n}{\omega\varepsilon_a \rho(t)} T'(t'-t_i') T(t-t_j) g_n \right]$$

$$\left(Z_n^{\phi t}\right)_{ij}^{JE} = \int_0^N dt' \int_0^N dt \left[\omega\mu_a T(t'-t_i') T(t-t_j) \sin\upsilon \frac{g_{n+1} - g_{n-1}}{2} - \frac{n}{\omega\varepsilon_a \rho'(t')} T(t'-t_i') T'(t-t_j) g_n \right]$$

$$\left(Z_n^{\phi\phi}\right)_{ij}^{JE} = \int_0^N dt' \int_0^N dt \left[j\omega\mu_a T(t'-t_i') T(t-t_j) \frac{g_{n+1} + g_{n-1}}{2} + \frac{n^2}{j\omega\varepsilon_a \rho'(t') \rho(t)} T(t'-t_i') T(t-t_j) g_n \right]$$

(C-19)

To reduce the number of integrations in eq.(C-19) an approximate evaluation was obtained by approximating each triangle function by four steps. . For the t

integration, the $T(t-t_j)$function is approximated by four pulses of amplitudes $\frac{1}{4},\frac{3}{4},\frac{3}{4},\frac{1}{4}$,as shown in Fig.(2- a). The derivative of $T(t-t_j)$ is represented exactly by four pulses of amplitude 1, 1, -1, -1 as shown in Fig.(2- b). The functions ρ, sinν, and cosν are assumed constant over each pulse, equal to them values at the midpoint of the pulse [8].

For the t' integration, the $T(t'-t_i')$ function is approximated by for impulse functions, of strengths $\frac{1}{8},\frac{3}{8},\frac{3}{8},\frac{1}{8}$, as shown in Fig.(2- a). The derivative of $T(t'-t_i')$ is approximated by four impulse functions of strengths $\frac{1}{2},\frac{1}{2},-\frac{1}{2},-\frac{1}{2}$, as shown in Fig.(2- b). The functions $\rho',\sin\nu'$, and $\cos\nu'$ are assumed constant over each pulse. We now define the numbers

$$T_1=\frac{1}{8} \qquad T_1'=\frac{1}{2}$$

$$T_2=\frac{3}{8} \qquad T_2'=\frac{1}{2} \tag{C-20a}$$

$$T_3=\frac{3}{8} \qquad T_3'=-\frac{1}{2}$$

$$T_4=\frac{1}{8} \qquad T_4'=-\frac{1}{2}$$

The midpoints of the pulses

$$t_p=j+\frac{p-2.5}{2} \qquad t_q=i+\frac{q-2.5}{2} \tag{C-20b}$$

and the pulse Green functions

$$G_n=2\int_{t_q-1/4}^{t_q+1/4}dt\int_0^{\pi}d\phi\frac{e^{-jK_aR_p}}{R_p}\cos(n\phi) \tag{C-21}$$

where $R_p=\sqrt{\rho^2+\rho_p{}^2-2\rho\rho_p\cos(\phi)+(z-z_p)^2}$

G_n is calculated for the above equation by combining the processes of analytical integration (t) and numerical (ϕ), as the period $0\langle\phi\langle\pi$ is divided

into periods of equal numbers ($M = 2N$), therefore the solution of (C-21) with some mathematical manipulation can take the form [8]

$$G_n = \frac{\pi}{M}\sum_{m=1}^{M}\cos(n\phi_m)\,f(\phi_m) \tag{C-22}$$

where $\int_0^{\pi}\cos(n\phi)d\phi \longrightarrow \frac{\pi}{M}\sum_{m=1}^{M}\cos(n\phi_m)$, $\phi_m = \frac{(m-1/2)\pi}{M}$ and

$$f(\phi_m) = e^{-jkR_{pq}}\left\{2(1+jK_aR_{pq})\ln\left[\frac{t_2+\left(t_2^2+d^2\right)^{1/2}}{t_1+\left(t_1^2+d^2\right)^{1/2}} - jK_a\right]\right\} \tag{C-23a}$$

$$R_{pq} = \sqrt{\rho_p{}^2 + \rho_q{}^2 - 2\rho_p\rho_q\cos\phi_m + (z_p - z_q)^2} \tag{C-23b}$$

with

$$\left.\begin{aligned} t_\circ &= \left|(z_p - z_q)\cos\upsilon_q + (\rho_p\cos\phi_m - \rho_q)\sin\upsilon_q\right| \\ d^2 &= R_{pq}^2 - t_\circ^2 \\ t_1 &= t_\circ - 1/4 \\ t_2 &= t_\circ + 1/4 \end{aligned}\right\} \tag{C-23c}$$

In terms of these definitions and approximations and using the relationships $\omega\mu_a = K_a\eta_a$ and $\omega\varepsilon_a = K_a/\eta_a$, the matrix elements of Eq.(C-19) for perfect electric conductor is reduced to:-

$$\left(Z_n^{tt}\right)_{ij}^{JE} = -jK_a\eta_a\sum_{p=1}^{4}\sum_{q=1}^{4}\left[T_p\,T_q\left\{\sin\nu_p\sin\nu_q\,\frac{G_{n+1}+G_{n-1}}{2} + \cos\nu_p\cos\nu_q\,G_n\right\} - \frac{1}{K_a^2}T_p'T_q'\,G_n\right]$$

$$\left(Z_n^{t\phi}\right)_{ij}^{JE} = -K_a\eta_a\sum_{p=1}^{4}\sum_{q=1}^{4}\left[T_p\,T_q\sin\nu_p\,\frac{G_{n+1}-G_{n-1}}{2} + \frac{n}{K_a^2}\frac{T_q}{\rho_q}T_p'\,G_n\right]$$

$$\left(Z_n^{\phi t}\right)_{ij}^{JE} = K_a\eta_a\sum_{p=1}^{4}\sum_{q=1}^{4}\left[T_p\,T_q\sin\nu_q\,\frac{G_{n+1}-G_{n-1}}{2} + \frac{n}{K_a^2}T_q'\frac{T_p}{\rho_p}G_n\right]$$

$$\left(Z_n^{\phi\phi}\right)_{ij}^{JE} = -jK_a\eta_a\sum_{p=1}^{4}\sum_{q=1}^{4}T_p\,T_q\left[\frac{G_{n+1}+G_{n-1}}{2} - \frac{n^2}{K_a^2\rho_p\rho_q}G_n\right] \tag{C-24}$$

Where the letter ***a*** in last equation referred to conducting medium, and ρ_p, ρ_q, ν_p, ν_q are the ρ and ν evaluated at t_p and t_q, respectively. In other way, the Eqs.(C-18) can be evaluated numerically by using gauss quadrature, without restoring to the pulse Green function, especially for dielectric bodies [88]. So, Eqs.(C-18) is re-written as follow:

$$G_1 = \int_0^{\pi} \cos(n\phi)\ \frac{e^{-jK_a R}}{R}\ d\phi \tag{C-25a}$$

$$G_2 = \int_0^{\pi} \cos\phi \cos(n\phi)\ \frac{e^{-jK_a R}}{R}\ d\phi \tag{C-25b}$$

$$G_3 = \int_0^{\pi} \sin\phi \sin(n\phi)\ \frac{e^{-jK_a R}}{R}\ d\phi \tag{C-25c}$$

Therefore, Eq.(C-24) becomes:-

$$\begin{aligned}
\left(Z_n^{tt}\right)_{ij}^{JE} &= -jK_a\eta_a \sum_{p=1}^{4}\sum_{q=1}^{4}\left[T_p\ T_q\ \left\{\sin\nu_p \sin\nu_q\ G_2 + \cos\nu_p \cos\nu_q\ G_1\right\} - \right. \\
&\qquad \left. \frac{1}{K_a^2} T_p' T_q'\ G_1\right] \\
\left(Z_n^{t\phi}\right)_{ij}^{JE} &= -K_a\eta_a \sum_{p=1}^{4}\sum_{q=1}^{4}\left[T_p\ T_q \sin\nu_p\ G_3 + \frac{n}{K_a^2}\frac{T_q}{\rho_q} T_p'\ G_1\right] \\
\left(Z_n^{\phi t}\right)_{ij}^{JE} &= K_a\eta_a \sum_{p=1}^{4}\sum_{q=1}^{4}\left[T_p\ T_q \sin\nu_q\ G_3 + \frac{n}{K_a^2} T_q'\frac{T_p}{\rho_p} G_1\right] \\
\left(Z_n^{\phi\phi}\right)_{ij}^{JE} &= -jK_a\eta_a \sum_{p=1}^{4}\sum_{q=1}^{4} T_p\ T_q\left[G_2 - \frac{n^2}{K_a^2\rho_p\rho_q} G_1\right]
\end{aligned} \tag{C-26}$$

where the letter *a* in above equation referred to dielectric medium.

Appendix (D)

The calculation of the R-submatrices elements

The first step to find the measurement matrices of BOR is the calculation of vectors dot product. These vectors can be summarized where θ_r and ϕ_r are the angles of field point ,as follow:

$$\begin{aligned}
&\bar{k} = k_\circ \hat{u}_r^r \\
&\bar{r} = \hat{x}x + \hat{y}y + \hat{z}z \\
&x = \rho\cos\theta \quad , \quad y = \rho\sin\theta \quad , \quad z = z \\
&\hat{u}_r^r = \hat{x}\sin\theta_r\cos\phi_r + \hat{y}\sin\theta_r\sin\phi_r + \hat{z}\cos\theta_r \\
&\hat{u}_\theta^r = \hat{x}\cos\theta_r\cos\phi_r + \hat{y}\cos\theta_r\sin\phi_r - \hat{z}\sin\theta_r \\
&\hat{u}_\phi^r = -\hat{x}\sin\phi_r + \hat{y}\cos\phi_r \\
&\hat{u}_t = \hat{x}\sin\upsilon\cos\phi + \hat{y}\sin\upsilon\sin\phi + \hat{z}\cos\upsilon \\
&\hat{u}_\phi = -\hat{x}\sin\phi + \hat{y}\cos\phi
\end{aligned} \tag{D-1}$$

The famous relations can be obtained from (D-1)

$$\hat{u}_t \cdot \hat{u}_\theta^r = \sin\upsilon\cos\theta_r\cos(\phi-\phi_r) - \cos\upsilon\sin\theta_r \tag{D-2}$$

$$\hat{u}_\phi \cdot \hat{u}_\theta^r = -\cos\theta_r\left(\sin\phi\cos\phi_r - \cos\phi\sin\phi_r\right) = -\cos\theta_r\sin(\phi-\phi_r) \tag{D-3}$$

$$\hat{u}_t \cdot \hat{u}_\phi^r = \sin\upsilon\left(\sin\phi\cos\phi_r - \cos\phi\sin\phi_r\right) = \sin\upsilon\sin(\phi-\phi_r) \tag{D-4}$$

$$\hat{u}_\phi \cdot \hat{u}_\phi^r = \cos\phi\cos\phi_r + \sin\phi\sin\phi_r = \cos(\phi-\phi_r) \tag{D-5}$$

$$\bar{k} \cdot \bar{r} = \left(k_\circ \hat{u}_r^r\right) \cdot \left(\hat{x}x + \hat{y}y + \hat{z}z\right) = k_\circ\left[\rho\sin\theta_r\cos(\phi-\phi_r) + z\cos\theta_r\right] \tag{D-6}$$

When ϕ_r =0 we get

$$\left.\begin{aligned}
&\hat{u}_t \cdot \hat{u}_\theta^r = \sin\upsilon\cos\theta_r\cos\phi - \cos\upsilon\sin\theta \\
&\hat{u}_\phi \cdot \hat{u}_\theta^r = -\cos\theta_r\sin\phi
\end{aligned}\right\} \tag{D-7}$$

$$\left.\begin{aligned}
&\hat{u}_t \cdot \hat{u}_\phi^r = \sin\upsilon\sin\phi \\
&\hat{u}_\phi \cdot \hat{u}_\phi^r = \cos\phi
\end{aligned}\right\} \tag{D-8}$$

$$\bar{k} \cdot \bar{r} = k_\circ\left[\rho\sin\theta_r\cos\phi + z\cos\theta_r\right] \tag{D-9}$$

For θ-polarized there are two components $\left(R_n^{t\theta}\right)_i$ and $\left(R_n^{\phi\theta}\right)_i$ which can be found, respectively, as follows :

$$\left(R_n^{t\theta}\right)_i = \int_0^N \int_0^{2\pi} \left(\hat{u}_t \cdot \hat{u}_\theta^r\right) f_i(t)\, e^{jn\phi} e^{jk\left(\rho\sin(\theta_r)\cos(\phi)+z\cos(\theta_r)\right)} \rho dt d\phi$$

$$= \int_0^N dt \int_0^{2\pi} \begin{bmatrix} \sin\upsilon\cos\theta_r\cos\phi\, e^{jn\phi} e^{jk\rho\sin(\theta_r)\cos(\phi)} e^{jkz\cos(\theta_r)} \\ -\cos\upsilon\sin\theta_r\, e^{jn\phi} e^{jk\rho\sin(\theta_r)\cos(\phi)} e^{jkz\cos(\theta_r)} \end{bmatrix} T(t-i) d\phi \qquad \text{(D-10)}$$

By using the integral formula of Bessel functions

$$J_n(x) = \frac{j^{-n}}{2\pi} \int_0^{2\pi} e^{jx\cos(\phi)} e^{jn\phi} d\phi \qquad \text{(D-11)}$$

Where $x = k\rho\sin\theta_r$, to obtained

$$\int_0^{2\pi} e^{jk\rho\sin\theta_r\cos\phi} e^{jn\phi} d\phi = 2\pi j^n J_n(k\rho\sin\theta_r) \qquad \text{(D-12)}$$

When $n \to n+1$ the last equation (D-12) is devolved to

$$\int_0^{2\pi} e^{jk\rho\sin\theta_r\cos\phi} e^{j(n+1)\phi} d\phi = 2\pi j^{(n+1)} J_{(n+1)}(k\rho\sin\theta_r)$$

$$= \pi j^{(n+1)} \left(J_{(n+1)}(k\rho\sin\theta_r) + J_{(n+1)}(k\rho\sin\theta_r)\right)$$

add and subtract $J_{(n-1)}(k\rho\sin\theta_r)$ to right side of above equation

$$\int_0^{2\pi} e^{jk\rho\sin\theta_r\cos\phi} e^{jn\phi} \left[\cos\phi + j\sin\phi\right] d\phi = \pi j^{(n+1)} \left[\left(J_{(n+1)} - J_{(n-1)}\right) + \left(J_{(n+1)} + J_{(n-1)}\right)\right]$$

when comparing both sides of this equation, we find

$$\begin{aligned} &\int_0^{2\pi} \cos\phi\, e^{jk\rho\sin\theta_r\cos\phi}\, e^{jn\phi} d\phi = \pi j^{(n+1)} \left(J_{(n+1)} - J_{(n-1)}\right) \\ &\int_0^{2\pi} \sin\phi\, e^{jk\rho\sin\theta_r\cos\phi}\, e^{jn\phi} d\phi = \pi j^n \left(J_{(n+1)} + J_{(n-1)}\right) \end{aligned} \qquad \text{(D-13)}$$

Eq.(D-10) can be take the form

$$\left(R_n^{t\theta}\right)_i = \int_0^N dt \begin{bmatrix} \sin\upsilon\cos\theta_r \int_0^{2\pi} \cos\phi e^{jn\phi} e^{jk\rho\sin\theta_r\cos\phi} d\phi \\ -\cos\upsilon\sin\theta_r \int_0^{2\pi} e^{jn\phi} e^{jk\rho\sin\theta_r\cos\phi} d\phi \end{bmatrix} e^{jkz\cos(\theta_r)} T(t-i) \qquad \text{(D-14)}$$

Therefore, the using of Eq.(D-13) in (D-14) is to give

$$\left(R_n^{t\theta}\right)_i = 2\pi j^{n+1}\int_0^N dt\left[\sin\upsilon\cos\theta_r\left(\frac{J_{(n+1)}-J_{(n-1)}}{2}\right)+j\cos\upsilon\sin\theta_r J_n\right]e^{jkz\cos(\theta_r)}T(t-i) \qquad \text{(D-15)}$$

As for the $\left(R_n^{\phi\theta}\right)_i$ can be found as follow:

$$\left(R_n^{\phi\theta}\right)_i = \int_0^N\int_0^{2\pi}\left(\hat{u}_\phi\cdot\hat{u}_\theta^r\right)f_i(t)e^{jn\phi}e^{jk(\rho\sin\theta_r\cos\phi+z\cos\theta_r)}\rho dtd\phi$$

$$=\int_0^N\int_0^{2\pi}-\cos\theta_r\sin\phi f_i(t)e^{jn\phi}e^{jk(\rho\sin\theta_r\cos\phi+z\cos\theta_r)}\rho dtd\phi$$

$$=-\int_0^N dt\left[\cos\theta_r\int_0^{2\pi}\sin\phi e^{jk\rho\sin\theta_r\cos\phi}e^{jn\phi}d\phi\right]e^{jkz\cos\theta_r}T(t-i) \qquad \text{(D-16)}$$

and by using eq.(D-13), we get

$$\left(R_n^{\phi\theta}\right)_i = -2\pi j^{n+1}\int_0^N dt\left[\cos\theta_r\left(\frac{J_{(n+1)}+J_{(n-1)}}{2j}\right)\right]e^{jkz\cos\theta_r}T(t-i) \qquad \text{(D-17)}$$

Also for ϕ-polarized there are two components $\left(R_n^{t\phi}\right)_i$ and $\left(R_n^{\phi\phi}\right)_i$, respectively. to find $\left(R_n^{t\phi}\right)_i$ we have:

$$\left(R_n^{t\phi}\right)_i = \int_0^N\int_0^{2\pi}\left(\hat{u}_t\cdot\hat{u}_\phi^r\right)f_i(t)e^{jn\phi}e^{jk(\rho\sin\theta_r\cos\phi+z\cos\theta_r)}\rho\,dt\,d\phi$$

$$=\int_0^N\int_0^{2\pi}\sin\upsilon\sin\phi\ f_i(t)\,e^{jn\phi}e^{jk(\rho\sin\theta_r\cos\phi+z\cos\theta_r)}\rho\,dt\,d\phi$$

$$=\int_0^N dt\left[\sin\upsilon\int_0^{2\pi}\sin\phi\,e^{jk\rho\sin\theta_r\cos\phi}\ e^{jn\phi}d\phi\right]e^{jkz\cos\theta_r}\ T(t-i) \qquad \text{(D-18)}$$

again using Eq.(D-13) is to obtained

$$\left(R_n^{t\phi}\right)_i = 2\pi j^{n+1}\int_0^N dt\left[\sin\upsilon\left(\frac{J_{(n+1)}+J_{(n-1)}}{2j}\right)\right]e^{jkz\cos\theta_r}\ T(t-i) \qquad \text{(D-19)}$$

For $\left(R_n^{\phi\phi}\right)_i$ it can be found with same steps as follow:

$$\left(R_n^{\phi\phi}\right)_i = \int_0^N\int_0^{2\pi}\left(\hat{u}_\phi\cdot\hat{u}_\phi^r\right)f_i(t)e^{jn\phi}e^{jk(\rho\sin\theta_r\cos\phi+z\cos\theta_r)}\ \rho\,dt\,d\phi$$

$$= \int_0^N \int_0^{2\pi} \cos\phi \; f_i(t) e^{jn\phi} e^{jk(\rho \sin\theta_r \cos\phi + z\cos\theta_r)} \; \rho \, dt \, d\phi$$

$$= \int_0^N dt \left[\int_0^{2\pi} \cos\phi \, e^{jk\rho \sin\theta_r \cos\phi} \; e^{jn\phi} d\phi \right] e^{jkz\cos\theta_r} \; T(t-i) \qquad \text{(D-20)}$$

with the application of (C-13) ,yields to

$$\left(R_n^{\phi\phi}\right)_i = 2\pi j^{n+1} \int_0^N dt \left(\frac{J_{(n+1)} - J_{(n-1)}}{2} \right) e^{jkz\cos\theta_r} \; T(t-i) \qquad \text{(D-21)}$$

the integrals (D-15) and (D-17) and (D-19) and (D-21) can be re-written with other formulas by using triangle function $\rho f_i(t) = T(t-i) \equiv T_q$ also used to $C_q = \pi j^{n+1} T_q e^{jkz_q \cos\theta_r}$ to obtained

$$\left.\begin{aligned}
\left(R_n^{t\theta}\right)_i &= \sum_{q=1}^{4} C_q \left[\sin\upsilon_q \cos\theta_r \left(J_{(n+1)} - J_{(n-1)}\right) + 2j \cos\upsilon_q \sin\theta_r \; J_n \right] \\
\left(R_n^{\phi\theta}\right)_i &= \sum_{q=1}^{4} j \, C_q \cos\theta_r \left(J_{(n+1)} + J_{(n-1)}\right) \\
\left(R_n^{t\phi}\right)_i &= \sum_{q=1}^{4} - j \, C_q \sin\upsilon_q \left(J_{(n+1)} + J_{(n-1)}\right) \\
\left(R_n^{\phi\phi}\right)_i &= \sum_{q=1}^{4} C_q \left(J_{(n+1)} - J_{(n-1)}\right)
\end{aligned}\right\} \qquad \text{(D-22)}$$

Appendix (E)

The calculation of the Y-submatrices elements

The main purpose of this appendix is to show the general procedure to find the admittance submatrices elements equations.

The starting point from Eq.(3-39a) is to show the mutual admittance between the source element i and an observation element j by the dot product of $\overline{W}_{mi}^{\alpha}$ and $\overline{H}^{a}\left(\overline{J}_{nj}^{\beta},0\right)$ as:-

$$\left(Y_{mn}^{\alpha\beta}\right)_{ij}^{JH} = \int_s \overline{W}_{mi}^{\alpha} \cdot \overline{H}^{a}\left(\overline{J}_{nj}^{\beta},0\right) ds \qquad \text{(E-1)}$$

In general, the magnetic field $\bar{H}^a(\bar{J}_{nj},0)$ is due to the electric current density $\bar{J}_{nj}(\bar{r}')$ may be written (see Eqs.(3-9) and (3-10)), as follow:-

$$\bar{H}^a(\bar{J}_{nj},0)=\int_{s'}\nabla\times\bar{J}_{nj}(\bar{r}')G^a(\bar{r},\bar{r}')\,ds' \tag{E-2}$$

Where the function $G^a(\bar{r},\bar{r}')$ is the scalar Green's function. By using the following vector identity [33]:-

$$\nabla\times\left(\bar{J}_{nj}(\bar{r}')G^a(\bar{r},\bar{r}')\right)=\nabla G^a(\bar{r},\bar{r}')\times\bar{J}_{nj}(\bar{r}')+G^a(\bar{r},\bar{r}')\left(\nabla\times\bar{J}_{nj}(\bar{r}')\right) \tag{E-3}$$

The function $G^a(\bar{r},\bar{r}')$ given in terms of source and observation coordinates. The operator ∇ is operated to the observation coordinates only and then the second term in Eq.(E-3) is vanish because $\nabla\times\bar{J}_{nj}(\bar{r}')=0$, it is possible to write Eq.(E-2) as:-

$$\bar{H}^a(\bar{J}_{nj},0)=\int_{s'}\nabla G^a(\bar{r},\bar{r}')\times\bar{J}_{nj}(\bar{r}')\,ds' \tag{E-4}$$

By using the chain rule, the grad ∇ of the Green's function can be written as follow:-

$$\nabla G^a(\bar{r},\bar{r}')=G_o^a(\bar{r},\bar{r}')\,\bar{R} \tag{E-5}$$

where

$$G_o^a(\bar{r},\bar{r}')=-\left(\frac{1+jK_aR}{R^2}\right)G^a(\bar{r},\bar{r}') \tag{E-6}$$

$$\bar{R}=\hat{u}_\rho\left(\rho-\rho'\cos(\phi'-\phi)\right)-\hat{u}_\phi\,\rho'\sin(\phi'-\phi)+\hat{u}_z(z-z') \tag{E-7}$$

Substituting Eq.(E-5) into Eq.(E-4), yields:-

$$\bar{H}^a(\bar{J}_{ni},0)=\int_{s'}G_o^a(\bar{r},\bar{r}')\left(\bar{R}\times\bar{J}_{nj}(\bar{r}')\right)ds' \tag{E-8}$$

The cross products on the right-hand side of Eq.(E-8) are evaluated by expressing all the vectors in terms of the unit vectors $\hat{u}_t,\hat{u}_n$ and $\hat{u}_\phi$.

The surface electric current $\bar{J}_{nj}(\bar{r}')$ has two components in $\hat{u}_{t'}-$ and $\hat{u}_{\phi'}-$directions only, as given in Eqs.(3-21), as:-

$$\bar{J}_{ni}^{t}(t',\phi') = \hat{u}_{t'}\ f_i(t')\ e^{jn\phi'} \tag{E-9a}$$

$$\bar{J}_{ni}^{\phi}(t',\phi') = \hat{u}_{\phi'}\ f_i(t')\ e^{jn\phi'} \tag{E-9b}$$

The relationship between the cylindrical and observation unit vectors are:-

$$\hat{u}_{\rho} = \hat{u}_n \cos\nu + \hat{u}_t \sin\nu \tag{E-10a}$$

$$\hat{u}_{\phi} = \hat{u}_{\phi} \tag{E-10b}$$

$$\hat{u}_z = -\hat{u}_n \sin\nu + \hat{u}_t \cos\nu \tag{E-10c}$$

Substituting Eqs.(E-10) into Eqs.(2-21c), and (2-21d) is to find the surface electric current of Eqs.(E-9) in terms of the unit vectors of observation point, we have:-

$$\hat{u}_{t'} = \hat{u}_t\left[\sin\nu\sin\nu'\cos(\phi'-\phi)+\cos\nu\cos\nu'\right]+\hat{u}_n\left[\cos\nu\sin\nu'\cos(\phi'-\phi)-\right.$$
$$\left.\sin\nu\cos\nu'\right]+\hat{u}_{\phi}\left[\sin\nu'\sin(\phi'-\phi)\right] \tag{E-11a}$$

Similarly with $\hat{u}_{\phi'}$:-

$$\hat{u}_{\phi'} = \hat{u}_t\left[-\sin\nu\sin(\phi'-\phi)\right]+\hat{u}_n\left[-\cos\nu\sin(\phi'-\phi)\right]+\hat{u}_{\phi}\left[\cos(\phi'-\phi)\right] \tag{E-11b}$$

Now, we can find the vector $\bar{R}$ in terms of the observation point unit vectors, by using Eqs.(E-10) into Eq.(E-7), as:-

$$\bar{R} = \hat{u}_t\left[\sin\nu\left\{\rho-\rho'\cos(\phi'-\phi)\right\}+\cos\nu(z-z')\right]+\hat{u}_n\left[\cos\nu\left\{\rho-\rho'\cos(\phi'-\phi)\right\}-\right.$$
$$\left.\sin\nu(z-z')\right]-\hat{u}_{\phi}\left[\rho'\sin(\phi'-\phi)\right] \tag{E-12}$$

To find the t- and ϕ - components of Eq.(E-8), the following products have to be found:-

$$\bar{R}\times\bar{J}_{nj}^{t}(\bar{r}') = \bar{R}\times\hat{u}_{t'}\ f_i(t')\ e^{jn\phi'} \tag{E-13a}$$

$$\bar{R}\times\bar{J}_{ni}^{\phi}(\bar{r}') = \bar{R}\times\hat{u}_{\phi'}\ f_i(t')\ e^{jn\phi'} \tag{E-13b}$$

Because the testing function $\overline{W}(\bar{r})$ has two components in $\hat{u}_t$- and $\hat{u}_\phi$- directions and from Eq.(E-1), then the two cross products in Eqs.(E-13) must be evaluated in terms of the $\hat{u}_t$ and $\hat{u}_\phi$ unit vectors only.

The t- and ϕ- components of the magnetic field (Eq.(E-8)), after substituting Eqs.(E-13), are:-

$$\overline{H}^a\left(\bar{J}_{ni}^t,0\right)=-\int_{s'} G_o^a\left(\bar{r},\bar{r}'\right) f_i\left(t'\right)\ e^{jn\phi'}\left[\hat{u}_t \sin\left(\phi'-\phi\right)\left(\rho'\cos\nu'\sin\nu+\sin\nu'\left\{\sin\nu\right.\right.\right.$$

$$\left.\left.\left.\left(z-z'\right)-\rho\cos\nu\right\}\right)+\hat{u}_\phi\left(\rho\cos\nu'-\cos\left(\phi'-\phi\right)\left\{\rho'\cos\nu'+\sin\nu'\left(z-z'\right)\right\}\right)\right]ds' \quad \text{(E-14a)}$$

$$\overline{H}^a\left(\bar{J}_{ni}^\phi,0\right)=-\int_{s'} G_o^a\left(\bar{r},\bar{r}'\right) f_i\left(t'\right)\ e^{jn\phi'}\left[\hat{u}_t\left(\rho'\cos\nu+\cos\left(\phi'-\phi\right)\left\{\sin\nu\left(z-z'\right)-\rho\cos\nu\right\}\right)\right.$$

$$\left.+\hat{u}_\phi\left(\sin\left(\phi'-\phi\right)\left(z-z'\right)\right)\right]\ ds' \quad \text{(E-14b)}$$

Substitution of Eqs.(E-14) and (2-17) into Eq.(E-1) and using the mode orthogonality in axis symmetric objects, i.e. (m=n), and using the same manner, in Appendix (C), with respect to t,t',ϕ and ϕ' integration the elements of the Y- matrix are given by:-

$$\left(Y_n^{tt}\right)_{ij}^{JH}=j\sum_{p=1}^{4}\sum_{q=1}^{4}T_pT_qG_6\left[\rho_q\cos\nu_q\sin\nu_p+\sin\nu_q\left\{\sin\nu_p\left(z_p-z_q\right)-\rho_p\cos\nu_q\right\}\right] \quad \text{(E-15a)}$$

$$\left(Y_n^{t\phi}\right)_{ij}^{JH}=\sum_{p=1}^{4}\sum_{q=1}^{4}T_pT_q\left[\rho_q\cos\nu_pG_4+\left\{\sin\nu_p\left(z_p-z_q\right)-\rho_p\cos\nu_p\right\}G_5\right] \quad \text{(E-15b)}$$

$$\left(Y_n^{\phi t}\right)_{ij}^{JH}=\sum_{p=1}^{4}\sum_{q=1}^{4}T_pT_q\left[\rho_p\cos\nu_qG_4-\left\{\sin\nu_q\left(z_p-z_q\right)+\rho_q\cos\nu_q\right\}G_5\right] \quad \text{(E-15c)}$$

$$\left(Y_n^{\phi\phi}\right)_{ij}^{JH}=j\sum_{p=1}^{4}\sum_{q=1}^{4}T_pT_q\left(z_p-z_q\right)G_6 \quad \text{(E-15d)}$$

Where

$$G_4=\int_0^\pi\cos\left(n\phi'\right)\frac{\left(1+jK_aR\right)}{R^3}e^{-jK_aR}d\phi' \quad \text{(E-16a)}$$

$$G_5 = \int_0^{\pi} \cos(n\phi')\cos\phi' \frac{(1+jK_aR)}{R^3} e^{-jK_aR} d\phi' \qquad \text{(E-16b)}$$

$$G_6 = \int_0^{\pi} \sin(n\phi')\sin\phi' \frac{(1+jK_aR)}{R^3} e^{-jK_aR} d\phi' \qquad \text{(E-16c)}$$

The matrix elements of Eqs.(2-35b) which produced from the electric field, is due to the magnetic current density $\overline{M}$, are described as:-

$$\left(Y_n^{\alpha\beta}\right)_{ij}^{ME} = -\left(Y_n^{\alpha\beta}\right)_{ij}^{JH} \qquad \text{(E-17)}$$

Basrah University
College of Science
Basrah Journal of Science

بسمه تعالى

جامعة البصرة
كلية العلوم
مجلة البصرة للعلوم

No.: العـــدد: 682 A
Date: التـــاريخ: ٢٠١٥/٤/٧

حضرة / عول سلمى طاهر

وائل عبدالطيف كريمي

احمد هاشم عبود

قسم الفيزياء / كلية العلوم / جامعة البصرة

- كلية العلوم / جامعة ميسان

تهديكم هيئة التحرير تحياتها ، ويسرها ان تعلمكم عن قبول بحثكم الموسوم..

((Electromagnetic scattering from dielectric bodies of revolution with attached wires))

للنشر في مجلة البصرة للعلوم وسوف يتم نشره في العدد القادم (القسم الانكليزي A) ان شاء الله.

www.bas-j-sci.net
bsj@bas-j-sci.net
Editor-in-chief:kadhim@bas-j-sci.net
Editorial secretory:karima@bas-j-sci.net

مجلة ميسان للدراسات الاكاديمية
ISSN: 1994-697X
Misan Journal of Academic Studies - Misan University - Iraq

no. العدد/ ١٣
date. التاريخ/ ٢٠١٥/١/م

إلى/ السيد عقيل سامي طاكر المحترم
أ.م.د. وائل عبد اللطيف كريم المحترم
جامعة البصرة / كلية العلوم
أ.د. احمد هاشم عبود المحترم
جامعة ميسان / كلية العلوم

م/ قبول نشر

نهديكم أطيب التحيات .....

تدارست هيئة تحرير المجلة بحثكم الموسوم :

Scattering from Dielectrically Coated Bodies of Revolution with Attached Wires

فوجدته صالحاً للنشر وسينشر في اعداد المجلة القادمة ان شاء الله.

مـع وافر الاحترام والتقدير ...

د. زين العابدين عبد علي
سكرتير التحرير
٢٠١٥/٢/

ISSN-1994-697X

الخلاصة

اعتمدت معالجة مسائل الإستطارة الكهرومغناطيسية في هذه الدراسة على الأجسام المعدنية والعازلة والمعدنية المطلية بطبقة عازلة ذات التناظر المحوري والمثبت عليها اسلاك او اجنحة معدنية بزاويا مختلفة والتي تعتبر من المسائل المهمة ذات التاثير على حساب مساحة المقطع الراداري، حيث تم تمثيل المسألة عن طريق مساهمة الجسم المتناظر وملحقاته الاسلاك والاجنحه والوصلات (الوصلة هي منطقة الاتصال بين السلك وسطح الجسم المتناظر) والاخذ بنظر الاعتبار المشاركة بينهم. وقد تم معالجة هذه المسائل باستخدام مبدا التكافؤ والذي يستخرج كثافة التيار الكهربائي المكافئة المجهولة على سطح الموصل وكثافات التيارات الكهربائية والمغناطيسية المكافئة المجهولة على سطح العازل. واستخدمت المعالجة المبنية على أساس المعادلة التكاملية للمجال الكهربائية EFIE لتحليل مسائل الاستطارة للاجسام المعدنية، اما بالنسبة للاجسام العازلة والمعدنية المطلية بطبقة عازلة فان الشروط الحدودية للمسالة تؤدي الى اربع معادلات تكاملية تختزل بواسطة المجموعات الخطية الى زوج من المعادلات التكاملية لذا استخدمت طريقة PMCHWT لمعالجة معادلة المجال التكاملية المركبة والتي تم تحويلها إلى مجموعة من المعادلات الخطية وحلها عدديا باستخدام طريقة العزوم MoM لتميزها باعطاء نتائج دقيقة فضلا عن انها يمكن ان تشمل جميع شروط الاستطارة للاجسام المنتظمة وغير المنتظمة، وتم اختيار تقنية كالركن لتكون اكثر موائمة في اختيار الدالة الوزنية الخاصة بالحل خصوصاً بعد أن تطورت تقنية الحاسوب ذو السرعة العالية والدقة الفائقة.

تم كتابة مجموعة من البرامجيات بلغة البرمجة فورتران Fortran Power Station90 لمحاكات الجزء النظري لهذه الاطروحة ولحساب مساحة المقطع الراداري في حالتي الاستطارة الكهرومغناطيسية الثنائية Bi-static والاحادية Mono-static للأجسام المعدنية والعازلة والمعدنية المطلية بطبقة عازلة بمختلف صفاتها كالتوصيلية σ وثابت العزل الكهربائي ε_r والنفاذية المغناطيسية μ_r ولحالتي وجود وعدم وجود الاسلاك والاجنحة والوصلات بين الاجسام والاسلاك. كانت النتائج التي تم الحصول عليها تؤكد صحة المعالجة العددية والبرمجية لمسائل الاستطارة، فضلا عن التقارب الكبير مع النتائج المنشورة من قبل باحثين آخرين.

ان احد الاهداف الاساسية والمهمة في بحثنا هو دراسة تاثير الشكل (بواسطة الاسلاك) بالاضافة الى الطلاء (بواسطة المواد الماصة للاشعة الرادارية) على البصمة الرادارية. هذه البصمة تكون معروفة للاجسام المنتظمة البسيطة , كما في الكرة والاسطوانة, قبل اضافة تاثير الاسلاك عليها وايجاد شكل جديد للبصمة الرادارية. اما التطبيق الاساسي هو ايجاد نموذج مطور لهذه الدراسة يحمل بصمة رادارية معروفة ولو كانت بشكل تقريبي مع اجسام اخرى قريبة له بالشكل.

أن النموذج المقترح في هذه الدراسة، والمستخدم لتقريب النتائج الى الواقع بالمقارنة مع اجسام ذات بصمة رادارية معروفة، عبارة عن صاروخ للقوة الجوية الامريكية مع اربعة اجنحة. تم دراسة ابعاد الاجنحة لهذا النموذج مع الجسم الموصل من حيث الطول والعرض والارتفاع وكذلك دراسة تاثير طبقة المادة العازلة المستخدمة في تقنية المواد الماصة لاشعة الرادار (RAM) لطلاء جسم الصاروخ من حيث سمكها ومعاملاتها المتمثلة بثابت العزل الكهربائي ε_r والنفاذية المغناطيسية μ_r، وان تاثير هذه العوامل كان واضحا على مساحة المقطع الراداري حيث بينت النتائج ان تاثير تقنية الطلاء تقلل من قيمة البصمة الرادارية مقارنة بالجسم المعدني، فضلا عن تاثير الاسلاك على البصمة الرادرية مع وجود الوصلات. ان الجزء الخيالي لثابت العزل الكهربائي والنفاذية المغناطيسية كان له تاثير كبير في تقليل وتشويه مساحة البصمة الرادارية للنموذج وهو من الاهداف الرئيسية في الدراسة الحالية عندما تتغيير مادة جسم الصاروخ وبقاء الاجنحة موصلة.

تخمين وتقليل مساحة المقطع الرادارية للاجسام المتناظرة محوريا مع الاسلاك الملحقة

(دراسة نظرية)

رسالة مقدمة الى
كلية العلوم - جامعة البصرة
كجزء من متطلبات نيلٍ شهادة
دكتوراه فلسفة في الفيزيـاُء
"الحسابات الكهرومغناطيسيةً"

من قبل

عقيل سامي طاهر

بكالوريوس فيزياء 1997 جامعة البصرة
ماجستيرفيزياء 2000 جامعة البصرة

بإشراف

أ.د . أحمد هاشم عبود
أ.م .د . وائل عبداللطيف كديمي

1436 هـ **2014 م**